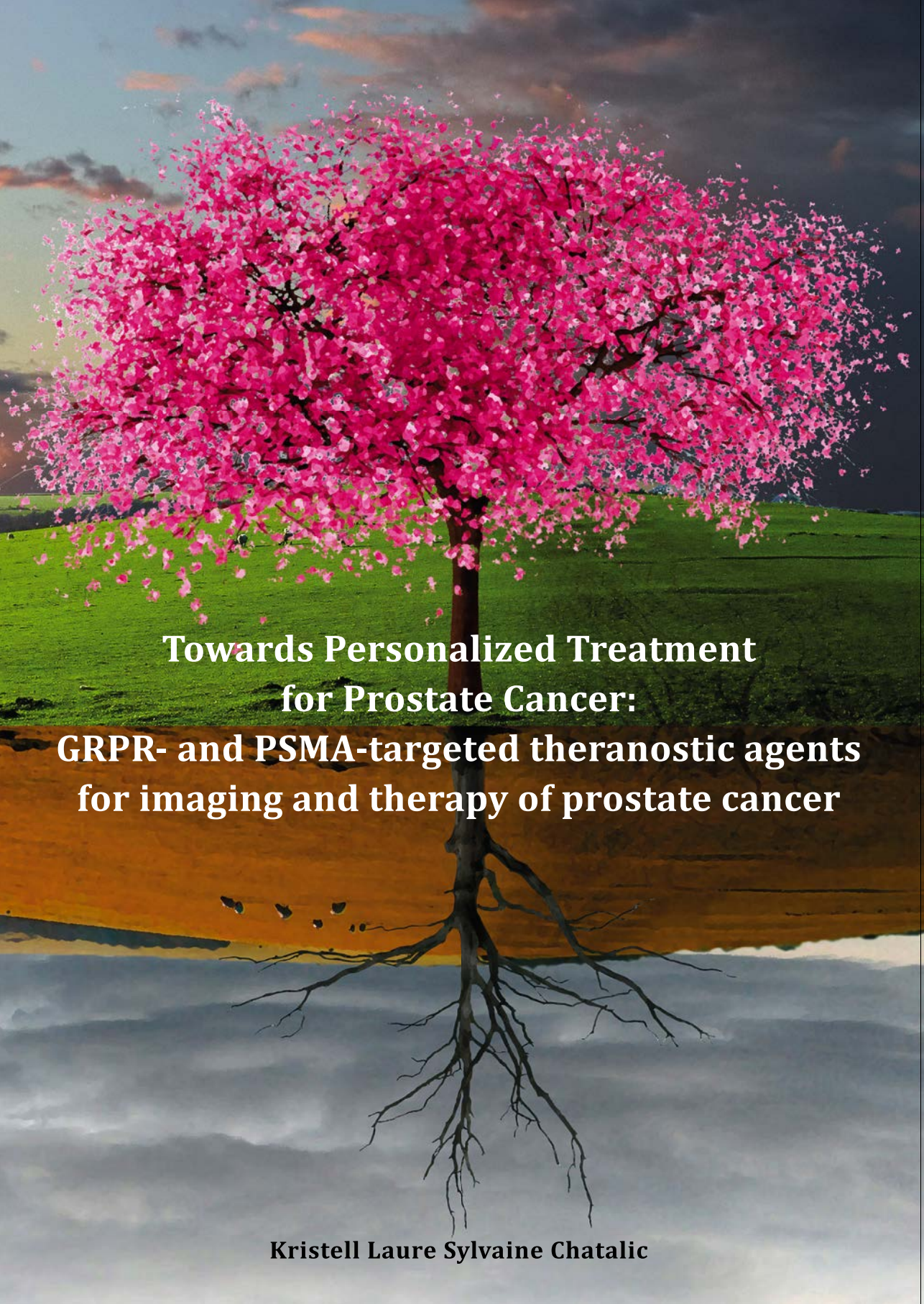

Towards Personalized Treatment for Prostate Cancer: GRPR- and PSMA-targeted theranostic agents for imaging and therapy of prostate cancer

Kristell Laure Sylvaine Chatalic

Towards Personalized Treatment for Prostate Cancer: GRPR- and PSMA-targeted theranostic agents for imaging and therapy of prostate cancer

Kristell Laure Sylvaine Chatalic

Cover design: Katie Shopland, Kristell Chatalic, Ton Everaers
Thesis layout: Concept: Ton Everaers Production: Legatron Electronic Publishing, Rotterdam
Printing: Ipskamp Printing, Enschede

ISBN/EAN: 978-94-028-0078-4

Towards Personalized Treatment for Prostate Cancer: GRPR- and PSMA-targeted theranostic agents for imaging and therapy of prostate cancer

Naar persoonlijke behandeling van prostaatkanker:
GRPR- en PSMA-gerichte theranostische radiofarmaca voor beeldvorming
en therapie van prostaatkanker

Proefschrift

ter verkrijging van de graad van doctor
aan de Erasmus Universiteit Rotterdam

op gezag van de rector magnificus

Prof.dr. H.A.P. Pols

en volgens besluit van het College voor Promoties.

De openbare verdediging zal plaatsvinden op
woensdag 16 maart 2016 om 15.30 uur

door
Kristell Laure Sylvaine Chatalic
geboren te Vitry-sur-Seine, Frankrijk

Erasmus University Rotterdam

PROMOTIECOMMISSIE

Promotoren:	Prof.dr.ir. M. de Jong Prof.dr. O.C. Boerman
Overige leden:	Prof.dr. C.H. Bangma Prof.dr.ir. T.J. Visser Prof.dr. H.J. Wester
Copromotor:	Dr.ir. W.M. van Weerden

Pour mes parents

CONTENTS

SECTION 1 - THERANOSTICS IN NUCLEAR MEDICINE 9

Chapter 1.1 **11**
General Introduction and Outline of the Thesis

Chapter 1.2 **39**
Radiopeptides for Imaging and Therapy: A Radiant Future
Journal of Nuclear Medicine, 2015; 56(12):1809-12

SECTION 2 - GASTRIN-RELEASING PEPTIDE RECEPTOR TARGETING 51

Chapter 2.1 **53**
Preclinical Comparison of Al^{18}F- and ^{68}Ga-labeled Gastrin-Releasing Peptide Receptor Antagonists for PET Imaging of Prostate Cancer
Journal of Nuclear Medicine 2014; 55(12):2050-6

Chapter 2.2 **71**
In Vivo Stabilization of a Gastrin-Releasing Peptide Receptor Antagonist enhances PET Imaging and Radionuclide Therapy of Prostate Cancer in Preclinical Studies
Theranostics 2016; 6(1):104-117

SECTION 3 - PROSTATE-SPECIFIC MEMBRANE ANTIGEN TARGETING 97

Chapter 3.1 **99**
A Novel ^{111}In-labeled Anti-PSMA Nanobody for Targeted SPECT/CT Imaging of Prostate Cancer
Journal of Nuclear Medicine 2015; 56(7):1094-9

Chapter 3.2 **119**
Towards Personalized treatment of Prostate Cancer: PSMA I&T, a Promising PSMA-Targeted Theranostic Agent
(Submitted for publication)

Chapter 3.3 **143**
Alpha Radionuclide Therapy of Prostate Cancer Targeting Prostate-Specific Membrane Antigen
(Submitted for publication)

SECTION 4 - EPILOGUE 157

General Discussion and Concluding Remarks *159*
Summary *169*
Samenvatting *175*
Curriculum Vitae *181*
List of Publications *185*
PhD Portfolio *189*
Acknowledgments *193*

Theranostics in Nuclear Medicine

1

Chapter 1.1
General Introduction and Outline of the Thesis

Chapter 1.2
Radiopeptides for Imaging and Therapy: A Radiant Future

1.1

General Introduction and Outline of the Thesis

PROSTATE CANCER

Statistics, Screening and Early Detection

According to GLOBOCAN estimates, 1.1 million new cases of prostate cancer (PCa) and 307,500 deaths occurred worldwide in 2012, rendering PCa as the second most frequently diagnosed cancer among men and the fifth leading cause of cancer death worldwide (*1*).

The highest PCa incidence rates are observed in more developed regions of the world, such as in Australia/New Zealand, Northern America, and Western and Northern Europe. Besides lifestyle and genetic factors, the use of prostate-specific antigen (PSA) testing in developed countries partially accounts for differences in incidence rate worldwide (*2*). The value of PSA screening is controversial. Although the European Randomized study of Screening for Prostate Cancer (ERSPC) has shown substantial reduction in mortality after 13 years follow-up (*3*), PSA-testing also leads to overdiagnosis (40-50% screen-detected cases) and unnecessary treatments with associated side effects (*4-6*). Modifications of PSA-screening approaches are being investigated to reduce the risk of overdiagnosis. New research methods are being developed to complement PSA-screening and separate low-risk cancers from more aggressive cancers, such as non-invasive assays for serum and urine biomarkers.

Diagnosis and Staging

Patients at risk for PCa are identified based on different factors, such as age, ethnicity, family history, PSA level, free/total PSA ratio and digital rectal examination (DRE). Diagnosis is established by transrectal ultrasound-guided prostate biopsy or magnetic resonance imaging (MRI)-transrectal ultrasound (TRUS) fusion biopsy, from which the Gleason score (GS) is derived (*7*). Clinical T stage is evaluated by DRE and patients with localized PCa are classified in risk groups (low-, intermediate- or high-risk) according to T stage, GS and PSA level. Staging of metastases is recommended for intermediate- or high-risk patients, using ^{99m}Tc bone scan, computed tomography (CT) scan, whole-body MRI or choline positron emission tomography (PET)/CT (*7*).

Treatment and Follow-up

Localized PCa

Watchful waiting and active surveillance are options for low-risk patients with localized disease. Curative treatment options for low- to intermediate-risk patients include radical prostatectomy, external beam radiotherapy and brachytherapy. For patients with high-risk or locally advanced PCa, treatment options include combinations of external beam radiotherapy with hormone treatment or radical prostatectomy with pelvic lymphadenectomy. Hormone treatment consisting of androgen-deprivation therapy can be given as neoadjuvant as well as adjuvant therapy (*7*).

Recurrent PCa and Castration-Resistant PCa
Patients showing recurrence of the disease as reflected by increased levels of circulating PSA (i.e. biochemical relapse) after radiotherapy and patient with hormone-naïve metastatic disease may receive androgen-deprivation therapy. For patients with castration-resistant PCa (CRPC), several options are currently available, such as chemotherapeutics (abiraterone, enzalutamide, docetaxel, sipuleucel-T, cabazitaxel), or the radiopharmaceutical Radium-223 (Xofigo) for treatment of bone metastases. Radiotherapy can be used to relief pain caused by bone metastases. Disease response/progression should be monitored by regular imaging studies in patients with CRPC (*7*).

THERANOSTICS CONCEPT

Clinical Relevance

Early diagnosis of PCa is essential, as patient prognosis is strongly diminished for advanced disseminated PCa. PSA-screening benefits are controversial, because of the risk of overdiagnosis and overtreatment. Initial diagnosis and staging is performed using DRE and prostate biopsies. More PCa-specific non-invasive methods are needed to complement currently available methods to facilitate staging and monitoring of treatment effect and disease progression. Moreover, there is an unmet need for a sensitive method to detect tumor lesions in patients with a rise in PSA from unknown source. In addition, there is a need for more effective treatment options of metastatic PCa. A single tool combining diagnosis and therapy in a “theranostic” approach could effectively contribute to a more personalized management of PCa patients, whereby imaging can guide the choice of the most suitable therapeutic option for each patient. Theranostic agents can be designed to specifically target biomarkers overexpressed on PCa cells. In nuclear medicine, theranostic agents can be designed with diagnostic and therapeutic radionuclides. This powerful combination would not only allow non-invasive detection of PCa lesions, but also monitoring of progression of disease and treatment efficacy (**Figure 1**).

Molecular Imaging

Imaging Modalities
Imaging can provide valuable insight about numerous pathologies, and multimodal imaging methods can provide complementary information. An overview of different imaging modalities used in preclinical research was recently given by de Jong et al. (*9*) (**Table 1**).

CT and MRI provide anatomical or physiological information with high spatial resolution, whereas nuclear and optical imaging techniques allow imaging of tumor-specific metabolic processes or biomarkers, with high sensitivity, but relatively low spatial resolution.

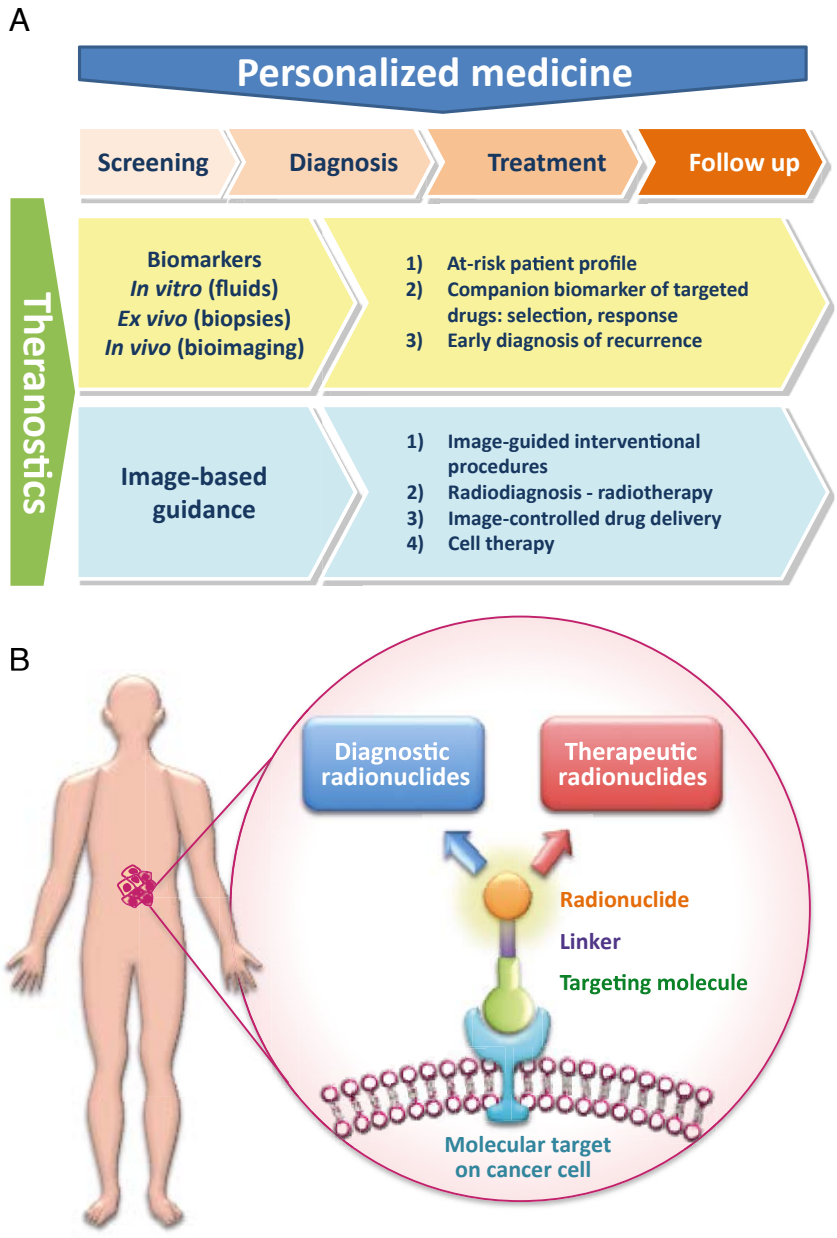

FIGURE 1. (A) Current concept of theranostics; diagram adapted from (*8*). (B) Schematic representation of the theranostic concept in nuclear medicine using radiolabeled molecules binding specific molecular targets overexpressed on cancer cells.

Nuclear imaging modalities are based on the detection of photons emitted during radioactive decay of radionuclides. Nuclear imaging techniques are very sensitive and allow visualization of molecular targets through attachment of radionuclides to targeting molecules. However, nuclear imaging should be combined with other modalities to provide anatomical references. PET imaging visualizes pairs of annihilation photons, which are emitted in opposite direction when a positron interacts with an electron. Image acquisition is based on the simultaneous detection of pairs of photons of 511 keV by a series of opposing detectors corresponding to several rings of scintillation crystals. A three-dimensional image is reconstructed after acquisition of sufficient events. In contrast to PET, single photon emission computed tomography (SPECT) measures single photons emitted by gamma (γ)-emitting radionuclides. Image acquisition is based on detection of photons by a set of rotating detectors, which acquire a series of two-dimensional projections images from multiples angles around the longitudinal axis of the patient. Several reconstruction algorithms are available to reconstruct these tomographic images. Clinical PET imaging systems offer higher spatial resolution and higher sensitivity than SPECT imaging system. In small-animal imaging, however, spatial resolution of SPECT is higher (**Table 1**). Therefore, SPECT imaging is widely used as well in preclinical studies.

Optical imaging techniques can also provide molecular information, but are restricted by the limited penetration range of light in tissue. Optical imaging techniques include bioluminescence- and fluorescence-based imaging, and are mostly restricted to preclinical studies. Bioluminescence allows quantitative imaging, but requires genetic modification of cells, which may impact biological processes. Fluorescence-based imaging is limited by tissue autofluorescence, which renders quantitation of signal challenging. Even though its use in the clinic is restricted, optical imaging has shown utility in the clinic for fluorescence-guided surgery, and sentinel node imaging (*10*).

PCa Imaging

Current conventional imaging techniques used to detect primary and metastatic PCa for staging include ultrasound, bone scintigraphy, and CT. Functional MRI techniques, e.g. diffusion-weighted MRI (DWI), or dynamic contrast-enhanced MRI (DCE-MRI), are becoming more prominent for imaging of PCa. The glucose metabolism imaging tracer ^{18}F-fluorodeoxyglucose (FDG) has shown promise for PET/CT imaging of numerous fast growing cancer types, but its utility for (re)staging of PCa is very limited (*11, 12*). Choline-based tracers imaging lipid metabolism, e.g. ^{11}C- and ^{18}F-choline, are more useful for staging of PCa, and are currently used in the clinic for assessment of distant metastases in high-risk PCa patients (*13*). However choline-based PET/CT has limited sensitivity for initial staging, lymph node detection, and restaging of patients with biochemical recurrence (*14-16*).

Tracers targeting PCa-specific biomarkers have shown promise for detection of PCa. Gastrin-releasing peptide receptor (GRPR)-targeted tracers are promising for the detection of primary tumors, and could be useful tools for initial staging (*17-20*). The recently developed prostate-specific membrane antigen (PSMA)-targeted tracers are

TABLE 1. Overview of in vivo small-animal imaging modalities (adapted from de Jong et al.)

Technology	Means of detection	Resolution	Depth*	Agents	Target	Costs‡	Use
CT	Ionizing radiation (X-rays)	50 µm	no limit	Iodinated molecules	Anatomical; physiological	€€	- Preclinical - Clinical
PET	Ionizing radiation (γ-rays)	1-2 mm	no limit	^{18}F-, ^{64}Cu-, ^{68}Ga-, ^{11}C- or ^{89}Zr-labelled compounds	Physiological; molecular	€€	- Preclinical - Clinical
SPECT	Ionizing radiation (γ-rays)	0.3-1 mm	no limit	^{99m}Tc-, ^{111}In- or ^{67}Ga-labelled compounds	Physiological; molecular	€€	- Preclinical - Clinical
MRI	Electromagnetism	10-100 µm	no limit	Paramagnetic and magnetic compounds; chelated Gd^{3+}	Anatomical; physiological	€€€	- Preclinical - Clinical
Ultrasound	Acoustic waves	50 µm	up to 3 cm	Microbubbles	Anatomical	€	- Preclinical - Clinical
Bioluminescence	Bioluminescent light	1-5 mm	up to <5 cm	Luciferin	Molecular	€	- Preclinical - Clinical and biochemical analysis
Fluorescence reflectance imaging§	Fluorescent light	2-3 mm	up to <1 cm	Fluorochromes; fluorescent proteins	Physiological; molecular	€	- Preclinical - Clinical use under development
Fluorescence-mediated tomography	Fluorescent light	1-2 mm	up to <5 cm	Near-infrared fluorochromes	Physiological; molecular	€€	- Preclinical - Clinical use under development
Intravital microscopy	Fluorescent light	200 nm	up to <1 mm	Fluorescent proteins; fluorochromes	Anatomical; Physiological; molecular	€€	- Preclinical - Clinical use under development

CT, computed tomography; MRI, magnetic resonance imaging; PET, positron emission tomography; SPECT, single photon emission computed tomography. *Resolution and depth limit is indicated for small-animal imaging systems. ‡€ represents €100,000-€200,000, €€ respresents €200,000-€400,000, €€€ represents >€400. §Not a quantitative method.

increasingly applied in the clinic for detection of PCa, and we foresee that these tracers will be useful tools for staging and follow up of (primary and) advanced PCa in the near future. Besides the utility of imaging for staging and follow-up of PCa, imaging techniques can be used for surgical guidance. Fluorescence-guided surgery using multimodal tracers is currently used in the clinic using non-targeted probes. Recently, a PSMA-targeted tracer was used for probe-guided surgery, allowing guidance of surgeon during metastatic lymph node dissection (*21*). A PSMA-targeted multimodal probe, combing fluorescence- and radiation-guidance could have a significant impact for PCa patient care.

Radionuclides

Diagnostic Radionuclides

Positron emitting radionuclides are used for PET (**Table 2**). PET visualizes annihilation photons of 511 keV, which are emitted when a positron interacts with an electron. Gamma-emitting radionuclides are used for SPECT (**Table 3**), which, in contrast with PET, visualizes single photons.

Positron emitting radionuclides with lower range in tissue provide higher spatial resolution, and higher sensitivity is achieved with high β^+ intensity. ^{18}F is one of the most widely used radionuclides for PET imaging, owing to its favorable physical characteristics for PET. ^{64}Cu is emerging as an interesting radionuclide for labeling of peptides and proteins for PET imaging, owing to its favorable physical characteristics and relatively long half-life (12.7 h). In addition, the combination of ^{64}Cu and ^{67}Cu provides a theranostic pair.

^{99m}Tc is the most widely radionuclide for clinical SPECT applications. ^{99m}Tc is readily available from $^{99}Mo/^{99m}Tc$ generators and emits photons of 140 keV, which is ideal for most SPECT cameras. In addition, the half-life of 6 h allows visualization of tumors while limiting radiation exposure to patients.

Therapeutic Radionuclides

Radionuclides applied for therapy are those emitting α or β particles, and Auger or conversion electrons (**Table 4-6**). These particles travel a relatively short distance through matter and can deliver most of their energy at localized area. Alpha particles have a very high energy and very short path length compared with β particles, resulting in high linear energy transfer (LET). Alpha-emitters are considered amongst the most powerful therapeutic radionuclides, because the high LET of α particles causes more complex DNA double-strand breaks (DSBs).

TABLE 2. Selected positron-emitting radionuclides used for radiolabeling of biomolecules for PET: physical characteristics, production mode and common labeling methods. $t_{1/2}$: half-life; E: energy; I: intensity; EC: electron capture. Nuclear data were obtained from (22). Data for mean range in tissue were taken from (23).

	$t_{1/2}$	Decay mode (%)	E_{β^+} (keV)	Endpoint E_{β^+} (keV)	I_{β^+} (%)	Mean E_{β^+} (MeV)	Mean dose β^+ (MeV/Bq.s)	Mean tissue range (mm)	Production mode	Labeling methods
^{68}Ga	67.71 m	EC + β^+ (100) β^+ (89)	836.02	1899.1	87.94	0.8295	0.7376	1.9	Generator ^{68}Ge/^{68}Ga	Bifunctional chelators
^{18}F	109.77 m	EC + β^+ (100) β^+(97)	249.8	633.5	96.73	0.2498	0.2416	0.2	Cyclotron ^{18}O(p,n)^{18}F ^{20}Ne(d,α)^{18}F	Direct labeling, prosthetic groups or Al^{18}F complex
^{44}Sc	3.97 h	EC + β^+ (100) β^+(94)	632.0	1473.5	94.27	0.632	0.5958	-	Generator ^{44}Ti/^{44}Sc Cyclotron ^{44}Ca(p,n)^{44g}Sc	Bifunctional chelators
^{64}Cu	12.701 h	EC + β^+ (61.5) β^+ (18) β^- (39)	278.21	653.03	17.60	0.278	0.0490	0.2	Cyclotron ^{64}Ni(p,n)^{64}Cu ^{67}Zn(p,α)^{64}Cu	Bifunctional chelators
^{86}Y	14.74 h	EC + β^+ (100) β^+ (32)	535.4	1221	11.9	0.66	0.21	0.7	Cyclotron ^{86}Sr(p,n)^{86}Y	Bifunctional chelators
^{76}Br	16.2 h	EC + β^+ (100) β^+ (55)	1532	3383	25.8	1.18	0.65	-	Cyclotron ^{76}Se(p.n)^{76}Br ^{75}As(α,3n)^{76}Br	Direct labeling or prosthetic groups
^{89}Zr	78.41 h	EC + β^+ (100) β^+ (23)	395.5	902	22.74	0.396	0.0899	0.3	Cyclotron ^{89}Y(p,n)^{89}Zr	Bifunctional chelators
^{124}I	4.1760 d	EC + β^+ (100) β^+ (23)	687.04 974.74	1534.9 2137.6	11.7 10.7	0.82	0.186	0.8	Cyclotron ^{124}Te(p,n)^{124}I	Direct labeling or prosthetic groups

TABLE 3. Selected γ-emitting radionuclides used for radiolabeling of biomolecules for SPECT. $t_{1/2}$: half-life; E: energy; I: intensity; EC: electron capture; IT: isomeric transition. Nuclear data were obtained from (22).

	$t_{1/2}$	Decay mode (%)	E_γ (keV) (Preferentially imaged)	I_γ %	Dose (MeV/Bq.s)	Production mode	Labeling methods
^{99m}Tc	6.01 h	IT (99.9963), β^- (0.0037)	140.511	89.06	0.125	Generator ^{99}Mo/^{99m}Tc	Direct labeling or bifunctional chelators
^{123}I	13.2234 h	EC (100)	158.97	83.3	0.1324	Cyclotron ^{124}Xe(p,2n)^{123}Cs→^{123}Xe→^{123}I ^{124}Xe(p,pn)^{123}I ^{123}Te(p,n)^{123}I	Direct labeling or prosthetic groups
^{111}In	2.8047 d	EC (100)	171.28	90.7	0.1553	Cyclotron	Bifunctional chelators
			245.35	94.1	0.2308	^{111}Cd(p,n)^{111m,g}In ^{112}Cd(p,2n)^{111m,g}In	
^{67}Ga	3.2617 d	EC (100)	93.310	38.81	0.03621	Cyclotron	Bifunctional chelators
			184.576	21.410	0.039518	^{nat}Zn(p,x)^{67}Ga	
			300.217	16.64	0.0500	^{68}Zn(p,2n)^{67}Ga	

TABLE 4. Selected β-emitting radionuclides used for radiolabeling of biomolecules for radionuclide therapy. $t_{1/2}$: half-life; E: energy; I: intensity; EC: electron capture. Nuclear data were obtained from (22). Data for mean range in tissue were taken from (23).

	$t_{1/2}$	Decay mode (%)	E_{β^-} (keV)	Endpoint E_{β^-}(keV)	I_{β^-} %	Mean E_{β^-} (MeV)	Mean β^- dose (MeV/Bq.s)	Mean tissue range (mm)	Production mode	Labeling methods
^{188}Re	17.004 h	β^- (100)	728.88 795.41	1965.4 2120.4	26.3 70.0	0.763	0.762	3.5	Generator ^{188}W/^{188}Re Reactor ^{187}Re(n,γ)^{188}Re	Direct labeling or bifunctional chelators
^{153}Sm	46.50 h	β^- (100)	199.5 225.3 264.3	634.7 704.4 807.6	31.3 49.4 18.4	0.224	0.224	1.2	Reactor ^{152}Sm(n,γ)^{153}Sm	Bifunctional chelators
^{67}Cu	61.83 h	β^- (100)	51.0 121 154 189	168.2 377.1 468.4 561.7	1.1 57 22.0 20.0	0.141	0.141	0.7	Cyclotron Reactor Several methods	Bifunctional chelators
^{90}Y	64.00 h	β^- (100)	933.7	2280.1	99.9885	0.9336	0.9336	3.9	Generator ^{90}Sr/^{90}Y Reactor ^{89}Y(n,γ)^{90}Y	Bifunctional chelators
^{186}Re	3.7183 d	EC (7) β^- (93)	306.1 359.2	932.3 1069.5	21.54 70.99	0.3467	0.3210	1.8	Cyclotron ^{186}W(p,n)^{186}Re Reactor ^{185}Re(n,γ)^{186}Re	Direct labeling or bifunctional chelators
^{177}Lu	6.647 d	β^- (100)	47.66 111.69 149.35	177.0 385.0 498.2	11.62 9.0 79.4	0.1342	0.1342	0.7	Reactor ^{176}Lu(n,γ)^{177}Lu ^{176}Yb(n,γ)^{177}Yb→^{177}Lu	Bifunctional chelators
^{131}I	8.0252 d	β^- (100)	96.2 191.58	333.8 606.3	7.23 89.6	0.1819	0.182	0.9	Reactor Several methods	Direct labeling or prosthetic groups
^{47}Sc	3.3492 d	β^- (100)	142.6 203.9	440.9 600.3	68.4 31.6	0.162	0.162	0.8	Reactor ^{47}Ti(n,p)^{47}Sc	Bifunctional chelators

TABLE 5. Selected α-emitting radionuclides used for radiolabeling of biomolecules for radionuclide therapy. $t_{1/2}$: half-life; E: energy; I: intensity; EC: electron capture. Nuclear data were obtained from (22). Data for mean range in tissue were taken from (23).

	$t_{1/2}$	Decay mode (%)	E_α (keV) (%)	I_α %	Dose (MeV/ Bq.s)	Mean tissue range (µm)	Production mode	Labeling methods
^{213}Bi	45.61 m	α (2)	5558	0.181	0.01005	85	Generator	Bifunctional chelators
		β^- (98)	5875	1.959	0.1151		^{225}Ac/^{213}Bi	
^{212}Bi	60.55 m	α (36)	6050.78	25.13	1.520	82	Generator	Bifunctional chelators
		β^- (64)	6089.88	9.75	0.594		^{224}Ra/^{212}Bi	
							^{212}Pb/^{212}Bi	
^{211}At	7.214 h	α (42)	5869.5	41.80	2.453	65	Cyclotron	Direct labeling or prosthetic groups
		EC (58)					^{209}Bi(α,2n)^{211}At	
^{225}Ac	10.0 d	α (100)	5637	4.4	0.248	69	Generator	Bifunctional chelators
			5724	3.1	0.18		^{229}Th/^{225}Ac	
			5732	8.0	0.46		Cyclotron	
			5790.6	8.6	0.50		^{226}Ra(p,2n)^{225}Ac	
			5792.5	18.1	1.05			
			5830	50.7	2.96			

TABLE 6. Selected auger and conversion electron-emitting radionuclides used for radiolabeling of biomolecules for radionuclide therapy. The range in tissue is only of a few nanometers. EC: electron capture; IT: isomeric transition; CE: conversion electron; E: energy; I: intensity; $t_{1/2}$: half-life. Nuclear data were obtained from (22).

	$t_{1/2}$	Decay mode (%)	Type np	E_{np} (keV)	I_{np} (%)	Mean E (keV)	Production mode	Labeling methods
^{67}Ga	3.2617 d	EC (100)	Auger L	0.99	168.3	0.001666	Cyclotron	Bifunctional chelators
			Auger K	7.35	60.7	0.00457	^{nat}Zn(p,x)^{67}Ga	
			CE - K	83.651	29.1	0.0244	^{68}Zn(p,2n)^{67}Ga	
^{111}In	2.8047 d	EC (100)	Auger L	2.72	100.4	0.002732	Cyclotron	Bifunctional chelators
			Auger K	19.3	15.5	0.00299	^{111}Cd(p,n)^{111m,g}In	
			CE – K	144.57	8.07	0.01166	^{112}Cd(p,2n)^{111m,g}In	
			CE - K	218.64	4.95	0.001885		
^{123}I	13.2234 h	EC (100)	Auger L	3.19	95.1	0.003035	Cyclotron	Direct labeling or prosthetic groups
			Auger K	22.7	12.4	0.00282	^{124}Xe(p,2n)^{123}Cs → ^{123}Xe → ^{123}I	
			CE – K	127.16	13.612	0.017309	^{124}Xe(p,pn)^{123}I	
							^{123}Te(p,n)^{123}I	
^{124}I	4.1760 d	EC + β^+ (100)	Auger L	3.19	63.8	0.00203	Cyclotron	Direct labeling or prosthetic groups
		β^+ (23)	Auger K	22.7	8.3	0.00188	^{124}Te(p,n)^{124}I	
^{125}I	59.400 d	EC (100)	Auger L	3.19	156.5	0.00499	Cyclotron/reactor	Direct labeling or prosthetic groups
			CE – K	3.68	78.1	0.00287	^{124}Xe(n,γ)^{125}Xe → ^{125}I	
			Auger K	22.7	19.8	0.00449		
			CE – L	30.55	10.7	0.00326		

Theranostic Pairs

In nuclear medicine, theranostic pairs are combinations of radionuclides that can be used for imaging and therapy. True theranostic pairs consist of different radionuclides of the same element, while matched pairs consist of radionuclides of different elements that can be complexed by the same chelator (**Table 7**).

TABLE 7. Examples of theranostic pairs in nuclear medicine.

True pairs		**Matched pairs**	
Diagnostic radionuclide	**Therapeutic radionuclide**	**Diagnostic radionuclide**	**Therapeutic radionuclide**
^{44}Sc	^{47}Sc	^{68}Ga/^{111}In	^{177}Lu/^{90}Y/^{213}Bi
^{64}Cu	^{67}Cu	^{99m}Tc	$^{186/188}$Re
^{68}Ga	^{67}Ga		
^{86}Y	^{90}Y		
^{124}I	^{131}I		
^{177}Lu	^{177}Lu		
^{131}I	^{131}I		

Radionuclide Therapy

Besides their application for molecular imaging, radionuclides can also be used for therapeutic applications. Interaction of α-particles, β-particles, Auger or conversion electrons with cells can induce several types of DNA damage, among which DSBs are the most genotoxic. Unrepaired DSBs can trigger cell cycle arrest, cell death (apoptosis) and chromosomal aberrations. Therefore, therapeutic radionuclides are being widely applied to destroy cancer cells. Bone-seeking radionuclides can be used for treatment of bone metastases. Tumor-targeted approaches are preferred to minimize exposure of healthy cells. For this purpose, tumor-targeting molecules are labeled with therapeutic radionuclides to selectively kill cancer cells.

TARGETS FOR PCA THERANOSTICS

Molecular targets for PCa theranostics include receptors and enzymes that are overexpressed on PCa cells. GRPR and PSMA are amongst the most widely explored targets for PCa theranostics.

Gastrin-Releasing Peptide Receptor

Bombesin Receptor Family

The mammalian bombesin (BBN) receptor family consists of three types of G-protein-coupled receptors: GRPR, neuromedin B receptor (NMBR) and bombesin receptor subtype 3 (BRS-3) (*24*). BBN is an amphibian 14-amino acid peptide, which was isolated from frog skin and was named after the European frog, *Bombina Bombina*. Two mammalian homologs, gastrin-releasing peptide (GRP) and neuromedin B (NMB), were isolated from porcine stomach and spinal cord, respectively. GRP and its C-terminal decapeptide, Neuromedin C (NMC, GRP(*18-27*)), share a seven-amino acid sequence with BBN (Trp-Ala-Val-Gly-His-Leu-Met-NH_2), accounting for a similar biological activity (*25, 26*). GRPRs exhibit high affinity for GRP and NMC, but low affinity for NMB. In contrast, NMBRs exhibit high affinity for NMB, but low affinity for GRP and NMC. GRP and NMB elicit a broad spectrum of biological/pharmacological responses in the gastrointestinal tract and central nervous system. GRP is involved in smooth muscle contraction and GI motility, release of GI hormones and neurotransmitters, and secretion and/or hormone release from numerous endocrine organs. In addition, BBN receptors are involved in tumor differentiation and growth. The biology of the BBN receptors was described in detail in a review of Jensen et al. (*24*)

Receptor Expression

BBN receptors are used as targets for imaging and therapy, owing to their overexpression on numerous malignancies, including small cell lung cancer, non-small cell lung cancer, pancreatic cancer, PCa, head/neck squamous cell cancers, glioblastomas, neuroblastomas, breast cancer, intestinal carcinoids and bronchial carcinoids (*27*). In PCa, GRPR expression was found in 45-100% of tested samples (*28*). In normal tissues, high levels of GRPR mRNAs were found in the pancreas and low levels were found in stomach, adrenal cortex and brain (*29*).

Prostate-Specific Membrane Antigen

PSMA, also referred to as glutamate carbopeptidase II (GPCII), *N*-acetyl-α-linked acidic dipeptidase I (NAALADase I), or folate hydrolase 1 (FOLH1), is a type II transmembrane glycoprotein exhibiting glutamate carboxypeptidase and folate hydrolase enzymatic activity. PSMA is a 750-amino-acid protein with 3 domains: a 19-amino-acid intracellular domain, a 24-amino-acid transmembrane domain, and a 707-amino-acid extracellular domain (*30*). PSMA is an interesting target for molecular imaging of PCa, as it is overexpressed in 90-100% of local PCa lesions, as well as in cancerous lymph nodes, and bone metastases (*31, 32*), with some reports indicating PSMA expression levels are further enhanced in high-grade, metastatic, and castration-resistant PCa (*31, 33, 34*). PSMA is also expressed in other tissues including normal prostate epithelium, small intestine, renal tubular cells, and salivary glands, but the expression in these organs is 100-1,000 fold less than in PCa (*35*).

Other Targets

Other targets have been envisaged for imaging and therapy of PCa, which are beyond the scope of this thesis. These include, but are not limited to, the prostate stem cell antigen (PSCA), the androgen receptor (AR), the CXC chemokine receptor 4 (CXCR4), and neuropeptide Y.

GRPR-TARGETED IMAGING AND RADIONUCLIDE THERAPY

GRPR-mediated imaging strategies have been described in detail in a review of Sancho et al. (*27*). In addition, the relevance of targeting GRPR in urological cancers was highlighted in a recent review of Mansi et al. (*36*). Both GRPR agonists and antagonists have been used for targeted imaging and therapy. The targeted imaging and radionuclide therapy approach with radiolabelled GRPR-targeting peptides is depicted in **Figure 2**.

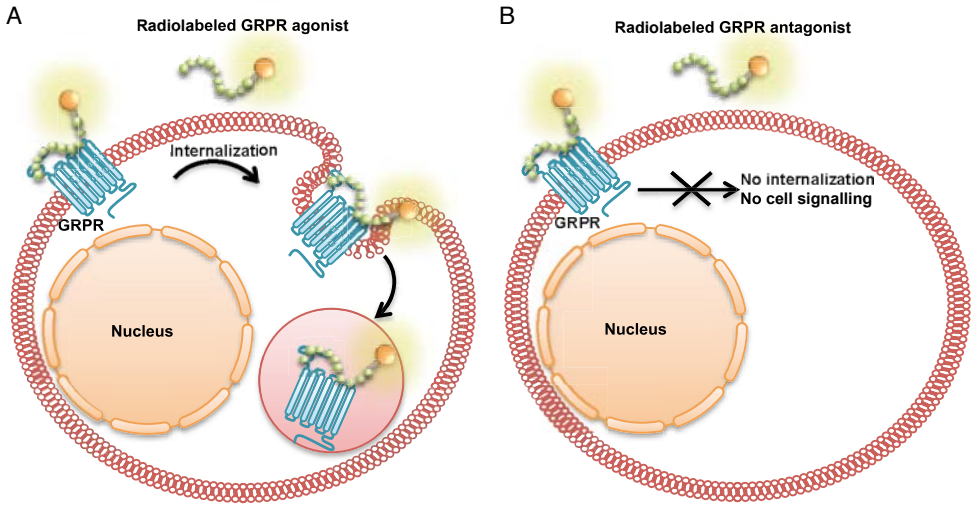

FIGURE 2: Targeted imaging and radionuclide therapy with radiolabeled bombesin analogues. (a) Radiolabeled GRPR agonists internalize after binding their receptor on the tumor cell and can be visualized (diagnostic radionuclides) or can trigger cell destruction (therapeutic radionuclides). (b) Radiolabeled GRPR antagonists are not internalized, but can be visualized or can trigger cell destruction from the cell membrane. Adapted from (36).

GRPR Agonists

Several GRPR agonists derived from BBN and GRP have been developed for imaging and therapy of PCa (**Table 8**). The BBN(7-14) sequence was the most widely explored motif, as radiolabeled tracers containing the BBN(7-14) sequence showed high

affinity for the GRPR. The first preclinical studies with BBN(7-14) analogs have used ^{99m}Tc as a radionuclide and have shown the effects of chelator, linker, and glycosylation on biodistribution profiles of the tracers in mice (*37-42*). Recently, ^{99m}Tc-labeled Demobesin-4 (N_4-Pro-Gln-Arg-Tyr-Gly-Asn-Gln-Trp-Ala-Val-Gly-His-Leu-Nle-NH_2 peptide conjugate, N_4 = 6-(p-carboxyl)-1,4,8,11-tetraazaundecane) was tested in patients. Primary PCa could be detected using ^{99m}Tc-Demobesin-4, whereas imaging of refractory PCa was suboptimal (*18*).

Recent studies have used DOTA- and NOTA-derived chelators to label BBN(7-14) with trivalent metal cations, in particular for therapeutic applications. Among those analogs, DOTA-8-AOC-BBN(7-14) (*43, 44*), DOTA-PESIN (*45*) and AMBA (*46*) appeared promising for imaging and therapy. However, in clinical studies, GRPR agonists were shown to induce severe side effects (*47, 48*).

TABLE 8. Examples of GRPR agonists used in preclinical in vivo imaging and therapy studies. Adapated from (27).

Name	Structure	Radionuclides
Bombesin (BBN)	Pyr-Gln-Arg-Leu-Gly-Asn-Gln-Trp-Ala-Val-Gly-His-Leu-Met-NH_2	^{125}I, ^{131}I, ^{18}F
[Tyr^4]BBN	Pyr-Gln-Arg-Tyr-Gly-Asn-Gln-Trp-Ala-Val-Gly-His-Leu-Met-NH_2	^{125}I
[Lys^3]BBN	Pyr-Gln-Lys-Leu-Gly-Asn-Gln-Trp-Ala-Val-Gly-His-Leu-Met-NH_2	^{99m}Tc, ^{18}F, ^{64}Cu
[Pro^1,Tyr^4]BBN	Pro-Gln-Arg-Tyr-Gly-Asn-Gln-Trp-Ala-Val-Gly-His-Leu-Met-NH_2	^{99m}Tc, ^{111}In, ^{64}Cu, ^{86}Y
[ε-Lys^3,Tyr^4]BBN	Pyr-Gln-ε-Lys-Tyr-Gly-Asn-Gln-Trp-Ala-Val-Gly-His-Leu-Met-NH_2	^{111}In
[Pro^1,Tyr^4,Nle^{14}]BBN	Pro-Gln-Arg-Tyr-Gly-Asn-Gln-Trp-Ala-Val-Gly-His-Leu-Nle-NH_2	^{99m}Tc
Litorin [pGlu^6,Phe^{13}]BBN(6-14)	pGlu-Gln-Trp-Ala-Val-Gly-His-Phe-MetNH_2	^{99m}Tc
[DPhe^6,Leu$^{13}\Psi$Phe^{14}]BBN(6-14)	DPhe-Gln-Trp-Ala-Val-Gly-His-LeuΨ-Phe-NH_2	
[DTyr^6, βAla^{11},Thi^{13},Nle^{14}] BBN(6-14)	DTyr-Gln-Trp-Ala-Val-βAla-His-Thi-Nle-NH_2	^{111}In, ^{68}Ga, ^{177}Lu
BBN(2-14)	Gln-Arg-Leu-Gly-Asn-Gln-Trp-Ala-Val-Gly-His-Leu-Met-NH_2	^{99m}Tc, ^{90}Y, ^{177}Lu
[Lys^{14}]BBN(2-14)	Gln-Arg-Leu-Gly-Asn-Gln-Trp-Ala-Val-Gly-His-Leu-Lys-NH_2	^{99m}Tc

BBN(7-14)	Gln-Trp-Ala-Val-Gly-His-Leu-Met-NH_2	^{99m}Tc, ^{111}In, ^{188}Re, ^{186}Re, ^{64}Cu, ^{68}Ga, ^{177}Lu, ^{213}Bi ^{149}Pm, ^{153}Sm, ^{18}F
[Nle^{14}]BBN(7-14)	Gln-Trp-Ala-Val-Gly-His-Leu-Nle-NH_2	^{99m}Tc
[βAla^{11},Phe^{13},Nle^{14}]BBN(7-14)	Gln-Trp-Ala-Val-βAla-His-Phe-Nle-NH_2	^{111}In
GRP (13-27)	H-Lys-Met-Tyr-Pro-Arg-Gly-Asn-His-Trp-Ala-Val-Gly-His-Leu-Met-NH_2	^{177}Lu, ^{111}In
GRP (14-27)	H-Met-Tyr-Pro-Arg-Gly-Asn-His-Trp-Ala-Val-Gly-His-Leu-Met-NH_2	^{111}In
GRP (17-27)	H-Arg-Gly-Asn-His-Trp-Ala-Val-Gly-His-Leu-Met-NH_2	^{111}In
GRP(18-27)	H-Gly-Asn-His-Trp-Ala-Val-Gly-His-Leu-Met-NH_2	^{111}In, ^{99m}Tc
[DAla^{24}]GRP(18-27)	H-Gly-Asn-His-Trp-Ala-Val-DAla-His-Leu-Met-NH_2	^{99m}Tc
[DAla^{24},Nle^{27}]GRP(18-27)	H-Gly-Asn-His-Trp-Ala-Val-DAla-His-Leu-Nle-NH_2	^{99m}Tc
[DAla^{24},Leu^{27}]GRP(18-27)	H-Gly-Asn-His-Trp-Ala-Val-DAla-His-Leu-Leu-NH_2	^{99m}Tc
[βAla^{24}]GRP(18-27)	H-Gly-Asn-His-Trp-Ala-Val-βAla-His-Leu-Met-NH_2	^{99m}Tc
[Sar^{24}]GRP(18-27)	H-Gly-Asn-His-Trp-Ala-Val-Sar-His-Leu-Met-NH_2	^{99m}Tc

GRPR Antagonists

Particular attention has been drawn to the development of GRPR antagonists after reports have described that GRPR antagonists show higher tumor uptake and lower accumulation in GRPR-positive nontarget tissues than GRPR agonists (*49, 50*). Several GRPR antagonists have been developed by the modification of C-terminal residues of GRPR agonists (**Table 9**), amongst which the statin-based BBN analog JMV594 (H-D-Phe-Gln-Trp-Ala-Val-Gly-His-Sta-Leu-NH_2) (*51*) is the most widely applied for imaging and therapy. ^{68}Ga-labeled GRPR-antagonists derived from the JMV594 sequence were developed for PET imaging, showing good targeting properties in preclinical studies (*50, 52-54*) and recently also in clinical trials (*55, 56*). ^{68}Ga-labeled GRPR antagonist BAY86-7548 (^{68}Ga-DOTA-4-amino-1-carboxymethylpiperidine-D-Phe-Gln-Trp-Ala-Val-Gly-His-Sta-Leu-NH_2) has shown a specificity, sensitivity, and accuracy of 88%, 81%, and 83%, respectively, for the detection of primary PCa. However, this tracer was suboptimal for the detection of lymph node metastases.

Recently, ^{18}F- and ^{64}Cu-labeled GRPR antagonists based on the J594 peptide sequence were also tested in clinical studies, showing no adverse events and clear delineation of primary PCa lesions during imaging (*17, 19, 20*).

TABLE 9. Examples of GRPR antagonists used in preclinical in vivo imaging and therapy studies. Adapated from (27).

Name	Structure	Radionuclides
[DPhe^{6},Leu-NHEt^{13},des-Met^{14}] BBN(6-13)	DPhe-Gln-Trp-Ala-Val-Gly-His-Leu-NHEt	^{99m}Tc, ^{18}F
[DPhe^{6},Sta^{13},Leu^{14}]BBN(6-14)	DPhe-Gln-Trp-Ala-Val-Gly-His-Sta-Leu-NH_2	^{99m}Tc, ^{111}In, ^{68}Ga, ^{18}F, ^{177}Lu, ^{64}Cu, ^{90}Y
[Cha^{13}]BBN(7-14)	Gln-Trp-Ala-Val-Gly-His-Cha-Met-NH_2	^{99m}Tc
[Cha^{13},Nle^{14}]BBN(7-14)	Gln-Trp-Ala-Val-Gly-His-Cha-Nle-NH_2	^{99m}Tc, ^{64}Cu
[DPhe^{6}, Leuψ(CHOH-CH_2-$(CH_2)_2$-CH_3^{13},des-Met^{14}]BBN(6-14)	DPhe-Gln-Trp-Ala-Val-Gly-His-Leuψ(CHOH-CH_2-$(CH_2)_2$-CH_3	^{111}In, ^{68}Ga
[DPhe^{6},Leu-OCH_3^{13},des-Met^{14}] BBN(6-14)	DPhe-Gln-Trp-Ala-Val-Gly-His-Leu-OCH_3	^{111}In
[DPhe^{6},Leu-$NHCH_2CH_2CH_3$^{13},des-Met^{14}]BBN(6-14)	DPhe-Gln-Trp-Ala-Val-Gly-His-Leu-NH-CH_2-CH_2-CH_3	^{111}In

des-Met indicates the deletion of the BBN 14th amino acid, Methionine.

PSMA-TARGETED IMAGING AND RADIONUCLIDE THERAPY

Antibodies

The murine anti-PSMA antibody 7E11, targeting an intracellular epitope of PSMA, was used to develop the first clinical tracer targeting PSMA for imaging of PCa: ^{111}In-capromab (ProstaScint®). ^{111}In-capromab was indicated for detection of soft-tissue metastases and recurrence of PCa (*57*), but was not reliable for detection of primary PCa and bone metastases (*58, 59*). The poor diagnostic accuracy of ^{111}In-capromab has been associated with the intracellular targeting of 7E11, and led to the development of next-generation anti-PSMA monoclonal antibodies (mAb), binding to the extracellular domain of PSMA, e.g. J591. ^{177}Lu- and ^{90}Y-radiolabeled J591 have shown promising therapeutic efficacy and moderate toxicity in patients (*60-62*). Furthermore, J591 was superior to ^{111}In-capromab to detect soft-tissue and bony metastases (*60, 63*). However, monoclonal antibodies exhibit slow clearance from nontarget tissues, and are therefore not considered ideal vectors for targeted molecular imaging and radionuclide therapy.

Antibody Fragments

To circumvent the long circulating time of antibodies, smaller variants of mAb have been engineered, such as antigen-binding fragments (Fab) and $F(ab')_2$ (*64*), minibodies, diabodies, and Nanobodies (*65-67*). These antibody fragments have shown faster target recognition and more rapid blood clearance, but they also showed unspecific accumulation in liver and kidneys.

Small-Molecule Inhibitors

Small-molecule inhibitors, binding the enzymatic site in the extracellular domain of PSMA, are increasingly used for imaging and therapy of PCa. These small-molecule PSMA inhibitors consist of zinc-binding compounds attached to a glutamate moiety and include phosphonate-, phosphate-, phosphoramidate-, thiol-, and urea-based inhibitors, which have been discussed in an extensive review by Mease et al. (*68*). Glu-NH-CO-NH-Lys-(Ahx)-^{68}Ga-HBED-CC, also known as ^{68}Ga-PSMA-11 or ^{68}Ga-PSMA-HBED-CC (**Figure 3**), is currently the most widely used small-molecule inhibitor in the clinic for imaging of PCa (*69, 70*). More recently, a promising ^{18}F-labeled PSMA inhibitor, ^{18}F-DCFPyL, was introduced in the clinic as well (*71*).

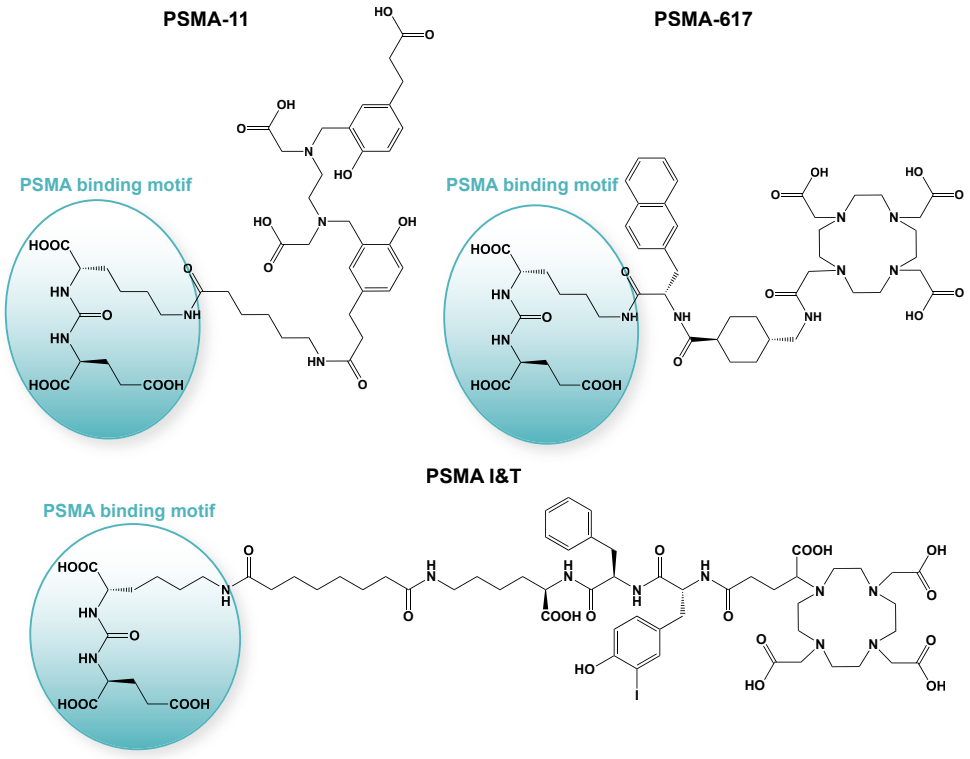

FIGURE 3. Chemical structures of small-molecule PSMA inhibitors PSMA-11, PSMA-617, and PSMA I&T.

For therapy, the small-molecule PSMA inhibitor [^{131}I]MIP-1095 (*72*) has shown reduction of bone pain in 85% of PCa patients with bone pain and mild hematological toxicity only. Recently, two PSMA tracers with DOTA- and DOTAGA chelators have been developed, namely PSMA-617 and PSMA I&T (**Figure 3 and 4**), allowing labeling with both diagnostic and therapeutic radionuclides (*73-76*).

Despite the encouraging preliminary therapeutic results of ^{177}Lu-labeled PSMA-617 and PSMA I&T, the high and specific uptake in kidneys and salivary glands represent a major disadvantage of small-molecule PSMA inhibitors for therapy. Research aiming to limit radiation-induced damage in those healthy organs is thus warranted.

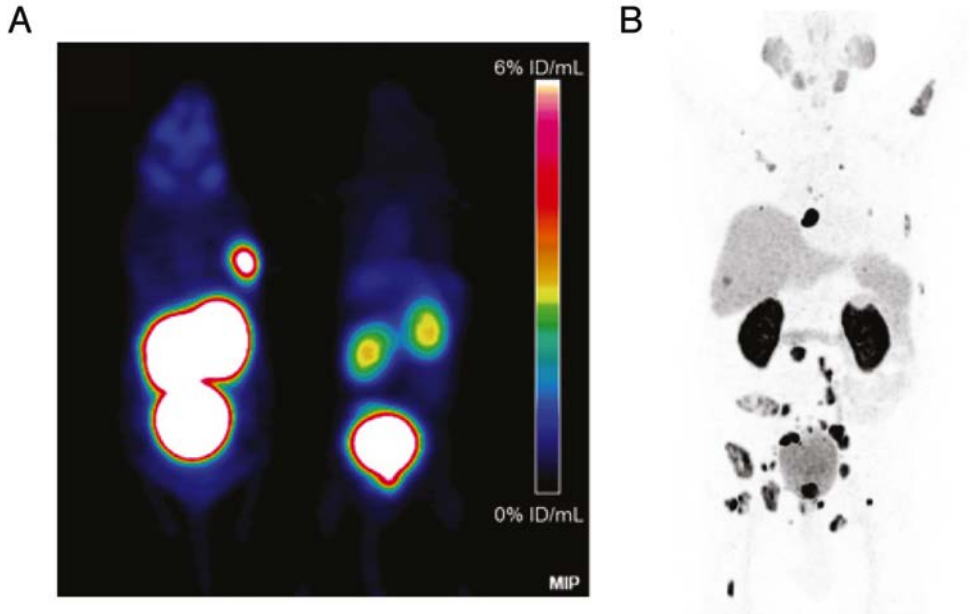

FIGURE 4. PET imaging of small-molecule PSMA inhibitor ^{68}Ga-PSMA I&T in a preclinical model of PCa (A) and in a PCa patient with liver, lymph node, and bone metastases (B); adapted from (75).

OUTLINE OF THIS THESIS

PCa is one of the most frequently diagnosed cancers in men worldwide. Early detection of PCa is essential, as treatment options for advanced disseminated PCa are limited. A single tool combining diagnosis and therapy in a "theranostic" approach could effectively contribute to a more personalized management of PCa patients, whereby imaging can guide the choice of the most suitable therapeutic option for each patient.

The studies described in this thesis focus on the development of theranostic approaches for PCa. The **first section** of this thesis presents the theranostic concept in nuclear medicine. **Chapter 1.1** provides a general introduction to PCa, tumor targeting, and the basic principles of molecular imaging and radionuclide therapy. Strategies to improve applications of radiolabeled peptides for imaging and therapy are discussed in **Chapter 1.2**.

The development of theranostic approaches for PCa targeting GRPR is described in the **second section**. First the development and comparison of ^{18}F- and ^{68}Ga-labeled GRPR antagonist JMV5132 and JMV4168 for PET/CT imaging of PCa is described (**Chapter 2.1**). In this study, a novel method was used for radiolabeling of peptides with Al^{18}F in a one-step procedure. The same GRPR antagonist was tested in a theranostic approach for PCa (**Chapter 2.2**). In this chapter an innovative method was investigated to stabilize the radiolabeled peptide using in vivo enzyme inhibition.

The **third section** focuses on PSMA targeting. A novel ^{111}In-labeled anti-PSMA Nanobody was developed for SPECT/CT imaging of PCa (**Chapter 3.1**). This Nanobody was engineered with a C-terminal cysteine for site-specific coupling of a chelator. In **Chapter 3.2**, the application of a PSMA small-molecule inhibitor for imaging and radionuclide therapy of PCa is described. In this chapter we investigated a strategy to decrease renal tracer uptake. Finally, α radionuclide therapy of PCa with the anti-PSMA Nanobody and the PSMA small-molecule inhibitor was explored to further improve therapeutic efficacy (**Chapter 3.3**).

REFERENCES

1. Torre LA, Bray F, Siegel RL, Ferlay J, Lortet-Tieulent J, Jemal A. Global cancer statistics, 2012. CA Cancer J Clin. 2015;65:87-108.
2. Center MM, Jemal A, Lortet-Tieulent J, et al. International variation in prostate cancer incidence and mortality rates. Eur Urol. 2012;61:1079-1092.
3. Schroder FH, Hugosson J, Roobol MJ, et al. Screening and prostate cancer mortality: results of the European Randomised Study of Screening for Prostate Cancer (ERSPC) at 13 years of follow-up. Lancet. 2014;384:2027-2035.
4. Draisma G, Boer R, Otto SJ, et al. Lead times and overdetection due to prostate-specific antigen screening: estimates from the European Randomized Study of Screening for Prostate Cancer. J Natl Cancer Inst. 2003;95:868-878.
5. Cooperberg MR, Lubeck DP, Meng MV, Mehta SS, Carroll PR. The changing face of low-risk prostate cancer: trends in clinical presentation and primary management. J Clin Oncol. 2004;22:2141-2149.
6. Heijnsdijk EA, Wever EM, Auvinen A, et al. Quality-of-life effects of prostate-specific antigen screening. N Engl J Med. 2012;367:595-605.
7. Parker C, Gillessen S, Heidenreich A, Horwich A. Cancer of the prostate: ESMO Clinical Practice Guidelines for diagnosis, treatment and follow-updagger. Ann Oncol. 2015;26 Suppl 5:v69-v77.
8. Idée J-M, Louguet S, Ballet S, Corot C. Theranostics and contrast-agents for medical imaging: a pharmaceutical company viewpoint. Quantitative Imaging in Medicine and Surgery. 2013;3:292-297.
9. de Jong M, Essers J, van Weerden WM. Imaging preclinical tumour models: improving translational power. Nat Rev Cancer. 2014;14:481-493.
10. Vahrmeijer AL, Hutteman M, van der Vorst JR, van de Velde CJ, Frangioni JV. Image-guided cancer surgery using near-infrared fluorescence. Nat Rev Clin Oncol. 2013;10:507-518.
11. Gambhir SS, Czernin J, Schwimmer J, Silverman DH, Coleman RE, Phelps ME. A tabulated summary of the FDG PET literature. J Nucl Med. 2001;42:1s-93s.
12. Jadvar H. Imaging evaluation of prostate cancer with 18F-fluorodeoxyglucose PET/CT: utility and limitations. Eur J Nucl Med Mol Imaging. 2013;40 Suppl 1:S5-10.
13. Mapelli P, Picchio M. Initial prostate cancer diagnosis and disease staging-the role of choline-PET-CT. Nat Rev Urol. 2015;12:510-518.
14. Kitajima K, Murphy RC, Nathan MA. Choline PET/CT for imaging prostate cancer: an update. Ann Nucl Med. 2013;27:581-591.
15. Umbehr MH, Muntener M, Hany T, Sulser T, Bachmann LM. The role of 11C-choline and 18F-fluorocholine positron emission tomography (PET) and PET/CT in prostate cancer: a systematic review and meta-analysis. Eur Urol. 2013;64:106-117.
16. Castellucci P, Ceci F, Graziani T, et al. Early biochemical relapse after radical prostatectomy: which prostate cancer patients may benefit from a restaging 11C-Choline PET/CT scan before salvage radiation therapy? J Nucl Med. 2014;55:1424-1429.
17. Wieser G, Mansi R, Grosu AL, et al. Positron emission tomography (PET) imaging of prostate cancer with a gastrin releasing peptide receptor antagonist--from mice to men. Theranostics. 2014;4:412-419.
18. Mather SJ, Nock BA, Maina T, et al. GRP receptor imaging of prostate cancer using [(99m)Tc]Demobesin 4: a first-in-man study. Mol Imaging Biol. 2014;16:888-895.
19. Sah BR, Burger IA, Schibli R, et al. Dosimetry and first clinical evaluation of the new 18F-radiolabeled bombesin analogue BAY 864367 in patients with prostate cancer. J Nucl Med. 2015;56:372-378.

20. Beheshti M, Kunit T, Haim S, et al. BAY 1075553 PET-CT for Staging and Restaging Prostate Cancer Patients: Comparison with [18F] Fluorocholine PET-CT (Phase I Study). Mol Imaging Biol. 2015;17:424-433.
21. Maurer T, Weirich G, Schottelius M, et al. Prostate-specific membrane antigen-radioguided surgery for metastatic lymph nodes in prostate cancer. Eur Urol. 2015;68:530-534.
22. NuDat 2.6. National Nuclear Data Center, Brookhaven National Laboratory. http://www.nndc.bnl.gov/nudat2/. Published January 12, 2012. Accessed October 1, 2015.
23. Cantone MC, Hoeschen C. Radiation Physics for Nuclear Medicine. Heidelberg: Springer; 2011.
24. Jensen RT, Battey JF, Spindel ER, Benya RV. International Union of Pharmacology. LXVIII. Mammalian bombesin receptors: nomenclature, distribution, pharmacology, signaling, and functions in normal and disease states. Pharmacol Rev. 2008;60:1-42.
25. Anastasi A, Erspamer V, Bucci M. Isolation and structure of bombesin and alytesin, 2 analogous active peptides from the skin of the European amphibians Bombina and Alytes. Experientia. 1971;27:166-167.
26. Erspamer V. Discovery, isolation, and characterization of bombesin-like peptides. Ann N Y Acad Sci. 1988;547:3-9.
27. Sancho V, Di Florio A, Moody TW, Jensen RT. Bombesin receptor-mediated imaging and cytotoxicity: review and current status. Curr Drug Deliv. 2011;8:79-134.
28. Ischia J, Patel O, Bolton D, Shulkes A, Baldwin GS. Expression and function of gastrin-releasing peptide (GRP) in normal and cancerous urological tissues. BJU Int. 2014;113 Suppl 2:40-47.
29. Xiao D, Wang J, Hampton LL, Weber HC. The human gastrin-releasing peptide receptor gene structure, its tissue expression and promoter. Gene. 2001;264:95-103.
30. Ghosh A, Heston WW. Understanding Prostate-Specific Membrane Antigen and Its Implication in Prostate Cancer. In: LaRochelle W, Shimkets R, eds. The Oncogenomics Handbook: Humana Press; 2005:597-615.
31. Bostwick DG, Pacelli A, Blute M, Roche P, Murphy GP. Prostate specific membrane antigen expression in prostatic intraepithelial neoplasia and adenocarcinoma: a study of 184 cases. Cancer. 1998;82:2256-2261.
32. Silver DA, Pellicer I, Fair WR, Heston WD, Cordon-Cardo C. Prostate-specific membrane antigen expression in normal and malignant human tissues. Clin Cancer Res. 1997;3:81-85.
33. Wright GL, Jr., Haley C, Beckett ML, Schellhammer PF. Expression of prostate-specific membrane antigen in normal, benign, and malignant prostate tissues. Urol Oncol. 1995;1:18-28.
34. Wright GL, Jr., Grob BM, Haley C, et al. Upregulation of prostate-specific membrane antigen after androgen-deprivation therapy. Urology. 1996;48:326-334.
35. Sokoloff RL, Norton KC, Gasior CL, Marker KM, Grauer LS. A dual-monoclonal sandwich assay for prostate-specific membrane antigen: levels in tissues, seminal fluid and urine. Prostate. 2000;43:150-157.
36. Mansi R, Fleischmann A, Macke HR, Reubi JC. Targeting GRPR in urological cancers--from basic research to clinical application. Nat Rev Urol. 2013;10:235-244.
37. Karra SR, Schibli R, Gali H, et al. 99mTc-labeling and in vivo studies of a bombesin analogue with a novel water-soluble dithiadiphosphine-based bifunctional chelating agent. Bioconjug Chem. 1999;10:254-260.
38. Smith CJ, Sieckman GL, Owen NK, et al. Radiochemical investigations of gastrin-releasing peptide receptor-specific [(99m)Tc(X)(CO)3-Dpr-Ser-Ser-Ser-Gln-Trp-Ala-Val-Gly-His-Leu-Met-(NH2)] in PC-3, tumor-bearing, rodent models: syntheses, radiolabeling, and in vitro/in vivo studies where Dpr = 2,3-diaminopropionic acid and X = H2O or P(CH2OH)3. Cancer Res. 2003;63:4082-4088.

39. Smith CJ, Gali H, Sieckman GL, Higginbotham C, Volkert WA, Hoffman TJ. Radiochemical investigations of (99m)Tc-N(3)S-X-BBN[7-14]NH(2): an in vitro/in vivo structure-activity relationship study where X = 0-, 3-, 5-, 8-, and 11-carbon tethering moieties. Bioconjug Chem. 2003;14:93-102.
40. Nock BA, Nikolopoulou A, Galanis A, et al. Potent bombesin-like peptides for GRP-receptor targeting of tumors with 99mTc: a preclinical study. J Med Chem. 2005;48:100-110.
41. Garcia Garayoa E, Schweinsberg C, Maes V, et al. Influence of the molecular charge on the biodistribution of bombesin analogues labeled with the [99mTc(CO)3]-core. Bioconjug Chem. 2008;19:2409-2416.
42. Schweinsberg C, Maes V, Brans L, et al. Novel glycated [99mTc(CO)3]-labeled bombesin analogues for improved targeting of gastrin-releasing peptide receptor-positive tumors. Bioconjug Chem. 2008;19:2432-2439. 43. Hoffman TJ, Gali H, Smith CJ, et al. Novel series of 111In-labeled bombesin analogs as potential radiopharmaceuticals for specific targeting of gastrin-releasing peptide receptors expressed on human prostate cancer cells. J Nucl Med. 2003;44:823-831.
44. Smith CJ, Gali H, Sieckman GL, et al. Radiochemical investigations of 177Lu-DOTA-8-Aoc-BBN[7-14] NH2: an in vitro/in vivo assessment of the targeting ability of this new radiopharmaceutical for PC-3 human prostate cancer cells. Nucl Med Biol. 2003;30:101-109.
45. Zhang H, Schuhmacher J, Waser B, et al. DOTA-PESIN, a DOTA-conjugated bombesin derivative designed for the imaging and targeted radionuclide treatment of bombesin receptor-positive tumours. Eur J Nucl Med Mol Imaging. 2007;34:1198-1208.
46. Lantry LE, Cappelletti E, Maddalena ME, et al. 177Lu-AMBA: Synthesis and characterization of a selective 177Lu-labeled GRP-R agonist for systemic radiotherapy of prostate cancer. J Nucl Med. 2006;47:1144-1152.
47. Basso N, Lezoche E, Speranza V. Studies with bombesin in man. World J Surg. 1979;3:579-585.
48. Bodei L, Ferrari M, Nunn A, et al. Lu-177-AMBA Bombesin analogue in hormone refractory prostate cancer patients: A phase I escalation study with single-cycle administrations. Eur J Nucl Med Mol Imaging. 2007;34:S221-S221.
49. Cescato R, Maina T, Nock B, et al. Bombesin receptor antagonists may be preferable to agonists for tumor targeting. J Nucl Med. 2008;49:318-326.
50. Mansi R, Wang X, Forrer F, et al. Evaluation of a 1,4,7,10-tetraazacyclododecane-1,4,7,10-tetraacetic acid-conjugated bombesin-based radioantagonist for the labeling with single-photon emission computed tomography, positron emission tomography, and therapeutic radionuclides. Clin Cancer Res. 2009;15:5240-5249.
51. Llinares M, Devin C, Chaloin O, et al. Syntheses and biological activities of potent bombesin receptor antagonists. J Pept Res. 1999;53:275-283.
52. Mansi R, Wang X, Forrer F, et al. Development of a potent DOTA-conjugated bombesin antagonist for targeting GRPr-positive tumours. Eur J Nucl Med Mol Imaging. 2011;38:97-107.
53. Abiraj K, Mansi R, Tamma ML, et al. Bombesin antagonist-based radioligands for translational nuclear imaging of gastrin-releasing peptide receptor-positive tumors. J Nucl Med. 2011;52:1970-1978.
54. Varasteh Z, Velikyan I, Lindeberg G, et al. Synthesis and characterization of a high-affinity NOTA-conjugated bombesin antagonist for GRPR-targeted tumor imaging. Bioconjug Chem. 2013;24:1144-1153.
55. Roivainen A, Kahkonen E, Luoto P, et al. Plasma pharmacokinetics, whole-body distribution, metabolism, and radiation dosimetry of 68Ga bombesin antagonist BAY 86-7548 in healthy men. J Nucl Med. 2013;54:867-872.

56. Kahkonen E, Jambor I, Kemppainen J, et al. In Vivo Imaging of Prostate Cancer Using [68Ga]-Labeled Bombesin Analog BAY86-7548. Clin Cancer Res. 2013;19:5434-5443.
57. Ellis RJ, Kaminsky DA, Zhou EH, et al. Ten-year outcomes: the clinical utility of single photon emission computed tomography/computed tomography capromab pendetide (Prostascint) in a cohort diagnosed with localized prostate cancer. Int J Radiat Oncol Biol Phys. 2011;81:29-34.
58. Apolo AB, Pandit-Taskar N, Morris MJ. Novel tracers and their development for the imaging of metastatic prostate cancer. J Nucl Med. 2008;49:2031-2041.
59. Bander NH, Nanus DM, Milowsky MI, Kostakoglu L, Vallabahajosula S, Goldsmith SJ. Targeted systemic therapy of prostate cancer with a monoclonal antibody to prostate-specific membrane antigen. Semin Oncol. 2003;30:667-676.
60. Milowsky MI, Nanus DM, Kostakoglu L, Vallabhajosula S, Goldsmith SJ, Bander NH. Phase I trial of yttrium-90-labeled anti-prostate-specific membrane antigen monoclonal antibody J591 for androgen-independent prostate cancer. J Clin Oncol. 2004;22:2522-2531.
61. Vallabhajosula S, Nikolopoulou A, Jhanwar YS, et al. Radioimmunotherapy of Metastatic Prostate Cancer with 177Lu-DOTA-huJ591 Anti Prostate Specific Membrane Antigen Specific Monoclonal Antibody. Curr Radiopharm. 2015.
62. Tagawa ST, Milowsky MI, Morris M, et al. Phase II study of Lutetium-177-labeled anti-prostate-specific membrane antigen monoclonal antibody J591 for metastatic castration-resistant prostate cancer. Clin Cancer Res. 2013;19:5182-5191.
63. Tagawa ST, Beltran H, Vallabhajosula S, et al. Anti-prostate-specific membrane antigen-based radioimmunotherapy for prostate cancer. Cancer. 2010;116:1075-1083.
64. Lutje S, van Rij CM, Franssen GM, et al. Targeting human prostate cancer with 111In-labeled D2B IgG, F(ab')2 and Fab fragments in nude mice with PSMA-expressing xenografts. Contrast Media Mol Imaging. 2015;10:28-36.
65. Viola-Villegas NT, Sevak KK, Carlin SD, et al. Noninvasive Imaging of PSMA in prostate tumors with (89)Zr-Labeled huJ591 engineered antibody fragments: the faster alternatives. Mol Pharm. 2014;11:3965-3973.
66. Kampmeier F, Williams JD, Maher J, Mullen GE, Blower PJ. Design and preclinical evaluation of a 99mTc-labelled diabody of mAb J591 for SPECT imaging of prostate-specific membrane antigen (PSMA). EJNMMI Res. 2014;4:13.
67. Evazalipour M, D'Huyvetter M, Tehrani BS, et al. Generation and characterization of nanobodies targeting PSMA for molecular imaging of prostate cancer. Contrast Media Mol Imaging. 2014;9:211-220.
68. Mease RC, Foss CA, Pomper MG. PET imaging in prostate cancer: focus on prostate-specific membrane antigen. Curr Top Med Chem. 2013;13:951-962.
69. Afshar-Oromieh A, Avtzi E, Giesel FL, et al. The diagnostic value of PET/CT imaging with the (68)Ga-labelled PSMA ligand HBED-CC in the diagnosis of recurrent prostate cancer. Eur J Nucl Med Mol Imaging. 2015;42:197-209.
70. Budaus L, Leyh-Bannurah SR, Salomon G, et al. Initial Experience of Ga-PSMA PET/CT Imaging in High-risk Prostate Cancer Patients Prior to Radical Prostatectomy. Eur Urol. 2015.
71. Szabo Z, Mena E, Rowe SP, et al. Initial Evaluation of [(18)F]DCFPyL for Prostate-Specific Membrane Antigen (PSMA)-Targeted PET Imaging of Prostate Cancer. Mol Imaging Biol. 2015;17:565-574.
72. Zechmann CM, Afshar-Oromieh A, Armor T, et al. Radiation dosimetry and first therapy results with a (124)I/ (131)I-labeled small molecule (MIP-1095) targeting PSMA for prostate cancer therapy. Eur J Nucl Med Mol Imaging. 2014;41:1280-1292.

73. Benesova M, Schafer M, Bauder-Wust U, et al. Preclinical Evaluation of a Tailor-Made DOTA-Conjugated PSMA Inhibitor with Optimized Linker Moiety for Imaging and Endoradiotherapy of Prostate Cancer. J Nucl Med. 2015;56:914-920.
74. Weineisen M, Simecek J, Schottelius M, Schwaiger M, Wester HJ. Synthesis and preclinical evaluation of DOTAGA-conjugated PSMA ligands for functional imaging and endoradiotherapy of prostate cancer. EJNMMI Res. 2014;4:63.
75. Weineisen M, Schottelius M, Simecek J, et al. 68Ga- and 177Lu-Labeled PSMA I&T: Optimization of a PSMA-Targeted Theranostic Concept and First Proof-of-Concept Human Studies. J Nucl Med. 2015;56:1169-1176.
76. Herrmann K, Bluemel C, Weineisen M, et al. Biodistribution and radiation dosimetry for a probe targeting prostate-specific membrane antigen for imaging and therapy. J Nucl Med. 2015;56:855-861.

1.1

1.2

Radiopeptides for Imaging and Therapy: A Radiant Future

Kristell L.S. Chatalic[1-3], Dik J. Kwekkeboom[1] and Marion de Jong[1,2]

[1]Department of Nuclear Medicine, Erasmus MC, Rotterdam, The Netherlands
[2]Department of Radiology, Erasmus MC, Rotterdam, The Netherlands
[3]Department of Urology, Erasmus MC, Rotterdam, The Netherlands

Adapted from: Journal of Nuclear Medicine, 2015; 56(12):1809-12

ABSTRACT

Radiopeptides are powerful tools for diagnostic imaging and radionuclide therapy of various diseases. Since the introduction of the first radiopeptide into the clinical setting to diagnose neuroendocrine tumors about 25 y ago, many advances have been made in the field. This short review highlights novel strategies to improve the application of radiopeptides for imaging and therapy.

INTRODUCTION

Radiopeptides targeting somatostatin receptor (SSTR) have contributed significantly to patient care. The SSTR agonist octreotide and modifications thereof ([Tyr^3]octreotide [TOC], [Tyr^3, Thr^8]octreotide [TATE], and [1-Nal^3]octreotide [NOC]) are widely used in routine clinical practice for diagnosis of neuroendocrine tumors (NETs). ^{111}In-diethylenetriaminepentaacetic acid-octreotide (OctreoScan; Mallinckrodt Inc.) was the first registered radiopeptide, and it has become the gold standard for diagnosis and staging of SSTR-positive tumors using SPECT and SPECT/CT. After the successful application of ^{111}In-octreotide for imaging of NETs in the clinic, somatostatin analogs radiolabeled with β-emitting isotopes (i.e. ^{177}Lu-DOTATATE and ^{90}Y-DOTATOC) were introduced as treatment. Peptide receptor radionuclide therapy (PRRT) using ^{177}Lu-DOTATATE and ^{90}Y-DOTATOC has given impressive results thus far.

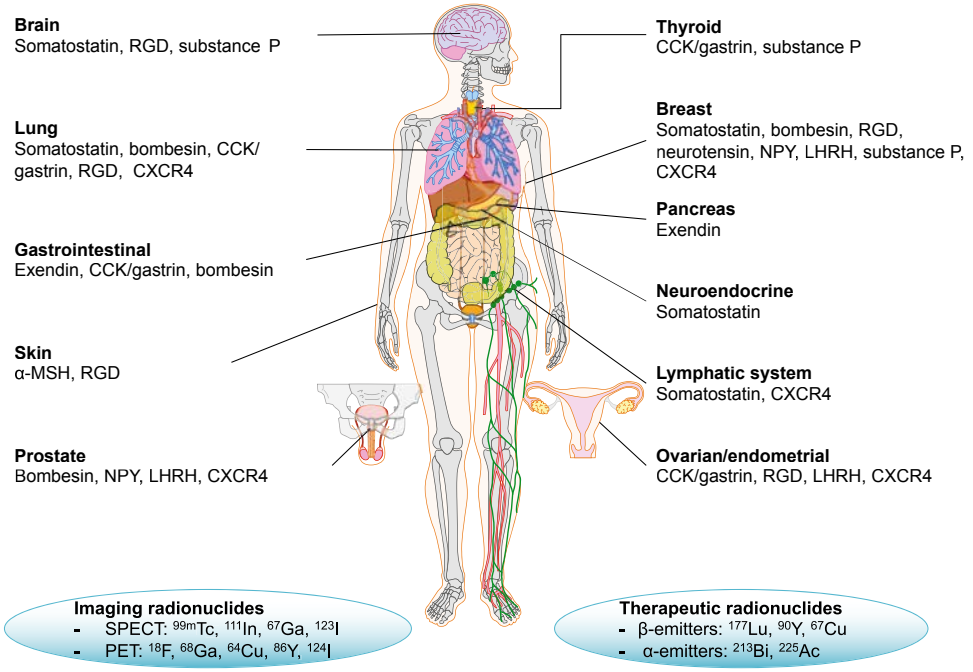

FIGURE 1. Examples of radiopeptide families, radionuclides and their applications for imaging of tumors. RGD = Arginylglycylaspartic acid.

The success of radiolabeled somatostatin analogs inspired the scientific community to develop radiopeptides targeting different receptor families, including gastrin-releasing peptide (GRP), cholecystokinin-2/gastrin (CCK-2/CCK-B), glucagonlike peptide-1 (GLP-1), $\alpha_v\beta_3$-integrin, neurokinin-1 (NK-1), melanocyte-stimulating

hormone (MSH), neuropeptide Y (NPY), luteinizing hormone-releasing hormone (LHRH) and chemokine receptor-4 (CXCR4) (*1*). Examples of radiopeptide families and their applications for tumor imaging and therapy are shown in **Figure 1**. Radiopeptides have established themselves as important agents for imaging, but also for PRRT. For medical imaging, peptides can be radiolabelled with radionuclides such as ^{99m}Tc, ^{111}In, ^{67}Ga, or ^{123}I for SPECT and ^{18}F, ^{68}Ga, ^{64}Cu, ^{86}Y, or ^{124}I for PET. For therapeutic purposes, peptides can be labeled with β-emitters such as ^{177}Lu, ^{90}Y or ^{67}Cu, and α-emitters such as ^{213}Bi or ^{225}Ac. Current applications of clinical radiopeptides for imaging and therapy have been described in detail by Ambrosini et al. (*2*). Approaches intending to improve the performance of radiopeptides for imaging and therapy and thereby widen their scope of application are discussed below.

NOVEL PERSPECTIVES FOR IMAGING

Intensive research efforts have improved pharmacokinetics and in vivo stability of radiopeptides, as well as boosting image quality by identifying radionuclides with more suitable nuclear physical properties or by combining nuclear imaging modalities with complementary modalities. Some examples of novel approaches for radionuclide therapy are shown in **Figure 2**.

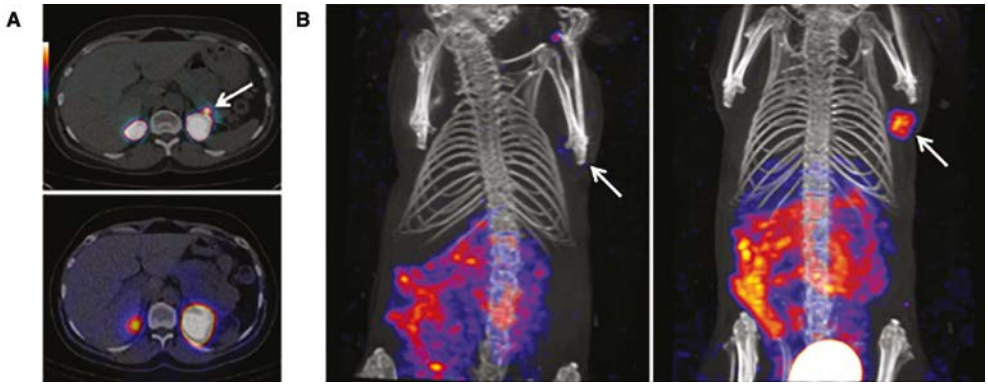

FIGURE 2. (A) PET/CT (top) of insulinoma patient showing focal ^{68}Ga-DOTA-exendin-4 uptake in distal pancreatic tail (consistent with surgically removed insulinoma) that was not shown by SPECT/CT (bottom) with ^{111}In-DOTA-exendin-4. (B) SPECT/CT images of mice with GRPR-expressing PC-3 tumors(arrows) 4 h after injection of bombesin analog ^{111}In-DOTA-PEG$_2$-DTyr-Gln-Trp-Ala-Val-βAla-His-Phe-Nle-NH$_2$ without (left) or with (right) coinjection of neutral endopeptidase inhibitor phosphoramidon (300 μg)

Change of Paradigm Using Receptor Antagonists

An important eye-opener in the field of radiopeptides has been the recent introduction of SSTR antagonists, which showed more favorable pharmacokinetics and better tumor visualization than agonists did, despite their poor internalization rate. In a clinical study, the SSTR antagonist ^{111}In-DOTA-BASS (^{111}In-DOTA-pNO$_2$-Phe-c(DCys-Tyr-DTrp-Lys-Thr-Cys)DTyrNH$_2$) resulted in higher tumor uptake and better visualization of metastatic NETs than did the SSTR agonist ^{111}In- diethylenetriaminepentaacetic acid-octreotide (*3*).

Subsequently, radiolabeled GRPR-targeted antagonists also entered the arena, showing a more favorable pharmacokinetic profile and fewer side effects than agonists. GRPR-targeted antagonists have shown high potential in early clinical trials for prostate cancer imaging (*4*).

Improving Pharmacokinetics and In Vivo Stability

Many efforts have been made to increase radiopeptide in vivo stability by introducing structural modifications, although such modifications can cause undesired changes in pharmacokinetics or impaired receptor affinity. A remarkable advance in this area is the discovery of the in vivo enzyme inhibition concept, in which radiopeptides are administered together with an enzyme inhibitor as a safeguard against enzymatic degradation. It has recently been shown that coinjection of a neutral endopeptidase inhibitor, such as phosphoramidon (PA), can stabilize radiolabeled bombesin, minigastrin, and somatostatin analogs in vivo, leading to enhanced tumor uptake and improved tumor visualization (*5*). We believe that this strategy will have a significant impact on patient care, as it may enhance the diagnostic sensitivity and therapeutic efficacy of radiopeptides. For that purpose, a neutral endopeptidase inhibitor already applied in patients (e.g. thiorphan) is the preferred choice.

^{68}Ga Versus ^{18}F

Recently, imaging quality has been boosted by selecting radionuclides with more suitable nuclear physical properties. For SPECT imaging, ^{99m}Tc is the radioisotope of choice. However, recent developments in PET/CT and PET/MR technologies are steering the field towards positron emitters.

^{68}Ga-radiopeptides are useful tools for PET/CT or PET/MR imaging of diseases, as ^{68}Ga can be obtained in-house from a ^{68}Ge/^{68}Ga generator. The introduction of ^{68}Ga-labeled DOTA-conjugated somatostatin analogs (TOC, TATE, NOC) into the clinic, enabling PET/CT imaging of NETs, is an important advance in somatostatin-based imaging. The superior performance of imaging techniques using these tracers for detection of NET lesions was described by Ambrosini et al. (*2*).

Recently, ^{68}Ga-labeled exendin-4 has been introduced in the clinic for the detection of GLP-1 receptor-positive insulinomas (*6*). ^{68}Ga-DOTA-exendin-4 PET/CT is preferred over ^{111}In-DOTA-exendin-4 SPECT/CT because of the higher spatial resolution and better quantification options obtained with PET/CT cameras.

^{18}F-labeled peptides have some advantages over ^{68}Ga-labeled peptides, such as a longer half-life. Moreover, physical properties of ^{18}F are more favorable for PET imaging than those of ^{68}Ga. Indeed, an ^{18}F-labeled GRPR-antagonist, BAY 864367 (3-cyano-4-^{18}F-fluorobenzoyl-Ala(SO_3H)-Ala(SO_3H)-Ava-Gln-Trp-Ala-Val-*N*MeGly-His-Sta-Leu-NH_2), has recently been implemented in the clinical setting (*4*). A drawback yet to be overcome with ^{18}F-labeled peptides is their higher lipophilicity, which gives rise to less favorable pharmacokinetics. An interesting approach consists of labeling peptides with Al^{18}F via radiometalation chemistry. Several peptides have been labeled with Al^{18}F, such as octreotide, E[c(RGDyK)]$_2$, exendin-4, the bombesin analog NOTA-8-Aoc-BBN(7-14)NH_2, and the GRPR-antagonist JMV4168 (DOTA-βAla-βAla-JMV594) (*7, 8*). The development of a kit-based method for labeling peptides with ^{18}F would make application of ^{18}F-labeled peptides possible in a wider range of hospitals.

Nuclear/Optical Multimodality Imaging

Nuclear imaging technologies available in the clinic (SPECT/CT, PET/CT, and PET/MR) are superior to any other clinical imaging modality in terms of specificity and sensitivity. However, optical imaging offers interesting applications as well and could complement the nuclear medicine uses (*9*). An important development in the field of radiopeptides has been the introduction of hybrid derivatives, containing both a fluorescent and radioactive label, as these have significant implications in the field of image-guide surgery. Several hybrid radiopeptides have been developed, including agents targeting SSTR, GRPR, interleukin-11 receptor-α, $\alpha_v\beta_3$-integrin, matrix metalloproteinase, CXCR4, and GLP-1R (*10-12*). Because of the size and lipophilicity of common fluorescent dyes, the main challenge lies in the optimization the chemical structures of hybrid tracers to preserve receptor affinity and biodistribution patterns while maximizing the range of tissue penetration.

NOVEL PERSPECTIVES FOR THERAPY

Novel strategies might improve the outcome of PRRT. These include the improvement of pharmacokinetics and in vivo stability, the combination of radionuclides, the combination of PRRT with chemotherapy, the use of α-emitting radionuclides, and the use of novel methods to predict therapy response. Recent developments to increase the therapeutic effects of PRRT have been described in detail by Bison et al. (*13*). Some examples of novel approaches for radionuclide therapy are shown in **Figure 3**.

Improving Pharmacokinetics and In Vivo Stability

The success of PRRT would presumably be improved by enhancing the dose delivered to the tumor or limiting the dose delivered to normal healthy tissues. The use of SSTR antagonists has enhanced tumor targeting and prolonged tumor retention compared to SSTR agonists, resulting in an enhanced tumor radiation dose during PRRT. In a clinical study, the SSTR antagonist ^{177}Lu-DOTA-JR11 exhibited higher tumor uptake

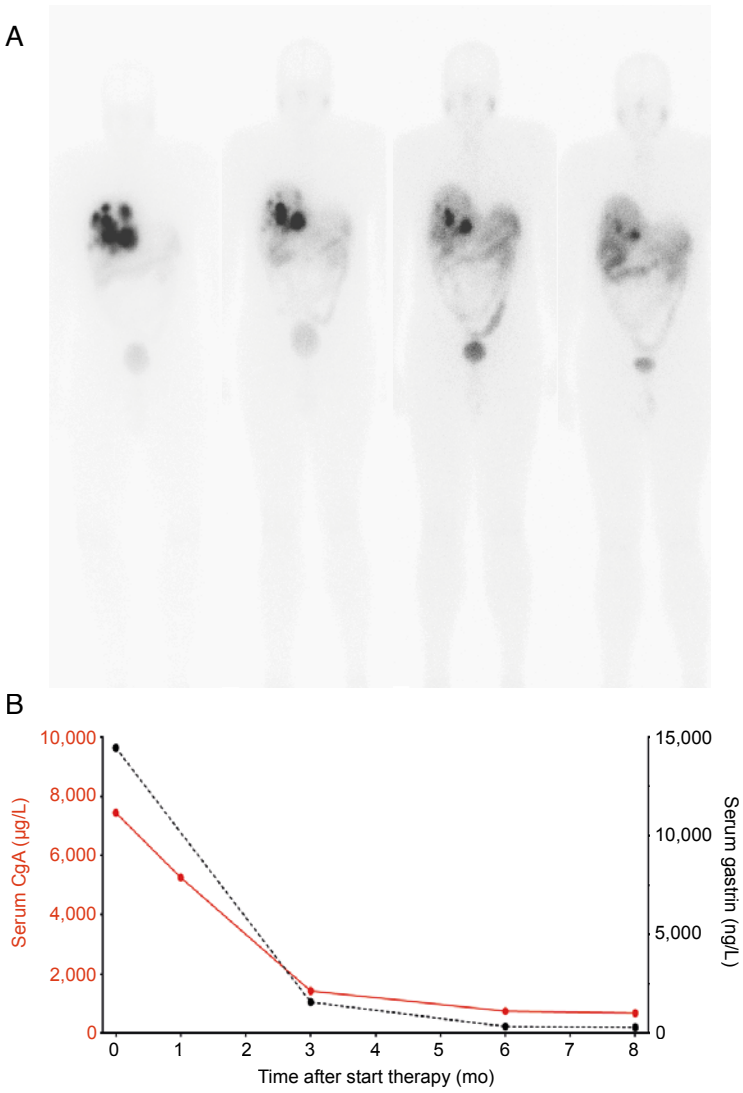

FIGURE 3. (A) Total body images after each cycle of PRRT with 7.4 GBq ^{177}Lu-octreotate in combination with low-dose capecitabine as chemosensitizer in patient with liver metastases of gastrinoma. Decreasing uptake in the liver metastases indicates and preludes tumor response, which was later confirmed with CT. (B) Course of tumor markers chromogranin-A (CgA) and gastrin.

and a longer intratumoral residence time than the SSTR agonist ^{177}Lu-DOTATATE (*14*). This study was performed on only a few patients, and more systematic clinical studies are needed now to fully evaluate the role of ^{177}Lu-DOTA-JR11 for therapy of NETs.

Patients with advanced prostate cancer could also benefit from PRRT, as treatment options for this patient group are limited. ^{177}Lu-GRPR antagonists have not been tested in clinical studies thus far, even though they have shown promising results in preclinical studies (*15*). Radionuclide therapy using PSMA-targeted tracers has been more widely explored, as PSMA expression has been validated in advanced prostate cancer in several reports. Extensive comparative studies showing target expression of PSMA and GRPR in advanced prostate cancer would guide the choice of therapeutic options for those patients.

Combination Therapies

In the search for increased therapeutic efficacy of PRRT, therapeutic radionuclides with different physical characteristics have been combined to target a wider range of tumor lesions. ^{90}Y and ^{177}Lu β-emitting isotopes suitable for treatment of large and small tumors have been combined in simultaneous or sequential treatment. A recent retrospective study (*16*) described the benefits of the combination of ^{90}Y-DOTATOC and ^{177}Lu-DOTATOC over treatment with either radiopeptide alone, with increased survival after the combination treatment. However, patient selection bias cannot be excluded; therefore, prospective, randomized trials are needed before firm conclusions can be drawn.

PRRT could also be combined with other therapies to increase tumor response. Chemotherapeutics can sensitize tumor cells to PRRT by modulating DNA damage and repair mechanisms, apoptosis, cell proliferation, cell-cycle synchronization and tumor cell oxygenation. However, careful design of such combination studies is needed, as chemotherapeutics could also alter receptor expression and tumor vascularization. For instance, the DNA alkylating drug temozolomide increased tumor perfusion in a preclinical study (*13*). Clinical studies combining PRRT using ^{177}Lu-DOTATATE with several chemotherapeutics have been reported. Capecitabine and temozolomide both increased the response rate of ^{177}Lu-DOTATATE in comparison with ^{177}Lu-DOTATATE alone (*17*). A recent proof-of-concept study described the combination of PRRT with everolimus (*18*). It was shown that everolimus could be safely combined with ^{177}Lu-octreotate to treat low-grade NETs.

Introduction of Powerful α-Emitters

An important development in the field of radionuclide therapy has been the introduction of α-particle-emitting radionuclides. A first-in-human study showed ^{213}Bi-DOTATOC can eradicate neuroendocrine liver metastases pretreated with

^{90}Y/^{177}Lu-DOTATOC. Only moderate acute and midterm hematologic and renal toxicity was observed at effective therapeutic doses (*19*). Nonoperable and critically located gliomas have been treated with α-targeted therapy, by local injection of ^{213}Bi-DOTA-substance P, providing local irradiation of the tumor. The short tissue range of ^{213}Bi prevents damage to adjacent brain areas. Up till now, this therapy has proven to be feasible and safe, with only mild adverse effects observed (*20*). Despite the promising preliminary results obtained with ^{213}Bi-DOTATOC and ^{213}Bi-substance P in patients, the short half-life of ^{213}Bi (45.6 min) and the costs and limited availability of ^{225}Ac/^{213}Bi generators limit clinical use. The recently described accelerator-driven production of ^{225}Ac may allow it to be produced in quantities sufficient to supply centers for clinical trials and make the treatment available to a wider range of centers (*21*).

Innovative Methods as Predictors of Therapeutic Response

There is a clear need for personalization and standardization of PRRT to optimize efficacy and minimize long-term toxicity, as emphasized in a recent review of Bodei et al. (*22*). They recommend collecting data on several parameters to construct a patient-specific treatment plan, taking into account various patient-specific characteristics to predict the probability of response and predisposition to toxicity. Dosimetry can be used as a predictor of therapy response and toxicity; a relationship between tumor-absorbed dose and response has already been demonstrated for ^{90}Y-DOTATOC (*23*).

Markers of DNA-damage and repair, such as phosphorylated variant H2A histone family member X (γ-H2AX), may predict tumor and normal-organ radiosensitivities. A recent paper described the use of a γ-H2AX-foci assay as a predictor of normal-tissue toxicity after PRRT (*24*). Genetic components can also predict disease stage and response to therapy (*25*).

CONCLUSION

Derived from natural peptide ligands, radiopeptides can be tailored and optimized to provide personalized treatment for several types of diseases. In recent years, several methods have been developed to optimize radiopeptides for imaging and therapy; these efforts and achievements may bridge the gap between the exciting promises of radiopeptides and their implementation in the clinic. Today, complex multimodal ligands are being designed for theranostic applications, whereas simple radiopeptides combine all key ingredients for effective theranostic applications, including easy manufacturing, fast clearance, low immunogenicity, and efficient targeting. We believe that the recent advances described in this article may lead the way to a radiant future for radiopeptides in the field of theranostics.

REFERENCES

1. Koopmans KP, Glaudemans AW. Rationale for the use of radiolabelled peptides in diagnosis and therapy. *Eur J Nucl Med Mol Imaging.* 2012;39(suppl 1):S4-S10.
2. Ambrosini V, Fani M, Fanti S, Forrer F, Maecke HR. Radiopeptide imaging and therapy in Europe. *J Nucl Med.* 2011;52(suppl 2):42s-55s.
3. Wild D, Fani M, Behe M, et al. First clinical evidence that imaging with somatostatin receptor antagonists is feasible. *J Nucl Med.* 2011;52:1412-1417.
4. Sah BR, Burger IA, Schibli R, et al. Dosimetry and first clinical evaluation of the new 18F-radiolabeled bombesin analogue BAY 864367 in patients with prostate cancer. *J Nucl Med.* 2015;56:372-378.
5. Nock BA, Maina T, Krenning EP, de Jong M. "To serve and protect": enzyme inhibitors as radiopeptide escorts promote tumor targeting. *J Nucl Med.* 2014;55:121-127.
6. Antwi K, Fani M, Nicolas G, et al. Localization of hidden insulinomas with 68Ga-DOTA-Exendin-4 PET/CT: a pilot study. *J Nucl Med.* 2015;56:1075-1078.
7. Laverman P, McBride WJ, Sharkey RM, Goldenberg DM, Boerman OC. Al(18) F labeling of peptides and proteins. *J Labelled Comp Radiopharm.* 2014;57:219-223.
8. Chatalic KL, Franssen GM, van Weerden WM, et al. Preclinical comparison of Al18F- and 68Ga-labeled gastrin-releasing peptide receptor antagonists for PET imaging of prostate cancer. *J Nucl Med.* 2014;55:2050-2056.
9. van Leeuwen FW, de Jong M. Molecular imaging: the emerging role of optical imaging in nuclear medicine. *Eur J Nucl Med Mol Imaging.* 2014;41:2150-2153.
10. Kuil J, Velders AH, van Leeuwen FW. Multimodal tumor-targeting peptides functionalized with both a radio- and a fluorescent label. *Bioconjug Chem.* 2010;21:1709-1719.
11. Azhdarinia A, Ghosh P, Ghosh S, Wilganowski N, Sevick-Muraca EM. Dual-labeling strategies for nuclear and fluorescence molecular imaging: a review and analysis. *Mol Imaging Biol.* 2012;14:261-276.
12. Brand C, Abdel-Atti D, Zhang Y, et al. In vivo imaging of GLP-1R with a targeted bimodal PET/fluorescence imaging agent. *Bioconjug Chem.* 2014;25:1323-1330.
13. Bison SM, Konijnenberg MW, Melis M, et al. Peptide receptor radionuclide therapy using radiolabeled somatostatin analogs: focus on future developments. *Clin Transl Imaging.* 2014;2:55-66.
14. Wild D, Fani M, Fischer R, et al. Comparison of somatostatin receptor agonist and antagonist for peptide receptor radionuclide therapy: a pilot study. *J Nucl Med.* 2014;55:1248-1252.
15. Dumont RA, Tamma M, Braun F, et al. Targeted radiotherapy of prostate cancer with a gastrin-releasing peptide receptor antagonist is effective as monotherapy and in combination with rapamycin. *J Nucl Med.* 2013;54:762-769.
16. Radojewski P, Dumont R, Marincek N, et al. Towards tailored radiopeptide therapy. *Eur J Nucl Med Mol Imaging.* 2015;42:1231-1237.
17. Claringbold PG, Turner JH. Pancreatic neuroendocrine tumor control: durable objective response to combination Lu-octreotate-capecitabine-temozolomide radiopeptide chemotherapy. *Neuroendocrinology.* June 10, 2015 [Epub ahead of print].
18. Claringbold PG, Turner JH. Neuroendocrine tumor therapy with lutetium-177-octreotate and everolimus (NETTLE): a phase I study. *Cancer Biother Radiopharm.* 2015;30:261-269.

19. Kratochwil C, Giesel FL, Bruchertseifer F, et al. (213)Bi-DOTATOC receptor-targeted alpha-radionuclide therapy induces remission in neuroendocrine tumours refractory to beta radiation: a first-in-human experience. *Eur J Nucl Med Mol Imaging.* 2014;41:2106-2119.
20. Krolicki L, Morgenstern A, Kunikowska J, et al. Alphaknife for glioma tumors: two years experiences with targeted alpha therapy of 213Bi-substance P [abstract]. *Eur J Nucl Med Mol Imaging.* 2014;41(suppl 2):S291-S292.
21. Weidner JW, Mashnik SG, John KD, et al. 225Ac and 223Ra production via 800 MeV proton irradiation of natural thorium targets. *Appl Radiat Isot.* 2012;70:2590-2595.
22. Bodei L, Kidd M, Baum RP, Modlin IM. PRRT: Defining the paradigm shift to achieve standardization and individualization. *J Nucl Med.* 2014;55:1753-1756.
23. Strigari L, Konijnenberg M, Chiesa C, et al. The evidence base for the use of internal dosimetry in the clinical practice of molecular radiotherapy. *Eur J Nucl Med Mol Imaging.* 2014;41:1976-1988.
24. Denoyer D, Lobachevsky P, Jackson P, Thompson M, Martin OA, Hicks RJ. Analysis of 177Lu-DOTA-octreotate therapy-induced DNA damage in peripheral blood lymphocytes of patients with neuroendocrine tumors. *J Nucl Med.* 2015;56:505-511.
25. Modlin IM, Oberg K, Taylor A, Drozdov I, Bodei L, Kidd M. Neuroendocrine tumor biomarkers: current status and perspectives. *Neuroendocrinology.* 2014;100:265-277.

Gastrin-Releasing Peptide Receptor Targeting

2

Chapter 2.1
Preclinical Comparison of $Al^{18}F$- and ^{68}Ga-labeled Gastrin-Releasing Peptide Receptor Antagonists for PET Imaging of Prostate Cancer

Chapter 2.2
In Vivo Stabilization of a Gastrin-Releasing Peptide Receptor Antagonist enhances PET Imaging and Radionuclide Therapy of Prostate Cancer in Preclinical Studies

2.1

Preclinical Comparison of Al^{18}F- and ^{68}Ga-labeled Gastrin-Releasing Peptide Receptor Antagonists for PET Imaging of Prostate Cancer

Kristell L.S. Chatalic[1,2], Gerben M. Franssen[3], Wytske M. van Weerden[2], William J. McBride[4], Peter Laverman[3], Erik de Blois[1], Bouchra Hajjaj[5], Luc Brunel[5], David M. Goldenberg[4], Jean-Alain Fehrentz[5], Jean Martinez[5], Otto C. Boerman[3], Marion de Jong[1]

[1]Department of Nuclear Medicine, Erasmus MC, Rotterdam, The Netherlands
[2]Department of Urology, Erasmus MC, Rotterdam, The Netherlands
[3]Department of Nuclear Medicine, Radboud University Medical Center, Nijmegen, The Netherlands
[4]Immunomedics, Inc., Morris Plains, New Jersey USA
[5]Institut des Biomolécules Max Mousseron, UMR 5247, CNRS-UM1-UM2, Montpellier, France

Adapted from: Journal of Nuclear Medicine 2014; 55(12):2050-6

ABSTRACT

Gastrin-releasing peptide receptor (GRPR) is overexpressed in human prostate cancer and is being used as a target for molecular imaging. In this study, we report on the direct comparison of 3 novel GRPR-targeted radiolabeled tracers: Al^{18}F-JMV5132, ^{68}Ga-JMV5132, and ^{68}Ga-JMV4168 (JMV5132 is NODA-MPAA-βAla-βAla-[H-D-Phe-Gln-Trp-Ala-Val-Gly-His-Sta-Leu-NH_2], JMV4168 is DOTA-βAla-βAla-[H-D-Phe-Gln-Trp-Ala-Val-Gly-His-Sta-Leu-NH_2], and NODA-MPAA is 2-[4-(carboxymethyl)-7-{[4-(carboxymethyl) phenyl]methyl}-1,4,7-triazacyclononan-1-yl]acetic acid).

Methods

The GRPR antagonist JMV594 (H-D-Phe-Gln-Trp-Ala-Val-Gly-His-Sta-Leu-NH_2) was conjugated to NODA-MPAA for labeling with Al^{18}F. JMV5132 was radiolabeled with ^{68}Ga and ^{18}F, and JMV4168 was labeled with ^{68}Ga for comparison. The inhibitory concentration of 50% values for binding GRPR of JMV4168, JMV5132, ^{nat}Ga-JMV4168 and ^{nat}Ga-JMV5132 were determined in a competition-binding assay using GRPR-overexpressing PC-3 tumors. The tumor-targeting characteristics of the compounds were assessed in mice bearing subcutaneous PC-3 xenografts. Small animal PET/CT images were acquired, and tracer biodistribution was determined by ex vivo measurements.

Results

JMV5132 was labeled with ^{18}F in a novel 1-pot, 1-step procedure within 20 min, without need for further purification and resulting in a specific activity of 35 MBq/nmol. Inhibitory concentration of 50% values (in nM) for GRPR binding of JMV5132, JMV4168, ^{nat}Ga-JMV5132, ^{nat}Ga-JMV4168 and Al^{nat}F-JMV5132 were 6.8 (95% confidence intervals [CIs], 4.6-10.0), 13.2 (95% CIs, 5.9-29.3), 3.0 (95% CIs, 1.5-6.0), 3.2 (95% CIs, 1.8-5.9) and 10.0 (95% CIs, 6.3-16.0), respectively. In mice with subcutaneous PC-3 xenografts, all tracers cleared rapidly from the blood, exclusively via the kidneys for ^{68}Ga-JMV4168 and partially hepatobiliary for ^{68}Ga-JMV5132 and Al^{18}F-JMV5132. Two hours after injection, the uptake of ^{68}Ga-JMV4168, ^{68}Ga-JMV5132 and Al^{18}F-JMV5132 in PC-3 tumors was 5.96 ± 1.39, 5.24 ± 0.29, 5.30 ± 0.98 (percentage injected dose per gram), respectively. GRPR specificity was confirmed by significantly reduced tumor uptake of the 3 tracers after coinjection of a 100-fold excess of unlabeled JMV4168 or JMV5132. Small animal PET/CT clearly visualized PC-3 tumors, with the highest resolution observed for Al^{18}F-JMV5132.

Conclusion

JMV5132 could be rapidly and efficiently labeled with ^{18}F. Al^{18}F-JMV5132, ^{68}Ga-JMV5132, and ^{68}Ga-JMV4168 all showed comparable high and specific accumulation in GRPR-positive PC-3 tumors. These new PET tracers are promising candidates for future clinical translation.

INTRODUCTION

Prostate cancer (PCa) is the most frequently diagnosed cancer and the second leading cause of cancer death among men in the United States (*1*). There is a strong need for improved imaging techniques that provide accurate staging and monitoring of this disease, particularly at early stages. Conventional diagnostic techniques, such as ultrasound-guided biopsy, are limited by high false-negative rates (*2*). Emerging functional imaging techniques, including diffusion-weighted MR imaging, dynamic contrast-enhanced MR imaging, and PET, have shown improved sensitivity and staging accuracy for detecting primary prostate tumors and metastatic lymph nodes (*3*). Several PET radiotracers have shown promising clinical utility, such as the metabolic agents, ^{18}F-FDG, ^{11}C-/^{18}F-choline, and ^{11}C-/^{18}F-acetate for the assessment of distant metastasis and ^{18}F-NaF for the detection of bone metastasis (*4*). However, their application is most valuable in late-stage, recurrent, or metastatic PCa. Increasing efforts are being made in developing PET imaging agents targeting specific biomarkers of PCa, such as gastrin-releasing peptide receptor (GRPR) (*5*) and prostate-specific membrane antigen (*6*).

The GRPR, or bombesin (BBN) receptor subtype II, has been shown to be overexpressed in several human tumors, including PCa (*7*). Overexpression of GRPR was found in 63-100% of primary prostate tumors and over 50% of lymph and bone metastases (*8, 9*). The GRPR density was reported to be 26-fold higher in prostate carcinoma than prostatic hyperplasia (*9*). Because of the low expression in benign prostatic hyperplasia and inflammatory prostatic tissues, imaging of GRPR in localized PCa has potential advantages over choline- and acetate-based radiotracers (*9, 10*).

A variety of radiolabeled BBN analogs have been developed for targeting GRPR-positive tumors and were evaluated in preclinical and clinical studies (*5*). Several recent reports have shown that GRPR antagonists show properties superior GRPR agonists, affording higher tumor uptake and lower accumulation in physiologic GRPR-positive nontarget tissues (*11, 12*). Moreover, GRPR agonists were shown to induce side effects in patients, mediated by virtue of their physiologic activity (*13, 14*). Therefore, particular attention has been drawn to the development of GRPR antagonists for imaging and radionuclide therapy of PCa. Several GRPR antagonists have since been developed by the modification of C-terminal residues of GRPR agonists, including the statin-based BBN analog, JMV594 (H-D-Phe-Gln-Trp-Ala-Val-Gly- His-Sta-Leu-NH_2) (*15*).

^{68}Ga-labeled GRPR antagonists were developed for PET imaging, showing good targeting properties in preclinical studies (*12, 16-18*) and recently also in clinical trials (*19, 20*). Clinical evaluation of the ^{68}Ga-labeled GRPR antagonist BAY86-7548 (^{68}Ga-DOTA-4-amino-1-carboxymethylpiperidine-D-Phe-Gln-Trp-Ala-Val-Gly-His-Sta-Leu-NH_2) has shown a specificity, sensitivity, and accuracy of 88%, 81%, and 83%, respectively, for the detection of primary PCa. In comparison, it was shown that ^{11}C-choline was not able to discriminate PCa from benign prostatic hyperplasia,

because maximum standardized uptake values in PCa were not significantly different from benign prostatic hyperplasia (*21*). Another study reported a specificity, sensitivity and accuracy of 80%, 29%, and 71%, respectively, for the detection of PCa using ^{11}C-choline (*22*). The detection of lymph node metastases with the ^{68}Ga-labeled GRPR antagonist was suboptimal, partially due to the suboptimal physical characteristics of ^{68}Ga, limiting the detection of small lesions (*20*).

Therefore, the aim of the present study was to develop an ^{18}F-labeled GRPR antagonist for high resolution and sensitive PET imaging of primary, recurrent, and metastatic PCa and to compare the imaging properties of this tracer with those of ^{68}Ga-labeled analogs. ^{18}F has superior physical characteristics for PET imaging, such as a lower positron range and a higher positron yield, offering higher resolution and sensitivity (*23*). However, most methods for labeling peptides with ^{18}F are laborious and require multistep procedures with moderate labeling yields. A good alternative is the Al^{18}F labeling method (*24*), allowing fast and facile labeling of peptides in a 1-step procedure. We designed a new GRPR-antagonist conjugate (JMV5132 [NODA-MPAA-βAla-βAla-(H-D-Phe-Gln-Trp-Ala-Val-Gly-His-Sta-Leu-NH_2); NODA-MPAA is 2-(4-(carboxymethyl)-7-{[4-(carboxy-methyl)phenyl]methyl}-1,4,7-triazacyclononan-1-yl)acetic acid]), analogous to the previously-described JMV4168 (DOTA-βAla-βAla-[H-D-Phe-Gln-Trp-Ala-Val-Gly-His-Sta-Leu-NH_2]) (*25*), with a NODA-MPAA chelator for high-yield complexation of Al^{18}F (*26*).

Here, we report on the direct preclinical comparison of 3 novel radiolabeled tracers (Al^{18}F-JMV5132, ^{68}Ga-JMV4168 and ^{68}Ga-JMV5132) for PET imaging of PCa. We determined the in vitro characteristics of the radiolabeled peptides and evaluated their tumor targeting properties in vivo in nude mice with subcutaneous human prostate tumors.

MATERIALS AND METHODS

Synthesis of JMV4168 and JMV5132

JMV4168 was synthesized using Fmoc-based solid-phase peptide synthesis as described previously (*25*). JMV5132 was synthesized in the same manner as JMV4168 but was coupled to tert-butyl (tBu)-protected NODA-MPAA instead of tBu-protected DOTA. NODA-MPAA was prepared as previously described using NO2AtBu (Chematech, Dijon, France) (*26*). The chemical structures of JMV4168 and JMV5132 are shown in **Figure 1**.

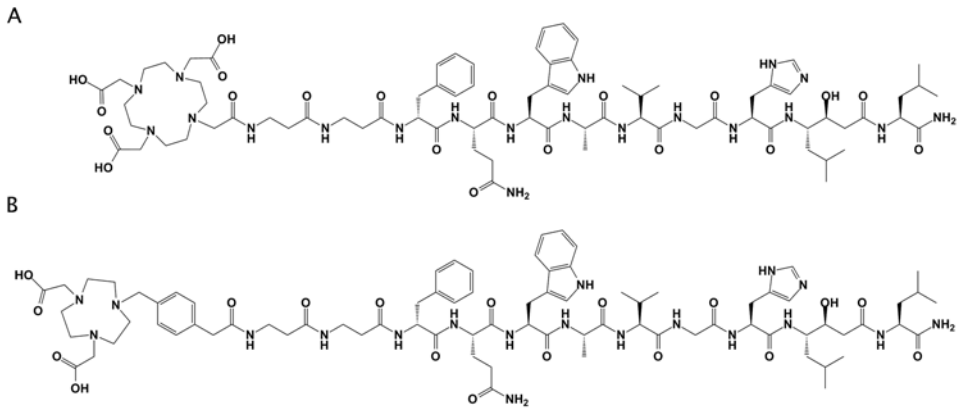

FIGURE 1. Chemical structures of DOTA-βAla-βAla-[H-D-Phe-Gln-Trp-Ala-Val-Gly-His-Sta-Leu-NH_2] (JMV4168) (A) and NODA-MPAA-βAla-βAla-[H-D-Phe-Gln-Trp-Ala-Val-Gly- His-Sta-Leu-NH_2] (JMV5132) (B).

Radiolabeling

Concentration and purification of $^{18}F^-$

$^{18}F^-$ solution in enriched water ($H_2{}^{18}O$, BV Cyclotron) was purified from metal impurities and concentrated before use. Briefly, a CM cartridge (weak cation-exchange cartridge, Waters, Sep-Pak Accell Plus CM, 130 mg) and a QMA cartridge (strong anion-exchange cartridge, Waters, Sep-Pak Waters Accell Plus QMA Plus Light, 130 mg) were prewashed with 10 mL metal-free ultrapure water (Milli-Q, Millipore). The $^{18}F^-$ solution (8-15 GBq) was pushed slowly through the CM cartridge connected to the QMA cartridge, followed by 6 mL wash with metal-free ultrapure water. Finally, the CM cartridge containing cationic metal impurities was disposed of and $^{18}F^-$ was eluted from the QMA cartridge with a small volume (150-200 µL) of saline.

Radiolabeling of JMV5132 with $Al^{18}F$

Labeling was performed by mixing $^{18}F^-$ solution (15-20 µL, 700-900 MBq), sodium acetate (NaOAc) (0.5 µL of 1 M solution, pH 4.1), Al^{3+} stock solution (20 nmol, 10 µl of 2 mM $AlCl_3.6H_2O$ in 0.1 M NaOAc, pH 4.2), acetonitrile (67 % v/v), quenchers (2.5 µL of 50 mM methionine, gentisic acid and ascorbic acid), and finally JMV5132 (20 nmol, 3.26 µL of solution [10 µg/µL] in 2 mM NaOAc pH 4.1). The reaction mixture was heated for 15 min at 105°C. To allow injection into mice, the peptide was diluted to less than 0.5 % (v/v) acetonitrile with 0.5% (w/v) bovine serum albumin (BSA), 0.5 % (w/v) polyoxyethylene (20) sorbitan monolaurate solution (polysorbate-20), and quenchers (1 mM methionine, gentisic acid and ascorbic acid) in phosphate-buffered saline (PBS), pH 7.4. Bovine serum albumin and polysorbate-20 were added to reduce binding of radiolabeled peptide to plastic disposables, whereas quenchers (methionine, gentisic acid, and ascorbic acid) were added to prevent radiolysis of radiolabeled peptides.

Radiolabeling of JMV4168 and JMV5132 with ^{68}Ga
Elution and purification of ^{68}Ga from a $^{68}Ga/^{68}Ge$ generator (IGG-100; Eckert & Ziegler Europe) was performed using the sodium chloride-based procedure described earlier (*27*). A volume of 375 µL of 4-(2-Hydroxyethyl)piperazine-1-ethanesulfonic acid (1 M, pH 3.6) was slowly added to 300 µL of purified ^{68}Ga eluate, followed by addition of quenchers (methionine, gentisic acid, and ascorbic acid, 1.25 mM) and peptide (2 nmol). The reaction mixture was heated for 10 min at 95°C. After reaction, ethylenediaminetetraacetic acid (50 mM) was added to a final concentration of 5 mM to complex free ^{68}Ga. For animal experiments, the labeled product was purified by reversed-phase high-performance liquid chromatography (RP-HPLC) using the gradient described in the "Quality Control" section and concentrated by evaporation. To allow injection into mice, the radiolabeled peptide was diluted with 0.5% (w/v) bovine serum albumin, 0.5 % (w/v) polysorbate-20, and quenchers (1 mM methionine, gentisic acid, and ascorbic acid) in PBS and neutralized with sodium carbonate ($NaHCO_3$) buffer (1 M, pH 8.5).

Cold labeling of JMV4168 and JMV5132 with ^{nat}Ga and ^{nat}F
2 µL of a $Ga(NO_3)_3$ solution (0.2 M) was added to 10 µL of 4-(2-Hydroxyethyl) piperazine-1-ethanesulfonic acid (HEPES) (1 M, pH 3.6), followed by addition of quenchers (methionine, gentisic acid and ascorbic acid, 5 mM) and peptide (100 nmol). Reaction mixture was heated for 10 min at 95°C. Reverse-phase high performance liquid chromatography (RP-HPLC) analysis was performed as described in the section "Quality Control", showing complete incorporation of ^{nat}Ga; no further purification was needed.

10 µL of a $AlCl_3$ solution (0.1 M) was mixed with 5 µL NaF (1 M) and 0.5 µL sodium acetate (NaAc, 2.5 M), followed by addition of 25 µL ethanol and 10 µL JMV5132 (5 mM). Reaction mixture was heated for 15 min at 106°C. $Al^{nat}F$-JMV5132 was purified by RP-HPLC.

Quality Control
Peptide synthesis
Purification of JMV5132 was accomplished by a preparative HPLC (Waters Delta Preparative, Waters 4000 system controller) with a C18 column (40 mm × 100 mm, Waters Delta Pack, column II). The final product was characterized by RP-HPLC (Beckman, LC-126) on a reverse phase-18 Chromatolith Speed ROD column (50 mm × 4.6 mm, Merck, column I) and ESI/MS (Waters micromass ZQ, Waters 2695 Separation Module).

Radiolabeling
Labeling efficiency and colloid formation were assessed by instant thin layer chromatography using silica gel coated paper (Agilent Technologies) and 0.1 M ammonium acetate (NH_4OAc) pH 5.5: 0.1 M ethylenediaminetetraacetic acid (1:1), or

1 M NH_4OAc:methanol (1:3), respectively. Radiochemical purity of labeled peptides was analyzed by RP-HPLC on an Agilent 1200 system (Agilent Technologies). A C-18 column (Onyx monolithic, 4.6 mm x 100 mm; Phenomenex) was used at a flow rate of 1 mL/min with the following buffer system: buffer A, 0.1% v/v trifluoroacetic acid in water; buffer B, 0.1% trifluoroacetic acid in acetonitrile; with a gradient as follows: 97% buffer A (0-5 min), 97 to 76% buffer A (5-8 min), 76 to 75% buffer A (8-13 min), 75% buffer A (13-25 min). The radioactivity of the eluate was monitored using an in-line NaI radiodetector (Raytest GmbH). Elution profiles were analyzed using Gina-star software (version 2.18; Raytest GmbH).

Lipophilicity
The octanol/PBS partition coefficients of ^{68}Ga-JMV4168, ^{68}Ga-JMV5132, and Al^{18}F-JMV5132 were determined as described previously (*28*).

Cell Culture and Competitive Cell Binding Assay
The human PCa cell line PC-3 was cultured in Ham's F-12K (Kaighn's) Medium (Life Technologies) supplemented with 10% fetal calf serum, penicillin (100 units/mL), and streptomycin (100 µg/mL). Cells were grown in tissue culture flasks at 37°C in a humidified atmosphere containing 5% CO_2.

The binding affinities of JMV4168, JMV5132, ^{nat}Ga-JMV4168, ^{nat}Ga-JMV5132, and Al^{nat}F-JMV5132 towards the GRPR were determined in a competitive binding assay using frozen cryostat sections (10-µm thick) of PC-3 xenografts and [^{125}I-Tyr^4]-BBN as a tracer. Tyr^4-BBN (Sigma Aldrich) was iodinated as described earlier (*29*). Tissue sections were preincubated for 5 min in ice-cold binding buffer (5 mM $MgCl_2$, 167 mM tris(hydroxymethyl)aminomethane hydrochloride, pH 7.6), followed by incubation for 1 h in binding buffer containing 1% w/v BSA, [^{125}I-Tyr^4]BBN (5.10-10 M) and JMV4168, JMV5132, ^{nat}Ga-JMV4168 or ^{nat}Ga-JMV5132 in increasing concentrations (range of 10^{-12} M to 10^{-6} M). After incubation, the sections were washed successively with ice-cold binding buffer with 0.25 % w/v BSA for 5 min, binding buffer without BSA for 5 min, and ice-cold Ultrapure water for 5 seconds. Dried sections were placed in apposition to phosphor screens (PerkinElmer, Super Resolution) for 1 day. Radioactivity was assessed using a phosphor imager system (Cyclone, Packard, model A431201) and quantified using Optiquant software (PerkinElmer, Waltham, MA).

Small-animal PET/CT and Biodistribution Studies
Male nude BALB/c mice (age, 6-8 wk) were injected subcutaneously near the right shoulder with a PC-3 cell suspension (5 x 10^6 cells, 200 µL, 66% RPMI, 33% Matrigel [BD Biosciences]). Two to 3 wk after inoculation, when tumor size averaged 200 mm^3, mice were injected intravenously with 5-10 MBq of radiolabeled peptide (200 pmol, 200 µL). To confirm the receptor specificity of the radiolabeled peptides,

additional animals were coinjected with an excess (20 nmol) of unlabeled peptide. Mice were euthanized 1 or 2 h after injection by CO_2/O_2 asphyxiation. Mice were first scanned prone on a small animal PET/CT scanner (Inveon; Siemens Preclinical Solutions). PET emission scans were acquired for 30-60 min, followed by a CT scan (spatial resolution 113.15 μm; 80 kV; and 500 μA). Scans were reconstructed using Inveon Acquisition Workplace software (version 1.5; Siemens Preclinical Solutions), using a 3-dimensional ordered-subset expectation maximization/maximization a posteriori algorithm with the following parameters: matrix, 256 x 256 x 161; pixel size, 0.40 x 0.40 x 0.796 mm; and β-value, 1.5, with uniform variance and FastMAP. After scanning, blood, tumor, and relevant organs and tissues were collected, weighed and counted in a γ-counter (1480 WIZARD automatic gamma counter, PerkinElmer, Waltham, MA) with a counting time of 60 seconds per sample, isotope-specific energy window and an error not exceeding 5%.

The percentage injected dose per gram (%ID/g) was determined for each tissue sample. All animal experiments were approved by local authorities and were in compliance with the institutions guidelines.

Statistical Analysis

Statistical analysis was performed using GraphPad Prism version 5.01 (version 5.01; GraphPad Software). IC_{50} values were determined with datasets from 3 independent experiments, each in duplicate. Data are represented as percentage of total binding (normalized), with standard error of the mean. An extra sum-of-squares F test was used to compare two best-fit values, and the level of significance was set at $P < 0.05$. Biodistribution data are represented as the mean %ID/g ± SD, with group sizes of 3 mice, except at 1 h after injection: n = 2 for $Al^{18}F$-JMV5132 and at 2 h after injection: n = 5 for ^{68}Ga-JMV4168, $Al^{18}F$-JMV5132. Statistical analysis of biodistribution data was performed using a 1-way ANOVA with a Bonferroni post-hoc test, and the level of significance was set at $P < 0.05$.

RESULTS

Synthesis of JMV4168 and JMV5132

JMV4168 and JMV5132 **(Figure 1)** were obtained with an average yield of approximately 40% and a purity greater than 97% as confirmed by RP-HPLC. Conjugates were characterized by electrospray ionization mass spectrometry (mass/charge, $[M+2H]^{2+}/2$: JMV4168, calculated: 815.9414, found: 815.9412; JMV5132, calculated: 821.4416, found: 821.4433).

Radiolabeling and Stability Studies

Al^{18}F-JMV5132 was obtained with a specific activity of 40 ± 4 MBq/nmol (88% non-decay-corrected yield) and ^{68}Ga-JMV4168 and ^{68}Ga-JMV5132 with a specific activity of 47 ± 2 and 47 ± 4 MBq/nmol after purification, respectively. RP-HPLC analysis indicated that the radiochemical purity of the Al^{18}F- or ^{68}Ga-labeled peptide preparations used in in vitro and in vivo experiments always exceeded 95%. Radio-HPLC elution profiles of Al^{18}F- and ^{68}Ga-labeled peptides are shown in **Figure 2A**. ^{68}Ga-JMV4168, ^{68}Ga-JMV5132 and Al^{18}F-JMV5132 had retention times of 13.8 min, 19.6 min and 21.9 min, respectively. The addition of quenchers (methionine, gentisic acid, and ascorbic acid) prevented oxidation of the radiolabeled peptides, as shown in **Figure 2B**.

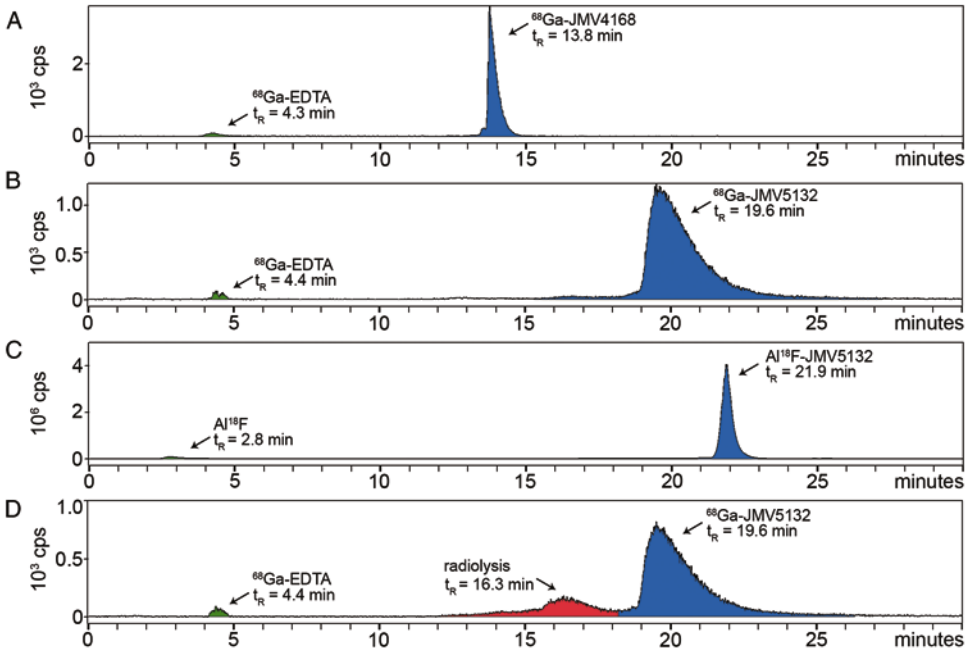

FIGURE 2. Radio-high-performance liquid chromatograms of ^{68}Ga-JMV4168 (A), ^{68}Ga-JMV5132 (B), and Al^{18}F-JMV5132 (C). (D) Radio-high-performance liquid chromatogram of ^{68}Ga-JMV5132 without added quenchers. Y-axis = radioactivity in count per second (cps); x-axis = retention time in min. EDTA = ethylenediaminetetraacetic acid; t_R = retention time.

Lipophilicity

The octanol/PBS partition coefficients were determined to estimate the lipophilicity of the Al^{18}F- or ^{68}Ga-labeled peptides. The log $P_{octanol/PBS}$ values for ^{68}Ga-JMV4168, ^{68}Ga-JMV5132 and Al^{18}F-JMV5132 were -2.53 ± 0.04, -1.40 ± 0.01, and -1.56 ± 0.08, respectively. This result shows that the ^{68}Ga-DOTA analog (JMV4168) was more hydrophilic than the ^{68}Ga- and ^{18}F-NODA-MPAA analogs (JMV5132).

Competitive Cell Binding Assay

The affinity of JMV4168, JMV5132, ^{nat}Ga-JMV4168, ^{nat}Ga-JMV5132, and Al^{nat}F-JMV5132 for the GRPR was determined in a competitive binding assay, using [^{125}I-Tyr^4]-BBN as radioligand. The displacement binding curves are shown in **Figure 3**. Inhibitory concentration of 50% (IC_{50}) values (in nM) for binding to GRPR for JMV5132 (NODA-MPAA), JMV4168 (DOTA) and ^{nat}AlF-JMV5132 were not significantly different: 6.8 (95% confidence interval [CI], 4.6-10.0) and 13.2 (95% CI, 5.9-29.3), and 10.0 nM

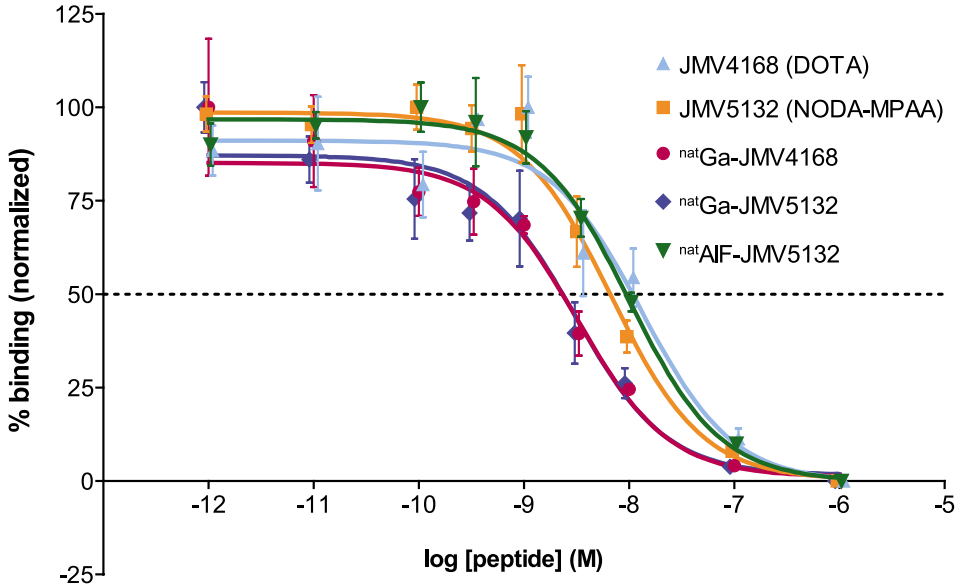

FIGURE 3. Competition binding curves. PC-3 frozen sections were incubated in presence of 5.10^{-10} M [^{125}I-Tyr^4]-BBN and increasing amounts of JMV4168, JMV5132, ^{nat}Ga-JMV4168, ^{nat}Ga-JMV5132, or Al^{nat}F-JMV5132. IC_{50} values (with 95% CIs in parentheses) were 6.8 nM (4.6-10.0) for JMV5132, 13.2 nM (5.9-29.3) for JMV4168, 3.0 nM (1.5-6.0) for ^{nat}Ga-JMV5132, 3.2 nM (1.8-5.9) for ^{nat}Ga-JMV4168, and 10.0 nM (6.3-16.0) for Al^{nat}F-JMV5132.

(95% CI, 6.3-16.0), respectively. IC_{50} values for ^{nat}Ga-JMV5132 (3.0 [95% CI, 1.5-6.0]) and ^{nat}Ga-JMV4168 (3.2 [95% CI, 1.8-5.9]) were lower than their unlabeled counterpart, indicating a higher binding affinity for the GRPR.

Small-Animal PET/CT and Biodistribution Studies

Fused PET and CT images obtained at 1 and 2 h after injection are shown in **Figure 4**. Maximum-intensity projections showed clear visualization of PC-3 tumors with very low background. Predominant renal excretion was observed for all 3

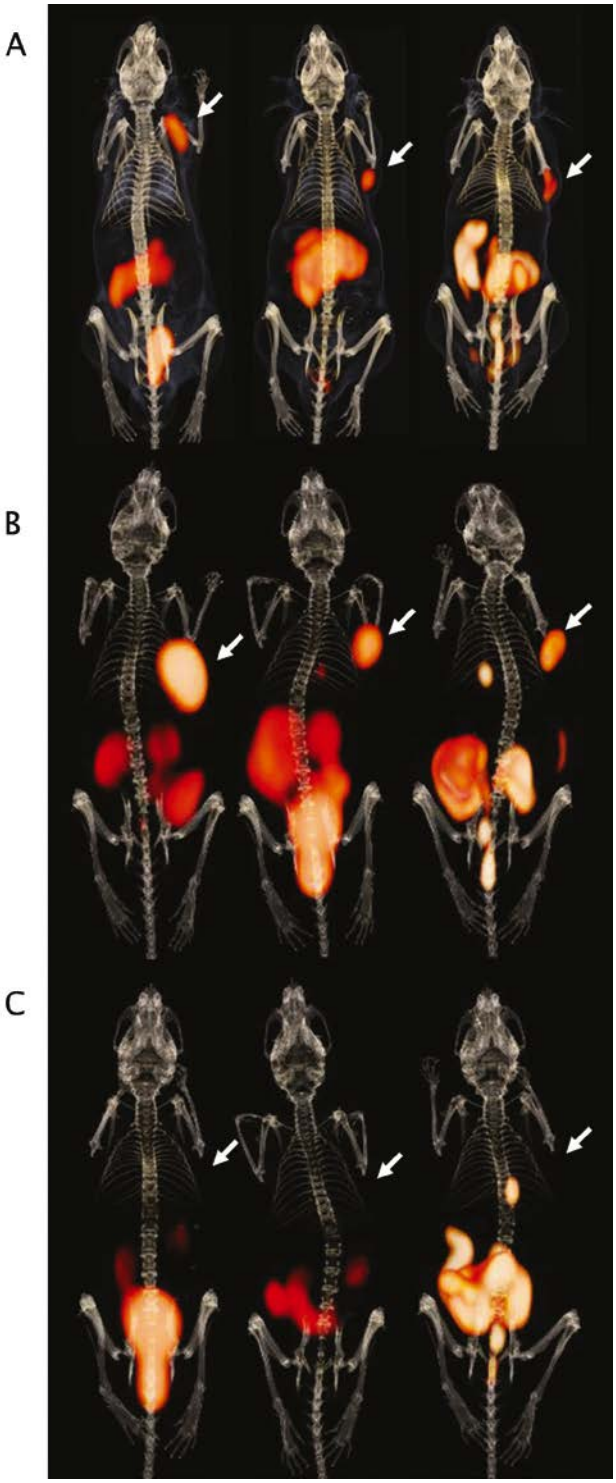

FIGURE 4. PET/CT images of mice bearing subcutaneous PC-3 xenografts on right shoulder (arrow) injected with ^{68}Ga-JMV4168 (left), ^{68}Ga-JMV5132 (center) or Al^{18}F-JMV5132 (right) at 1 h after injection (A), 2 h after injection (B), and 2 h after injection with coinjection of excess unlabeled peptide (C). Beside tumor (arrow), pancreas, intestines, and kidneys can be observed in the abdominal region. Bladder can be distinguished by hot spot below abdomen. Gallbladder can be recognized as hot spot below rib cage.

radiolabeled peptides. Partial hepatobiliary excretion was observed for Al^{18}F-JMV5132 and ^{68}Ga-JMV5132, as indicated by the nonspecific uptake in the gallbladder and intestines. PET images obtained at 2 h after injection showed partial clearance of radioactivity in nontarget tissues such as pancreas, kidney, and intestines as compared to the images obtained at 1 h after injection.

The results of the biodistribution studies of ^{18}F- and ^{68}Ga-labeled peptides are summarized in **Figure 5**. These pharmacokinetic data obtained at 1 and 2 h after injection were in line with the PET images. High and specific uptake of the tracer was observed in the PC-3 tumors. There were no significant difference for ^{68}Ga-JMV4168, ^{68}Ga-

JMV5132, and Al^{18}F-JMV5132, with uptake values (in %ID/g) of 4.46 ± 0.33, 4.73 ± 0.68, 4.96 ± 1.20, respectively, at 1 h after injection and 5.96 ± 1.39, 5.24 ± 0.29, 5.30 ± 0.98, respectively, at 2 h after injection. The uptake in GRPR-positive organs, such as tumor, pancreas, stomach, and intestines, was significantly decreased by coinjection of an excess of unlabeled peptide, indicating GRPR-specific targeting. All tracers displayed fast blood clearance, with 0.09 ± 0.04, 0.19 ± 0.13, and 0.05 ± 0.01 %ID/g remaining in blood at 2 h after injection for ^{68}Ga-JMV4168, ^{68}Ga-JMV5132, and Al^{18}F-JMV5132, respectively. The 3 tracers cleared rapidly from the GRPR-positive pancreas between 1 h (6.14 ± 0.68, 11.42 ± 0.84, 4.21 ± 1.34 %ID/g) and 2 h after injection (1.00 ± 0.24, 1.33 ± 0.25, and 1.41 ± 0.15 %ID/g) for ^{68}Ga-JMV4168, ^{68}Ga-JMV5132, and Al^{18}F-JMV5132, respectively, whereas PC-3 tumor uptake was preserved. The uptake and retention of all tracers in blood, muscle, heart, lung, liver, and bone were relatively low as measured at 2 h after injection (all ≤0.5 %ID/g). Mice injected with Al^{18}F-JMV5132 showed a (significantly) higher uptake in spleen and bone.

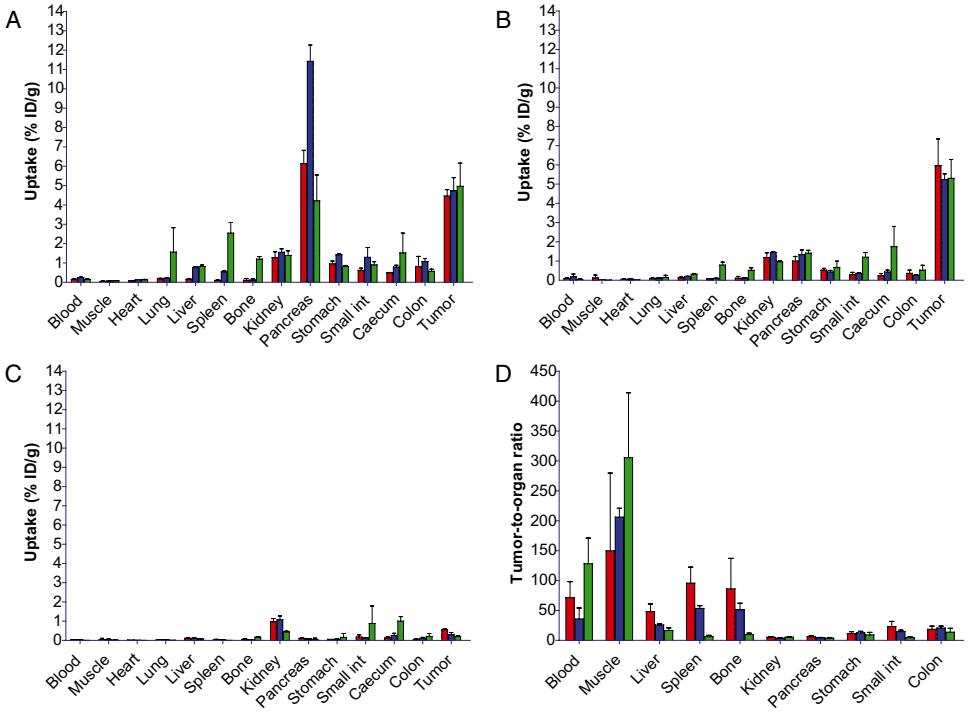

FIGURE 5. Biodistribution of ^{68}Ga-JMV4168 (red), ^{68}Ga-JMV5132 (blue) and Al^{18}F-JMV5132 (green) in mice bearing PC-3 xenografts at 1 h after injection (A), 2 h after injection (B), and 2 h after injection with coinjection of excess unlabeled peptide (C) and tumor-to-organ ratios at 2 h after injection (D). Int = intestines.

DISCUSSION

The use of radiolabeled GRPR antagonists for targeting tumors in vivo has attracted considerable attention, starting with somatostatin receptor antagonists showing higher tumor uptake and targeting more receptor-binding sites than their agonists (*30*). This finding was also extended to GRPR antagonists, with the seminal work of Cescato et al. (*11*). Recently, more articles have appeared showing the promise of novel radiolabeled GRPR antagonists for GRPR-positive tumor imaging (*12, 16-18, 25*). The studies revealed favorable pharmacokinetics of radiolabeled antagonists, including high tumor uptake and fast clearance from nontargeted tissues. Several ^{64}Cu- and ^{68}Ga-labeled receptor antagonists developed for PET imaging of prostate tumors have shown pharmacokinetics superior to ^{64}Cu- or ^{18}F-labeled GRPR agonists described in earlier literature (*12, 16, 17*). Beside a favorable pharmacokinetic profile, the use of antagonists should reduce the occurrence of side effects. In a study in which BBN was infused intravenously in a dose of 15 ng/kg/min over a 90-min period, side effects – among which were nausea, hot flush, and sweating – were observed in 80% of the patients (*13*).

Here, we report on the development of a NODA-MPAA-conjugated GRPR antagonist (JMV5132) labeled with ^{18}F for PET imaging of GRPR-positive tumors and the direct comparison with ^{68}Ga-radiolabeled analogs. In our previous work, the statin-based GRPR antagonist JMV594 was linked to DOTA via a $(\beta Ala)_2$ linker and labeled with ^{111}In. It showed very good tumor targeting in PC-3 xenografts in mice (*25*). In the present study, we conjugated JMV594 to NODA-MPAA for radiolabeling with ^{18}F. The NODA-MPAA-$(\beta Ala)_2$–JMV594 peptide (JMV5132) was labeled with ^{18}F and ^{68}Ga and compared with the ^{68}Ga-labeled DOTA-$(\beta Ala)_2$–JMV594 peptide (JMV4168).

The radiolabeling of peptides via complexation of Al^{18}F by a NOTA chelator was first described by McBride et al. (*24*). This novel technique has been successfully applied to several peptides, including a GRPR agonist (*28*) and recently to GRPR antagonists (*31, 32*). Recently, McBride et al. reported the labeling of peptides with Al^{18}F in a 1-pot, 1-step procedure using the NODA-MPAA chelator (*26, 33*), leading to a kit formulation, after which the labeled peptide could be purified by solid-phase extraction.

In the present study, we further optimized the labeling conditions to achieve Al^{18}F-labeled JMV5132 in less than 20 min with complete incorporation of ^{18}F-fluoride, resulting in a high specific activity (35 MBq/nmol), without the need for purification by solid-phase exctraction. In receptor-binding studies using PC-3 tumor sections, the in vitro affinities of JMV5132 and JMV4168 were comparable, as shown by the similar IC_{50} values, indicating that both chelators apparently affected receptor affinity in a similar way. The peptides labeled with ^{nat}Ga had slightly higher receptor affinities than their unlabeled counterpart, indicating that the presence of Ga^{3+} in the chelator enhanced the affinity of the peptides for the GRPR. The affinity of the peptide labeled with ^{nat}AlF, on the other hand, was not significantly different from its unlabeled counterpart, indicating that the presence of AlF in the chelator did not affect the affinity of the peptide for the GRPR.

The PET images obtained with $Al^{18}F$-JMV5132 showed higher spatial resolution than the images obtained with the ^{68}Ga-labeled tracers, which is most likely due to the longer positron range of ^{68}Ga (*34*) as compared with ^{18}F.

The comparative biodistribution study showed GRPR-specific accumulation of all 3 radiolabeled GRPR antagonists in the tumor. ^{68}Ga-JMV4168, ^{68}Ga-JMV5132, and $Al^{18}F$-JMV5132 tracers showed similar uptake in the GRPR-positive tumor and organs, including PC-3 tumor, pancreas, stomach, and colon. The uptake was receptor-mediated, as confirmed by the reduction of uptake in tumor and other receptor-positive organs after coinjection of excess unlabeled peptide. The washout from receptor-positive organs occurred at different rates. The pancreas uptake decreased from 1 to 2 h after injection by a factor of 6.1, 8.6, and 3.0, whereas tumor uptake was increased by a factor of 1.3, 1.1, and 1.1 for ^{68}Ga-JMV4168, ^{68}Ga-JMV5132, and $Al^{18}F$-JMV5132, respectively. This outcome indicates a higher retention of the tracers in the tumor than in the pancreas.

Despite their low internalization rate, the high and persistent tumor uptake of these radiolabeled antagonists was expected, as it was previously described for a few other radiolabeled antagonists (*11, 12, 16, 18*). This might be explained by a higher number of binding sites for receptor antagonists than agonists, a higher metabolic stability of antagonists, or a strong interaction of the antagonist with the receptor (*11, 16*). In previous studies using radiolabeled GRPR antagonists, a faster clearance from the pancreas and abdominal organs was already observed between 1 and 4 h after injection, in contrast with data concerning radiolabeled GRPR agonists, which showed more sustained retention of activity in the abdominal region. Several reasons for these differences in tissue clearance kinetics have been postulated, including species differences or more efficient perfusion in the pancreas and intestine (*16*). Possible metabolic degradation of the peptide by enzymes in the pancreas might also explain the faster washout from the pancreas.

Clearance from background tissues, such as blood, muscle, heart, lung, liver, and bone, was very fast for all tracers tested, leading to high tumor-to-background ratios, which allowed clear visualization of the tumor. Overall, $Al^{18}F$-JMV5132 showed improved imaging properties, compared with the previously reported $Al^{18}F$-NOTA-8-Aoc-BBN(7-14)NH_2 GRPR agonist (*28*), because that analog showed lower tumor uptake, much higher pancreatic uptake, and higher liver and intestinal uptake in the same animal model.

The slightly higher uptake of $Al^{18}F$-JMV5132 in bone may be due to the presence of trace amounts (<1%) of uncomplexed $Al^{18}F$ or ^{18}F-fluoride or partial defluorination of the tracer in vivo. The uptake of $Al^{18}F$-JMV5132 in bone was relatively low (0.52 ± 0.13 %ID/g 2 h after injection), in comparison with the values reported for the $Al^{18}F$-labeled RM1 derivative (1.58 %ID/g 2 h after injection) (*31*). The increased uptake of $Al^{18}F$-JMV5132 and ^{68}Ga-JMV5132 in the gallbladder, liver, and gastrointestinal excretions indicates partial hepatobiliary excretion of the tracers, because of their

higher lipophilicity, which may be caused by the benzyl group. Considering the clinical application of the tracers, high signal intensity in the intestines may affect visualization of prostate-confined tumor or spread to lymph nodes. Nevertheless, considering the superior imaging characteristics of ^{18}F, further development of Al^{18}F-JMV5132 as a tracer for PCa diagnostic and therapy follow-up is certainly warranted.

CONCLUSION

Highly sensitive and receptor-specific imaging of PCa with PET/CT can be achieved using ^{68}Ga- and ^{18}F-labeled GRPR antagonists. In this study, labeling of JMV5132 with Al^{18}F was completed within 20 min with high specific activity without a need for purification. The ^{68}Ga-JMV4168 tracer showed the most favorable biodistribution, because of its lower hepatobiliary excretion, but the PET images showed a higher resolution with the ^{18}F-JMV5132 tracer. These new PET tracers are promising candidates for future clinical translation.

REFERENCES

1. Siegel R, Naishadham D, Jemal A. Cancer statistics, 2012. CA Cancer J Clin. 2012;62:10-29.
2. Roehl KA, Antenor JA, Catalona WJ. Serial biopsy results in prostate cancer screening study. J Urol. 2002;167:2435-2439.
3. Talab SS, Preston MA, Elmi A, Tabatabaei S. Prostate cancer imaging: what the urologist wants to know. Radiol Clin North Am. 2012;50:1015-1041.
4. Mari Aparici C, Seo Y. Functional imaging for prostate cancer: therapeutic implications. Semin Nucl Med. 2012;42:328-342.
5. Sancho V, Di Florio A, Moody TW, Jensen RT. Bombesin receptor-mediated imaging and cytotoxicity: review and current status. Curr Drug Deliv. 2011;8:79-134.
6. Osborne JR, Akhtar NH, Vallabhajosula S, Anand A, Deh K, Tagawa ST. Prostate-specific membrane antigen-based imaging. Urol Oncol. 2013;31:144-154.
7. Reubi JC, Wenger S, Schmuckli-Maurer J, Schaer JC, Gugger M. Bombesin receptor subtypes in human cancers: detection with the universal radioligand (125)I-[D-TYR(6), beta-ALA(11), PHE(13), NLE(14)] bombesin(6-14). Clin Cancer Res. 2002;8:1139-1146.
8. Ananias HJ, van den Heuvel MC, Helfrich W, de Jong IJ. Expression of the gastrin-releasing peptide receptor, the prostate stem cell antigen and the prostate-specific membrane antigen in lymph node and bone metastases of prostate cancer. Prostate. 2009;69:1101-1108.
9. Markwalder R, Reubi JC. Gastrin-releasing peptide receptors in the human prostate: relation to neoplastic transformation. Cancer Res. 1999;59:1152-1159.
10. Beer M, Montani M, Gerhardt J, et al. Profiling gastrin-releasing peptide receptor in prostate tissues: clinical implications and molecular correlates. Prostate. 2012;72:318-325.
11. Cescato R, Maina T, Nock B, et al. Bombesin receptor antagonists may be preferable to agonists for tumor targeting. J Nucl Med. 2008;49:318-326.
12. Mansi R, Wang X, Forrer F, et al. Evaluation of a 1,4,7,10-tetraazacyclododecane-1,4,7,10-tetraacetic acid-conjugated bombesin-based radioantagonist for the labeling with single-photon emission computed tomography, positron emission tomography, and therapeutic radionuclides. Clin Cancer Res. 2009;15:5240-5249.
13. Basso N, Lezoche E, Speranza V. Studies with bombesin in man. World J Surg. 1979;3:579-585.
14. Bodei L, Ferrari M, Nunn A, et al. Lu-177-AMBA Bombesin analogue in hormone refractory prostate cancer patients: A phase I escalation study with single-cycle administrations. Eur J Nucl Med Mol Imaging. 2007;34:S221-S221.
15. Llinares M, Devin C, Chaloin O, et al. Syntheses and biological activities of potent bombesin receptor antagonists. J Pept Res. 1999;53:275-283.
16. Mansi R, Wang X, Forrer F, et al. Development of a potent DOTA-conjugated bombesin antagonist for targeting GRPr-positive tumours. Eur J Nucl Med Mol Imaging. 2011;38:97-107.
17. Abiraj K, Mansi R, Tamma ML, et al. Bombesin antagonist-based radioligands for translational nuclear imaging of gastrin-releasing peptide receptor-positive tumors. J Nucl Med. 2011;52:1970-1978.
18. Varasteh Z, Velikyan I, Lindeberg G, et al. Synthesis and characterization of a high-affinity NOTA-conjugated bombesin antagonist for GRPR-targeted tumor imaging. Bioconjug Chem. 2013;24:1144-1153.
19. Roivainen A, Kahkonen E, Luoto P, et al. Plasma pharmacokinetics, whole-body distribution, metabolism, and radiation dosimetry of 68Ga bombesin antagonist BAY 86-7548 in healthy men. J Nucl Med. 2013;54:867-872.

20. Kahkonen E, Jambor I, Kemppainen J, et al. In vivo imaging of prostate cancer using [68Ga]-labeled bombesin analog BAY86-7548. Clin Cancer Res. 2013;19:5434-5443.
21. Souvatzoglou M, Weirich G, Schwarzenboeck S, et al. The sensitivity of [11C]choline PET/CT to localize prostate cancer depends on the tumor configuration. Clin Cancer Res. 2011;17:3751-3759.
22. Jambor I, Borra R, Kemppainen J, et al. Functional imaging of localized prostate cancer aggressiveness using 11C-acetate PET/CT and 1H-MR spectroscopy. J Nucl Med. 2010;51:1676-1683.
23. Sanchez-Crespo A. Comparison of Gallium-68 and Fluorine-18 imaging characteristics in positron emission tomography. Appl Radiat Isot. 2013;76:55-62.
24. McBride WJ, Sharkey RM, Karacay H, et al. A novel method of 18F radiolabeling for PET. J Nucl Med. 2009;50:991-998.
25. Marsouvanidis PJ, Nock BA, Hajjaj B, et al. Gastrin releasing peptide receptor-directed radioligands based on a bombesin antagonist: synthesis, (111)in-labeling, and preclinical profile. J Med Chem. 2013;56:2374-2384.
26. D'Souza CA, McBride WJ, Sharkey RM, Todaro LJ, Goldenberg DM. High-yielding aqueous 18F-labeling of peptides via Al18F chelation. Bioconjug Chem. 2011;22:1793-1803.
27. Mueller D, Klette I, Baum RP, Gottschaldt M, Schultz MK, Breeman WA. Simplified NaCl based (68)Ga concentration and labeling procedure for rapid synthesis of (68)Ga radiopharmaceuticals in high radiochemical purity. Bioconjug Chem. 2012;23:1712-1717.
28. Dijkgraaf I, Franssen GM, McBride WJ, et al. PET of tumors expressing gastrin-releasing peptide receptor with an 18F-labeled bombesin analog. J Nucl Med. 2012;53:947-952.
29. de Blois E, Chan HS, Breeman WA. Iodination and stability of somatostatin analogues: comparison of iodination techniques. A practical overview. Curr Top Med Chem. 2012;12:2668-2676.
30. Ginj M, Zhang H, Waser B, et al. Radiolabeled somatostatin receptor antagonists are preferable to agonists for in vivo peptide receptor targeting of tumors. Proc Natl Acad Sci U S A. 2006;103:16436-16441.
31. Liu Y, Hu X, Liu H, et al. A Comparative Study of Radiolabeled Bombesin Analogs for the PET Imaging of Prostate Cancer. J Nucl Med. 2013;54:2132-2138.
32. Varasteh Z, Aberg O, Velikyan I, et al. In Vitro and In Vivo Evaluation of a (18)F-Labeled High Affinity NOTA Conjugated Bombesin Antagonist as a PET Ligand for GRPR-Targeted Tumor Imaging. PLoS One. 2013;8:e81932.
33. McBride WJ, D'Souza CA, Karacay H, Sharkey RM, Goldenberg DM. New lyophilized kit for rapid radiofluorination of peptides. Bioconjug Chem. 2012;23:538-547.
34. Disselhorst JA, Brom M, Laverman P, et al. Image-quality assessment for several positron emitters using the NEMA NU 4-2008 standards in the Siemens Inveon small-animal PET scanner. J Nucl Med. 2010;51:610-617.

2.2

In Vivo Stabilization of a Gastrin-Releasing Peptide Receptor Antagonist Enhances PET Imaging and Radionuclide Therapy of Prostate Cancer in Preclinical Studies

Kristell L.S. Chatalic[1,2,3], Mark Konijnenberg[1], Julie Nonnekens[1,4], Erik de Blois[1], Sander Hoeben[3], Corrina de Ridder[3], Luc Brunel[5], Jean-Alain Fehrentz[5], Jean Martinez[5], Dik C. van Gent[4], Berthold A. Nock[6], Theodosia Maina[6], Wytske M. van Weerden[3], Marion de Jong[1,2]

[1]Department of Nuclear Medicine, Erasmus MC, Rotterdam, The Netherlands
[2]Department of Radiology, Erasmus MC, Rotterdam, The Netherlands
[3]Department of Urology, Erasmus MC, Rotterdam, The Netherlands
[4]Department of Genetics, Erasmus MC, Rotterdam, The Netherlands
[5]IBMM, UMR 5247, CNRS, Université Montpellier, ENSCM, France
[6]Molecular Radiopharmacy, INRASTES, NCSR Demokritos, Athens, Greece

Adapted from: Theranostics 2016; 6(1):104-117

ABSTRACT

A single tool for early detection, accurate staging, and personalized treatment of prostate cancer (PCa) would be a major breakthrough in the field of PCa. Gastrin-releasing peptide receptor (GRPR) targeting peptides are promising probes for a theranostic approach for PCa overexpressing GRPR. However, the successful application of small peptides in a theranostic approach is often hampered by their fast in vivo degradation by proteolytic enzymes, such as neutral endopeptidase (NEP). Here we show for the first time that coinjection of a NEP inhibitor (phosphoramidon (PA)) can lead to an impressive enhancement of diagnostic sensitivity and therapeutic efficacy of the theranostic ^{68}Ga-/^{177}Lu-JMV4168 GRPR antagonist. Coinjection of PA (300 μg) led to stabilization of ^{177}Lu-JMV4168 in murine peripheral blood. In PC-3 tumor-bearing mice, PA coinjection led to a 2-fold increase in tumor uptake of ^{68}Ga-/^{177}Lu-JMV4168, 1 h after injection. In positron emission tomography (PET) imaging with ^{68}Ga-JMV4168, PA coinjection substantially enhanced PC-3 tumor signal intensity. Radionuclide therapy with ^{177}Lu-JMV4168 resulted in significant regression of PC-3 tumor size. Radionuclide therapy efficacy was confirmed by production of DNA double strand breaks, decreased cell proliferation, and increased apoptosis. Increased survival rates were observed in mice treated with ^{177}Lu-JMV4168 plus PA as compared to those without PA. This data shows that coinjection of the enzyme inhibitor PA greatly enhances the theranostic potential of GRPR radioantagonists for future application in PCa patients.

INTRODUCTION

Prostate cancer (PCa) is the most frequently diagnosed cancer and the second leading cause of cancer-related death among men in the United States (*1*). The 5-year relative survival rate for localized and regional PCa is 100%, but decreases to 29% when the cancer has spread to distant sites (*2*). Prognosis and treatment options are strongly related to disease stage and grade at time of diagnosis. Early diagnosed and locally confined tumors can be treated by radical prostatectomy and/or local radiation therapy, whereas for advanced, disseminated PCa curative treatment is not available (*2*). This underlines the importance of early detection and accurate staging for the successful management of PCa patients.

Currently, local staging is mostly based on ultrasound, biopsies, and level of serum prostate-specific antigen. Recent advances in molecular imaging techniques have highlighted the potential of PET imaging, providing a sensitive and noninvasive detection method for PCa lesions. Metabolic PET radiotracers, such as ^{18}F-fluoro-2-deoxy-D-glucose (FDG) or ^{18}F-fluoro-choline have been used to detect recurrent metastatic PCa with high metabolic rates, but are suboptimal for the detection of slow-growing primary tumors.

An alternative strategy focuses on the development of receptor-directed PET imaging agents. PET radiotracers targeting prostate-specific membrane antigen (PSMA) and gastrin-releasing peptide receptor (GRPR) have shown promising results for detection of primary and metastasized PCa in early clinical studies (*3-6*). Besides their use for diagnostic imaging, these targeting agents may also be used as therapeutic agents for tumor-targeted radionuclide therapy of PCa. PSMA-targeted agents labeled with the β-emitting radioisotope ^{177}Lu are currently evaluated in clinical studies (*7, 8*). The powerful combination of diagnosis and therapy by one single probe in a "theranostic" strategy could effectively contribute to a more personalized management of PCa patients, whereby imaging can guide the choice of the most suitable therapeutic option for each patient.

The aim of the present study was to develop a theranostic agent based on a GRPR-antagonist with application prospects in the personalized treatment of PCa patients.

GRPRs are overexpressed in the majority of primary prostate tumors and in a subset of patients with lymph node and/or bone metastasis (*9, 10*), making it an interesting target for radionuclide therapy. GRPR antagonists are promising molecular probes, owing to their superior tumor-targeting and pharmacokinetic properties compared to agonists (*11*). GRPR agonists were also shown to induce side effects in patients, owing to their physiologic activity (*12, 13*). The potential of the ^{68}Ga-labeled GRPR antagonist, JMV4168, for PET imaging of prostate cancer was reported previously in preclinical studies (*14*).

However, delivery of radiopeptides to the tumor will be challenged by the action of proteolytic enzymes present in blood, vasculature walls, liver, lungs, kidneys, and gastrointestinal tract. In vivo degradation of radiopeptides by proteolytic enzymes may hamper their targeting properties, thereby limiting their successful application as theranostic probes. One of the key proteolytic enzymes is neutral endopeptidase 24.11 (NEP, EC 3.4.24.11, neprilysin, CD10, MME), a cell surface metallopeptidase responsible for catalytic inactivation of many neuropeptide substrates, including bombesin-like peptides (*15-17*). NEP is abundantly expressed in the human body, including vasculature walls, major organs, and tissues, potentially hampering radiopeptide-based imaging and therapy by cleaving radiopeptides on the amino side of hydrophobic amino acids. The released inactive radiometabolites will not be able to interact with the tumor-associated target-receptors, and as a result, diagnostic sensitivity and therapeutic efficacy will be severely compromised. In previous studies we have shown that coinjection of a single enzyme inhibitor, phosphoramidon (PA), could stabilize radiopeptides in vivo by inhibition of NEP. This strategy led to notable enhancement of tumor uptake of radiopeptides, whereas uptake in most nontarget healthy tissues was not affected (*18*). We hypothesize that this strategy would be particularly interesting to enhance the therapeutic efficacy of radionuclide therapy as well, by delivering a higher cytotoxic radiation dose to cancer cells at similar dose exposure of healthy tissues.

The aim of this study was to investigate the effect of in vivo stabilization by PA on diagnostic sensitivity and therapeutic efficacy of the GRPR-targeted theranostic agent ^{68}Ga/^{177}Lu-JMV4168 in nude mice with subcutaneous (sc) human prostate tumors.

MATERIALS AND METHODS

Peptide, Reagents, Cell Line, and Mice

JMV4168 (DOTA-βAla-βAla-[H-D-Phe-Gln-Trp-Ala-Val-Gly-His-Sta-Leu-NH_2], **Figure 1**) was synthesized as described previously (*19*). Chemicals were purchased from Sigma-Aldrich, unless otherwise stated. Phosphoramidon (PA) was purchased from Peptides International Inc. $^{177}LuCl_3$ was purchased from IDB Holland and no-carrier added (n.c.a.) ItG $^{177}LuCl_3$ was obtained from ITG Isotope Technologies Garching GmbH. ^{175}Lu was obtained from Merck as 1 g/L standard solution in nitric acid. The human PCa cell line PC-3 was obtained from the American Type Culture Collection (CRL 1435) and cell culture reagents from Life Technologies. Cells were cultured in Ham's F-12K (Kaighn's) Medium supplemented with 10% fetal bovine serum, penicillin (100 units/mL), and streptomycin (100 μg/mL). Cells were grown in tissue culture flasks at 37°C in a humidified atmosphere containing 5% CO_2. Male nude BALB/c mice (age, 8 wk) were obtained from Janvier. All animal experiments were approved by the Animal Experiments Committee under the Dutch Experiments on Animal Act and adhered to the European Convention for Protection of Vertebrate Animals used for Experimental Purposes (Directive 86/609/EEC).

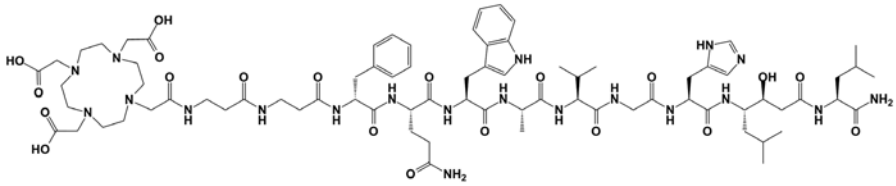

FIGURE 1. Chemical structure of JMV4168 (DOTA-βAla-βAla-[H-D-Phe-Gln-Trp-Ala-Val-Gly-His-Sta-Leu-NH_2]).

Labeling of JMV4168 with ^{68}Ga, ^{177}Lu, and ^{175}Lu

Elution of ^{68}Ga from a ^{68}Ga/^{68}Ge generator (IGG-100, Eckert & Ziegler AG) was performed using fractionated elution with 0.1 M HCl (Rotem Industries Ltd). For PET imaging and biodistribution studies, JMV4168 (1-2 nmol) was mixed with ^{68}Ga eluate (200 µL), sodium acetate (0.5 M, 50 µL) and ethanol (30 µL). The reaction mixture was heated for 10 min at 95°C. After reaction, ethylenediaminetetraacetic acid (EDTA, 4 mM) was added to complex free ^{68}Ga, and the reaction mixture was filtered (0.02 µm Whatman™ filter, GE Healthcare) to remove ^{68}Ga-hydroxides (*20*).

JMV4168 was labeled with carrier-added $^{177}LuCl_3$ (IDB Holland) with a specific activity (ratio between amount of bound radioactivity and total molar quantity of peptide) of 125 MBq/nmol for in vivo stability studies and 60 MBq/nmol for biodistribution studies. Labeling was performed in 20 mM sodium acetate, for 15 min at 80°C. Radioprotectants (gentisic acid, ascorbic acid and methionine, 3.5 mM) were added to prevent radiolysis.

To obtain higher specific activity (i.e. 250 MBq/nmol) for in vivo therapy studies, JMV4168 was labeled with n.c.a. $^{177}LuCl_3$ (ITG Munich) as the presence of ^{176}Lu in carrier-added $^{177}LuCl_3$ limits the maximum achievable specific activity to 125 MBq/nmol. Labeling was performed in 50 mM sodium acetate for 15 min at 80°C with radioprotectants. An excess of diethylenetriaminepentaacetic acid (DTPA, 4 mM) was added to complex free $^{177}LuCl_3$ after reaction.

For control experiments, JMV4168 was labeled with the stable isotope ^{175}Lu. JMV4168 was incubated with a 2-fold molar excess ^{175}Lu in 80 mM sodium acetate, for 15 min at 80°C.

Vehicle for Animal Injection

To allow for injection into mice, the radiolabeled peptide was diluted in a vehicle. For biodistribution studies, vehicle consisted of 5% (v/v) ethanol, 0.05% (w/v) bovine serum albumin (BSA) in phosphate-buffered saline (PBS), pH 7.4, containing a mixture of 0.5 mM radioprotectants. For therapy studies with higher activity concentration, vehicle consisted of 5% (v/v) ethanol, 0.05% (w/v) BSA in PBS, pH 7.4, containing 5 mM radioprotectants.

Quality Control
Labeling efficiency was assessed by instant thin layer chromatography (iTLC) using silica gel coated paper (Varian Medical Systems, Inc.) and 0.1 M citrate buffer pH 5 as eluent. Colloid formation was determined by iTLC using silica gel-coated paper and 1 M NH4OAc:methanol (1:3) as eluent. Radiochemical purity of labeled peptides was analyzed by RP-HPLC on a Breeze system (Waters). A C-18 column (Symmetry Shield, 4.6 mm x 250 mm; particle size 5 µm, Waters) was used at a flow rate of 1 mL/min with the following buffer system: buffer A, 0.1% v/v trifluoroacetic acid in water; buffer B, methanol; with a gradient as follows: 100% buffer A (0-5 min), 60% buffer B (5-5.01 min), 80% buffer B (5.01-20 min), 100% buffer B (20.01-25 min), 100% buffer A (25.01-30 min). The radioactivity of the eluate was monitored using an in-line NaI radiodetector, digital multichannel analyzer and dedicated software (MetorX B.V.). Elution profiles were analyzed using Empower 3 software (Waters).

In Vivo Stability Studies
Non-tumor bearing mice were injected intraperitoneally (ip) with ^{177}Lu-JMV4168 (25 MBq, 200 pmol) in vehicle, or in vehicle containing PA (300 µg). Blood was drawn 15 min after injection and collected in a polypropylene tube coated with EDTA containing PA (30 µg), and 50 nmol of radioprotectants on ice. Plasma proteins were precipitated by adding 50% ethanol, centrifuged for 10 min at 4°C and the extract was analyzed by radio-HPLC. HPLC fractions were collected every min and counted in a γ-counter to quantify intact radiopeptide and degradation products.

Prostate Cancer Xenograft Model
Mice were injected subcutaneously on the right shoulder with a PC-3 cell suspension (3 x 10^6 cells, 200 µL, 67% RPMI, 33% Matrigel [BD Bioscience]). Three to 4 wk after inoculation, tumor size averaged 200 mm^3 and mice were used for biodistribution, PET imaging and therapy studies.

Biodistribution Studies
^{68}Ga-JMV4168 (1 MBq, 200 pmol) was injected intravenously (iv) with vehicle (control) or with PA (300 µg) in vehicle. Mice were euthanized 1 h or 2 h after injection. ^{177}Lu-JMV4168 (0.7 MBq, 200 pmol) was injected iv or ip with or without PA (300 µg) in vehicle. Mice were sacrificed at 1 h, 4 h or 24 h after injection for ^{177}Lu-JMV4168 in controls, and 1 h or 4 h for ^{177}Lu-JMV4168 with PA. Blood, tumor, and relevant organs and tissues were collected, weighed, and counted in a γ-counter (WIZARD, PerkinElmer) with a counting time of 60 sec per sample, isotope-specific energy window and an error not exceeding 5%. The percentage of the injected dose per gram (%ID/g) was determined for each tissue sample.

Dosimetry

Biodistribution data of ^{177}Lu-JMV4168 in controls (iv and ip) were used to estimate the absorbed radiation doses to the organs with physiologic uptake and tumor. A single-exponential expression was fitted to the activity data at 1, 4, and 24 h, and the cumulative activity concentration in each organ was calculated by analytic integration of the fitted expression. Absorbed radiation doses of ^{177}Lu-JMV4168 with PA were estimated assuming equivalent clearance as without PA from 4 to 24 h.

Absorbed radiation doses to the organs were estimated according to the MIRD-scheme (*21*) with the following equation: $D(r_T) = \sum_{r_S} \tilde{A}(r_S) \times S(r_T \leftarrow r_S)$, with $D(r_T)$ the absorbed dose to a target organ r_T, $\tilde{A}(r_S)$ the time-integrated activity in a source organ r_S and $S(r_T \leftarrow r_S)$ the absorbed dose rate per unit activity of ^{177}Lu. The S-values were obtained for a standardized 25 g mouse from the RADAR realistic animal models (*22*). The biodistribution data are measured in activity concentration and hence the time-integrated activity concentration is obtained and this is multiplied with the source organ mass, as used in the phantom for the S-value calculation.

The Linear Quadratic (LQ) model was used to predict cell survival for PC-3 radiation response (α = 0.13 /Gy, β = 0.024 /Gy^2, doubling time of 11 d, sub-lethal repair half-life Tμ = 1 h, clonogenic cell density; 10^7/g) (*23*). Radiation sensitivity was estimated by external ^{137}Cs gamma irradiation (data not shown), resulting in LQ model fit (Pearson R^2 = 0.99) with α= 0.13 ± 0.02 /Gy, β = 0.025 ± 0.005 /Gy^2 (α/β = 5.5 Gy). Doubling time was estimated by fitting an exponential growth expression into PC-3 tumor growth curve in our model. Tumor control as a function of absorbed dose *D* over time T was expressed by Poisson statistics expressing the probability for survival S of 1 or more clonogenic cells from the original number of clonogenic cells $N_{clonogens}$ by:

$TCP = \exp\left(-N_{clonogens} S(D)\right)$, with the survival

$$S(D,T) = \exp\left(-\alpha D(T)\left(1 + \frac{G(T)}{\alpha/\beta} \times \frac{D(T)}{N}\right) + \gamma T\right)$$

with γ the tumor growth constant and N the number of therapy cycles used.

The dose prolongation factor G(T) can be approximated by the value integrated to infinity for single exponential dose buildup with effective half-life T_{eff}: $G(\infty) = \frac{T_\mu}{T_\mu + T_{eff}}$ (*24*). A Tumor Control Probability of > 90% was considered as being successful.

Small-Animal PET

Mice were injected iv with 2-8 MBq of ^{68}Ga-JMV4168 (200 pmol) in vehicle or vehicle containing PA (300 µg). Mice were scanned 2 h after injection, on a heated bed under

isoflurane/O_2 anesthesia, in a small animal PET scanner (Inveon; Siemens Preclinical Solutions). PET emission scans were acquired for 45 min, followed by a transmission scan (402 s). Scans were reconstructed using Inveon Acquisition Workplace software (version 1.5; Siemens Preclinical Solutions), using a 3-dimensional ordered-subset expectation maximization/maximization a posteriori algorithm with the following parameters: matrix, 256 x 256 x 161; pixel size, 0.40 x 0.40 x 0.796 mm; and β-value, 1.0, with uniform variance and OPMAP. Images were rescaled to account for differences in injected dose.

Therapy Studies

Mice received 4 ip injections in 2-d intervals of either PBS, ^{177}Lu-JMV4168 (50 MBq, 200 pmol) in vehicle or ^{177}Lu-JMV4168 (50 MBq, 200 pmol) in vehicle containing PA (300 μg). To exclude a possible antitumor effect of radioprotectants, GRPR-antagonist or PA, a separate experiment was performed: mice received 4 ip injections of PBS, ^{175}Lu-JMV4168 in vehicle, or ^{175}Lu-JMV4168 in vehicle containing PA (300 μg). Tumor size was followed twice weekly by caliper measurements, endpoints were tumor size exceeding 1.5 cm^3, or survival of 94 d after the first injection.

GRPR Expression, Histology, and Molecular Characteristics

In order to study the molecular response of tumor cells to therapy, 2 mice of each group were sacrificed 8 d after start of therapy, and tumor was dissected. At the endpoint of the experiment, tumor, kidney, and pancreas from sacrificed animals of each group were dissected. For each organ half was frozen in liquid nitrogen and half was fixed in 10% neutral buffered formalin at 4°C. After fixation and routine dehydration, tissue samples were embedded in paraffin.

GRPR expression after radionuclide therapy treatment was assessed on frozen tumor sections (10 μm) using autoradiography as described earlier (*14*). In brief, frozen tissue sections were incubated with ^{177}Lu-JMV4168 (10^{-10} M) for 1 h in binding buffer containing 1% w/v BSA. Unlabeled JMV4168 was used for blocking (10^{-6} M). Radioactivity was measured using a phosphor imager system (Cyclone, Packard A431201, PerkinElmer) and data obtained on different phosphor screens was normalized against a positive control slide (PC-295 xenograft tumor (*25*)).

Histology was performed on paraffin-embedded kidney and pancreas sections (4 μm). Sections were stained with hematoxylin and eosin for microscopic examination using standard protocols. Immunofluorescence and TUNEL staining were performed on paraffin-embedded tumor sections (4 μm) of mice sacrificed 8 d after therapy.

For immunofluorescence staining, tumor sections were deparaffinized, rehydrated, and target antigen retrieval was performed using DAKO Antigen Retrieval buffer (pH

6.9) for 15 min at 100°C. Cells were permeabilized in PBS containing 0.1% Triton X-100 for 10 min and incubated in blocking buffer [PBS, 0.1% Triton X-100, 2% BSA]. Primary antibodies [anti-GEMININ (10802-1-AP, Proteintech Group, 1/400 dilution), anti-53BP1 (NB100-304, Novus Biologicals, dilution 1/1000), or anti-γH2AX (05-636, Merck-Millipore, dilution 1/500)] were diluted in blocking buffer and incubated for 90 min at room temperature. Secondary antibodies (Alexa Fluor 594 or 488, Life Technologies; dilution 1/1000) were diluted in blocking buffer and incubated for 60 min at room temperature.

For apoptotic cell detection TUNEL staining was performed. Tumor sections were stained using an *in situ* cell death detection kit (11684795910, Roche). Briefly, cells were deparaffinized, rehydrated and incubated in PBS containing 0.5% Triton X-100 and proteinase K (20 µg/ml) for 15 min at room temperature. Cells were incubated in PBS containing 0.1% Triton X-100 and 0.1% sodium citrate for 2 min on ice, followed by TUNEL labeling for 1 h at 37°C. Imaging was performed using a DM4000 fluorescent microscope (Leica).

γH2AX and 53BP1 imaging was performed using a TCS SP5 confocal microscope (Leica) and GEMININ imaging using a DM4000 fluorescent microscope (Leica).

53BP1/γH2AX foci quantification was performed with ImageJ software using automated threshold settings. GEMININ and TUNEL positive cells were counted manually and compared to the total number of DAPI-positive cells. Approximately 1000 (53BP1/γH2AX) or 400 (GEMININ/TUNEL) DAPI-positive cells from different microscope fields per condition were evaluated.

Statistical Analysis

Statistical analysis was performed using GraphPad Prism version 5.01. Biodistribution data are represented as the mean %ID/g ± SD, with group sizes of 3-4 mice. Statistical analysis of biodistribution data was performed using a 2-way ANOVA with a Tukey's multiple comparisons test, and the level of significance was set at $P < 0.05$.

Mean tumor size with 95% confidence interval were displayed for the period that all mice of one group were still in the experiments. Mice were sacrificed when tumor exceeded 1.5 cm^3, causing the mean size to drop, which made the comparison of the means not fair after that period. Survival analysis is displayed up to day 94, corresponding to a maximum follow up time.

Statistical analysis of mean tumor size of all groups was performed up to day 24, when all animals were still in the experiment. A 2-way ANOVA with repeated measures was used to compare the 3 groups, with a Tukey's multiple comparison test. Tumor size of the two treated groups was compared up to day 66, with a 2-tailed paired t-test. Statistical analysis of survival data was performed using a Mantel-Cox Chi square

test, with a level of significance set at $P < 0.05$, corrected to 0.0167 for multiple comparisons.

Tumor growth was analyzed by performing a nonlinear regression fit of an exponential growth curve to the control group. The Aikake information criterion was used to determine whether the growth was exponential or showed a Gompertzian type of growth. The tumor growth data of the treated animals were fitted by an initial exponential growth curve till the onset time of shrinkage and an exponential regrowth curve. Extrapolations of the growth curves for animals that were taken out of the experiment because of too large tumor sizes enabled establishment of a mean growth curve.

RESULTS

Radiolabeling of JMV4168 with ^{68}Ga and ^{177}Lu

^{68}Ga-JMV4168 was obtained with a specific activity of 50 MBq/nmol. ^{177}Lu-JMV4168 could be obtained with a specific activity of up to 125 MBq/nmol using carrier added ^{177}Lu/^{176}Lu and 250 MBq/nmol using n.c.a. ^{177}Lu. Labeling efficiency for ^{68}Ga-JMV4168 and ^{177}Lu-JMV4168 exceeded 97% as determined by iTLC. Radiopeptides were not purified and radiochemical purity of preparations used in in vivo experiments exceeded 96% for ^{68}Ga-JMV4168 and 94% for ^{177}Lu-JMV4168, as determined by RP-HPLC. An excess of EDTA/DTPA was added to complex free ^{68}Ga/^{177}Lu and limit accumulation in bone. Protection of ^{177}Lu-JMV4168 with radioprotectants (methionine, gentisic acid, and ascorbic acid) was required to preserve the peptide from radiolysis (*26*). Radioprotectants were added in the labeling reaction,

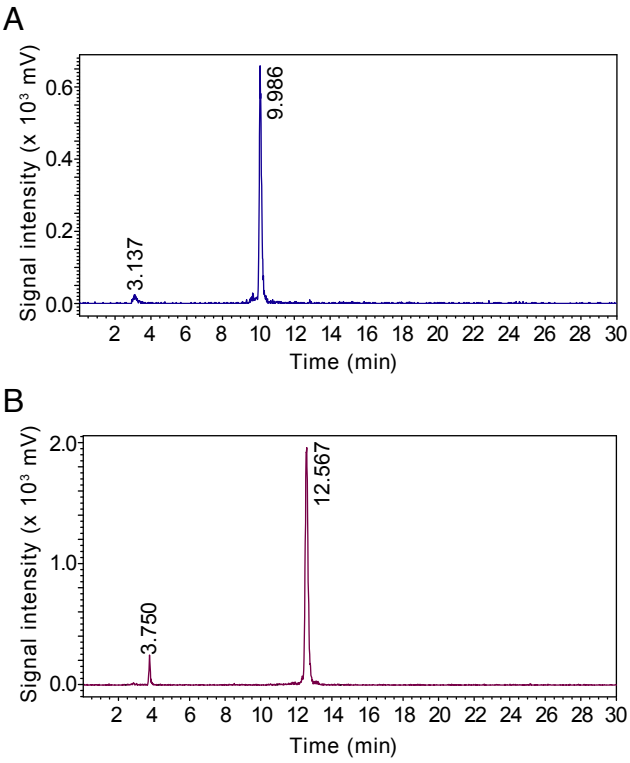

FIGURE 2. Radio-HPLC chromatograms of ^{68}Ga-JMV4168 (A) and ^{177}Lu-JMV4168 (B).

as well as in the formulation for mouse injection. Radio-HPLC elution profiles of ^{68}Ga- and ^{177}Lu-JMV4168 are shown in **Figure 2**. ^{68}Ga-JMV4168 and ^{177}Lu-JMV4168 had retention times of 9.99 min and 12.57 min, respectively.

PA Stabilizes ^{177}Lu-JMV4168 in Murine Peripheral Blood

In vivo stability studies resulted in 48% intact ^{177}Lu-JMV4168 in peripheral blood after 15 min, and an increase to 84% intact radiopeptide upon coinjection of PA.

PA Enhances Tumor Uptake of ^{68}Ga- and ^{177}Lu-JMV4168 in PC-3 Xenograft Mice

The results of the biodistribution studies of ^{68}Ga- and ^{177}Lu-JMV4168 are summarized in **Figure 3**. Biodistribution patterns of ^{68}Ga- and ^{177}Lu-JMV4168 at 1 h after injection were comparable ($p > 0.05$ for all organs). Tumor uptake (in %ID/g ± SD) at 1 h after iv injection increased from 9.9 ± 1.3 to 19.1 ± 2.6 (^{68}Ga-JMV4168, $p < 0.0001$) and from 9.0 ± 3.9 to 17.2 ± 1.7 (^{177}Lu-JMV4168, $p < 0.0001$) upon coinjection of PA. Uptake in the GRPR-positive pancreas was increased at 1 h after iv injection for ^{68}Ga-JMV4168 ($p < 0.0001$), but not for ^{177}Lu-JMV4168, upon coinjection of PA. No significant increase in uptake in non-target tissue was observed, resulting in high tumor-to-background ratios. A 3-fold decrease in pancreatic uptake was observed for ^{68}Ga-JMV4168 from 1 to 2 h after injection, whereas tumor uptake remained stable, leading to increased tumor/pancreas ratio over time. Biodistribution patterns of ^{177}Lu-JMV4168 after iv or ip injection were fairly comparable. Increased uptake in pancreas was observed at 1 h after ip injection in comparison with iv injection ($p < 0.0001$), but no differences were observed at later time points. Tumor uptake values (in %ID/g ± SD) at 1, 4, and 24 h after injection were 9.0 ± 3.9, 8.3 ± 1.7, and 4.2 ± 1.0 after iv, versus 8.9 ± 2.4, 7.2 ± 2.1, and 4.5 ± 0.7 after ip injection, respectively. Tumor uptake at 4 h after injection increased to 12.9 ± 3.5 (iv), and 14.5 ± 3.7 (ip) upon coadministration of PA.

Dosimetry of ^{177}Lu-JMV4168 in PC-3 Xenograft Mice

Single-exponential curves could be fitted to the biodistribution data; the tumor showed comparable clearance half-lives for the two types of injection (20.8 ± 8.5 h (iv) and 24.4 ± 8.3 h (ip)). Estimated absorbed radiation doses (in Gy) from 50 MBq ^{177}Lu-JMV4168 in tumor, kidneys, and pancreas were 10, 3.5, 2.5 Gy, and 11, 7.3, 4.4 Gy after iv and ip injections, respectively. Absorbed doses for tumor, kidneys, and pancreas for ^{177}Lu-JMV4168 with PA were 16, 3.7, 3.1 and 20, 7.6, 4.8 Gy after iv and ip injections, respectively, assuming equivalent clearance from 4 to 24 h as without PA. No significant differences were observed for absorbed radiation doses of normal organs for ^{177}Lu-JMV4168 and ^{177}Lu-JMV4168 with PA.

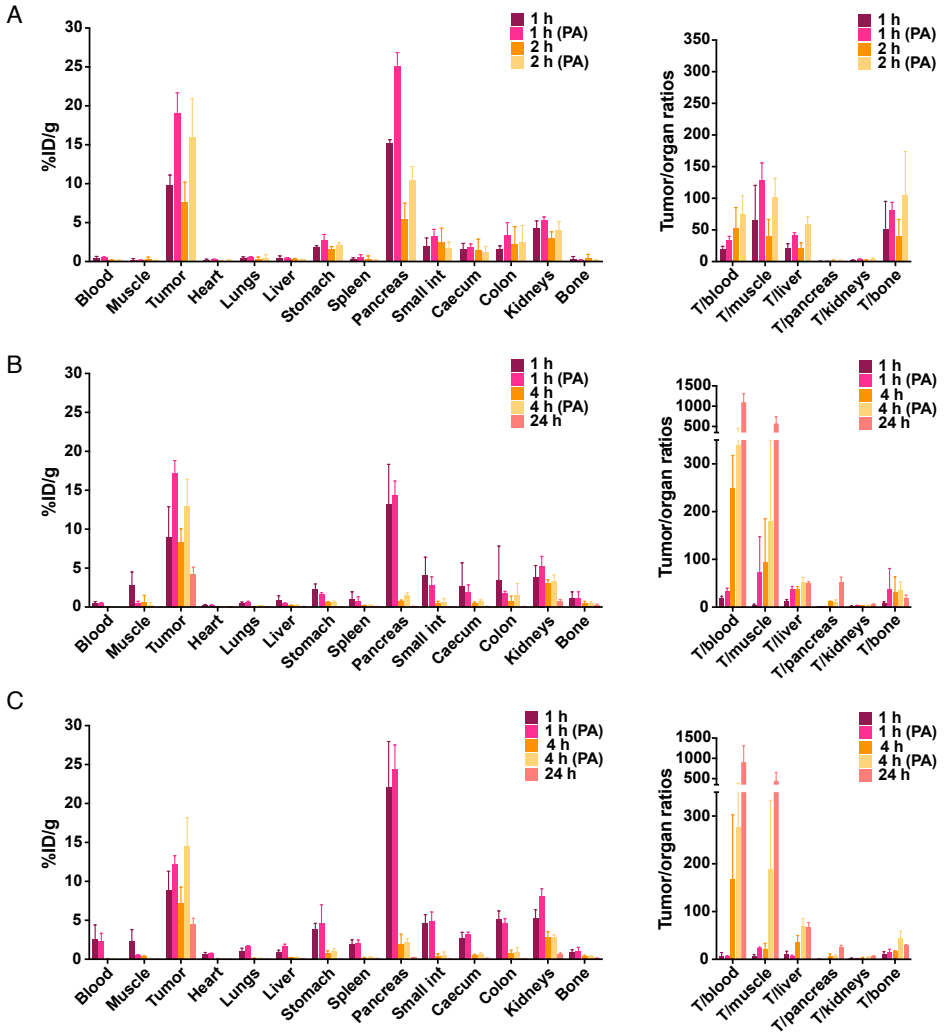

FIGURE 3. Effect of phosphoramidon (PA) on the biodistribution of ^{68}Ga-JMV4168 (200 pmol, 1 MBq) administered intravenously (iv) at 1 and 2 h after injection (A) and ^{177}Lu-JMV4168 (200 pmol, 0.7 MBq) administered intravenously (B) or intraperitoneally (C) at 1, 4, and 24 h after injection (n=3-4 per group). Biodistribution of ^{68}Ga-JMV4168 and ^{177}Lu-JMV4168 at 1 h after injection were comparable. Tumor uptake of ^{177}Lu-JMV4168 injected intraperitoneal and intravenously were comparable. Tumor uptake and tumor-to-background ratios were increased in the presence of PA.

Based on the absorbed doses in PC-3 tumors, it was predicted that a single ip dose of 367 MBq (81 Gy) ^{177}Lu-JMV4168 would have a 95% probability to elicit full tumor control. However, a maximum of 50 MBq (200 pmol) could be administered per injection (specific activity of 250 MBq/nmol). For ^{177}Lu-JMV4168 alone, 8 cycles of therapy (8 x 50 MBq, ip) with 2-d intervals would be needed to reach 98% TCP. Upon

coadministration of ^{177}Lu-JMV4168 and PA, 4 cycles of therapy (4 x 50 MBq, ip) with 2-d intervals would be needed to reach 93% TCP (**Figure 4**).

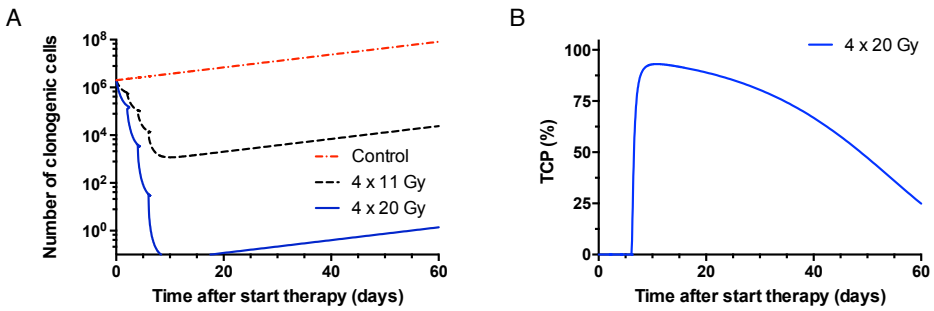

FIGURE 4. Theoretical survival curve of clonogenic cells in PC-3 xenograft (200 mg, 2 x 10^6 clonogenic cells at the start) after therapy with 4 injections (2-d intervals) of 50 MBq of ^{177}Lu-JMV4168 (4 x 11 Gy) and ^{177}Lu-JMV4168 + phosphoramidon (4 x 20 Gy) (A). Tumor control probability (TCP) curve for the therapy with phosphoramidon is shown, reaching a 93% TCP after 9 d (B).

PA Enhances Sensitivity of Small-Animal PET Imaging of ^{68}Ga-JMV4168 in PC-3 Xenograft Mice

PET images obtained at 2 h after iv injection of ^{68}Ga-JMV4168 are presented in **Figure 5**, showing clear, high-contrast visualization of PC-3 tumors. Visualization of PC-3 tumors was substantially improved by coinjection of PA, as shown by the increased signal intensity in the tumors.

PA Augments Therapeutic Efficacy of ^{177}Lu-JMV4168 in PC-3 Xenograft Mice

Therapy studies were conducted in PC-3 tumor-bearing mice receiving 4 cycles of PBS, ^{177}Lu-JMV4168, or ^{177}Lu-JMV4168 plus PA (**Figures 6 and 7**). The ^{177}Lu-JMV4168-treated mice showed significant reduction in tumor size as compared to control (PBS) mice. At day 24 after start of therapy, mean tumor volumes (in mm^3 ±SD) were 1181 ± 402, 146 ± 35 and 145 ± 45 for PBS, ^{177}Lu-JMV4168 and ^{177}Lu-JMV4168 plus PA, respectively. Tumor regrowth was observed for both treated groups, with mean tumor volumes (in mm^3 ± SD) of 770 ± 456 and 381 ± 264 at day 66 for ^{177}Lu-JMV4168 and ^{177}Lu-JMV4168 plus PA, respectively. Consequently, mice in both treated groups had an increased survival as compared to the control group ($P < 0.0001$) and mice treated with ^{177}Lu-JMV4168 plus PA had an increased survival as compared to mice treated with ^{177}Lu-JMV4168 alone ($P = 0.0157$). Median survival increased from 35 to 79 d upon treatment with ^{177}Lu-JMV4168, whereas the median survival in mice treated with ^{177}Lu-JMV4168 plus PA was > 94 d, which was the endpoint of the experiment. Animal body weight remained stable during the course of the experiment and no apparent toxicity was observed (**Figure 7**).

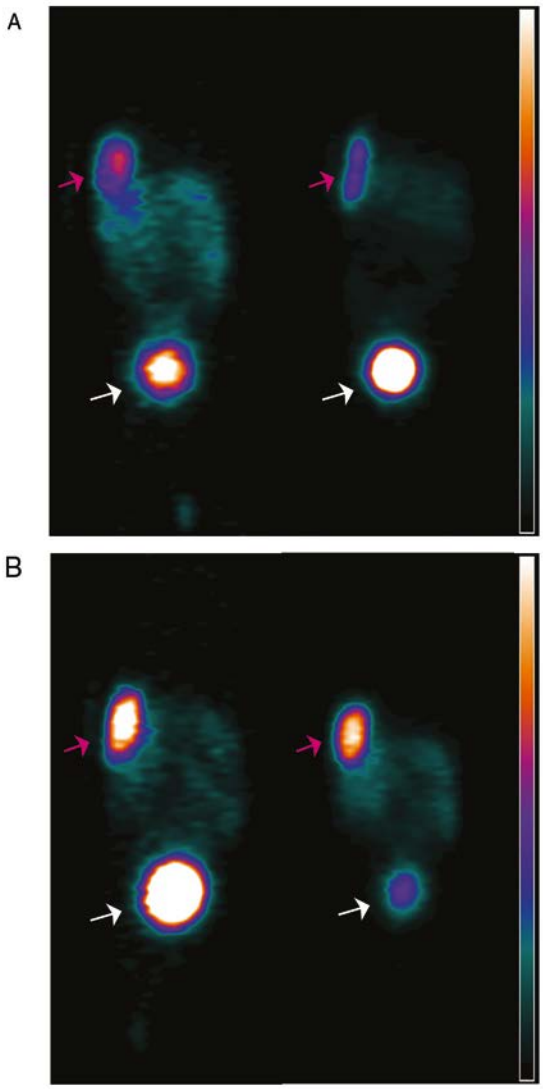

FIGURE 5. PET images of duplicate mice bearing subcutaneous PC-3 xenografts near the shoulder (pink arrow) injected with ^{68}Ga-JMV4168 (A), or ^{68}Ga-JMV4168 with phosphoramidon (B) at 2 h after injection, illustrating the higher tumor uptake in the presence of phosphoramidon. Excretion of the radiolabeled peptide in the bladder (white arrow) can be observed. Scale bar; 0 to 10^5 kBq/mL.

No significant differences in tumor growth and survival were observed for the groups treated with PBS, ^{175}Lu-JMV4168 or ^{175}Lu-JMV4168 plus PA, showing that vehicle, ^{175}Lu-JMV4168 and PA had no effect on tumor growth (**Figure 6**).

^{177}Lu-JMV4168 Radionuclide Therapy Results in DNA Damage, Apoptosis, and Decreased Proliferation and Does Not Affect GRPR Expression of PC-3 Tumors

Histological analysis of tumors, kidneys, and pancreas dissected at the endpoint of the experiment showed overall healthy tissue, with some necrotic areas in the tumors (data not shown). Staining of molecular characteristics (DNA damage, replication, apoptosis, and GRPR expression) of tumors from mice sacrificed 8 d after the last injection is presented in **Figures 8-10**.

Tumors from the groups treated with ^{177}Lu-JMV4168 and ^{177}Lu-JMV4168 plus PA showed an increased number of DNA double strand breaks (DSBs) as shown by phosphorylated histone 2AX (γH2AX) and p53-binding protein 1 (53BP1) foci formation in the tumor cell nuclei. Coinjection with PA increased the amount of produced DSBs. Furthermore, decreased numbers of cells expressing GEMININ (replicating cells) and increased numbers of TUNEL-positive cells (apoptotic cells)

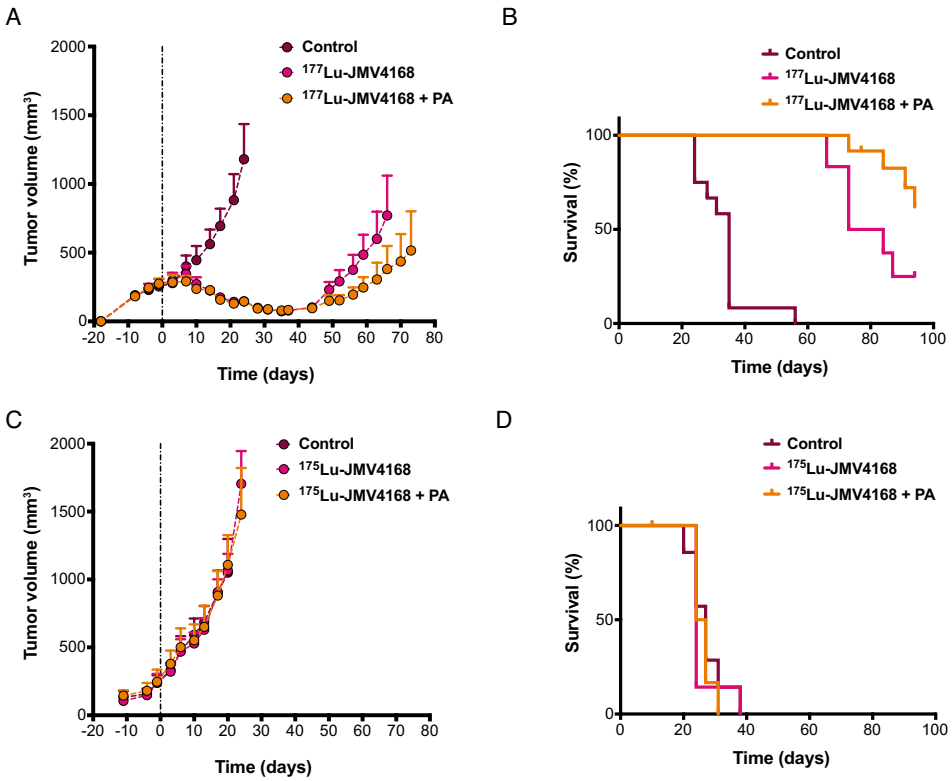

FIGURE 6. Effect of phosphoramidon (PA) on therapeutic efficacy of ^{177}Lu-JMV4168 to treat subcutaneous PC-3 tumors. Mice were treated with 4 injections of ^{177}Lu-JMV4168 (50 MBq, 200 pmol, n=12 per group) or ^{175}Lu-JMV4168 (200 pmol, n=7 per group) on d 0, 2, 4, and 6, with or without PA. Mean tumor volume with 95% confidence interval (A, C) are displayed for the duration that no data point was missing. Kaplan-Meier survival curves (B, D) are displayed for the event of tumor volume exceeding 1500 mm^3. All growth curves of the control mice could be fitted by an exponential growth curve, none should evidence for Gompertzian type of growth. The mean tumor volume doubling time was 11.2 ± 1.2 d. Regrowth of tumors in the treated animals was found after a kick-off time of 32 ± 4 d (^{177}Lu-JMV4168) and 35 ± 6 d (^{177}Lu-JMV4168 + PA) and showed comparable regrowth doubling times to the initial and control growth curves. No significant differences in tumor growth and survival were observed for the groups treated with PBS, ^{175}Lu-JMV4168 or ^{175}Lu-JMV4168 with PA.

were observed after ^{177}Lu-JMV4168 treatment. GRPR binding of ^{177}Lu-JMV4168 on frozen tumor sections was preserved in PC-3 tumors from all groups.

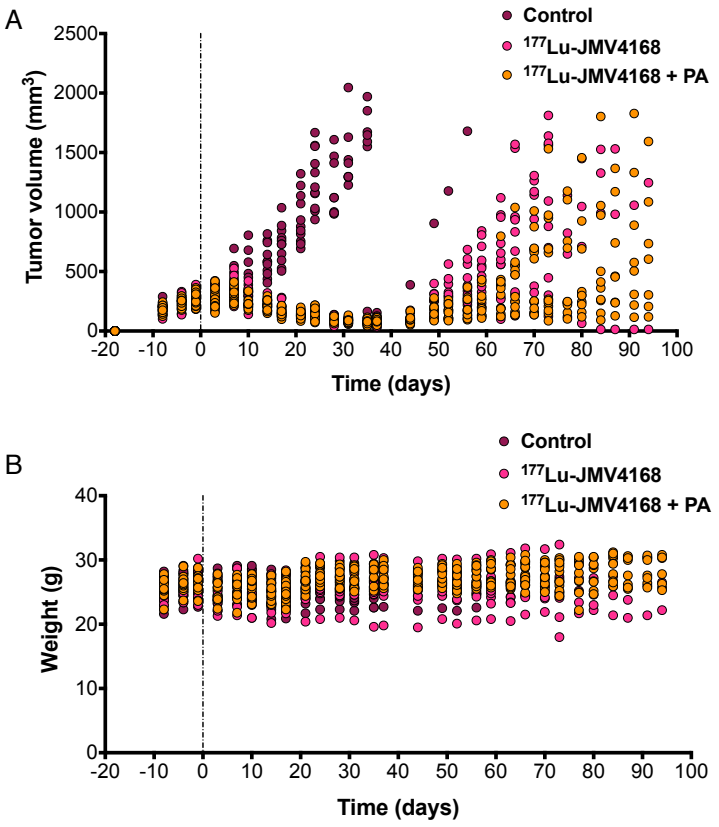

FIGURE 7. Therapeutic efficacy of ^{177}Lu-JMV4168 to treat subcutaneous PC-3 tumors. Tumor size (A) and weight (B) followup of mice treated with 4 injections of ^{177}Lu-JMV4168 (50 MBq, 200 pmol) on d 0, 2, 4, and 6, with or without PA (n=12 per group).

DISCUSSION

In the search for an improved personalized cancer management, the field of theranostics is emerging, applying imaging diagnostics into the choice of the most suitable therapy for each patient. Bombesin analogs have been widely used for molecular imaging (*27*) and radionuclide therapy (*28-30*) of PCa. The field was initially focused on bombesin agonists until a change in paradigm was introduced with somatostatin receptor (SSTr) antagonists, which despite their poor internalization rate have shown more favorable pharmacokinetics and higher tumor uptake than agonists (*31-33*). Similarly to SSTr antagonists, GRPR antagonists have shown superior tumor-targeting and pharmacokinetic properties as compared to agonists (*11*), with promising characteristics for imaging (*3, 4*) and therapeutic applications (*34*).

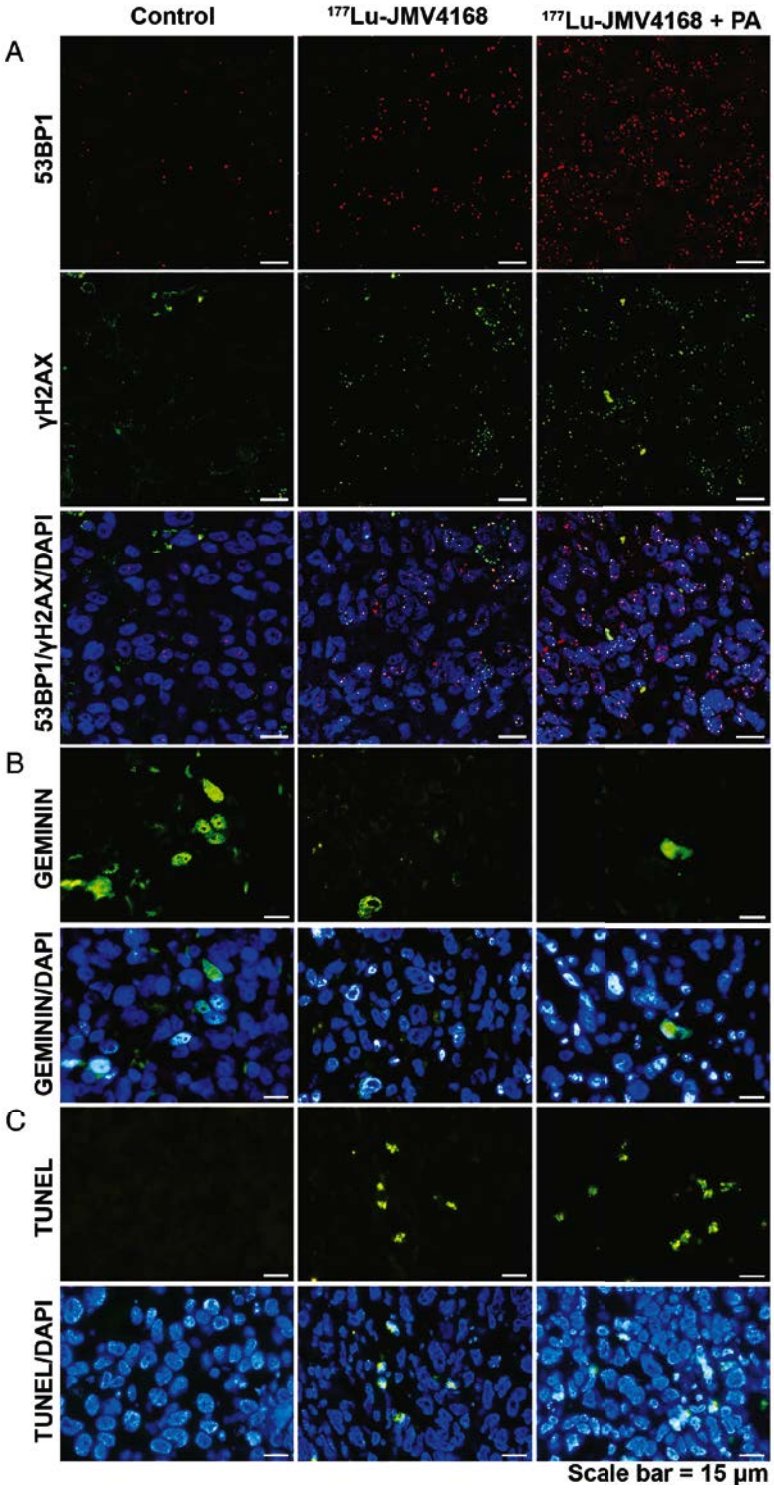

FIGURE 8.
Representative pictures of 53BP1 and γ H2AX staining (A), GEMININ staining (B) and TUNEL assay (C) on PC-3 paraffin-embedded tissues, 8 d after radionuclide therapy (control, ^{177}Lu-JMV4168, and ^{177}Lu-JMV4168 with phosphoramidon (PA)).
Scale bar = 15 μm.

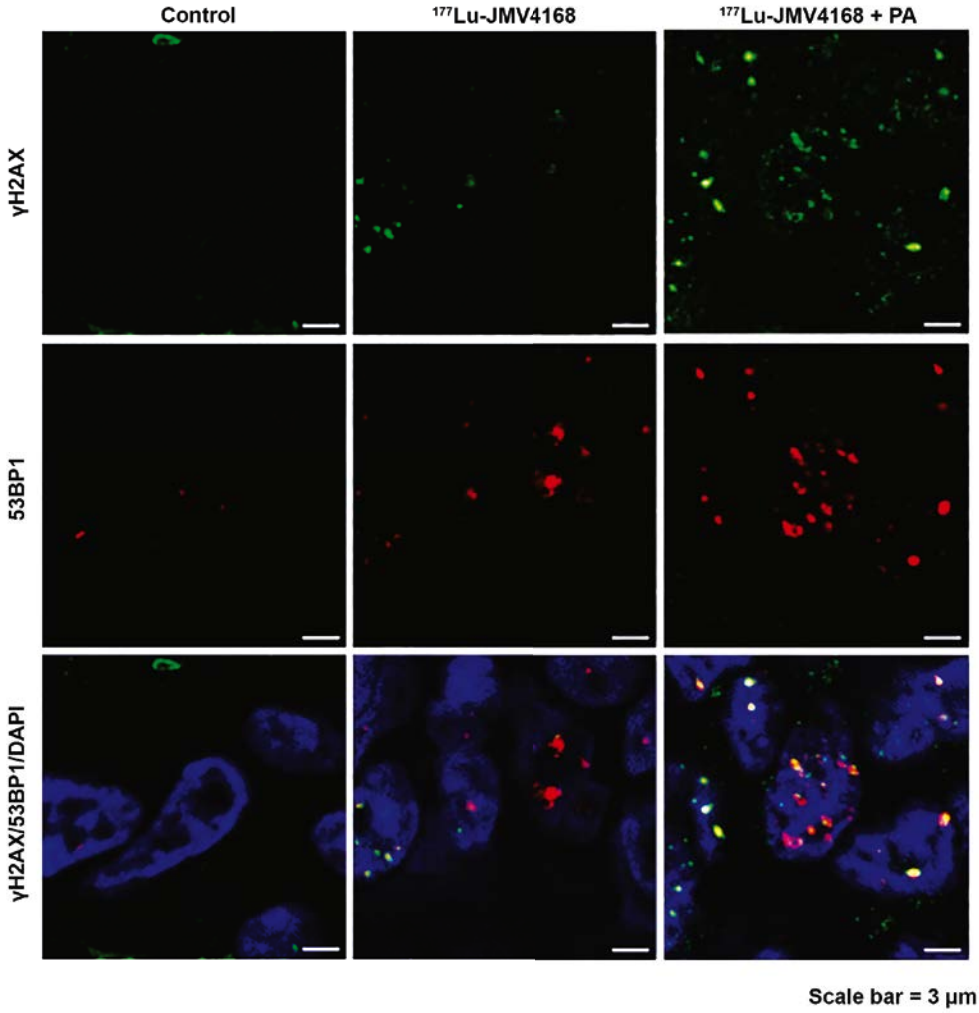

FIGURE 9. Representative pictures of γH2AX and 53BP1 foci staining on PC-3 paraffin-embedded tissues 8 d after radionuclide therapy (control, ^{177}Lu-JMV4168 and ^{177}Lu-JMV4168 with phosphoramidon (PA)). Scale bar = 3 µm.

Moreover, the use of GRPR antagonists should prevent side effects such as nausea, hot flush, and sweating, which were previously observed in patients injected with a bombesin receptor agonist (*12, 13*). In a previous study performed by Dumont et al. (*34*) the potential of GRPR-targeted radionuclide therapy using a GRPR antagonist, ^{177}Lu-RM2, and enhancement of therapeutic efficacy in combination with rapamycin were reported.

GRPR antagonists can be used as theranostic agents for PCa, but rapid in vivo degradation of these peptides by proteolytic enzymes may strongly hamper their

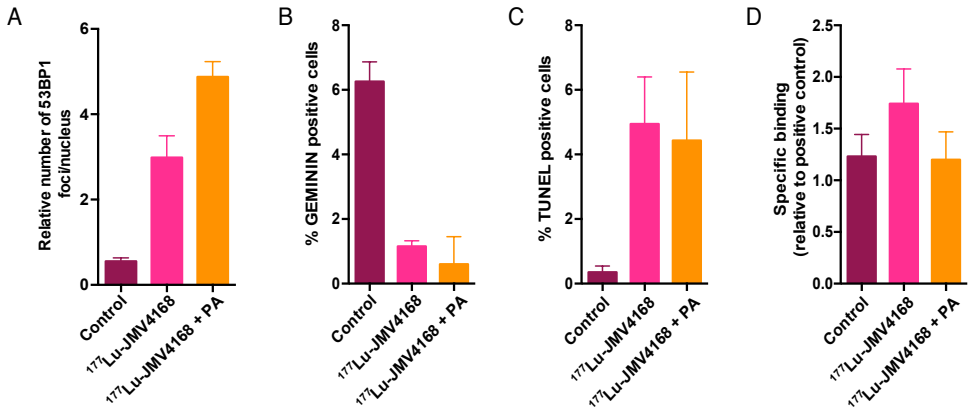

FIGURE 10. Quantification of number of 53BP1 foci per nucleus (A), and number of cells scored positive for GEMININ (B) or TUNEL (C) on PC-3 paraffin-embedded tissue, 8 d after radionuclide therapy. (D) GRPR binding of ^{177}Lu-JMV4168 on PC-3 frozen sections after radionuclide therapy (endpoint).

targeting properties. Strategies to improve in vivo stability of radiolabeled peptides include various structural modifications, such as key amino acid substitutions, reduction/methylation of biodegradable bonds or cyclization, but these modifications can cause undesired changes in pharmacokinetics and/or impair receptor affinity (*35-37*). The proteolytic enzyme NEP, which is abundant in the human body (*38-40*), cleaves peptides on the amino side of hydrophobic amino acids, thereby inactivating a broad range of neuropeptides, including bombesin-like peptides (*15-17*). Recently we have shown that coinjection of the NEP inhibitor PA (*41*) could stabilize radiolabeled bombesin, minigastrin, and somatostatin analogs in vivo, leading to enhanced tumor uptake (*18, 42*).

In this preclinical study, we have brought this in vivo stabilization concept to the next level, showing that coinjection of PA can contribute to an impressive enhancement in diagnostic sensitivity and therapeutic efficacy of a GRPR-targeted theranostic agent. We labeled the GRPR antagonist JMV4168 with ^{68}Ga for PET imaging and ^{177}Lu for radionuclide therapy. All in vivo studies were performed with 200 pmol JMV4168, which appeared to be the optimal peptide dose in previous experiments (data not shown). The dose of 300 µg of PA was chosen based on previous experience (*18*). Optimization of PA-dose for this ^{68}Ga-/^{177}Lu-JMV4168 theranostic pair has not been conducted, because the major purpose of the present study has been to show the PA-effect in therapy in a qualitative "proof-of-principle" approach. ^{177}Lu-labeling of JMV4168 with very high specific activities (250 MBq/nmol) could be achieved using n.c.a. ^{177}Lu. In vivo stability studies in mice showed excellent stabilization of ^{177}Lu-JMV4168 in peripheral blood upon coinjection of PA.

Biodistribution of ^{68}Ga-JMV4168 and ^{177}Lu-JMV4168 was compared in nude mice with sc PC-3 human tumors. The similar biodistribution patterns of ^{68}Ga-JMV4168

and ^{177}Lu-JMV4168 at 1 h after injection indicate that ^{68}Ga-JMV4168 could serve as a surrogate to ^{177}Lu-JMV4168 for PET imaging-based patient selection and followup of therapy outcome. Tumor uptake of ^{177}Lu-JMV4168 was similar to tumor uptake of ^{177}Lu-RM2 reported by Dumont et al. (*34*). Tumor uptake of ^{68}Ga- and ^{177}Lu-JMV4168 was doubled by coinjection of PA, whereas most nontarget background organs and blood levels were not enhanced, leading to higher tumor-to-background ratios. Although uptake of ^{68}Ga-JMV4168 in the GRPR-positive pancreas was also increased by coinjection of PA at 1 h after injection, rapid washout from the pancreas was observed between 1 h and 2 h after injection, in agreement with previous findings (*14*). These increased tumor uptake values were visualized on PET images acquired at 2 h after injection, showing higher signal intensity in the PC-3 tumors in mice that received coinjection of PA, with unaltered low intensity in the pancreas area. This suggests that PA could increase sensitivity of detection of small PCa lesions in patients.

Dosimetry of ^{177}Lu-JMV4168 was evaluated to predict therapy outcome and to optimize the design of therapy studies. Administration of ^{177}Lu-JMV4168 via the ip route was preferred to reduce injection failure rate and radiation exposure rate to researchers. Based on dosimetry calculations, therapy studies were conducted in nude mice with sc PC-3 tumors with 4 cycles of 50 MBq of ^{177}Lu-JMV4168 (ip) with 2-d intervals. This schedule resulted in an impressive decrease and stabilization of tumor size as compared to that in untreated mice. More strikingly, coadministration of PA to ^{177}Lu-JMV4168 resulted in increased survival. Several reports have suggested a role of NEP in PCa progression (*43-45*). Minimal effect of NEP inhibition on PC-3 tumor growth was expected, because previous studies have shown lack of NEP expression in PC-3 cells (*45-47*). Consistently, our results revealed no effect of PA on PC-3 xenograft tumor growth. However, we would recommend testing the effect of PA for each new model being investigated in similar studies.

In order to confirm the efficacy of radionuclide therapy at the molecular level, we evaluated the occurrence of DSBs, proliferation and apoptosis in PC-3 tumors. The β-particles emitted by the radionuclide ^{177}Lu induce several types of DNA damage, among which DSBs are the most genotoxic; because unrepaired DSBs can trigger cell cycle arrest, cell death (apoptosis) or chromosomal aberrations. DSBs produced by ionization radiation activate a cascade of events, including protein modifications (such as γH2AX) and accumulation of several DNA damage response proteins (one of these proteins is the key DSB repair regulator 53BP1) (*48*). After DSB induction, γH2AX, and 53BP1 can be visualized as nuclear foci at the DSBs providing a measure of DSB induction.

PC-3 tumors dissected 8 d after the last therapeutic injection revealed increased number of DSBs, as shown by the increase in γH2AX and 53BP1 foci for the groups treated with ^{177}Lu-JMV4168 and ^{177}Lu-JMV4168 with PA. Furthermore, an increased production of DSBs was observed in mice that received coadministration of PA, which was consistent with the higher ^{177}Lu-JMV4168 tumor uptake and the improved therapeutic outcome.

In both treated groups, we also observed decreased replication, as shown by the reduction in the number of cell expressing the cell cycle marker GEMININ. In line with these results, TUNEL staining showed an increased level of apoptosis after treatment. No significant difference in the number of GEMININ- and TUNEL-positive cells was observed between both treated groups, unlike DNA damage data. This could be due to different kinetics of DNA damage repair, proliferation, and apoptosis.

Altogether, these parameters confirm tissue damage and subsequent tumor volume reduction induced by the radionuclide treatment with ^{177}Lu-JMV4168. Importantly, GRPR expression was maintained on regrowing PC-3 tumors after radionuclide therapy, excluding the possibility of a selection of GRPR-negative cells, and allowing repeated treatment with the same probe.

CONCLUSION

In conclusion, this study highlights the potential of the GRPR-targeted peptide-based theranostic approach for imaging and treatment of PCa. Besides treatment of PCa patients, this approach could be applied to a wider range of GRPR-expressing tumors, such as breast tumors (*49*). Moreover, it shows how coinjection of the NEP inhibitor PA can greatly enhance diagnostic sensitivity and therapeutic efficacy. We believe that this strategy may contribute to an improved management of PCa patients and warrants translation into a clinical setting. For that purpose, clinically certified NEP inhibitors should be preferred to facilitate translation.

REFERENCES

1. Siegel R, Naishadham D, Jemal A. Cancer statistics, 2012. CA Cancer J Clin. 2012;62:10-29.
2. Siegel R, DeSantis C, Virgo K, et al. Cancer treatment and survivorship statistics, 2012. CA Cancer J Clin. 2012;62:220-241.
3. Roivainen A, Kahkonen E, Luoto P, et al. Plasma pharmacokinetics, whole-body distribution, metabolism, and radiation dosimetry of 68Ga bombesin antagonist BAY 86-7548 in healthy men. J Nucl Med. 2013;54:867-872.
4. Kahkonen E, Jambor I, Kemppainen J, et al. In vivo imaging of prostate cancer using [68Ga]-labeled bombesin analog BAY86-7548. Clin Cancer Res. 2013;19:5434-5443.
5. Afshar-Oromieh A, Malcher A, Eder M, et al. PET imaging with a [68Ga]gallium-labelled PSMA ligand for the diagnosis of prostate cancer: biodistribution in humans and first evaluation of tumour lesions. Eur J Nucl Med Mol Imaging. 2013;40:486-495.
6. Afshar-Oromieh A, Zechmann CM, Malcher A, et al. Comparison of PET imaging with a (68)Ga-labelled PSMA ligand and (18)F-choline-based PET/CT for the diagnosis of recurrent prostate cancer. Eur J Nucl Med Mol Imaging. 2014;41:11-20.
7. Tagawa ST, Milowsky MI, Morris M, et al. Phase II study of Lutetium-177-labeled anti-prostate-specific membrane antigen monoclonal antibody J591 for metastatic castration-resistant prostate cancer. Clin Cancer Res. 2013;19:5182-5191.
8. Vallabhajosula S, Nikolopoulou A, Jhanwar YS, et al. Radioimmunotherapy of Metastatic Prostate Cancer with 177Lu-DOTA-huJ591 Anti Prostate Specific Membrane Antigen Specific Monoclonal Antibody. Curr Radiopharm. 2015;[Epub ahead of print].
9. Ananias HJ, van den Heuvel MC, Helfrich W, de Jong IJ. Expression of the gastrin-releasing peptide receptor, the prostate stem cell antigen and the prostate-specific membrane antigen in lymph node and bone metastases of prostate cancer. Prostate. 2009;69:1101-1108.
10. Markwalder R, Reubi JC. Gastrin-releasing peptide receptors in the human prostate: relation to neoplastic transformation. Cancer Res. 1999;59:1152-1159.
11. Cescato R, Maina T, Nock B, et al. Bombesin receptor antagonists may be preferable to agonists for tumor targeting. J Nucl Med. 2008;49:318-326.
12. Basso N, Lezoche E, Speranza V. Studies with bombesin in man. World J Surg. 1979;3:579-585.
13. Bodei L, Ferrari M, Nunn A, et al. Lu-177-AMBA Bombesin analogue in hormone refractory prostate cancer patients: A phase I escalation study with single-cycle administrations. Eur J Nucl Med Mol Imaging. 2007;34:S221-S221.
14. Chatalic KL, Franssen GM, van Weerden WM, et al. Preclinical comparison of Al18F- and 68Ga-labeled gastrin-releasing peptide receptor antagonists for PET imaging of prostate cancer. J Nucl Med. 2014;55:2050-2056.
15. Shipp MA, Tarr GE, Chen CY, et al. CD10/neutral endopeptidase 24.11 hydrolyzes bombesin-like peptides and regulates the growth of small cell carcinomas of the lung. Proc Natl Acad Sci U S A. 1991;88:10662-10666.
16. Erdos EG, Skidgel RA. Neutral endopeptidase 24.11 (enkephalinase) and related regulators of peptide hormones. Faseb j. 1989;3:145-151.
17. Roques BP, Noble F, Dauge V, Fournie-Zaluski MC, Beaumont A. Neutral endopeptidase 24.11: structure, inhibition, and experimental and clinical pharmacology. Pharmacol Rev. 1993;45:87-146.
18. Nock BA, Maina T, Krenning EP, de Jong M. "To serve and protect": enzyme inhibitors as radiopeptide escorts promote tumor targeting. J Nucl Med. 2014;55:121-127.

19. Marsouvanidis PJ, Nock BA, Hajjaj B, et al. Gastrin releasing peptide receptor-directed radioligands based on a bombesin antagonist: synthesis, (111)in-labeling, and preclinical profile. J Med Chem. 2013;56:2374-2384.
20. Ali M, Hsieh W, Smyth D, Tsopelas C. A simple and rapid method to quantify (68)Ga-hydroxides in a (68)Ga-DOTATATE formulation. Intern Med J. 2014;44:36-37.
21. Bolch WE, Eckerman KF, Sgouros G, Thomas SR. MIRD pamphlet No. 21: a generalized schema for radiopharmaceutical dosimetry--standardization of nomenclature. J Nucl Med. 2009;50:477-484.
22. Keenan MA, Stabin MG, Segars WP, Fernald MJ. RADAR realistic animal model series for dose assessment. J Nucl Med. 2010;51:471-476.
23. Konijnenberg M, Breeman W, de Blois E, et al. Therapeutic application of CCK2R-targeting PP-F11: influence of particle range, activity and peptide amount. EJNMMI Research. 2014;4:1-15.
24. O'Donoghue JA, Bardies M, Wheldon TE. Relationships between tumor size and curability for uniformly targeted therapy with beta-emitting radionuclides. J Nucl Med. 1995;36:1902-1909.
25. de Visser M, van Weerden WM, de Ridder CM, et al. Androgen-dependent expression of the gastrin-releasing peptide receptor in human prostate tumor xenografts. J Nucl Med. 2007;48:88-93.
26. de Blois E, Chan HS, Konijnenberg M, de Zanger R, Breeman WA. Effectiveness of quenchers to reduce radiolysis of (111)In- or (177)Lu-labelled methionine-containing regulatory peptides. Maintaining radiochemical purity as measured by HPLC. Curr Top Med Chem. 2012;12:2677-2685.
27. Sancho V, Di Florio A, Moody TW, Jensen RT. Bombesin receptor-mediated imaging and cytotoxicity: review and current status. Curr Drug Deliv. 2011;8:79-134.
28. Lantry LE, Cappelletti E, Maddalena ME, et al. 177Lu-AMBA: Synthesis and characterization of a selective 177Lu-labeled GRP-R agonist for systemic radiotherapy of prostate cancer. J Nucl Med. 2006;47:1144-1152.
29. Johnson CV, Shelton T, Smith CJ, et al. Evaluation of combined (177)Lu-DOTA-8-AOC-BBN (7-14)NH(2) GRP receptor-targeted radiotherapy and chemotherapy in PC-3 human prostate tumor cell xenografted SCID mice. Cancer Biother Radiopharm. 2006;21:155-166.
30. Wild D, Frischknecht M, Zhang H, et al. Alpha- versus beta-particle radiopeptide therapy in a human prostate cancer model (213Bi-DOTA-PESIN and 213Bi-AMBA versus 177Lu-DOTA-PESIN). Cancer Res. 2011;71:1009-1018.
31. Ginj M, Zhang H, Waser B, et al. Radiolabeled somatostatin receptor antagonists are preferable to agonists for in vivo peptide receptor targeting of tumors. Proc Natl Acad Sci U S A. 2006;103:16436-16441.
32. Cescato R, Waser B, Fani M, Reubi JC. Evaluation of 177Lu-DOTA-sst2 antagonist versus 177Lu-DOTA-sst2 agonist binding in human cancers in vitro. J Nucl Med. 2011;52:1886-1890.
33. Wild D, Fani M, Behe M, et al. First clinical evidence that imaging with somatostatin receptor antagonists is feasible. J Nucl Med. 2011;52:1412-1417.
34. Dumont RA, Tamma M, Braun F, et al. Targeted radiotherapy of prostate cancer with a gastrin-releasing peptide receptor antagonist is effective as monotherapy and in combination with rapamycin. J Nucl Med. 2013;54:762-769.
35. Pernot M, Vanderesse R, Frochot C, Guillemin F, Barberi-Heyob M. Stability of peptides and therapeutic success in cancer. Expert Opin Drug Metab Toxicol. 2011;7:793-802.
36. Adessi C, Soto C. Converting a peptide into a drug: strategies to improve stability and bioavailability. Curr Med Chem. 2002;9:963-978.
37. Vlieghe P, Lisowski V, Martinez J, Khrestchatisky M. Synthetic therapeutic peptides: science and market. Drug Discov Today. 2010;15:40-56.

38. Shipp MA, Richardson NE, Sayre PH, et al. Molecular cloning of the common acute lymphoblastic leukemia antigen (CALLA) identifies a type II integral membrane protein. Proc Natl Acad Sci U S A. 1988;85:4819-4823.
39. Erdos EG, Schulz WW, Gafford JT, Defendini R. Neutral metalloendopeptidase in human male genital tract. Comparison to angiotensin I-converting enzyme. Lab Invest. 1985;52:437-447.
40. Sato Y, Itoh F, Hinoda Y, et al. Expression of CD10/neutral endopeptidase in normal and malignant tissues of the human stomach and colon. J Gastroenterol. 1996;31:12-17.
41. Oefner C, D'Arcy A, Hennig M, Winkler FK, Dale GE. Structure of human neutral endopeptidase (Neprilysin) complexed with phosphoramidon. J Mol Biol. 2000;296:341-349.
42. Marsouvanidis PJ, Melis M, de Blois E, et al. In vivo enzyme inhibition improves the targeting of [177Lu] DOTA-GRP(13-27) in GRPR-positive tumors in mice. Cancer Biother Radiopharm. 2014;29:359-367.
43. Osman I, Dai J, Mikhail M, et al. Loss of neutral endopeptidase and activation of protein kinase B (Akt) is associated with prostate cancer progression. Cancer. 2006;107:2628-2636.
44. Albrecht M, Doroszewicz J, Gillen S, et al. Proliferation of prostate cancer cells and activity of neutral endopeptidase is regulated by bombesin and IL-1beta with IL-1beta acting as a modulator of cellular differentiation. Prostate. 2004;58:82-94.
45. Dawson LA, Maitland NJ, Turner AJ, Usmani BA. Stromal-epithelial interactions influence prostate cancer cell invasion by altering the balance of metallopeptidase expression. Br J Cancer. 2004;90:1577-1582.
46. Usmani BA, Harden B, Maitland NJ, Turner AJ. Differential expression of neutral endopeptidase-24.11 (neprilysin) and endothelin-converting enzyme in human prostate cancer cell lines. Clin Sci (Lond). 2002;103 Suppl 48:314s-317s.
47. Ho ME, Quek SI, True LD, et al. Prostate cancer cell phenotypes based on AGR2 and CD10 expression. Mod Pathol. 2013;26:849-859.
48. van Gent DC, van der Burg M. Non-homologous end-joining, a sticky affair. Oncogene. 2007;26:7731-7740.
49. Dalm SU, Martens JW, Sieuwerts AM, et al. In vitro and in vivo application of radiolabeled gastrin-releasing Peptide receptor ligands in breast cancer. J Nucl Med. 2015;56:752-757.

Prostate-Specific Membrane Antigen Targeting

3

Chapter 3.1
A Novel ^{111}In-labeled Anti-PSMA Nanobody for Targeted SPECT/CT Imaging of Prostate Cancer

Chapter 3.2
Towards Personalized treatment of Prostate Cancer: PSMA I&T, a Promising PSMA-Targeted Theranostic Agent

Chapter 3.3
Alpha Radionuclide Therapy of Prostate Cancer Targeting Prostate-Specific Membrane Antigen

3.1

A Novel ^{111}In-Labeled Anti-Prostate-Specific Membrane Antigen Nanobody for Targeted SPECT/CT Imaging of Prostate Cancer

Kristell L.S. Chatalic[1,2], Joke Veldhoven-Zweistra[1], Michiel Bolkestein[3], Sander Hoeben[1], Gerben A. Koning[3], Otto C. Boerman[4], Marion de Jong[2], and Wytske M. van Weerden[1]

[1]Department of Urology, Erasmus MC, Rotterdam, The Netherlands
[2]Departments of Nuclear Medicine and Radiology, Erasmus MC, Rotterdam, The Netherlands
[3]Laboratory Experimental Surgical Oncology, Department of Surgery, Erasmus MC, Rotterdam, The Netherlands
[4]Department of Radiology and Nuclear Medicine, Radboud University Medical Center, Nijmegen, The Netherlands

Adapted from: Journal of Nuclear Medicine 2015; 56(7):1094-9

ABSTRACT

Prostate-specific Membrane Antigen (PSMA) is overexpressed in prostate cancer (PCa) and a promising target for molecular imaging and therapy. Nanobodies (single-domain antibodies, V_{HH}) are the smallest antibody-based fragments possessing ideal molecular imaging properties, such as high target specificity and rapid background clearance. We developed a novel anti-PSMA Nanobody (JVZ-007) for targeted imaging and therapy of PCa. Here, we report on the application of the ^{111}In-radiolabeled Nanobody for SPECT/CT imaging of PCa.

Methods
A Nanobody library was generated by immunization of a llama with 4 human PCa cell lines. Anti-PSMA Nanobodies were captured by biopanning on PSMA-overexpressing cells. JVZ-007 was selected for evaluation as an imaging probe. JVZ-007 was initially produced with a c-*myc*-hexahistidine (his) tag allowing purification and detection. The c-*myc*-his tag was subsequently replaced by a single cysteine at the C terminus, allowing site-specific conjugation of chelates for radiolabeling. JVZ-007-c-*myc*-his was conjugated to 2-(4-isothiocyanatobenzyl)-diethylene-triaminepentaacetic acid (p-SCN-DTPA) via the lysines, whereas JVZ-007-cys was conjugated to maleimide-DTPA via the C-terminal cysteine. PSMA targeting was analyzed in vitro by cell-binding experiments using flow cytometry, autoradiography, and internalization assays with various PCa cell lines and patient-derived xenografts (PDXs). The targeting properties of radiolabeled Nanobodies were evaluated in vivo in biodistribution and SPECT/CT imaging experiments, using nude mice bearing PSMA-positive PC-310 and PSMA-negative PC-3 tumors.

Results
JVZ-007 was successfully conjugated to DTPA for radiolabeling with ^{111}In at room temperature. ^{111}In-JVZ007-c-*myc*-his and ^{111}In-JVZ007-cys internalized in LNCaP cells and bound to PSMA-expressing PDXs and, importantly, not to PSMA-negative PDXs and human kidneys. Good tumor targeting and fast blood clearance were observed for ^{111}In-JVZ-007-c-*myc*-his and ^{111}In-JVZ-007-cys. Renal uptake of ^{111}In-JVZ-007-c-*myc*-his was initially high but was efficiently reduced by coinjection of gelofusine and lysine. The replacement of the c-*myc*-his tag by the cysteine contributed to further reduction of renal uptake without loss of targeting. PC-310 tumors were clearly visualized by SPECT/CT with both tracers, with very low renal uptake (< 4 percentage injected dose per gram) for ^{111}In-JVZ-007-cys already at 3 h after injection.

Conclusion
We developed an ^{111}In-radiolabeled anti-PSMA Nanobody, showing good tumor targeting, low uptake in nontarget tissues, and low renal retention, allowing excellent SPECT/CT imaging of PCa within a few hours after injection.

INTRODUCTION

Prostate cancer (PCa) is the second leading cause of cancer-related death among men in the western world. Early detection and accurate staging of PCa is crucial because the survival rate decreases dramatically when the cancer has spread beyond the prostate (*1*). Because of the heterogeneity of PCa, and the lack of specificity of conventional imaging techniques, there is currently no universal imaging method approved for detection of early PCa lesions. Prostate-specific membrane antigen (PSMA) is an interesting target for molecular imaging of PCa, as it is overexpressed in 90-100% of local PCa lesions, as well as on cancerous lymph nodes, and bone metastases (*2, 3*), with some reports suggesting PSMA expression levels are further enhanced in high-grade, metastatic, and castration-resistant PCa (*2, 4, 5*). PSMA is also expressed in other tissues including normal prostate epithelium, small intestine, renal tubular cells, and salivary glands, but the expression in these organs is 100-1,000 fold less than in PCa (*6*).

PSMA, also referred to as glutamate carbopeptidase II (GPCII), *N*-acetyl-α-linked acidic dipeptidase I (Naaladase I), or folate hydrolase, is a type II transmembrane glycoprotein exhibiting glutamate carboxypeptidase and folate hydrolase enzymatic activity. The first clinical tracer for imaging PSMA was based on the murine anti-PSMA antibody 7E11, binding to an epitope on the intracellular domain of PSMA. The ^{111}In-labeled version of 7E11, ^{111}In-capromab, commonly known as ProstaScint (Cytogen Corp.), was approved by the Food and Drug Administration in 1997 for detection of soft-tissue metastases and recurrence of PCa (*7*). Its use for staging primary PCa is suboptimal, with an average sensitivity and specificity of 60% and 70%, respectively (*8*). ^{111}In-capromab was also not reliable for the detection of bone metastases, which are often the initial site of metastasis in advanced PCa (*9*). After the discovery of 7E11, next-generation monoclonal antibodies (mAb) binding to the extracellular domain of PSMA were developed, including mAb J591. Initially developed for therapeutic purposes, J591 was also evaluated for SPECT imaging in clinical trials, showing characteristics superior to ^{111}In-capromab, revealing most soft-tissue and bony metastases (*10, 11*). Despite improved targeting of J591 and next-generation PSMA mAb, the major disadvantage of the use of antibodies for imaging is the slow clearance from nontarget tissues, often requiring several days between tracer administration and imaging.

An interesting alternative for molecular imaging of PSMA is the development of small-molecule PSMA inhibitors. Because PSMA possesses an enzymatic site in its extracellular domain that cleaves endogenous substrates such as *N*-acetylaspartylglutamate and poly-γ-glutamyl folic acid, a series of substrates has been designed. These small-molecule PSMA inhibitors consist of zinc-binding compounds attached to a glutamate moiety. Several radiolabeled PSMA small-molecules inhibitors have been synthetized, starting with phosphonate and phosphate inhibitors, followed by phosphoramidate-, thiol-, and urea-based inhibitors, which are discussed in an extensive review by Mease et al. (*12*). Some have shown promising results in early clinical studies, such

as ^{123}I-MIP-1072, ^{123}I-MIP-1095 (*13*), *N*-[*N*-[(*S*)-1,3-dicarboxypropyl]carbamoyl]-4-^{18}F-fluorobenzyl-L-cysteine (*14*), ^{68}Ga-HBED-CC (*15*), and BAY1075553 (*16*). These compounds localize rapidly to tumor lesions, including soft-tissue and bone metastases, but also show high uptake in kidneys and salivary glands, attributed to PSMA expression in these organs.

Another approach aiming at circumventing the long circulation time of mAbs, is the use of antibody fragments, such as single-domain antibodies (V_{HH}). Nanobodies display attractive features for molecular imaging, including fast nontarget tissue clearance, good tumor penetration capability, and recognition of unique epitopes that are less accessible for mAbs (*17*). In this study, we describe the development of a Nanobody targeting PSMA and showing good tumor targeting and fast blood clearance, resulting in impressive tumor-to-background ratios within a few hours after injection. The Nanobody was conjugated to a diethylenetriamine-pentaacetic acid (DTPA) chelator allowing facile and stable radiolabeling with ^{111}In at room temperature in a 1-step procedure. The structure of the Nanobody was optimized to minimize renal retention using a novel method for production and labeling of cys-tagged Nanobodies. We report on the production and radiolabeling of anti-PSMA Nanobodies as well as in vitro and in vivo evaluation in patient-derived PCa xenograft models.

MATERIALS AND METHODS

Immunization and V_{HH} Library Construction

A llama (Lama glama) was immunized subcutaneously at days 1, 30, 60, and 90 with 4 androgen-responsive human-derived PCa cell lines (33 x 10^6 cells per cell line) – LNCaP, PC346C, VCaP, and MDA-PCa-2b – to generate a V_{HH} library targeting PCa. Blood was collected after the third immunization and peripheral blood lymphocytes were isolated. Library construction was performed as previously described (*18*). Briefly, RNA was isolated and cDNA was synthetized with reverse transcriptase. V_{HH} (variable domains of camelid heavy-chain antibodies) genes were amplified by polymerase chain reaction introducing NotI and SfiI restriction enzyme sites (forward and backward primers). V_{HH} fragments were isolated from a 1% agarose gel, digested with Sfil and Notl, ligated into the pHEN1-6HISGS phagemid and transformed into TG1 Escherichia coli cells to generate a library of 3.3 x 10^9 transformants (L1P4 library). The V_{HH} library was kindly provided by Dr. Patrick Chames (IBISA).

Selection and Screening by Phage Display

A phage display library was produced by infecting the Nanobody library with M13 K07ΔpIII hyperphages (Progen Biotechnik). PSMA-specific Nanobodies were captured by 3 rounds of biopanning. Each round consisted of a negative selection using wild-type B16 cells followed by a positive selection on B16-PSMA-transfected

cells. Briefly, 10^7 B16 cells were scraped in phosphate-buffered saline (PBS)/10% fetal calf serum (FCS). B16 cells and phages were incubated in PBS/10%FCS/2% protivar milk (Nutrica) for 30 min at RT. B16 cells were incubated with 2 x 10^{11} phages in PBS/10%FCS/2% protivar milk for 45 min at RT. Meanwhile, B16-PSMA cells were scraped in PBS/10%FCS and incubated in PBS/10%FCS/2% protivar milk (Nutrica) for 30 min at RT. B16 cells were then spin down, and the supernatant containing unbound phages was incubated with 10^7 B16-PSMA transfected cells in PBS/1% bovine serum albumin (BSA)/2% protivar milk for 45 min at RT. Cells were washed 10 times with PBS/1%BSA/2% protivar milk and 2 times with PBS. Phages bound to PSMA-transfected B16 cells were eluted with 200 mM triethylamine (Sigma) and reamplified in TG1 cells. Colonies were grown on 2YT (16 g/L tryptone, 10 g/L yeast extract, and 5 g/L NaCl)/ampicillin (100 µg/mL)/glucose (2%) agar plates. Colonies were scraped from the 2YT plates, and stored at –80°C in the presence of 20% glycerol.

Selected single clones were plated in 100 µl 2YT/ampicillin (100 µg/mL)/glucose (2%) broth in 96-well plates and shaken overnight at 30°C. From each well, 5 µl was replated in 150 µl 2YT/ampicillin (100 µg/mL)/glucose (2%) broth and shaken for 2.5 h at 37°C. Phages presenting a V_{HH} were produced by adding 0.5 x 10^9 M13K07ΔpIII helper phage to each well and incubating for 30 minutes at 37°C. Plates were centrifuged (1700 rpm, 10 minutes). Bacterial pellet was resuspended in 2YT/ampicillin (100 µg/mL)/kanamycin (25 µg/mL) and grown under vigorous shaking overnight at 30°C.

Phage-containing supernatants were tested for binding to PSMA by enzyme-linked immunosorbent assay using B16 and B16-PSMA cells. Briefly, B16 and B16-PSMA cells were collecting by scraping in PBS containing 1% BSA. Cells were incubated with phage supernatant for 1.5 h at room temperature, shaking. Binding of phages to PSMA was detected with a horseradish peroxidase-conjugated anti-M13 mouse antibody (27-9421-01, GE Healthcare). Cells were then incubated with o-phenylenediamine dihydrochloride substrate (Sigma) and optical density was measured at 490 nm.

Clones found positive in cell enzyme-linked immunosorbent assay were further analyzed by flow cytometry. Binding of phages was detected with an anti-M13 mouse antibody (GE Healthcare), followed by a phycoerythrin (PE)-conjugated anti-mouse goat antibody (550589, BD Biosciences). Fluorescence was measured on a FACScan (BD).

Nanobody Sequencing, Production and Purification

Selected clones were sequenced, and distinct Nanobody clones were identified. Sequence of JVZ-007 clone is shown in **Figure 1**. Selected clones were produced as c-*myc*-his-tagged proteins to facilitate purification by affinity chromatography and detection by flow cytometry. The plasmid containing JVZ-007 sequence was isolated from the TG1 cells (JetStar™ 2.0 plasmid purification MIDI kit, Genomed) and

transformed into HB2151 cells. Production in HB2151 cells was performed overnight at 37°C in 2YT (16 g/L tryptone, 10 g/L yeast extract and 5 g/L NaCl) medium supplemented with 100 µg/mL ampicillin and 0.1% glucose. Cells were collected by centrifugation for 30 min at 4000 rpm, washed with PBS and lysed by freeze-thaw cycles in lysis buffer (50 mM KPO_4 pH 7.8, 400 mM NaCl, 100 mM KCl, 10% glycerol, 0.5% TritonX-100). Lysate was centrifuged and filtered (40 µm filter), and c-*myc*-his-tagged Nanobodies were trapped on a HisTrap FF column (GE Healthcare) on a ÄKTA preparative protein purification system (GE Healthcare) and eluted with 500 mM imidazole. Buffer was changed for PBS using a Vivaspin sample concentrator (5-kDa cut-off, GE Healthcare). C-*myc*-his-tagged Nanobody purity was assessed with reducing sodium dodecyl sulfate polyacrylamide gel electrophoresis (SDS-PAGE) and western blot analysis with anti-c-*myc* mouse antibody (M4439, Sigma), followed by horseradish peroxidase-anti-mouse goat antibody (p0447, Dako) and visualized with

A

```
1               10              20              30              40              50
|               |               |               |               |               |
EVQLVESGGGLVQPGGSLTLSCAASRFMISEYSMHWVRQAPGKGLEWVSTINPAGTTDY

60              70              80              90              100             110
|               |               |               |               |               |
AESVKGRFTISRDNAKNTLYLQMNSLKPEDTAVYYCDGYGYRGQGTQVTVSS
```

B

```
1               10              20              30              40              50
|               |               |               |               |               |
EVQLVESGGGLVQPGGSLTLSCAASRFMISEYSMHWVRQAPGKGLEWVSTINPAGTTDY

60              70              80              90              100             110
|               |               |               |               |               |
AESVKGRFTISRDNAKNTLYLQMNSLKPEDTAVYYCDGYGYRGQGTQVTVSSTGT
```

FIGURE 1. Amino acid sequence of JVZ-007 Nanobody (A) and JVZ-007 Nanobody with a cysteine residue at the C terminus (B).

a Chemiluminescence kit (Thermo Fisher Scientific). The protein concentration was determined using a bicinchoninic acid assay kit (Thermo Fisher Scientific).

Production of JVZ-007-cys

JVZ-007 Nanobody was cloned from the pHEN vector, introducing a cysteine at the C terminus, and expressed as a fusion protein to SUMO3 (Smt3 ubiquitin-like protein) using the pETM11-SUMO3GFP vector (EMBL). The Nanobody sequence was cloned from the pHEN vector using 2 primers (**Figure 2**).

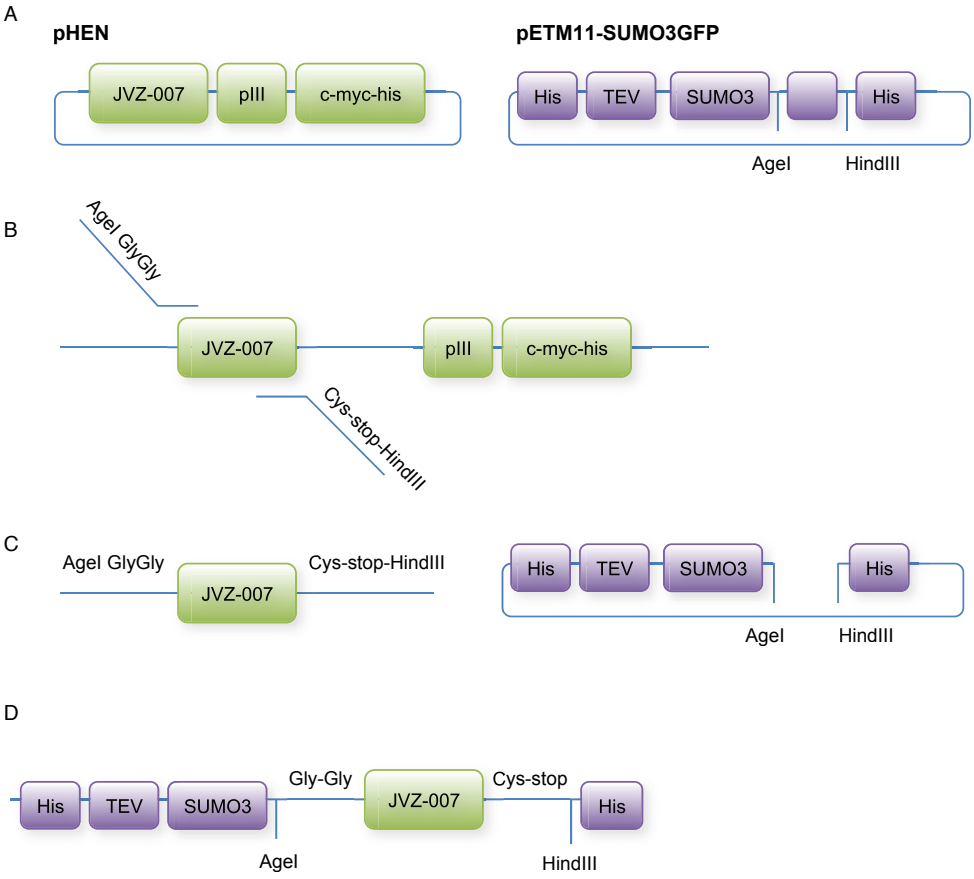

FIGURE 2. Cloning of JVZ-007 from pHEN vector to pETM11-SUMO3GFP vector. (A) pHEN vector containing JVZ-007 and pETM11-SUMO3GFP. (B) Forward primer containing a restriction enzyme site AgeI and two glycine molecules, necessary for SenP2 digestion. Backward primer containing a cysteine sequence, a stop sequence, and a HindIII restriction enzyme site. (C) Products resulting from digestion with AgeI and HindIII. (D) Ligation product of JVZ-007 into the pETM11-SUMO3GFP vector.

The forward primer contains a restriction enzyme site AgeI and 2 glycine molecules, necessary for Sentrin-specific protease 2 (SenP2) digestion (5' ACT ATG ACC GGT GGA GAG GTG CAG CTG GTG 3'). The backward primer contains a cysteine sequence, a stop sequence and a HindIII restriction enzyme site (3' TCA GTA AAG CTT TCA ACA TGA GGA GAC GGT GAC 5'). The Nanobody was ligated into the pETM11-SUMO3GFP vector after digestion with AgeI and HindIII. After expression of the recombinant plasmid in BL21 bacteria and protein extraction, JVZ-007-cys-SUMO3 was isolated with a HisTrap column. The SUMO3 protein was cleaved off by a SUMO-specific protease, SenP2, (Addgene (*19*)). Digestion was performed overnight at 4°C with a ratio of 1:10 (w/w) of SenP2 to JVZ-007-cys-SUMO3. His-tagged SenP2 and SUMO3 were removed with a

HisTrap FF column (GE Healthcare). JVZ-007-cys Nanobody purity was assessed with reducing SDS-PAGE. FPLC elution profile and SDS-PAGE are shown in **Figure 3**. The sequence of JVZ-007-cys is depicted in **Figure 1**.

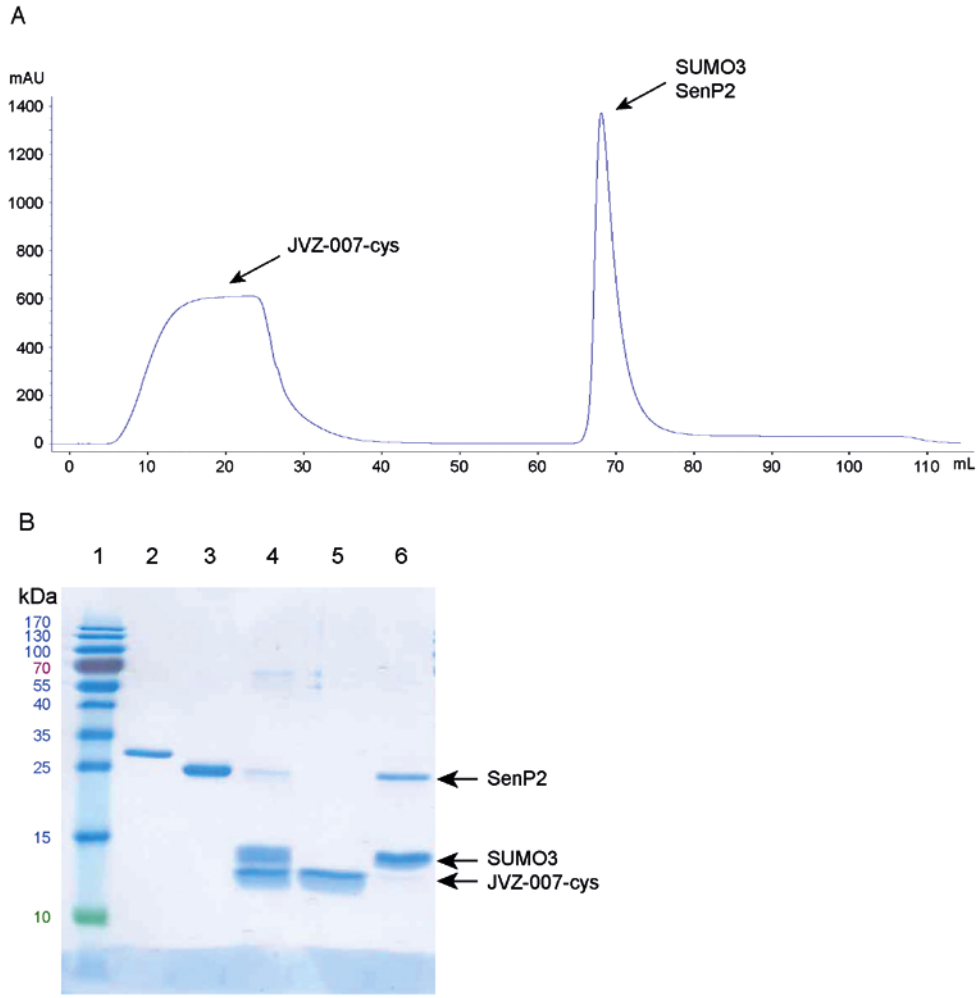

FIGURE 3. FPLC elution profile (A) and SDS-PAGE (B) showing purification of JVZ-007-cys Nanobody from His-tagged SenP2 and SUMO3. X-axis = volume (milliliter, mL); y-axis = UV signal (milliabsorbance unit, mAU). Lane 1 = PageRuler Prestained Protein Ladder (10 to 180 kDa); lane 2 = JVZ-007-cys-SUMO3 (fusion protein); lane 3 = SenP2; lane 4 = SenP2, SUMO3 and JVZ-007 (digestion product); lane 5 = JVZ-007-cys (FPLC flow through); lane 6 = SenP2 and SUMO3 (FPLC elution).

Flow Cytometry

PSMA-specific binding was assessed by flow cytometry on PC-346C, LNCaP, and PC-3 cells, using an anti-c-*myc* mouse primary antibody and a PE-conjugated antimouse goat secondary antibody. Briefly, cells were collected by scrapping in polypropylene tubes and incubated with the c-*myc*-his-tagged Nanobody for 60 min at 4°C, followed by incubation with an anti-c-*myc* mouse antibody (M4439, Sigma) for 30 min and finally PE-conjugated anti-mouse goat antibody (550589, BD Biosciences) for 30 min. As negative control, cells were incubated using the same procedure, without the Nanobody. As positive control, cells were incubated with an anti-PSMA mouse antibody (SAB4200257, Sigma), and a PE-conjugated goat anti-mouse antibody (550589, BD Biosciences). Flow cytometry was performed using a BD FACScan system (Becton Dickinson).

Conjugation to DTPA and Radiolabeling

JVZ-007-c-*myc*-his was incubated with a 5-fold molar excess of p-SCN-Bn-DTPA (Macrocyclics) in 0.1 M sodium carbonate buffer (pH 9.5) for 2.5 h at room temperature. JVZ-007-cys was reduced with 1 mM 2-mercaptoethylamine-HCl in phosphate-buffered saline (·), 5 mM ethylenediaminetetraacetic acid for 90 min at 37°C. Reduced JVZ-007-cys was then incubated with 5 mM maleimide-DTPA for 2 h at 37°C. Conjugated Nanobodies were then dialyzed for 3 d in a Slide-A-Lyzer (3.5-kDa cut-off; Life Technologies) against 0.25 M ammonium acetate (NH_4Ac), pH 5.5.

Nanobody-DTPA conjugates were labeled with $^{111}InCl_3$ (Covidien) in 20 mM sodium acetate, pH 5.0, for 30 min at room temperature. Radioprotectants (3.5 mM ascorbic acid, gentisic acid and methionine) were used to prevent radiolysis. Labeling efficiency was assessed by instant thin-layer chromatography using silica gel-coated paper (Varian Inc.) and 0.1 M citrate buffer, pH 5.0, as mobile phase. After incubation, an excess of DTPA (final concentration: 0.15 mM) was added to complex free $^{111}InCl_3$.

Cell Culture

Cell lines were purchased from the American Type Culture Collection. B16-PSMA was kindly provided by Marco Colombatti (University of Verona). Cell cultures media and reagents were obtained from Lonza unless stated otherwise. LNCaP, VCaP and PC-3 cells were cultured in RPMI 1640 medium containing 10% (5% for PC-3) FCS. PC-346C cells were cultured in Dulbecco's modified Eagle's F12 medium supplemented with 2% FCS, 0.01% BSA (Boehringer-Mannheim), 1% insulin-transferrin-selenium (Life Technologies), 0.1 µg/mL fibronectin (Alfa Aesar), 0.1 nM R1881 androgen, 10 ng/mL epidermal growth factor, 0.5 µg/mL dexametason, 1 nM triiodothyronine, 0.1 mM phosphoethanolamine, 50 ng/mL cholera toxin, and 20 µg/mL fetuin (all from Sigma). B16 cells were cultured in Dulbecco's modified Eagle's medium containing 10% FCS, 10 mM HEPES (Sigma), 20 µM 2-mercaptoethanol (Sigma), and 2 mM glutamine. For B16-PSMA, 1200 µg/mL geneticin (G418, Gibco) was added to this medium. MDA-

PCa2b cells were grown in Ham's F12 medium containing 15% FCS, 25 ng/mL cholera toxin, 10 ng/mL epidermal growth factor, 5 μM phosphoethanolamine, 120 pg/mL hydrocortisone, and 1% insulin-transferrin-selenium. Penicillin (100 units/mL) and streptomycin (100 μg/mL) were added to cell culture media. Cells were grown in tissue culture flasks at 37°C in a humidified atmosphere containing 5% CO_2.

Autoradiography and Internalization

Binding of ^{111}In-JVZ-007-c-*myc*-his and ^{111}In-JVZ-007-cys to frozen cryostat section of PDXs and kidneys (mouse/human) was evaluated using autoradiography, as described previously (*20*). Tissue sections were incubated for 1 h with ^{111}In-JVZ-007-c-*myc*-his or ^{111}In-JVZ-007-cys (10^{-9} M). In saturation binding experiments, concentrations ranging from 10^{-6} M to 10^{-12} M of ^{111}In-JVZ-007-c-*myc*-his were used.

The internalization of ^{111}In-JVZ-007-c-*myc*-his and ^{111}In-JVZ-007-cys was assessed using LNCaP and PC-3 cells. Cells were trypsinized and incubated with ^{111}In-JVZ-007-c-*myc*-his or ^{111}In-JVZ-007-cys (10^{-10} M) in RPMI 1640/GlutaMAX (Life Technologies)/20 mM HEPES/1% BSA (pH 7.4) for 90 min at 37°C or 4°C. JVZ-007-c-*myc*-his was used for blocking (10^{-6} M). After incubation, the cells were centrifuged, and washed 2 times with PBS. Cell surface-bound Nanobodies were eluted using a solution of 50 mM glycine/100 mM NaCl (pH 2.8), and cells were washed with PBS. Cells were then lysed in 1 M sodium hydroxide to collect internalized Nanobody. Membrane-bound and internalized fractions were counted in a γ counter. Binding was expressed as percentage of added amount of radioactivity per number of cells.

Biodistribution and SPECT/CT Imaging

Male NMRI *nu/nu* mice (8 wk old) were transplanted with PC-310 tumor fragments near the left shoulder and injected subcutaneously near the right shoulder with PC-3 cells (3 x 10^6 cells, 200 μL, 66% RPMI, 33% Matrigel [BD Bioscience]). Three to 4 wk after inoculation, when tumor size averaged 200 mm^3, mice were injected intravenously with radiolabeled Nanobody (200 μL). Radiolabeled Nanobody was diluted in PBS containing 0.1% v/w BSA. When coinjection of lysine (20 mg) and gelofusine (4 mg) was performed, radiolabeled Nanobody was mixed 1:1 with a solution of lysine (400 mg/mL) and 100 μL of this solution were coinjected with 100 μL of gelofusine (40 mg/mL).

Mice were injected with 0.7 MBq of radiolabeled Nanobody (amount ranging from 1 μg to 100 μg) and euthanized 4 or 24 h after injection for biodistribution studies. Blood, tumor, and relevant organs and tissues were collected, weighed, and counted in a γ counter, with a counting time of 60 s per sample, isotope-specific energy window, and a counting error not exceeding 5%. The percentage injected dose per gram (%ID/g) was determined for each tissue sample.

For SPECT/CT imaging experiments, mice were injected with 30 MBq of ^{111}In-JVZ007-c-*myc*-his (10 µg) or 15 MBq of ^{111}In-JVZ007-cys (10 µg). Mice were scanned under isoflurane/O_2 anesthesia at 3 and 24 h after injection on a small-animal nano-SPECT scanner (Mediso) with heated bed. SPECT emission scans were acquired for 30-42 min, with a matrix of 256 x 256 and 20 projections (120 s per projection). Multi-pinhole mouse collimators with 9 pinholes (1.4 mm diameter) per head were used. SPECT scans reconstruction and processing were performed with InVivoScope/VivoQuant software 2.0 (inviCRO).

All animal experiments were approved by the Animal Experiments Committee under the Dutch Experiments on Animal Act and adhered to the European Convention for Protection of Vertebrate Animals used for Experimental Purposes (Directive 86/609/EEC).

Statistical Analysis

Statistical analysis was performed using GraphPad Prism version 5.01 (GraphPad Software). Biodistribution data are represented as the mean %ID/g ± SD, with group sizes of 4 mice. Statistical analysis of biodistribution data was performed using a 1-way ANOVA with Bonferroni post-hoc test, and the level of significance was set at $P < 0.05$.

RESULTS

Generation of Anti-PSMA Nanobodies

A PCa-specific Nanobody library was generated by immunization of a llama with 4 PCa cell lines (LNCaP, PC346C, VCaP and MDA-PCa-2b). PSMA-specific Nanobodies were retrieved by biopanning using phage display for 3 positive and negative selection rounds with B16-PSMA and B16 cell lines, respectively. Selection on PSMA-expressing cells was preferred rather than using the recombinant PSMA protein, to increase the chance of capturing Nanobodies binding to an accessible epitope on the extracellular domain of PSMA. Several distinct PSMA-specific Nanobodies were isolated and sequenced (data not shown). Selected clones were produced as c-*myc*-his-tagged proteins to facilitate purification by affinity chromatography and detection by flow cytometry. PSMA-specific binding was assessed by flow cytometry on PC-346C, LNCaP, and PC-3 cells. Results of flow cytometry analysis of a few selected Nanobodies are displayed in **Figure 4**. JVZ-005, JVZ-007, and JVZ-012 all bound to PSMA-expressing LNCaP and PC346C, as shown by the increase in the geometric mean of the fluorescence intensity. No binding was observed on the PSMA-negative PC3 cells, showing the specificity of the Nanobodies for PSMA. JVZ-007, showing the highest binding, was selected for further evaluation as the imaging probe. Its sequence is indicated in **Figure 1**. JVZ-007-c-*myc*-his and JVZ-007-cys were successfully produced in bacteria using the pHEN and pETM11-SUMO3GFP expression vectors, respectively.

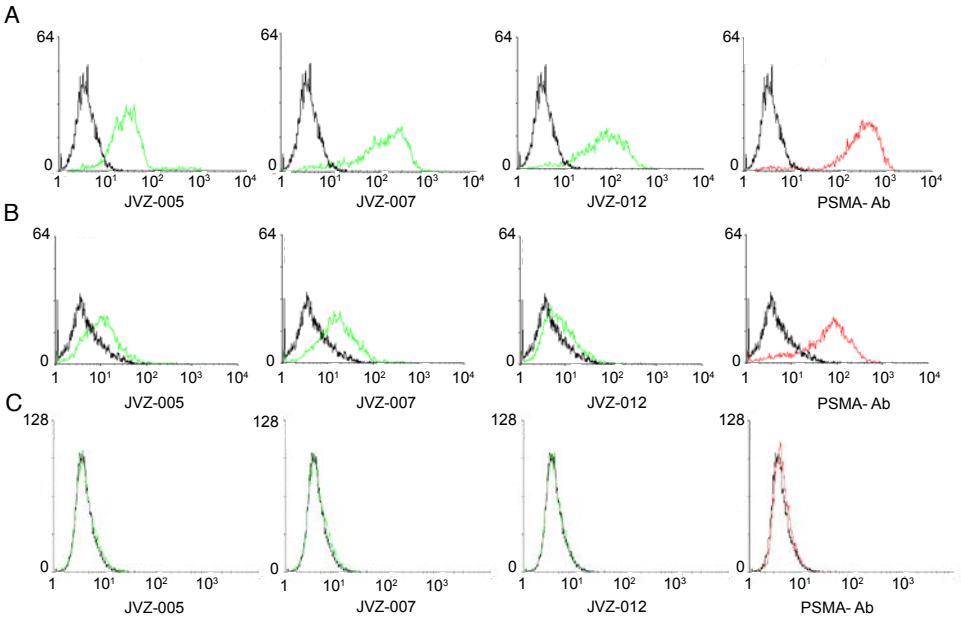

FIGURE 4. Flow cytometry analysis of JVZ-005, JVZ-007, and JVZ-012 on LNCaP (A), PC346C (B), and PC-3 cells (C). Binding was observed on PSMA-positive LNCaP and PC346C cells, whereas no binding was observed on PSMA-negative PC3 cells. Green = in presence of Nanobody; red = in presence of PSMA-antibody (PSMA-Ab); black = control, in absence of Nanobody; x-axis = fluorescence intensity; y-axis = number of events.

Labeling and In Vitro Binding Studies

JVZ-007-c-*myc*-his was conjugated to p-SCN-Bn-DTPA via lysine residues, to allow radiolabeling with ^{111}In for SPECT imaging of PCa. JVZ-007-cys was site-specifically conjugated with DTPA by reacting it with maleimide-DTPA. JVZ-007-cys formed dimers via cysteine bridging and mild reduction was necessary to free the thiol in the cysteine. ^{111}In-radiolabeling was performed, with specific activities up to 60 MBq/nmol, whereas the labeling efficiency always exceeded 90%. No release of ^{111}In was observed at 4°C up to 72 h after radiolabeling. Binding to frozen sections of PDXs and kidney using autoradiography is shown in **Figure 5** and **Figure 6**. Binding affinity of ^{111}In-JVZ-007-c-*myc*-his was estimated by saturation binding on the PSMA-positive PC-310 tumor, resulting in an equilibrium dissociation constant value of 27.4 nM (14.1 – 40.7, 95% confidence interval). ^{111}In-JVZ-007-c-*myc*-his and ^{111}In-JVZ-007-cys showed high binding to all PSMA-expressing tumor sections (PC310, LNCaP, PC82, and PC295), with lower binding to the weakly PSMA-positive PC346c. The absence of binding was observed on the PSMA-negative tumors (PC3, VCaP, PC133, PC339, and PC324). These results are in line with previous PSMA RNA expression data of these PDXs (Affymetrix data not shown). Binding to mouse and human kidneys was very low (<1%) in comparison with PSMA-positive tumors.

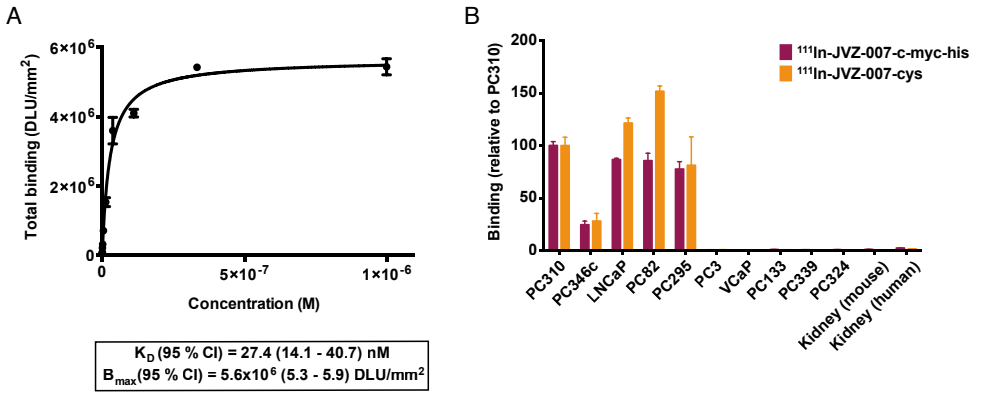

FIGURE 5. (A) Saturation binding of ^{111}In-JVZ-007-c-myc-his on PC-310 frozen sections using autoradiography. (B) Binding of ^{111}In-JVZ-007-c-myc-his and ^{111}In-JVZ-007-cys to tumor and kidney frozen sections using autoradiography. High binding is observed on PSMA-expressing tumor sections (PC310, PC346c, LNCaP, PC82 and PC295) whreas no binding is observed on the PSMA-negative tumors PC3, VCaP, PC133, PC339, PC324) and kidneys (mouse or human). B_{max} = maximum binding; DLU = digital light unit; K_D = equilibrium dissociation constant.

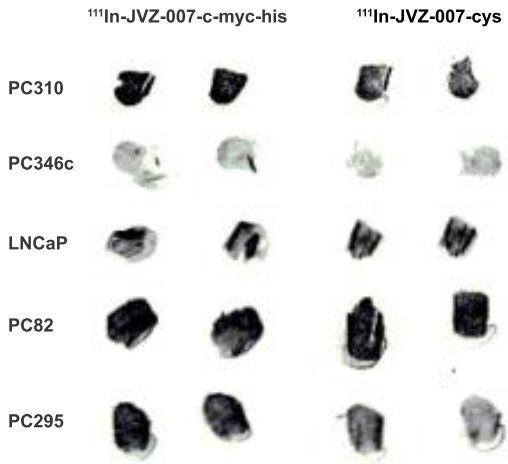

FIGURE 6. Binding of ^{111}In-JVZ-007-c-myc-his and ^{111}In-JVZ-007-cys to PSMA-expressing tumor frozen sections (PC310, PC346c, LNCaP, PC82 and PC295) using autoradiography.

Cell binding assays on PSMA-positive LNCaP cells (**Figure 7**) showed 30% and 37% internalization after 90 min at 37°C, for ^{111}In-JVZ-007-c-*myc*-his and ^{111}In-JVZ-007-cys, respectively. Cell binding of both tracers was blocked in the presence of an excess of unlabeled JVZ-007-c-*myc*-his, confirming target specificity. Internalization of ^{111}In-JVZ-007-c-*myc*-his was confirmed by the strongly reduced amount of radioactivity in the internalized fraction (0.05% of total binding) observed at 4°C. Low binding (<1% relative to LNCaP cells) and absence of internalization of ^{111}In-JVZ-007-c-*myc*-his was observed for the PSMA-negative cell line PC-3, confirming Nanobody specificity for PSMA.

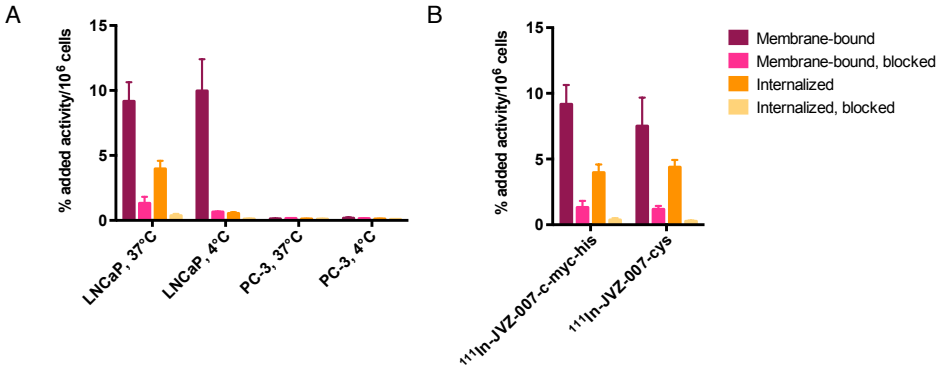

FIGURE 7. (A) Internalization of ^{111}In-JVZ-007-c-myc-his in LNCaP and PC-3 cells, after incubation for 90 min at 37°C and 4°C. (B) Comparison of internalization of ^{111}In-JVZ-007-c-myc-his and ^{111}In-JVZ-007-cys in LNCaP cells after incubation for 90 min at 37°C. ^{111}In-JVZ-007-c-myc-his and ^{111}In-JVZ-007-cys internalized in PSMA-expressing LNCaP cells at 37°C.

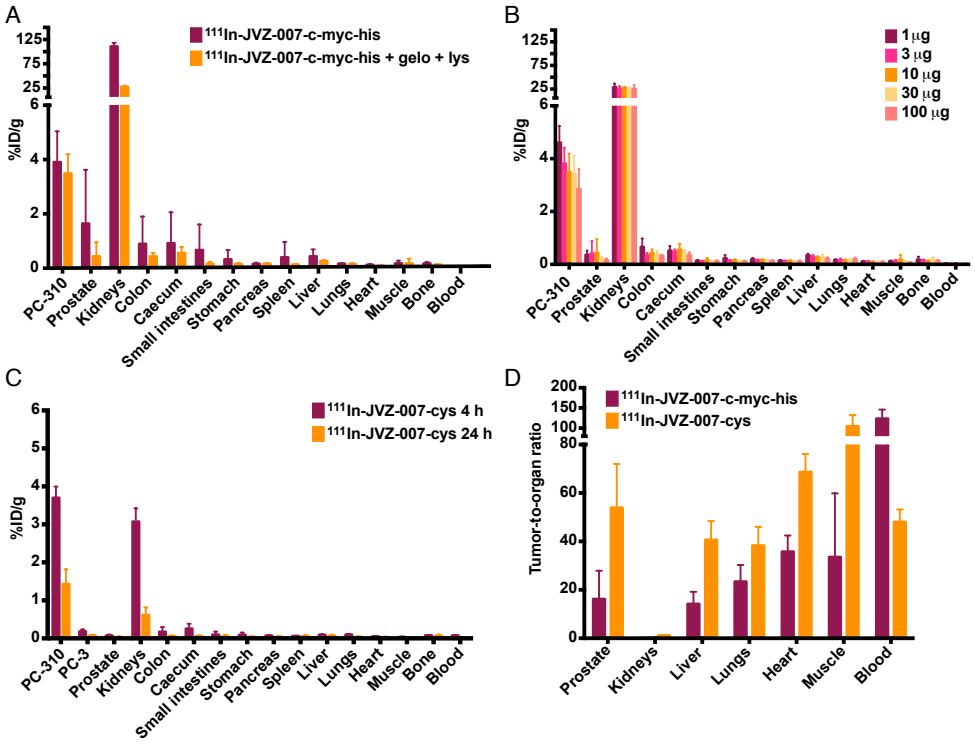

FIGURE 8. Biodistribution studies in mice bearing PC-310 and PC-3 tumors. Effect of coinjection of gelofusine and lysine (A) and dose (B) on biodistribution of ^{111}In-JVZ-007-c-myc-his (10 µg) at 4 h after injection. (C) Biodistribution at 4 and 24 h after injection of ^{111}In-JVZ-007-cys (10 µg) with coinjection of gelofusine and lysine. (D) Tumor-to-organ ratios at 4 h after injection of ^{111}In-JVZ-007-c-myc-his (10 µg) or ^{111}In-JVZ-007-cys (10 µg) with coinjection of gelofusine and lysine.

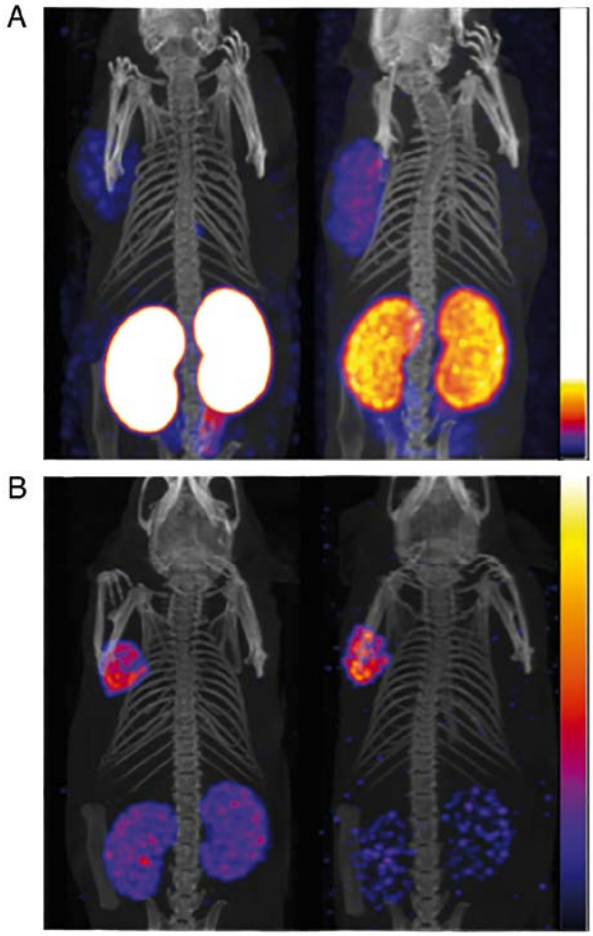

FIGURE 9. SPECT/CT images of mice bearing PC-310 (left shoulder) and PC-3 (right shoulder) tumors. (A) Images acquired 3 h after injection of ^{111}In-JVZ-007-c-myc-his with coinjection of PBS (left) or gelofusine and lysine (right). (B) Images acquired 3 h (left) and 24 h (right) after injection of ^{111}In-JVZ-007-cys with coinjection of gelofusine and lysine. Scale from 0 to 0.2 kBq (A); 0 to 0.015 kBq (B, left); 0 to 0.005 kBq (B, right). PSMA-expressing PC-310 tumor could be clearly visualized with high contrast on the left shoulder, whereas no uptake was observed in PC-3 tumor on the right shoulder.

Biodistribution and SPECT/CT Imaging

The PSMA-targeting properties of ^{111}In-JVZ-007-c-*myc*-his and ^{111}In-JVZ-007-cys were evaluated further in mice bearing PC-310 and PC-3 tumors. Biodistribution studies are displayed in **Figure 8**, showing good tumor targeting, with low background intensity except for the kidneys. Four hours after injection, the uptake of ^{111}In-JVZ-007-c-*myc*-his in the PC-310 tumor was 3.91 ± 1.13 %ID/g. Uptake in the kidneys was 110.89 ± 7.35 %ID/g but could be reduced to 27.77 ± 2.02 %ID/g by coinjection of gelofusine and lysine. Increasing doses of JVZ-007-c-*myc*-his showed a slight decrease in tumor uptake. Similarly, ^{111}In-JVZ-007-cys in combination with gelofusine and lysine showed uptake in PC-310 and PC-3 tumors of 3.70 ± 0.29 %ID/g and 0.18 ± 0.05 %ID/g at 4 h after injection, respectively. Importantly, kidney uptake was approximately 10-fold lower than that of JVZ-007-c-*myc*-his, with values of only 3.13 ± 0.30 and 0.61 ± 0.20 %ID/g, at 4 h and 24 h after injection, respectively. Moreover, ^{111}In-JVZ-007-cys showed higher tumor-to-background ratios at 4 h after injection than ^{111}In-JVZ-007-c-*myc*-his, with a tumor-to-muscle ratio of 104.8 ± 27.4 and tumor-to-kidney ratio of 1.2 ± 0.1. The tumor-to-blood ratio was significantly lower for ^{111}In-JVZ-007-cys (48.1 ± 5.1) than for ^{111}In-JVZ-007-c-*myc*-his.

SPECT/CT images of mice bearing PC-310 and PC-3 tumors 3 h after injection of ^{111}In-JVZ-007-c-*myc*-his and ^{111}In-JVZ-007-cys are shown in **Figure 9**. PSMA-expressing PC-310 tumor could be clearly visualized with high contrast on the right shoulder, whereas no uptake was observed in PC-3 tumor on the left shoulder. Signal intensity in kidneys of ^{111}In-JVZ-007-c-*myc*-his was very high but could be efficiently reduced by coadministration of gelofusine and lysine. Importantly, kidney signal intensity of ^{111}In-JVZ-007-cys was markedly lower.

DISCUSSION

Development of PSMA-based imaging tracers for PCa has increased tremendously in the past few years. After the approval of the PSMA mAb ^{111}In-capromab as an imaging agent in 1997, a panel of novel PSMA-targeted imaging agents was developed, including next-generation antibodies, antibody fragments, aptamers, and PSMA inhibitors (*12*). PSMA small-molecule inhibitors localize rapidly to tumor lesions, including soft-tissue and bone metastases, but also show high uptake in kidneys and salivary glands. The high uptake of PSMA inhibitors in these organs was attributed to PSMA expression, although the expression of PSMA in these organs was shown to be 100- to 1,000-fold lower than in PCa (*6*). This lower PSMA expression in normal organs may suggest that other (receptor-mediated) processes may be involved in tracer uptake in normal organs as well.

In parallel to these developments, alternative strategies have been pursued using smaller variants of mAb, such as antigen-binding fragments (Fab) and F(ab')$_2$ (*21*), and minibodies or diabodies (*22, 23*), aiming to circumvent the long circulation time of mAb. These antibody fragments have shown fast target recognition and rapid blood clearance but also show unspecific accumulation in the liver and kidneys. A more recent approach is the use of Nanobodies (V_{HH}), the smallest antibody-based fragments (12-15 kDa), offering ideal characteristics for molecular imaging. Because of their small size below the renal threshold for glomerular filtration (60 kDa), they are mainly cleared via the renal pathway. Moreover, it is possible to humanize Nanobodies for clinical translation using the recently described universal humanized Nanobody scaffold technique (*24*). Nanobodies targeting PSMA were developed, showing moderate tumor targeting, low liver uptake, and high kidney uptake (*25*). Retention of tracers in the kidneys might be the result of a combination of different factors, including glomerular filtration by the kidney, PSMA-specific binding, and trapping of metabolites in the lysosomes of renal tubular cells. Tracer retention in the kidneys is not desirable, because it may interfere with visualization of small tumor lesions in the vicinity of the kidneys and especially with staging of PCa. Renal tracer retention also limits the application of the PSMA tracer for radionuclide therapy by inflicting a high dose to the kidneys. We have developed a Nanobody (JVZ-007) that shows good tumor targeting in PSMA-expressing PC-310 PDX tumors. JVZ-007 was initially produced with a c-*myc*-his-tag and conjugated to p-SCN-Bn-DTPA via the lysine residues, to allow radiolabeling with ^{111}In for SPECT imaging of PCa. ^{111}In-JVZ-007-c-*myc*-his was internalized in LNCaP cells and showed high binding

on all PSMA-expressing PDX sections in vitro, whereas low binding to the PSMA-negative PDX sections was observed and 50-fold lower binding to the human kidney than the PC-310 tumor, indicating the markedly lower expression levels of PSMA in the kidney. ^{111}In-JVZ-007-c-*myc*-his was evaluated further in mice bearing PC-310 tumors, showing good tumor targeting as early as 4 h after injection, with low background intensity, except for the kidneys. It was recently described that renal retention of an anti-epidermal growth factor receptor Nanobody could be reduced by coinjection of gelofusine and lysine (*26*). Indeed, efficient reduction of renal uptake of our anti-PSMA Nanobody was obtained when gelofusine and lysine were coadministered. These results support that high renal uptake may be due to reabsorption in the renal promixal tubule after glomerular filtration. Moreover, studies from D'Huyvetter et al. (*27*) have also shown that the his-tag plays a major role in the high retention of radiolabeled Nanobodies in the kidneys. Therefore, we have engineered a new Nanobody construct, based on JVZ-007, in which the c-*myc*-his tag was removed. In addition, we introduced a cysteine at the C terminus for site-specific coupling to maleimide-DTPA. For this purpose we used the pETM11-SUMO3GFP expression vector, allowing production of a protein with a C-terminal cysteine and retrieval of the protein by cleavage of SUMO3 by a specific protease. ^{111}In-JVZ-007-cys showed similar binding on PSMA-expressing cells and PDXs. More importantly, a further drop in renal uptake to 3 %ID/g was observed at 4 h after injection, without loss of tumor targeting. In comparison, these renal uptake values in mice were inferior to those found with other PSMA tracers: 100 %ID/g for ^{68}Ga-HBED-CC-PSMA (1 h) (*28*) and ^{111}In-D_2B-Fab fragments (4 h) (*21*). Kidney uptake of 78 and 36 %ID/g were reported for ^{123}I-MIP-1095 and ^{123}I-MIP-1072 (4 h), respectively (*29*). Tumor-to-blood and tumor-to-muscle ratios obtained with ^{111}In-JVZ-007-cys at 4 h after injection were superior to those obtained with ^{111}In-D_2B-Fab fragments (*21*) and comparable to those obtained with ^{123}I-MIP-1095, in LNCaP xenograft mice (4 h) (*29*). The novel method described here for production and site-specific labeling of cys-tagged Nanobodies could have a significant impact for the clinical implementation of a wide range of Nanobodies. The site-specific coupling offers a well-defined labeling procedure, while the absence of the c-*myc*-his-tag limits reabsorption in renal tubular cells. This minimal renal retention also broadens the applicability of this Nanobody to radionuclide therapy.

CONCLUSION

We developed a specific anti-PSMA Nanobody containing a cysteine for site-specific conjugation to radioactive labels. The ^{111}In-radiolabeled anti-PSMA Nanobody shows good tumor targeting and fast blood clearance, allowing SPECT/CT imaging within a few hours after injection. Unlike most radiolabeled small-molecule PSMA inhibitors, anti-PSMA Nanobody JVZ-007 displays a low kidney uptake. These results warrant further evaluation of anti-PSMA Nanobody JVZ-007 for detection and radionuclide therapy of metastatic lesions in PSMA-expressing PCa, for which few treatment options are currently available.

REFERENCES

1. Siegel R, Naishadham D, Jemal A. Cancer statistics, 2012. CA Cancer J Clin. 2012;62:10-29.
2. Bostwick DG, Pacelli A, Blute M, Roche P, Murphy GP. Prostate specific membrane antigen expression in prostatic intraepithelial neoplasia and adenocarcinoma: a study of 184 cases. Cancer. 1998;82:2256-2261.
3. Silver DA, Pellicer I, Fair WR, Heston WD, Cordon-Cardo C. Prostate-specific membrane antigen expression in normal and malignant human tissues. Clin Cancer Res. 1997;3:81-85.
4. Wright GL, Jr., Haley C, Beckett ML, Schellhammer PF. Expression of prostate-specific membrane antigen in normal, benign, and malignant prostate tissues. Urol Oncol. 1995;1:18-28.
5. Wright GL, Jr., Grob BM, Haley C, et al. Upregulation of prostate-specific membrane antigen after androgen-deprivation therapy. Urology. 1996;48:326-334.
6. Sokoloff RL, Norton KC, Gasior CL, Marker KM, Grauer LS. A dual-monoclonal sandwich assay for prostate-specific membrane antigen: levels in tissues, seminal fluid and urine. Prostate. 2000;43:150-157.
7. Ellis RJ, Kaminsky DA, Zhou EH, et al. Ten-year outcomes: the clinical utility of single photon emission computed tomography/computed tomography capromab pendetide (Prostascint) in a cohort diagnosed with localized prostate cancer. Int J Radiat Oncol Biol Phys. 2011;81:29-34.
8. Apolo AB, Pandit-Taskar N, Morris MJ. Novel tracers and their development for the imaging of metastatic prostate cancer. J Nucl Med. 2008;49:2031-2041.
9. Bander NH, Nanus DM, Milowsky MI, Kostakoglu L, Vallabahajosula S, Goldsmith SJ. Targeted systemic therapy of prostate cancer with a monoclonal antibody to prostate-specific membrane antigen. Semin Oncol. 2003;30:667-676.
10. Milowsky MI, Nanus DM, Kostakoglu L, Vallabhajosula S, Goldsmith SJ, Bander NH. Phase I trial of yttrium-90-labeled anti-prostate-specific membrane antigen monoclonal antibody J591 for androgen-independent prostate cancer. J Clin Oncol. 2004;22:2522-2531.
11. Tagawa ST, Beltran H, Vallabhajosula S, et al. Anti-prostate-specific membrane antigen-based radioimmunotherapy for prostate cancer. Cancer. 2010;116:1075-1083.
12. Mease RC, Foss CA, Pomper MG. PET imaging in prostate cancer: focus on prostate-specific membrane antigen. Curr Top Med Chem. 2013;13:951-962.
13. Barrett JA, Coleman RE, Goldsmith SJ, et al. First-in-man evaluation of 2 high-affinity PSMA-avid small molecules for imaging prostate cancer. J Nucl Med. 2013;54:380-387.
14. Cho SY, Gage KL, Mease RC, et al. Biodistribution, tumor detection, and radiation dosimetry of 18F-DCFBC, a low-molecular-weight inhibitor of prostate-specific membrane antigen, in patients with metastatic prostate cancer. J Nucl Med. 2012;53:1883-1891.
15. Afshar-Oromieh A, Avtzi E, Giesel FL, et al. The diagnostic value of PET/CT imaging with the (68) Ga-labelled PSMA ligand HBED-CC in the diagnosis of recurrent prostate cancer. Eur J Nucl Med Mol Imaging. 2015;42:197-209.
16. Beheshti M, Kunit T, Haim S, et al. BAY 1075553 PET-CT for Staging and Restaging Prostate Cancer Patients: Comparison with [F] Fluorocholine PET-CT (Phase I Study). Mol Imaging Biol. 2014;17:424-433.
17. Cortez-Retamozo V, Lauwereys M, Hassanzadeh Gh G, et al. Efficient tumor targeting by single-domain antibody fragments of camels. Int J Cancer. 2002;98:456-462.
18. Behar G, Siberil S, Groulet A, et al. Isolation and characterization of anti-FcgammaRIII (CD16) llama single-domain antibodies that activate natural killer cells. Protein Eng Des Sel. 2008;21:1-10.

19. Mikolajczyk J, Drag M, Bekes M, Cao JT, Ronai Z, Salvesen GS. Small ubiquitin-related modifier (SUMO)-specific proteases: profiling the specificities and activities of human SENPs. J Biol Chem. 2007;282:26217-26224.
20. Chatalic KL, Franssen GM, van Weerden WM, et al. Preclinical comparison of Al18F- and 68Ga-labeled gastrin-releasing peptide receptor antagonists for PET imaging of prostate cancer. J Nucl Med. 2014;55:2050-2056.
21. Lutje S, van Rij CM, Franssen GM, et al. Targeting human prostate cancer with 111In-labeled D2B IgG, F(ab')2 and Fab fragments in nude mice with PSMA-expressing xenografts. Contrast Media Mol Imaging. 2015;10:28-36.
22. Viola-Villegas NT, Sevak KK, Carlin SD, et al. Noninvasive Imaging of PSMA in prostate tumors with (89)Zr-Labeled huJ591 engineered antibody fragments: the faster alternatives. Mol Pharm. 2014;11:3965-3973.
23. Kampmeier F, Williams JD, Maher J, Mullen GE, Blower PJ. Design and preclinical evaluation of a 99mTc-labelled diabody of mAb J591 for SPECT imaging of prostate-specific membrane antigen (PSMA). EJNMMI Res. 2014;4:13.
24. Vincke C, Loris R, Saerens D, Martinez-Rodriguez S, Muyldermans S, Conrath K. General strategy to humanize a camelid single-domain antibody and identification of a universal humanized nanobody scaffold. J Biol Chem. 2009;284:3273-3284.
25. Evazalipour M, D'Huyvetter M, Tehrani BS, et al. Generation and characterization of nanobodies targeting PSMA for molecular imaging of prostate cancer. Contrast Media Mol Imaging. 2014;9:211-220.
26. Gainkam LO, Caveliers V, Devoogdt N, et al. Localization, mechanism and reduction of renal retention of technetium-99m labeled epidermal growth factor receptor-specific nanobody in mice. Contrast Media Mol Imaging. 2011;6:85-92.
27. D'Huyvetter M, Vincke C, Xavier C, et al. Targeted radionuclide therapy with A 177Lu-labeled anti-HER2 nanobody. Theranostics. 2014;4:708-720.
28. Eder M, Schafer M, Bauder-Wust U, et al. 68Ga-complex lipophilicity and the targeting property of a urea-based PSMA inhibitor for PET imaging. Bioconjug Chem. 2012;23:688-697.
29. Hillier SM, Maresca KP, Femia FJ, et al. Preclinical evaluation of novel glutamate-urea-lysine analogues that target prostate-specific membrane antigen as molecular imaging pharmaceuticals for prostate cancer. Cancer Res. 2009;69:6932-6940.

3.2

Towards Personalized Treatment of Prostate Cancer: PSMA I&T, a Promising Prostate-Specific Membrane Antigen-Targeted Theranostic Agent

Kristell L.S. Chatalic[1,2,3†], Sandra Heskamp[4†], Mark Konijnenberg[1], Janneke D.M. Molkenboer-Kuenen[4], Gerben M. Franssen[4], Marian C. Clahsen-van Groningen[5], Margret Schottelius[6], Hans-Jürgen Wester[6], Wytske M. van Weerden[3], Otto C. Boerman[4], Marion de Jong[1,2]

[†]These authors contributed equally to this work.
[1]Department of Nuclear Medicine, Erasmus MC Rotterdam, The Netherlands
[2]Department of Radiology, Erasmus MC Rotterdam, The Netherlands
[3]Department of Urology, Erasmus MC, Rotterdam, The Netherlands
[4]Department of Radiology and Nuclear Medicine, Radboud University Medical Center, Nijmegen, The Netherlands
[5]Department of Pathology, Erasmus MC, Rotterdam, The Netherlands
[6]Pharmaceutical Radiochemistry, Technische Universität München, Garching, Germany

Submitted for publication

ABSTRACT

Prostate-specific membrane antigen (PSMA) is a well-established target for nuclear imaging and therapy of prostate cancer (PCa). Radiolabeled small-molecule PSMA inhibitors are excellent candidates for PCa theranostics – they rapidly and efficiently localize in tumor lesions. However, high tracer uptake in kidneys and salivary glands are major concerns for therapeutic applications. Here, we present the preclinical application of PSMA I&T, a DOTAGA-chelated urea-based PSMA inhibitor, for SPECT/CT imaging and radionuclide therapy of PCa. ^{111}In-PSMA I&T showed dose-dependent uptake in PSMA-expressing tumors, kidneys, spleen, adrenals, lungs and salivary glands. Coadministration of 2-(phosphonomethyl)pentane-1,5-dioic acid (2-PMPA) efficiently reduced PSMA-mediated renal uptake of ^{111}In-PSMA I&T, with the highest tumor/kidney radioactivity ratios being obtained using a dose of 50 nmol 2-PMPA. SPECT/CT clearly visualized subcutaneous tumors and sub-millimeter intraperitoneal metastases; however, high renal and spleen uptake in control mice (no 2-PMPA) interfered with visualization of metastases in the vicinity of those organs. Coadministration of 2-PMPA increased the tumor-to-kidney absorbed dose ratio during ^{177}Lu-PSMA I&T radionuclide therapy. Hence, at equivalent absorbed dose to the tumor (36 Gy), coinjection of 2-PMPA decreased absorbed dose to the kidneys from 30 Gy to 12 Gy. Mice injected with ^{177}Lu-PSMA I&T only, showed signs of nephrotoxicity at 3 months after therapy, whereas mice injected with ^{177}Lu-PSMA I&T + 2-PMPA did not. These data indicate that PSMA I&T is a promising theranostic tool for PCa. PSMA-specific uptake in kidneys can be successfully tackled using blocking agents such as 2-PMPA.

INTRODUCTION

Prostate cancer (PCa) is a major health problem in men. Prognosis is dependent on stage of the disease and the five-year survival rate for advanced, disseminated PCa is only 29% (*1*). Metastatic castration-resistant PCa (mCRPC) is associated with poor prognosis and diminished quality of life. Treatment options for mCRPC patients include taxane-based therapies (docetaxel, cabazitaxel) and novel second-line hormonal therapies (enzalutamide and abiterone), all showing moderate survival benefits. Unfortunately, those therapies are only temporarily effective and development of treatment resistance is observed (*2, 3*). The bone-seeking alpha-emitting radiopharmaceutical Radium-223 chloride (Xofigo™) has recently been introduced, resulting in reduction of bone pain and moderately improved survival in mCRPC patients with bone metastases (*4, 5*). However, the use of this promising radiopharmaceutical is limited to the treatment of bone metastases. Therefore, there is an urgent need to develop more specific therapies that target PCa visceral lesions as well.

Recent developments in PCa-targeted radiopharmaceuticals have focused on prostate-specific membrane antigen (PSMA) ligands. PSMA is a favorable target for imaging and radionuclide therapy of PCa, because it is overexpressed in 90-100% of local PCa lesions, as well as in cancerous lymph node metastases and bone lesions. Furthermore, reports indicate that PSMA expression levels are further enhanced in high-grade, metastatic and castration-resistant PCa (*6-9*).

Numerous studies have shown the value of radiolabeled PSMA-targeted agents to visualize PCa lesions, including PCa metastases (*10-18*). Among the different PSMA-targeting tracers available, several tracers have made their way to the clinic. For PET imaging of PCa, Glu-NH-CO-NH-Lys-(Ahx)-^{68}Ga-HBED-CC, also known as ^{68}Ga-PSMA-11 or ^{68}Ga-PSMA-HBED-CC, is the most commonly used compound (*14, 18*). Unfortunately, HBED-CC (N,N'-bis[2-hydroxy-5-(carboxyethyl)benzyl] ethylenediamine-N,N'-diacetic acid), the chelator used in this tracer, is not suitable for radiolabeling with radiometals for therapeutic applications (e.g. ^{177}Lu, ^{90}Y, ^{213}Bi). More recently, a novel ^{18}F-labeled PSMA inhibitor, ^{18}F-DCFPyL, was introduced in the clinic (*19*). For therapy, anti-PSMA monoclonal antibodies (J591) radiolabeled with ^{177}Lu and ^{90}Y (*11, 20, 21*) and the small-molecule PSMA inhibitor [^{131}I]MIP-1095 (*22*) have shown promising therapeutic efficacy, although with moderate toxicity. Moreover, PSMA ligands with DOTA-derived chelators have been developed, which can be labeled with diagnostic radionuclides, e.g. ^{68}Ga for PET and ^{111}In for SPECT, as well as therapeutic radionuclides, e.g. ^{177}Lu, ^{90}Y or ^{213}Bi for radionuclide therapy. Such theranostic compounds, i.e. PSMA I&T and PSMA-617, are of great interest because they combine the potential of diagnosis and radionuclide therapy using one PSMA targeting molecule (*23-27*).

Radioligand properties, e.g. lipophilicity, target affinity and metabolic stability have been carefully optimized for theranostic applications. Monoclonal antibodies showed

slow blood clearance, which may result in myelotoxicity. Small-molecule PSMA inhibitors showed the advantage to localize rapidly in tumor lesions, including soft-tissue and bone metastases. On the other hand, these small inhibitors showed high and specific uptake in PSMA-expressing kidneys and salivary glands, which is of major concern for its application for radionuclide therapy. Strategies should therefore be investigated to limit radiation-induced damage in healthy organs. Here we report on the preclinical application of the DOTAGA-chelated urea-based PSMA inhibitor PSMA I&T for SPECT/CT imaging and radionuclide therapy of PCa. In this study we investigated if coinjection of ^{111}In-PSMA I&T with 2-(phosphonomethyl)pentane-1,5-dioic acid (2-PMPA) could contribute to increasing tumor-to-kidney uptake ratio, thereby facilitating visualization of metastatic lesions in the vicinity of the kidneys, and most importantly reducing toxicity during radionuclide therapy.

MATERIALS AND METHODS

Cell Culture

The human prostate cancer cell line LNCaP was cultured in RPMI 1640 medium (GIBCO, BRL Life Sciences Technologies, The Netherlands), supplemented with 2 mM glutamine (GIBCO) and 10% fetal calf serum (FCS, Sigma-Aldrich Chemie BV, The Netherlands) at 37 °C in a humidified atmosphere with 5% CO_2. LS174T colon carcinoma cells were stably transfected with human PSMA using the plasmid pcDNA3.1-hPSMA and cultured in RPMI 1640 medium supplemented with 2 mM glutamine, 10% FCS, and 0.3 mg/ml G418 (*28*).

Radiolabeling

^{111}In labeling

PSMA I&T (**Figure 1**), a DOTAGA-chelated urea-based PSMA inhibitor, was synthetized as described previously (*25*) and kindly provided by the Technical University Munich. PSMA I&T was radiolabeled with $^{111}InCl_3$ (Mallinckrodt BV, Petten, The Netherlands) in 0.5 M 2-(N-morpholino)ethanesulfonic acid (MES) buffer (twice volume of $^{111}InCl_3$), pH 5.5, for 10 min at 95 °C under metal-free conditions (*29*). After incubation, 4 mM diethylenetriaminepentaacetic acid (DTPA) was added to a final concentration of 0.2 mM to complex free $^{111}InCl_3$. Labeling efficiency was determined by instant thin-layer chromatography (ITLC) using silica gel coated paper (Agilent Technologies, Palo Alto, CA) and 0.1 M ammonium acetate containing 0.1 M ethylenediaminetetraacetic acid (EDTA), pH 5.5, as the mobile phase. Labeling efficiency exceeded 95% in all experiments.

^{177}Lu labeling

No-carrier added (n.c.a.) $^{177}LuCl_3$ was obtained from Isotope Technologies Garching (ITG) GmbH (Garching, Germany). Labeling was performed in 0.5 M MES buffer

(twice volume of $^{177}LuCl_3$), pH 5.5, for 20 min at 95 °C. EDTA was added to a final concentration of 5 mM to complex free $^{177}Lu^{3+}$ after reaction. Labeling efficiency was determined by ITLC and radiochemical purity by reverse-phase high performance liquid chromatography (RP-HPLC) on an Agilent 1200 system (Agilent Technologies). A monolithic C18 column (Onyx, 4.6 x 100 mm; Phenomenex, Torrance, CA) was used at a flow rate of 1 ml/min with the following buffer system: buffer A, 0.1% v/v TFA in water; buffer B, 0.1% v/v TFA in acetonitrile; and a gradient of 97% to 0% buffer A (5-15 min). The radioactivity of the eluate was monitored using an in-line NaI radiodetector (Raytest GmbH, Straubenhardt, Germany). Elution profiles were

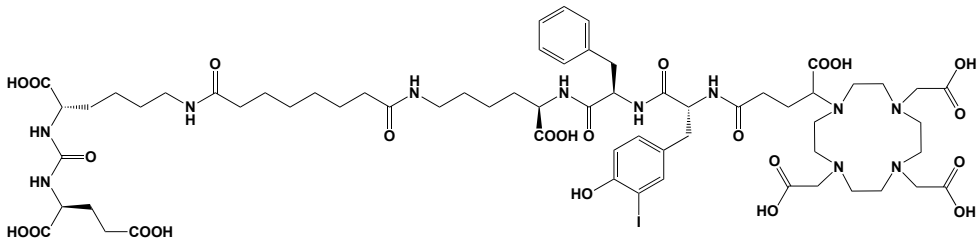

FIGURE 1. Chemical structure of PSMA I&T

analyzed using Gina-star software (version 2.18; Raytest GmbH). Labeling efficiency was 95% and radiochemical purity was 93-95%.

Scatchard Analysis of PSMA I&T

Scatchard analysis was performed to determine the dissociation constant (K_d) of ^{111}In-PSMA I&T and to quantitatively measure PSMA expression on LNCaP and LS174T-PSMA cells. Cells were cultured to confluence in six-well plates and incubated for 4 h on ice with increasing concentrations ^{111}In-PSMA I&T (0.03 – 30 nM) in 1 ml RPMI 1640 containing 0.5% BSA. Nonspecific binding was determined by coincubation with 100 µM PSMA I&T. After incubation, cells were washed with PBS and the cell-associated activity was measured in a shielded well-type gamma counter. The specific binding (total binding – nonspecific binding) was plotted against the bound/free ratio. Data were analyzed by linear regression to determine PSMA antigen density per cell and to determine the K_d of ^{111}In-PSMA I&T.

Autoradiography

Binding of ^{111}In-PSMA I&T to 10-mm frozen sections of patient-derived xenografts (PDXs) and of human and mouse kidneys was evaluated using autoradiography, as described previously (*30*). Tissue sections were incubated for 1 h with ^{111}In-PSMA I&T (10^{-9} M).

Animal Studies

Animal experiments were performed in male BALB/c nude mice (Janvier, le Genest-Saint-Isle, France) and were conducted in accordance with the principles laid out by the revised Dutch Act on Animal Experimentation (1997) and approved by the institutional Animal Welfare Committee of the Radboud University Nijmegen. At 6-8 weeks of age, mice were inoculated subcutaneously with 3 x 10^6 LNCaP cells (in RPMI-1640 medium:matrigel 2:1, BD Biosciences, Pharmingen) and/or 2.5 x 10^6 LS174T in RPMI-1640 medium. Because LS174T-PSMA xenografts showed better tumor take and more reproducible growth, the LS174T-PSMA model was selected for pharmacokinetic and therapeutic experiments. The tracer was injected when tumors reached a size of approximately 0.1 cm^3. For SPECT/CT imaging of intraperitoneal tumors, mice were inoculated with 1 x 10^6 LS174T-PSMA cells in RPMI-1640 medium intraperitoneally and imaged 2-3 weeks after inoculation.

Dose Escalation Study

Four groups of five mice with subcutaneous PSMA-expressing xenografts (right flank: LNCaP, left flank: LS174T-PSMA) received an intravenous injection of 0.2 MBq ^{111}In-PSMA I&T (specific activity 2 MBq/nmol) in the tail vein. The effect of the dose of PSMA I&T on the biodistribution of ^{111}In-PSMA I&T was studied by administering different doses (0.1 – 0.3 – 1 – 10 nmol/mouse) to groups of five mice. Two hours post injection, mice were euthanized using CO_2/O_2-asphyxiation and the biodistribution of ^{111}In-PSMA I&T was determined ex vivo. Tumors, blood, and relevant organs and tissues were dissected, weighed, and radioactivity in each sample was quantified using a γ-counter. The results were expressed as percentage of injected dose per gram of tissue (%ID/g).

Reduction of Renal Tracer Uptake with 2-PMPA

Five groups of five mice with subcutaneous LS174T-PSMA and LNCaP xenografts received an intravenous injection of 0.2 MBq ^{111}In-PSMA I&T (0.3 nmol) in vehicle (PBS/ 0.5% BSA) in the tail vein. Mice were injected with either ^{111}In-PSMA I&T alone or in combination with 2-PMPA (10, 20, 50 nmol) to reduce specific binding in kidneys. One additional group was injected with 4 mg gelofusine 6 min before injection of ^{111}In-PSMA I&T to investigate tubular reabsorption mediated renal uptake. Two hours after injection, mice were euthanized and the biodistribution was determined ex vivo.

To determine the best time point of 2-PMPA injection, five groups of five mice with subcutaneous LS174T-PSMA xenografts received an intravenous injection of 0.2 MBq ^{111}In-PSMA I&T (0.3 nmol) with a preinjection (15 or 60 min), a coinjection, or a postinjection (15 or 60 min) of 50 nmol of 2-PMPA. Two hours after injection, mice were euthanized and the biodistribution was determined ex vivo.

Pharmacokinetics

To determine the pharmacokinetics of ^{111}In-PSMA I&T, eight groups of four mice with subcutaneous LS174T-PSMA xenografts received an intravenous injection of 0.2 MBq ^{111}In-PSMA I&T (0.3 nmol) followed by ex vivo biodistribution at 1, 4, 24, and 48 h after injection. Mice were injected with or without 2-PMPA (50 nmol) coinjection to study the effect of 2-PMPA on tumor and kidney retention of ^{111}In-PSMA I&T.

Dosimetry

Biodistribution data obtained in the pharmacokinetic study were used to estimate the absorbed radiation doses to the organs and tumor. A single-exponential expression was fitted to the activity data at 1, 4, 24 and 48 h, and the cumulative activity concentration in each organ was calculated by analytic integration of the fitted expression.

Absorbed doses to the organs were calculated according to the MIRD-scheme (*31*) with the following equation: $D\left(r_T\right)=\sum_{r_S}\tilde{A}\left(r_S\right)\times S\left(r_T\leftarrow r_S\right)$, with $D\left(r_T\right)$ the absorbed dose to a target organ r_T, $\tilde{A}\left(r_S\right)$ the time-integrated activity in a source organ r_S and $S\left(r_T\leftarrow r_S\right)$ the absorbed dose rate per unit activity of ^{177}Lu. The S-values were obtained for a standardized 25 g mouse from the RADAR realistic animal models (*32*). The biodistribution data were measured in activity concentration and hence the time-integrated activity concentration was obtained and this was multiplied with the source organ mass, as used in the phantom for the S-value calculation. The dosimetry calculations assume comparable biodistribution of ^{111}In-PSMA I&T and ^{177}Lu-PSMA I&T. Absorbed doses to renal cortex were estimated assuming localization of ^{177}Lu-PSMA I&T in the cortex (*33*).

SPECT/CT Imaging

Mice with subcutaneous (n = 4) or intraperitoneal (n = 12) LS174T-PSMA tumors were injected with 20 MBq ^{111}In-PSMA I&T (0.3 nmol, specific activity 67 MBq/nmol), with or without coinjection of 2-PMPA (50 nmol). One hour after injection, mice were euthanized by CO_2/O_2 asphyxation and images were acquired with the U-SPECT-II/CT (MILabs, Utrecht, The Netherlands) (*34*). Mice were scanned for 50 min using the 1.0 mm diameter pinhole mouse high sensitivity collimator tube, followed by a CT scan (spatial resolution 160 µm, 65 kV, 615 µA) for anatomical reference. Scans were reconstructed with MILabs reconstruction software, using an ordered-subset expectation maximization algorithm, energy window 154 – 188 kEv, 3 iterations, 16 subsets, voxel size of 0.2 mm, and Gaussian filter 0.4 mm. SPECT/CT scans were analyzed and maximum intensity projections (MIPs) were created using the Inveon Research Workplace software (IRW, version 4.1).

Radionuclide Therapy

To assess potential renal toxicity of ^{177}Lu-PSMA I&T, three groups of four mice with subcutaneous LS174T-PSMA xenografts were injected intravenously with 100 MBq ^{177}Lu-PSMA I&T (0.35 nmol) with or without 2-PMPA (50 nmol) coinjection, or with vehicle (PBS/ 0.5% BSA). Body weight was monitored twice weekly. Renal function was assessed three months after treatment by quantification of renal uptake of ^{99m}Tc-dimercaptosuccinic acid (^{99m}Tc-DMSA) using SPECT (**J**) and by measuring plasma creatinine levels. DMSA (Renocis, IBA Molecular, The Netherlands) was radiolabeled with $^{99m}TcO_4^-$, which was eluated from a ^{99}Mo/^{99m}Tc-generator (GE Healthcare, The Netherlands). Mice were injected with 29 ± 5 MBq ^{99m}Tc-DMSA and images were acquired with the U-SPECT-II/CT, 2 h post injection, 20 min acquisition, scan range of 2.6 x 2.6 x 5.2 cm, using the 1.0 mm diameter pinhole mouse high sensitivity collimator tube. Scans were reconstructed with MILabs reconstruction software, using an ordered-subset expectation maximization algorithm, energy window 126-154 kEv, 3 iterations, 16 subsets, voxel size of 0.2 mm, and Gaussian filter 0.4 mm. Standards containing ^{99m}Tc-DMSA (0.036-3.36 MBq) were scanned using the same scanning protocol and a standard curve was derived for quantification. Scans were quantified by drawing a volume of interest (VOI) around the kidneys using the IRW software. Four days prior to scanning, plasma samples were collected and creatinine levels were analyzed by Aeroset (Abbott Diagnostics). Endpoint criteria were defined as body weight loss of > 20% of the initial body weight or body weight loss of > 15% within two days. One mouse reached a humane endpoint criterion 111 days after the start of therapy. The other mice were euthanized 118 days after the start of therapy for histopathological analysis of the kidneys. Two-µm sections of paraffin-embedded kidneys were stained with periodic acid Schiff following routine diagnostic procedures and analyzed for morphological alterations by an experienced pathologist (MC).

To determine the therapeutic efficacy of ^{177}Lu-PSMA I&T, three groups of ten mice with subcutaneous LS174T-PSMA xenografts were injected intraveneously with 100 MBq ^{177}Lu-PSMA I&T (0.35 nmol) with or without 2-PMPA (50 nmol) coinjection, or with vehicle (PBS/ 0.5% BSA). Tumor growth was monitored by caliper measurements in three dimensions twice weekly. Body weight was monitored twice weekly. Endpoint criteria were defined as (1) body weight loss of > 20% of the initial body weight or body weight loss of > 15% within two days, (2) tumor volume of 2000 mm^3, (3) ulceration of the tumor.

Statistical Analysis

Statistical analyses were performed using PASW Statistics version 18.0 (Chicago, IL) and GraphPad Prism version 5.03 (San Diego, CA). Differences in uptake of ^{111}In-PSMA I&T were tested for significance using the nonparametric Kruskal-Wallis and Mann-Whitney U test. Survival was described with the median survival, and survival curves were compared with the log-rank test. A p-value below 0.05 was considered significant.

RESULTS

^{111}In-PSMA I&T Shows High Specificity to PSMA-Expressing PCa Cells, PCa Xenografts, and Kidneys In Vitro

Binding of ^{111}In-PSMA I&T was assessed in vitro on LNCaP and LS174T-PSMA cells in saturation binding experiments. The equilibrium binding constant (K_d) of ^{111}In-PSMA I&T was 3.9 ± 1.2 nM for LNCaP and 5.6 ± 1.2 nM for LS174T-PSMA. The number of ^{111}In-PSMA I&T binding sites was 43,000 ± 6,000 for LS174T-PSMA and 137,000 ± 13,000 sites/cell for LNCaP.

Binding of ^{111}In-PSMA I&T was also evaluated on frozen xenograft tumors and kidney sections using autoradiography as shown in **Figure 2**. ^{111}In-PSMA I&T showed high binding to all PSMA-expressing xenograft sections (LNCaP, PC310, PC346c, PC295 and PC82) and PSMA-expressing kidneys (mouse and human). Binding to LNCaP tumors was 6 times higher than binding to human kidneys and binding to mouse kidney was 2 times higher than binding to human kidneys. Binding to the PSMA-negative tumors (PC3, VCaP, PC133, PC339, PC324) was very low, showing the target-specificity of the tracer.

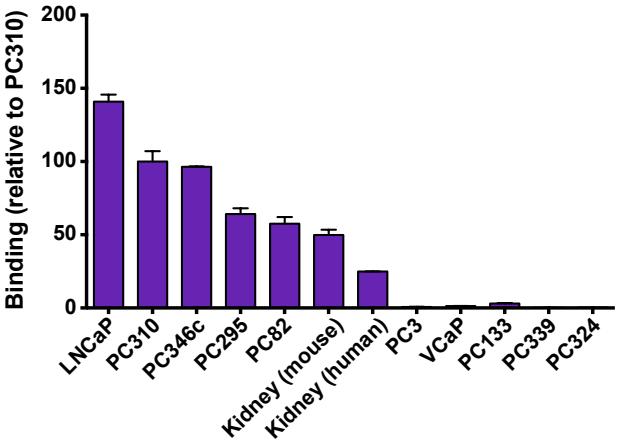

FIGURE 2. Specificity of ^{111}In-PSMA I&T for detecting PSMA-expressing tumors and tissues. High binding was observed on PSMA-expressing tumor sections (LNCaP, PC310, PC346c, PC295 and PC82) and PSMA-expressing kidneys (mouse and human), whereas no binding was observed to the PSMA-negative tumors (PC3, VCaP, PC133, PC339, PC324).

^{111}In-PSMA I&T Specifically Accumulates in PSMA-Expressing Human Xenografts in Mice

The optimal tumor targeting doses of ^{111}In-PSMA I&T were 0.1 – 0.3 nmol for LS174T-PSMA tumors and 0.1 – 1.0 nmol for LNCaP tumors (**Figure 3A**). Tumor uptake with 0.3 nmol ^{111}In-PSMA I&T was 17.0 ± 2.4 %ID/g and 11.7 ± 5.5 %ID/g for LS174T-PSMA and LNCaP, respectively ($p = 0.095$). Tumor uptake was significantly reduced from 0.3 nmol to 1 nmol tracer ($p = 0.008$) and 1 nmol to 10 nmol tracer ($p = 0.008$)

for LS174T-PSMA and LNCaP, respectively. The tracer also specifically accumulated in kidneys, spleen, lungs, salivary glands, and adrenals. The highest uptake was measured in kidneys (122 ± 27.0 %ID/g for 0.3 nmol ^{111}In-PSMA I&T).

Coinjection of 2-PMPA Significantly Reduces Renal Uptake of ^{111}In-PSMA I&T

To reduce renal retention, different kidney protecting strategies were evaluated (**Figure 3B**). Coinjection of 4 mg gelofusine did not significantly reduce renal uptake of ^{111}In-PSMA I&T ($p = 0.42$), whereas coinjection of 10 nmol 2-PMPA significantly reduced uptake in kidneys ($p = 0.008$), spleen ($p = 0.016$), lung ($p = 0.032$), adrenals ($p = 0.032$), and LS174T-PSMA tumors ($p = 0.008$), but not in LNCaP tumors ($p = 0.310$). The highest tumor-to-kidney ratios for LS174T-PSMA were obtained with 50 nmol 2-PMPA. Coinjection of 50 nmol 2-PMPA resulted in a 7-fold reduction in renal uptake (from 135.9 ± 31.2 %ID/g to 19.5 ± 1.8 %ID/g), whereas tumor uptake was only reduced two-fold: from 14.9 ± 2.8 %ID/g to 6.8 ± 1.0 %ID/g (LS174T-PSMA) and from 11.0 ± 6.0 %ID/g to 5.4 ± 2.3 %ID/g (LNCaP). Timing of 2-PMPA injection significantly influenced the tumor/kidney tracer uptake ratios ($p<0.001$). Most effective renal tracer uptake reduction was obtained by coinjection of ^{111}In-PSMA I&T with 2-PMPA or preinjection of 2-PMPA 15 min before ^{111}In-PSMA I&T. Kidney/tumor tracer uptake ratio was significantly higher after coinjection as compared to 15 min preinjection ($p = 0.008$) of 2-PMPA (**Figure 3C**).

Coinjection of 2-PMPA Improves the Tumor-to-Kidney Absorbed Dose Ratio

The optimal ^{111}In-PSMA I&T tracer dose (0.3 nmol) was selected to determine the tracer pharmacokinetics. Biodistribution studies were performed with and without 2-PMPA (coinjection of 50 nmol) for renal protection. For ^{111}In-PSMA I&T alone, uptake in tumor was the highest at 1 and 4 h after injection, and significantly decreased between 4 and 24 h after injection ($p = 0.029$) (**Figure 4A**). For ^{111}In-PSMA I&T with 2-PMPA coinjection, tumor uptake was the highest at 1 h after injection and significantly decreased from 1 to 4 h after injection already ($p = 0.029$) (**Figure 4B**). Uptake in PSMA-expressing healthy organs significantly decreased for both groups between 4 and 24 h after injection ($p = 0.029$).

Single-exponential curves were fitted to the biodistribution data and estimated absorbed doses to tumor and organs were calculated (**Figure 4C**). Estimated absorbed doses from 100 MBq ^{177}Lu-PSMA I&T in tumor, kidneys, spleen, and adrenals were 36, 30, 1, and 2 Gy, respectively, for ^{177}Lu-PSMA I&T alone and 15, 5, 0.2, and 0.3 Gy, respectively, for ^{177}Lu-PSMA I&T with 2-PMPA. Tumor-to-kidney dose ratio was substantially improved from 1.2 to 3.0 when ^{177}Lu-PSMA I&T was co-injected with 2-PMPA. Consequently, at an equivalent absorbed dose to the tumor (36 Gy), coinjection of 2-PMPA decreases absorbed dose to the kidneys from 30 Gy to 12 Gy. These absorbed doses to kidneys were calculated assuming uniform distribution of radioactivity. However, SPECT

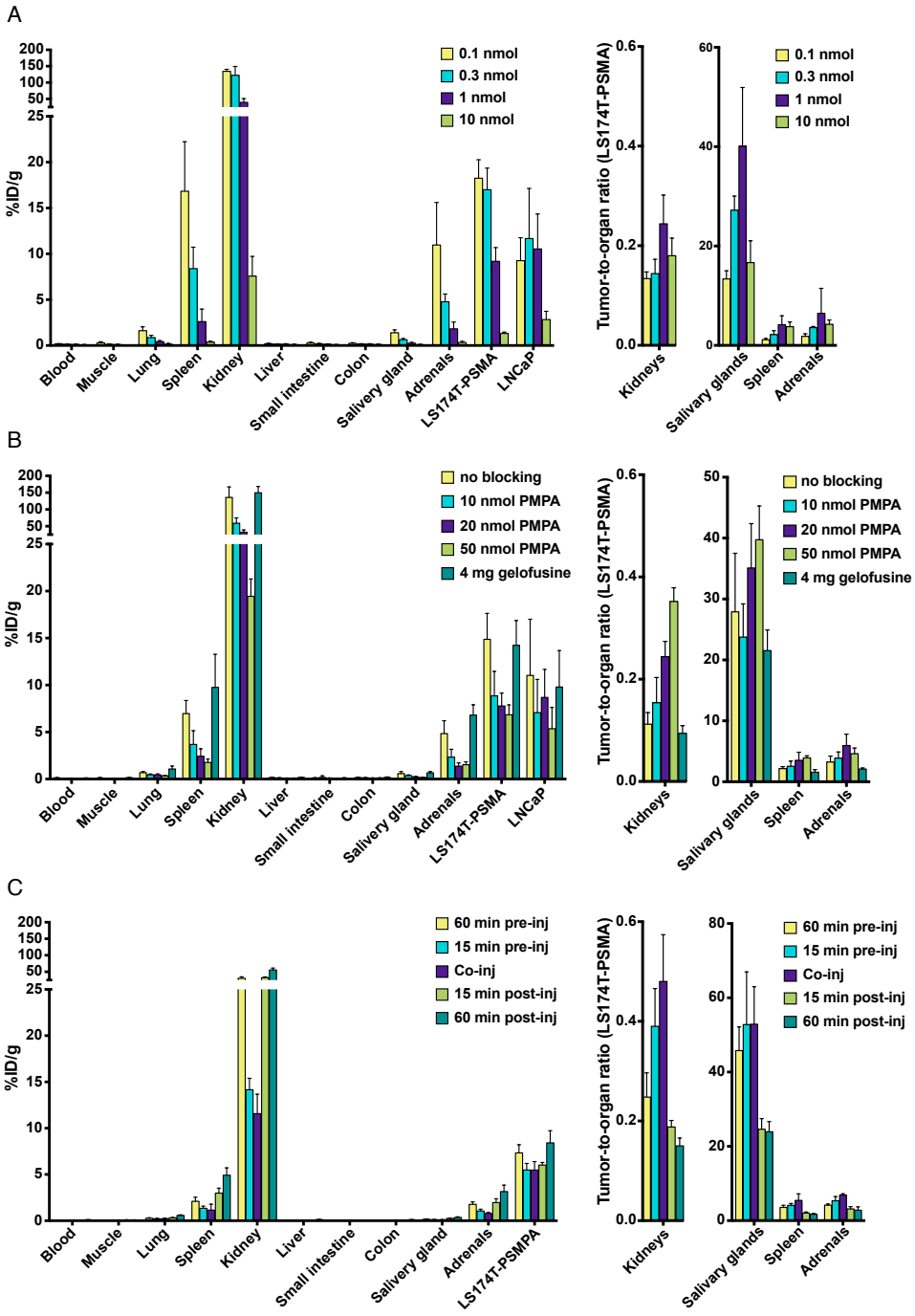

FIGURE 3. Biodistribution of ^{111}In-PSMA I&T in mice bearing LS174T-PSMA and LNCaP xenografts. Dose optimization (A), effect of 2-PMPA coinjection (10-50 nmol) or preinjection of gelofusine (B), and time schedule optimization of 2-PMPA injection (C) are depicted.

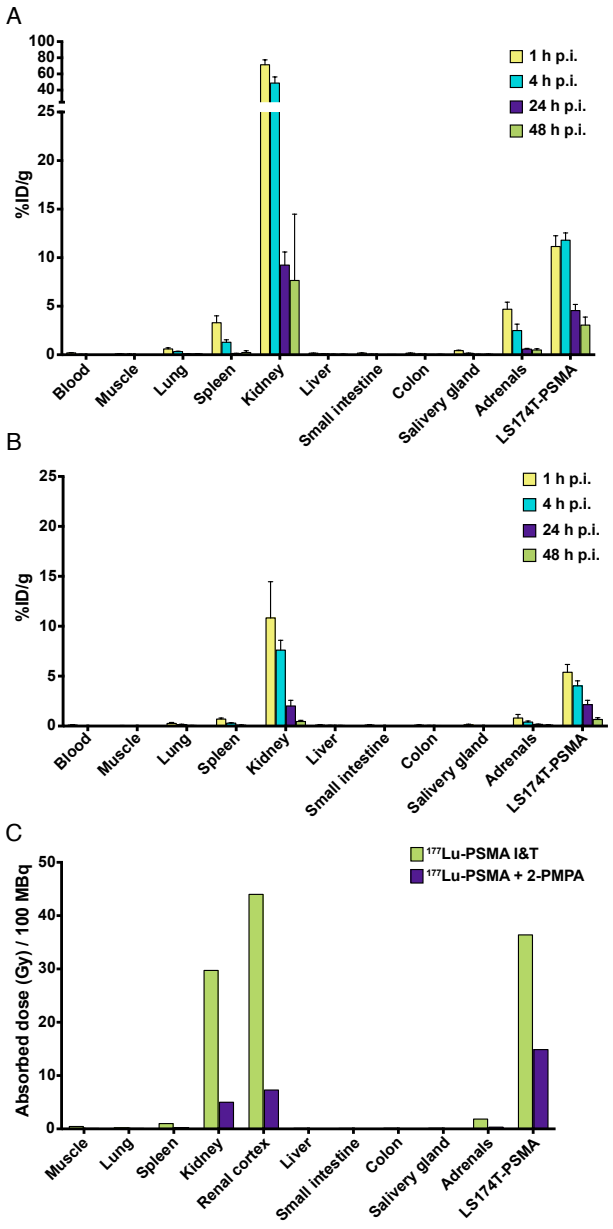

FIGURE 4. Pharmacokinetics and dosimetry of ^{111}In-PSMA I&T in mice bearing LS174T-PSMA xenografts. Biodistribution of ^{111}In-PSMA I&T (0.3 nmol) alone (A) or with coinjection of 50 nmol 2-PMPA (B) at different time points after injection. Absorbed doses (in Gy/100 MBq ^{177}Lu-PSMA I&T) were extrapolated from biodistribution data with and without 2-PMPA coinjection (C).

scans obtained 1 h after injection of ^{177}Lu-PSMA I&T clearly showed preferential localization of radioactivity in the renal cortex (**Figure 5**). Therefore, dosimetric calculations were adjusted to estimate absorbed doses to renal cortex, taking into account this preferential localization of ^{177}Lu-PSMA I&T in the cortex. Absorbed doses to renal cortex were 44 and 7.3 Gy for ^{177}Lu-PSMA I&T alone and ^{177}Lu-PSMA I&T with 2-PMPA, respectively. Absorbed doses to other organs from 100 MBq of ^{177}Lu-PSMA I&T were below 1 Gy.

Coinjection of 2-PMPA Improves Visualization of Metastatic Tumor Lesions Located Near Kidneys and Spleen

SPECT/CT imaging with ^{111}In-PSMA I&T, with or without 2-PMPA, clearly visualized subcutaneously growing LS174T-PSMA tumors and intraperitoneally growing LS174T-PSM metastases, whereas no uptake was observed in PSMA-negative LS174T tumors

(**Figure 6A**). High renal and spleen tracer uptake was observed in mice that did not receive coinjection of 2-PMPA, which interfered with visualization of metastases growing in the vicinity of these organs (**Figure 6B**).

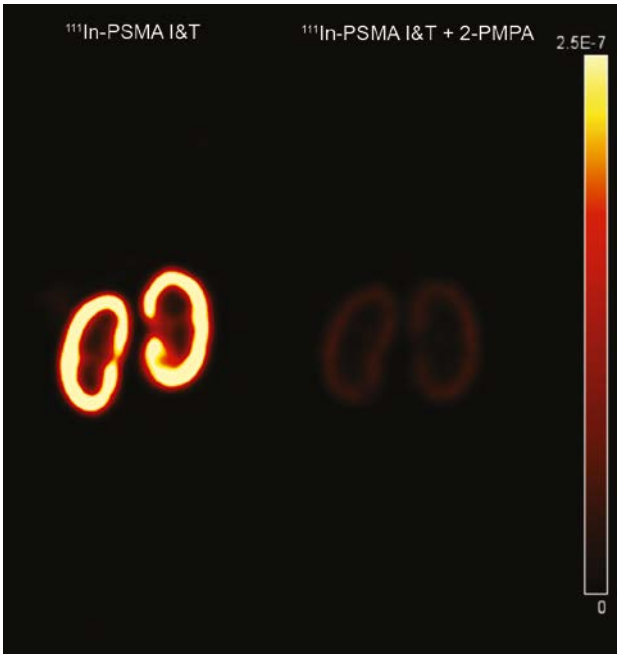

FIGURE 5. Localization of ^{111}In-PSMA I&T in mouse kidneys. SPECT/CT images of mice 1 h after injection of ^{111}In-PSMA I&T (0.3 nmol, 20 MBq) without (left) or with (right) coinjection of 50 nmol 2-PMPA, showing tracer localization in the renal cortex.

Coinjection of 2-PMPA Protects from Nephrotoxicity During ^{177}Lu-PSMA I&T Radionuclide Therapy

Non-tumor bearing mice treated with vehicle or ^{177}Lu-PSMA I&T + 2-PMPA gained body weight over 110 days (**Figure 7A**). In contrast, an increase in body weight was observed up to 50 days for mice treated with ^{177}Lu-PSMA I&T only, followed by a slow decline in body weight up to 110 days. Three months after therapy, renal function was monitored by measuring renal uptake of ^{99m}Tc-DMSA and plasma creatinine levels. Renal uptake of ^{99m}Tc-DMSA was significantly reduced in mice treated with ^{177}Lu-PSMA I&T (1.0 ± 0.3 %ID/g) as compared to mice treated with vehicle (10.5 ± 1.0 %ID/g, $p<0.001$) or ^{177}Lu-PSMA I&T + 2-PMPA (9.8 ± 1.6 %ID/g, $p<0.001$) (**Figures 7B and 7C**). Plasma creatinine levels were increased in mice treated with ^{177}Lu-PSMA I&T (8.2 ± 1.7 %ID/g) as compared to mice treated with vehicle (4.2 ± 1.6 %ID/g, $p = 0.029$) or ^{177}Lu-PSMA I&T + 2-PMPA (4.7 ± 2.1 %ID/g, $p = 0.114$) (**Figure 7D**). Kidneys of mice treated with ^{177}Lu-PSMA I&T + 2-PMPA or vehicle showed normal morphology, whereas kidneys of mice treated with ^{177}Lu-PSMA I&T showed extensive cortical damage (**Figure 7E**). Glomerular damage was denoted by segmental glomerular basement membrane thickening and wrinkling, and mesangial matrix increase, with pyknotic endothelial cells and podocytes. In addition, there was focal, global glomerular sclerosis. The tubular interstitial compartment of the cortex showed extreme acute tubular necrosis with atypia of the epithelial cells.

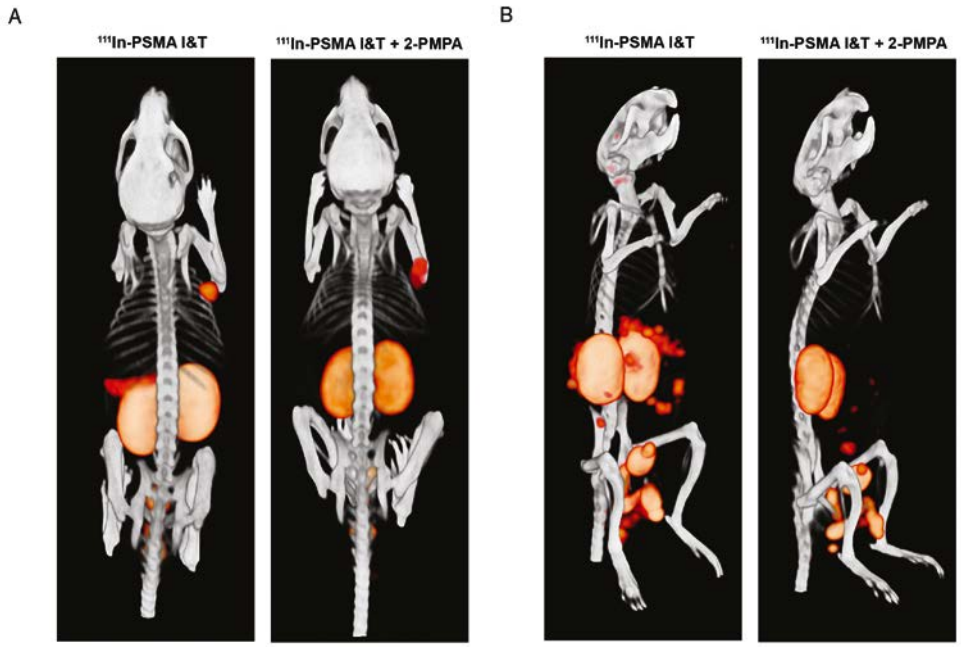

FIGURE 6. SPECT/CT imaging of ^{111}In-PSMA I&T in PSMA-expressing xenografts. (A) Representative SPECT/CT images of subcutaneous LS174T-PSMA xenografts (right shoulder) and LS174T (left shoulder) 1 h after injection of ^{111}In-PSMA I&T (0.3 nmol, 20 MBq) without (left) or with (right) coinjection of 50 nmol 2-PMPA. (B) Representative SPECT/CT images of intraperitoneal metastatic lesions of LS174T-PSMA cells 1 h after injection of ^{111}In-PSMA I&T (0.3 nmol, 20 MBq) without (left) or with (right) coinjection of 50 nmol 2-PMPA. Metastatic lesions were located around intestines, spleen and pancreas. High signal intensity in kidneys and spleen interfered with visualization of metastases in this area when 2-PMPA was not administered.

Therapeutic Efficacy of ^{177}Lu-PSMA I&T is Influenced by 2-PMPA

LS174T-PSMA tumor growth was significantly inhibited by 100 MBq of ^{177}Lu-PSMA I&T. A more effective growth inhibition was observed with ^{177}Lu-PSMA I&T alone as compared to ^{177}Lu-PSMA I&T + 2-PMPA. Mean doubling time for tumors of mice treated with vehicle, ^{177}Lu-PSMA, and ^{177}Lu-PSMPA + 2-PMPA were 6.1 ± 1.1 days, 13.9 ± 1.7 days, and 7.3 ± 1.7 days, respectively (**Figure 8A**). Median survival for these groups was 13 days, 29 days, and 19 days, respectively ($p<0.0001$, **Figure 8B**). Median survival significantly decreased in the group that received 2-PMPA in comparison with ^{177}Lu-PSMA I&T alone ($p = 0.0007$).

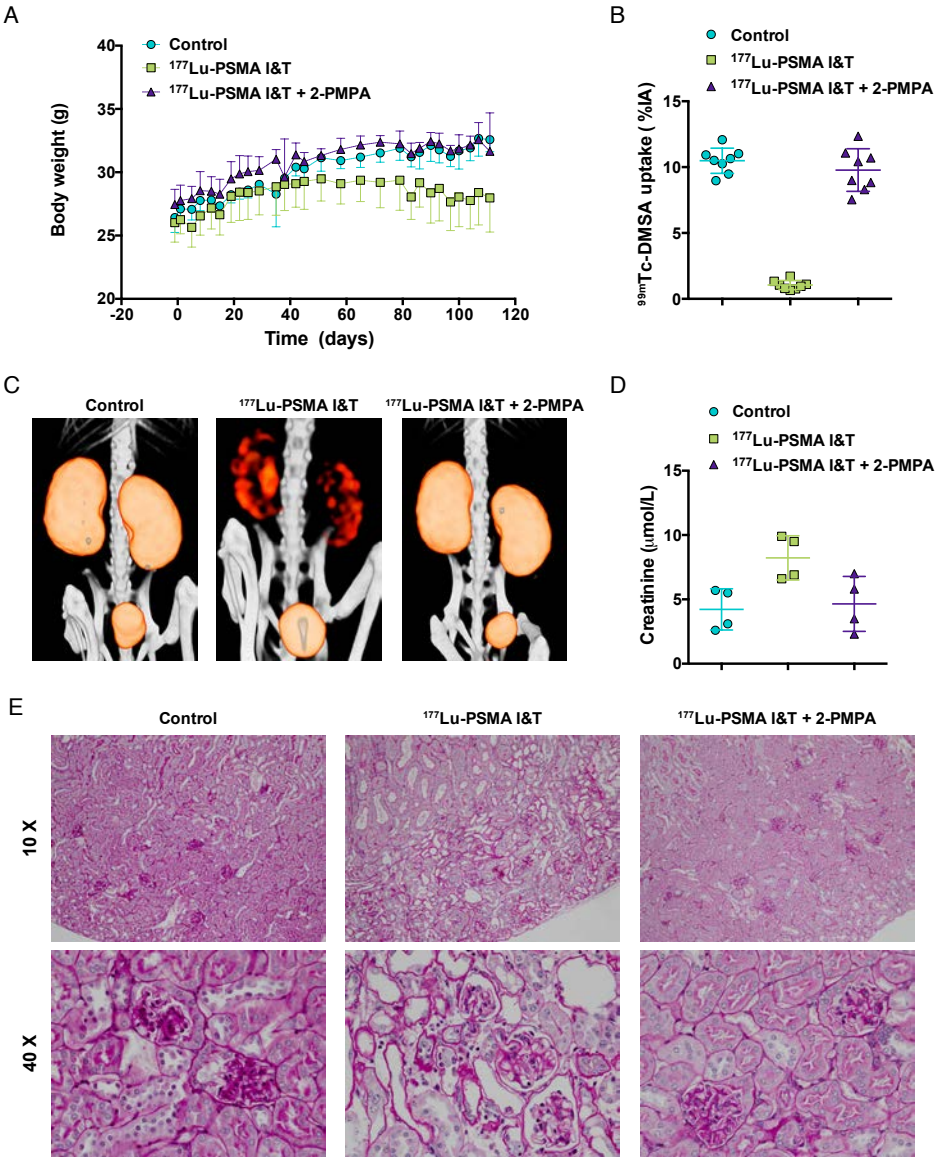

FIGURE 7. Toxicity of ^{177}Lu-PSMA I&T in non-tumor bearing mice. Mice (n = 4 per group) were treated with ^{177}Lu-PSMA I&T (100 MBq, 0.35 nmol) with or without 2-PMPA (50 nmol) on day 0. Control mice were injected with vehicle. Body weight follow-up (A), quantification of ^{99m}Tc-DMSA uptake (B), ^{99m}Tc-DMSA SPECT/CT scans (C), plasma creatinine levels (D), and periodic acid Schiff stained kidneys from treated mice (E) are displayed. Body weight loss, decreased renal uptake of ^{99m}Tc-DMSA, and increased plasma creatinine levels are observed for the group treated with ^{177}Lu-PSMA I&T without 2-PMPA. Kidneys of mice treated with ^{177}Lu-PSMA I&T + 2-PMPA or vehicle show normal morphology, whereas kidneys of mice treated with ^{177}Lu-PSMA I&T show extensive cortical damage. Tubular damage can be visualized by loss of epithelial cells and atypia of the remaining cells (10 X image). In addition, glomerular damage can be visualized by endothelial cell and podocyte pyknosis, focal glomerular basement membrane wrinkling and mesangial matrix increase (40 X image).

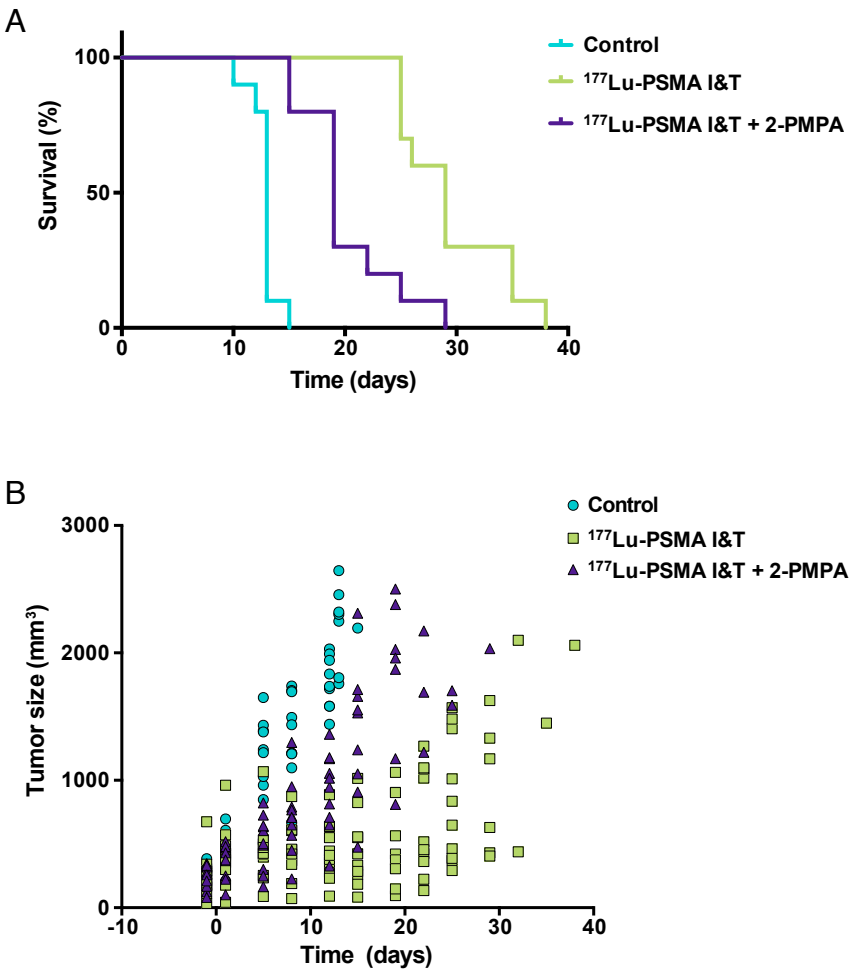

FIGURE 8. Therapeutic efficacy of ^{177}Lu-PSMA I&T in LS174T-PSMA tumors. Mice (n = 8 per group) were treated with ^{177}Lu-PSMA I&T (100 MBq, 0.35 nmol), with or without coinjection of 2-PMPA (50 nmol) on day 0. Control mice were injected with vehicle. Kaplan-Meier survival curves (A) and tumor size follow-up (B) are displayed.

DISCUSSION

A theranostic approach for detection, staging, treatment, and follow-up of PCa would be highly valuable to achieve personalized PCa treatment. PSMA is a very interesting target for such a theranostic approach, due to its consistent overexpression on PCa at all stages of disease. In recent years the number of PSMA-targeted agents for diagnostics and therapeutic applications has increased tremendously (*36*). Currently, two theranostic PSMA-ligands are being evaluated in the clinic, namely PSMA I&T

(*25-27*) and PSMA-617 (*23, 37-39*). These two compounds have been shown to efficiently detect PCa lesions with high contrast, but also display very high uptake in kidneys and salivary glands, which raises concerns regarding potential toxicity during radionuclide therapy. Preliminary results of ^{177}Lu-PSMA-617 therapy in patients showed no acute renal insufficiencies in 2 months follow-up time, but longer follow-up is needed to get more insight into late-stage renal toxicity (*37*). Similarly, no signs of renal insufficiencies were reported for patients treated with ^{177}Lu-PSMA I&T over a follow-up period of more than 6 months (*40, 41*).

Our study aimed to investigate the impact of healthy tissue uptake on the theranostic potential of PSMA I&T for SPECT imaging and radionuclide therapy of PCa. Our data showed that ^{111}In-PSMA I&T accumulated in PSMA-positive tumors, but not in PSMA negative tumors. In addition, PSMA-mediated uptake was observed in several normal murine tissues, including kidneys, spleen, salivary glands, adrenals, and lungs, of which kidneys showed the highest uptake. Our biodistribution data of ^{111}In-PSMA I&T were consistent with previously published data for ^{177}Lu-PSMA I&T (*25*). Moreover, we show that uptake of ^{111}In-PSMA I&T in PSMA-expressing tissues can be blocked by coinjection of 2-PMPA in a dose-dependent manner, with the highest effect being obtained in the kidneys. Coadministration of 2-PMPA significantly reduced tumor uptake as well, but to a lower extent than kidney uptake, resulting in increased tumor-to-kidney ratios at all doses tested. Hillier et al. have shown that coinjection of 50 mg/kg 2-PMPA, a phosphonate-based PSMA inhibitor, nearly completely blocked tumor and kidney uptake of the PSMA inhibitor [^{123}I]MIP1095 (*42*). More recently, Kratochwil et al. have shown the potential of 2-PMPA to selectively block kidney uptake without reducing tumor uptake by injecting 2-PMPA (0.2 – 50 mg/kg) 1 or 16 hours after injection of the PSMA inhibitors ^{99m}Tc-MIP1404 and ^{125}I-MIP1095, respectively (*43*). They reported rapid and efficient displacement of renal tracer uptake with minimal effects on tumor uptake and suggested that a higher internalization rate by tumor cells in comparison with renal cells could explain these differential effects on tumor and kidneys.

In contrast with data obtained by Kratochwil et al. for ^{125}I-MIP1095 and ^{99m}Tc-MIP1404, injection of 2-PMPA (50 nmol per 25 g mouse ~ 0.45 mg/kg) 1 hour after injection of ^{111}In-PSMA I&T did not reduce renal uptake. In our study, only coinjection or 15 min preinjection resulted in effective inhibition of ^{111}In-PSMA I&T renal uptake. This resulted in a seven-fold reduction in renal uptake at 2 h after injection, whereas tumor uptake was reduced only by a factor of two. The differential effect on tumor and kidneys might be explained by differences in the kinetics of tumor and renal uptake of 2-PMPA and PSMA I&T. Because of its small size (Mw = 226 g/mol), high hydrophilicity, and low tissue penetration (*44*), 2-PMPA might be cleared rapidly from the circulation, resulting in higher accumulation in kidneys than in tumor. Additional studies are needed to determine the kinetics of 2-PMPA uptake in tumor and kidneys, providing more insight into this mechanism and facilitating optimization of 2-PMPA injection schedule in patients. Pre- or coinjection of blocking agents is preferred over postinjection, because the kidneys will be protected from radiation-induced damage

from the start of therapy, which could be especially beneficial with short half-life radionuclides, e.g. ^{213}Bi.

In the case of application of PSMA inhibitors for PET imaging, high uptake observed in kidneys and salivary glands is not of major concern for detection of primary tumors or distant metastases. However, if metastases are situated in the vicinity of organs showing tracer uptake, this could interfere with the interpretation of the images. Our metastatic model indicates that coinjection of ^{111}In-PSMA I&T with 2-PMPA improved the visualization of intraperitoneal tumor lesions in the vicinity of kidneys, adrenals, and spleen.

For PSMA-targeted radionuclide therapy, high uptake observed in kidneys and salivary glands are major concerns. To investigate the potential protective effect of 2-PMPA on renal toxicity, a therapeutic study was performed with 100 MBq ^{177}Lu-PSMA I&T with and without coinjection of 2-PMPA. Several groups have reported radiation-induced nephropathy in mice between 15 and 30 weeks after therapy using ^{177}Lu-labeled therapeutic agents, translating into reduced ^{99m}Tc-DMSA clearance and increased serum creatinine levels (*33, 45, 46*). Svensson et al. have reported a threshold dose value of 24 Gy to renal cortex for ^{177}Lu-DOTATATE in nude mice (*33*). In our study, estimated absorbed doses to renal cortex were 44 Gy and 7.3 Gy, for ^{177}Lu-PSMA I&T and ^{177}Lu-PSMA I&T + 2-PMPA, respectively. Consistently, nephrotoxicity was observed in mice treated with 100 MBq ^{177}Lu-PSMA I&T at 3 months after start of therapy, as shown by the decreased ^{99m}Tc-DMSA uptake and increased serum creatinine levels. On the contrary, nephrotoxicity was not observed when 2-PMPA was coadministered.

Therapeutic efficacy of ^{177}Lu-PSMA I&T was significantly reduced by coinjection of 2-PMPA, which can be explained by the two-fold higher dose delivered to the tumor cells for ^{177}Lu-PSMA I&T alone in comparison with ^{177}Lu-PSMA I&T with 2-PMPA. To improve therapeutic efficacy, the dose delivered to the tumor for ^{177}Lu-PSMA I&T with 2-PMPA could be increased by administering a double dose of ^{177}Lu-PSMA I&T. This would result in an estimated absorbed dose of 30 Gy to the tumor and 14.6 Gy to the renal cortex, provided that receptor saturation has not been reached. Alternatively, 2 doses of ^{177}Lu-PSMA I&T could be administered at an interval allowing clearance of the tracer.

These preclinical results illustrate the potential of PSMA I&T for theranostic approaches in PCa. However, the extrapolation of these data to the clinical situation should be performed carefully. Pitfalls might include differences in expression of PSMA in human and its murine homolog Folh1 in mice, differences in affinities for PSMA expressed on human (xenograft) tumors and Folh1 expressed on murine tissues, and differences in pharmacokinetics in mice and humans. Moreover, safety and pharmacokinetics of 2-PMPA should be tested in patients. In preclinical models, PSMA inhibitors have shown utility for treatment of neurological diseases in which excessive excitatory glutamate transmission is pathogenic (*47*). Indeed, PSMA inhibition could limit detrimental excess glutamate release in the nervous system,

by blocking conversion of N-acetylaspartylglutamate into glutamate. Importantly, PSMA inhibition had no effect on basal glutamate transmission in healthy animals (*48*). Even though 2-PMPA has shown high affinity and selectivity towards PSMA, it was not evaluated in patients because of its poor oral bioavailability and limited brain penetration. A more lipophilic PSMA inhibitor, 2-(-3-mercaptopropyl)pentanedioic acid, which is almost as potent as 2-PMPA, was found to be safe and well tolerated in healthy subjects (*49*). For our application, however, the use of a hydrophilic PSMA inhibitor with poor brain penetration would be preferred, because it would less likely induce adverse events. In conclusion, future research is warranted to address the identified pitfalls and translate this concept in PCa patients.

CONCLUSION

In conclusion, PSMA I&T is a highly promising theranostic agent for radionuclide imaging and therapy of PCa. Coinjection of 2-PMPA efficiently reduced renal uptake, thereby improving visualization of intraperitoneal tumor lesions in the vicinity of kidneys, adrenals, and spleen and protecting from nephrotoxicity after radionuclide therapy. Because 2-PMPA also reduced tumor uptake, it might hamper therapeutic efficacy, which could be resolved by increasing amounts of injected activity.

REFERENCES

1. Siegel R, DeSantis C, Virgo K, et al. Cancer treatment and survivorship statistics, 2012. CA Cancer J Clin. 2012;62:220-241.
2. Heidenreich A, Bastian PJ, Bellmunt J, et al. EAU guidelines on prostate cancer. Part II: Treatment of advanced, relapsing, and castration-resistant prostate cancer. Eur Urol. 2014;65:467-479.
3. Heidenreich A, Porres D. Prostate cancer: treatment sequencing for CRPC--what do we know? Nat Rev Urol. 2014;11:189-190.
4. Hoskin P, Sartor O, O'Sullivan JM, et al. Efficacy and safety of radium-223 dichloride in patients with castration-resistant prostate cancer and symptomatic bone metastases, with or without previous docetaxel use: a prespecified subgroup analysis from the randomised, double-blind, phase 3 ALSYMPCA trial. Lancet Oncol. 2014;15:1397-1406.
5. Humm JL, Sartor O, Parker C, Bruland OS, Macklis R. Radium-223 in the treatment of osteoblastic metastases: a critical clinical review. Int J Radiat Oncol Biol Phys. 2015;91:898-906.
6. Bostwick DG, Pacelli A, Blute M, Roche P, Murphy GP. Prostate specific membrane antigen expression in prostatic intraepithelial neoplasia and adenocarcinoma: a study of 184 cases. Cancer. 1998;82:2256-2261.
7. Silver DA, Pellicer I, Fair WR, Heston WD, Cordon-Cardo C. Prostate-specific membrane antigen expression in normal and malignant human tissues. Clin Cancer Res. 1997;3:81-85.
8. Wright GL, Jr., Haley C, Beckett ML, Schellhammer PF. Expression of prostate-specific membrane antigen in normal, benign, and malignant prostate tissues. Urol Oncol. 1995;1:18-28.
9. Wright GL, Jr., Grob BM, Haley C, et al. Upregulation of prostate-specific membrane antigen after androgen-deprivation therapy. Urology. 1996;48:326-334.
10. Ellis RJ, Kaminsky DA, Zhou EH, et al. Ten-year outcomes: the clinical utility of single photon emission computed tomography/computed tomography capromab pendetide (Prostascint) in a cohort diagnosed with localized prostate cancer. Int J Radiat Oncol Biol Phys. 2011;81:29-34.
11. Milowsky MI, Nanus DM, Kostakoglu L, Vallabhajosula S, Goldsmith SJ, Bander NH. Phase I trial of yttrium-90-labeled anti-prostate-specific membrane antigen monoclonal antibody J591 for androgen-independent prostate cancer. J Clin Oncol. 2004;22:2522-2531.
12. Tagawa ST, Beltran H, Vallabhajosula S, et al. Anti-prostate-specific membrane antigen-based radioimmunotherapy for prostate cancer. Cancer. 2010;116:1075-1083.
13. Barrett JA, Coleman RE, Goldsmith SJ, et al. First-in-man evaluation of 2 high-affinity PSMA-avid small molecules for imaging prostate cancer. J Nucl Med. 2013;54:380-387.
14. Afshar-Oromieh A, Avtzi E, Giesel FL, et al. The diagnostic value of PET/CT imaging with the (68) Ga-labelled PSMA ligand HBED-CC in the diagnosis of recurrent prostate cancer. Eur J Nucl Med Mol Imaging. 2015;42:197-209.
15. Beheshti M, Kunit T, Haim S, et al. BAY 1075553 PET-CT for Staging and Restaging Prostate Cancer Patients: Comparison with [F] Fluorocholine PET-CT (Phase I Study). Mol Imaging Biol. 2014.
16. Pandit-Taskar N, O'Donoghue JA, Durack JC, et al. A Phase I/II Study for Analytic Validation of 89Zr-J591 ImmunoPET as a Molecular Imaging Agent for Metastatic Prostate Cancer. Clin Cancer Res. 2015.
17. Rowe SP, Gage KL, Faraj SF, et al. 18F-DCFBC PET/CT for PSMA-Based Detection and Characterization of Primary Prostate Cancer. J Nucl Med. 2015;56:1003-1010.
18. Budaus L, Leyh-Bannurah SR, Salomon G, et al. Initial Experience of Ga-PSMA PET/CT Imaging in High-risk Prostate Cancer Patients Prior to Radical Prostatectomy. Eur Urol. 2015.

19. Szabo Z, Mena E, Rowe SP, et al. Initial Evaluation of [(18)F]DCFPyL for Prostate-Specific Membrane Antigen (PSMA)-Targeted PET Imaging of Prostate Cancer. Mol Imaging Biol. 2015;17:565-574.
20. Vallabhajosula S, Nikolopoulou A, Jhanwar YS, et al. Radioimmunotherapy of Metastatic Prostate Cancer with 177Lu-DOTA-huJ591 Anti Prostate Specific Membrane Antigen Specific Monoclonal Antibody. Curr Radiopharm. 2015.
21. Tagawa ST, Milowsky MI, Morris M, et al. Phase II study of Lutetium-177-labeled anti-prostate-specific membrane antigen monoclonal antibody J591 for metastatic castration-resistant prostate cancer. Clin Cancer Res. 2013;19:5182-5191.
22. Zechmann CM, Afshar-Oromieh A, Armor T, et al. Radiation dosimetry and first therapy results with a (124)I/ (131)I-labeled small molecule (MIP-1095) targeting PSMA for prostate cancer therapy. Eur J Nucl Med Mol Imaging. 2014;41:1280-1292.
23. Benesova M, Schafer M, Bauder-Wust U, et al. Preclinical Evaluation of a Tailor-Made DOTA-Conjugated PSMA Inhibitor with Optimized Linker Moiety for Imaging and Endoradiotherapy of Prostate Cancer. J Nucl Med. 2015;56:914-920.
24. Weineisen M, Simecek J, Schottelius M, Schwaiger M, Wester HJ. Synthesis and preclinical evaluation of DOTAGA-conjugated PSMA ligands for functional imaging and endoradiotherapy of prostate cancer. EJNMMI Res. 2014;4:63.
25. Weineisen M, Schottelius M, Simecek J, et al. 68Ga- and 177Lu-Labeled PSMA I&T: Optimization of a PSMA-Targeted Theranostic Concept and First Proof-of-Concept Human Studies. J Nucl Med. 2015;56:1169-1176.
26. Herrmann K, Bluemel C, Weineisen M, et al. Biodistribution and radiation dosimetry for a probe targeting prostate-specific membrane antigen for imaging and therapy. J Nucl Med. 2015;56:855-861.
27. Maurer T, Weirich G, Schottelius M, et al. Prostate-specific membrane antigen-radioguided surgery for metastatic lymph nodes in prostate cancer. Eur Urol. 2015;68:530-534.
28. Lutje S, Rijpkema M, Franssen GM, et al. Dual-Modality Image-Guided Surgery of Prostate Cancer with a Radiolabeled Fluorescent Anti-PSMA Monoclonal Antibody. J Nucl Med. 2014;55:995-1001.
29. Brom M, Joosten L, Oyen WJ, Gotthardt M, Boerman OC. Improved labelling of DTPA- and DOTA-conjugated peptides and antibodies with 111In in HEPES and MES buffer. EJNMMI Res. 2012;2:4.
30. Chatalic KL, Franssen GM, van Weerden WM, et al. Preclinical comparison of Al18F- and 68Ga-labeled gastrin-releasing peptide receptor antagonists for PET imaging of prostate cancer. J Nucl Med. 2014;55:2050-2056.
31. Bolch WE, Eckerman KF, Sgouros G, Thomas SR. MIRD pamphlet No. 21: a generalized schema for radiopharmaceutical dosimetry--standardization of nomenclature. J Nucl Med. 2009;50:477-484.
32. Keenan MA, Stabin MG, Segars WP, Fernald MJ. RADAR realistic animal model series for dose assessment. J Nucl Med. 2010;51:471-476.
33. Svensson J, Molne J, Forssell-Aronsson E, Konijnenberg M, Bernhardt P. Nephrotoxicity profiles and threshold dose values for [177Lu]-DOTATATE in nude mice. Nucl Med Biol. 2012;39:756-762.
34. van der Have F, Vastenhouw B, Ramakers RM, et al. U-SPECT-II: An Ultra-High-Resolution Device for Molecular Small-Animal Imaging. J Nucl Med. 2009;50:599-605.
35. Forrer F, Valkema R, Bernard B, et al. In vivo radionuclide uptake quantification using a multi-pinhole SPECT system to predict renal function in small animals. Eur J Nucl Med Mol Imaging. 2006;33:1214-1217.
36. Kiess A, Banerjee S, Mease R, et al. Prostate-Specific Membrane Antigen as a target for cancer imaging and therapy. Q J Nucl Med Mol Imaging. 2015.

37. Ahmadzadehfar H, Rahbar K, Kurpig S, et al. Early side effects and first results of radioligand therapy with (177)Lu-DKFZ-617 PSMA of castrate-resistant metastatic prostate cancer: a two-centre study. EJNMMI Res. 2015;5:114.
38. Kabasakal L, AbuQbeitah M, Aygun A, et al. Pre-therapeutic dosimetry of normal organs and tissues of Lu-PSMA-617 prostate-specific membrane antigen (PSMA) inhibitor in patients with castration-resistant prostate cancer. Eur J Nucl Med Mol Imaging. 2015.
39. Afshar-Oromieh A, Hetzheim H, Kratochwil C, et al. The novel theranostic PSMA-ligand PSMA-617 in the diagnosis of prostate cancer by PET/CT: biodistribution in humans, radiation dosimetry and first evaluation of tumor lesions. J Nucl Med. 2015.
40. Kulkarni HR, Singh A, Schuchardt C, Klette I, Wester HJ, Baum RP. Peptide Radioligand Therapy (PRLT) Using Lu-177 Labeled DOTAGA-PSMA Inhibitor Yields Objective Responses in Metastatic Castrate-resistant Prostate Cancer. European Journal of Nuclear Medicine and Molecular Imaging. 2015;42:S59-S60.
41. Schuchardt C, Wiessalla S, Ozkan A, et al. Therapy of Metastasized Prostate Cancer Using a Lu-177 Labeled PSMA Inhibitor (I&T): First Dosimetric Results in Patients. European Journal of Nuclear Medicine and Molecular Imaging. 2015;42:S99-S99.
42. Hillier SM, Maresca KP, Femia FJ, et al. Preclinical evaluation of novel glutamate-urea-lysine analogues that target prostate-specific membrane antigen as molecular imaging pharmaceuticals for prostate cancer. Cancer Res. 2009;69:6932-6940.
43. Kratochwil C, Giesel FL, Leotta K, et al. PMPA for nephroprotection in PSMA-targeted radionuclide therapy of prostate cancer. J Nucl Med. 2015;56:293-298.
44. Rais R, Rojas C, Wozniak K, et al. Bioanalytical method for evaluating the pharmacokinetics of the GCP-II inhibitor 2-phosphonomethyl pentanedioic acid (2-PMPA). J Pharm Biomed Anal. 2014;88:162-169.
45. Haller S, Reber J, Brandt S, et al. Folate receptor-targeted radionuclide therapy: preclinical investigation of anti-tumor effects and potential radionephropathy. Nucl Med Biol. 2015;42:770-779.
46. Reber J, Haller S, Leamon CP, Muller C. 177Lu-EC0800 combined with the antifolate pemetrexed: preclinical pilot study of folate receptor targeted radionuclide tumor therapy. Mol Cancer Ther. 2013;12:2436-2445.
47. Rahn KA, Slusher BS, Kaplin AI. Glutamate in CNS neurodegeneration and cognition and its regulation by GCPII inhibition. Curr Med Chem. 2012;19:1335-1345.
48. Slusher BS, Vornov JJ, Thomas AG, et al. Selective inhibition of NAALADase, which converts NAAG to glutamate, reduces ischemic brain injury. Nat Med. 1999;5:1396-1402.
49. van der Post JP, de Visser SJ, de Kam ML, et al. The central nervous system effects, pharmacokinetics and safety of the NAALADase-inhibitor GPI 5693. Br J Clin Pharmacol. 2005;60:128-136.

3.3

Alpha Radionuclide Therapy of Prostate Cancer Targeting Prostate-Specific Membrane Antigen

Kristell L.S. Chatalic[1,2,3†], Julie Nonnekens[1,4†], Janneke D.M. Molkenboer-Kuenen[5], Cecile E.M.T. Beerens[4], Frank Bruchertseifer[6], Alfred Morgenstern[6], Joke Veldhoven-Zweistra[3], Margret Schottelius[7], Hans-Jürgen Wester[7], Dik C. van Gent[4], Wytske M. van Weerden[3], Otto C. Boerman[5], Marion de Jong[1,2], Sandra Heskamp[5]

[†]These authors contributed equally to this work.
[1]Department of Nuclear Medicine, Erasmus MC, Rotterdam, The Netherlands
[2]Department of Radiology, Erasmus MC, Rotterdam, The Netherlands
[3]Departments of Urology, Erasmus MC, Rotterdam, The Netherlands
[4]Departments of Genetics, Erasmus MC, Rotterdam, The Netherlands
[5]Department of Radiology and Nuclear Medicine, Radboud University Medical Center, Nijmegen, The Netherlands
[6]European Commission, Joint Research Centre, Institute for Transuranium Elements, Karlsruhe, Germany
[7]Pharmaceutical Radiochemistry, Technische Universität München, Garching, Germany

Submitted for publication

ABSTRACT

In this study we report on 2 novel ^{213}Bi-labeled tracers targeting prostate-specific membrane antigen (PSMA) for α radionuclide therapy of prostate cancer (PCa). Small-molecule inhibitor PSMA I&T and nanobody JVZ-008 were labeled with ^{213}Bi and their biodistribution profiles were evaluated in mice bearing LNCaP xenografts. DNA damage response was followed after ^{213}Bi-PSMA I&T and ^{213}Bi-JVZ-007-cys-DOTA (^{213}Bi-JVZ-008) treatment using LNCaP cells and LNCaP xenografts. Treatment of LNCaP cells in vitro with ^{213}Bi-PSMA I&T and ^{213}Bi-JVZ-008 induced DNA double-strand breaks (DSBs), as indicated by the presence of increased numbers of 53BP1 and γH2AX nuclear foci. ^{213}Bi-PSMA I&T showed clearly higher tumor uptake than ^{213}Bi-JVZ-008 in mice. ^{213}Bi-PSMA I&T and ^{213}Bi-JVZ-008 induced DSBs in vivo in LNCaP tumors at 1 h after injection. DSBs were still observed 24 h after injection. These promising preliminary results warrant further evaluation of the therapeutic potential of ^{213}Bi-labeled tracers for treatment of metastasized PCa.

INTRODUCTION

Late stage metastasized prostate cancer (PCa) is associated with a poor survival and diminished quality of life. Taxane-based therapies and second-line hormonal therapies show only moderate survival benefits and are often associated with toxicity (*1*). The recently introduced bone-seeking radiopharmaceutical $^{223}RaCl_2$ (Xofigo™) results in an overall survival advantage of 3.6 months in castration-resistant prostate cancer patients with bone metastases (*2*). The short range and high linear energy transfer (LET) of α-particles, as emitted by ^{223}Ra, generates localized DNA double-strand breaks (DSBs) in bone lesions, with limited myelotoxicity. A PCa-targeted α therapy approach would enable α-particles to target and treat potentially all PCa metastases and circulating tumor cells. Recent developments in PCa-targeted radiopharmaceuticals have focused on prostate-specific membrane antigen (PSMA), overexpressed in the majority of PCa at all stages. In this study we evaluated 2 tracers targeting PSMA coupled to the α-emitter ^{213}Bi. The small molecule inhibitor PSMA I&T and the nanobody JVZ-008, both showing rapid accumulation in PSMA-expressing tumors, represent ideal molecular carriers for the short-lived α-emitter ^{213}Bi (*3-5*). In this short report, we describe radiolabeling, tumor targeting and biodistribution profiles of ^{213}Bi-PSMA I&T and ^{213}Bi-JVZ-007-cys-DOTA (^{213}Bi-JVZ-008), as well as the resulting DNA damage response in vitro and in vivo using the PSMA-expressing LNCaP PCa model.

MATERIALS AND METHODS

All reagents used were purchased from Sigma-Aldrich unless stated otherwise.

Synthesis and Radiolabeling of ^{213}Bi-PSMA I&T and ^{213}Bi-JVZ-008

PSMA I&T was kindly provided by the Technical University Munich (*3*) and JVZ-007-cys was synthetized as described previously (*5*). JVZ-008 was obtained by conjugation of JVZ-007-cys to maleimide-DOTA (Chematech) according to the protocol described for maleimide-DTPA (*5*). ^{213}Bi was eluted as BiI_{4-}/BiI_5^{2-} from a $^{225}Ac/^{213}Bi$ generator (Institute for Transuranium Elements) using 600 µL 0.1 M HCl/0.1 M NaI. For PSMA I&T labeling, the ^{213}Bi eluate was added to a labeling vial containing 120 µL 2 M TRIS, 50 µL 20% ascorbic acid and 2-4 nmol PSMA I&T (pH 8.7). For JVZ-008 labeling, the ^{213}Bi eluate was added to a labeling vial containing 80 µL 2 M TRIS, 50 µL 20% ascorbic acid and 4 nmol JVZ-008 (pH 7.9). The reaction mixture was heated for 10 min at 95°C. After reaction, DTPA was added to a final concentration of 0.03 mM to complex free ^{213}Bi. Incorporation yield was determined by instant thin-layer chromatography (iTLC, Agilent Technologies) using 0.1 M NH_4OAc/ 0.1 M EDTA (pH 5.5) and 0.1 M sodium citrate (pH 6.0) as eluent for ^{213}Bi-PSMA I&T and ^{213}Bi-JVZ-008, respectively. Radioactivity corresponding to ^{213}Bi-PSMA I&T (Rf = 0.5), ^{213}Bi-JVZ-008 (Rf = 0) and

free ^{213}Bi (Rf = 1) was quantified using a gamma counter (Perkin Elmer). Incorporation yield always exceeded 95%.

For animal experiments radiolabeled tracers were purified and formulated in a physiological buffer. ^{213}Bi-PSMA I&T was purified using a OasisTM HLB column (Waters) preconditioned with 1 mL ethanol and 2 mL water. ^{213}Bi-PSMA I&T was loaded on the column and eluted with 500 µL ethanol. The volume was reduced to 50 µL by evaporation, 50 nmol 2-(phosphonomethyl)pentane-1,5-dioic acid (PMPA; Santa Cruz) was added and PBS/ 0.5% BSA was added up to 1 mL. Mice received 200 µL of this solution. ^{213}Bi-JVZ-008 was purified by size exclusion chromatography using an illustra NAP-5 column (GE Healthcare Life Sciences) preconditioned with 5 volumes of 0.5% BSA and eluted with 1 mL PBS in 100 µL fractions. The first 5 fractions were pooled and mice were coinjected with 100 µL of this solution combined with 100 µL gelofusine (40 mg/ml). Specific activity was 30 MBq/nmol and 7 MBq/nmol at time of injection for ^{213}Bi-PSMA I&T and ^{213}Bi-JVZ-008, respectively.

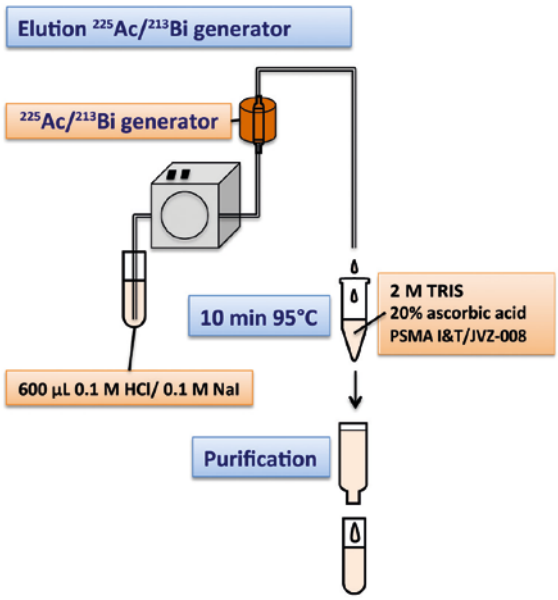

FIGURE 1: Scheme depicting labeling procedure with ^{213}Bi.

Cell Culture

The human PCa cell line LNCaP was cultured in RPMI1640 (Life Technologies), with 2 mM glutamine (Life Technologies) and 10% fetal calf serum at 37 °C with 5% CO_2.

In Vitro Experiments

Cells were seeded in 12-well plates (5 x 10^4 cells in 1 mL/well) on sterile 13-mm diameter coverslips (VWR) and allowed to grow for 2 days. Subsequently, cells were treated for 20 min at 37°C with 300 µL of ^{213}Bi-PSMA I&T (10^{-7} M, 0.3 MBq), ^{213}Bi-JVZ-008 (10^{-7} M, 0.3 MBq), ^{213}Bi-DTPA (2 x 10^{-6} M, 0.3 MBq), or medium containing labeling buffer. Immediately after treatment, cells were washed with 1 mL phosphate-buffered saline (PBS) and incubated with normal medium for 1, 2, 4, 24 or 48 h.

After incubation, cells were washed with 2 mL PBS, fixed for 15 min in 0.5 mL 2% paraformaldehyde, and washed with 1 mL PBS.

In Vivo Experiments

All animal experiments were conducted in accordance with the revised Dutch Act on Animal Experimentation (1997) and approved by the institutional Animal Welfare Committee of the Radboud University Nijmegen.

Female nude BALB/c mice (age, 6-8 wk; Janvier) were inoculated subcutaneously with LNCaP cells (3 x 10^6 cells, 200 µL, 33% RPMI/67% matrigel). Three weeks after inoculation (tumors 4-5 mm in diameter), ^{213}Bi-PSMA I&T (0.2 nmol, 5.4-6.6 MBq) was injected intravenously with 10 nmol 2-(phosphonomethyl)pentane-1,5-dioic acid (2-PMPA) for renal protection (*6*). ^{213}Bi-JVZ-008 (0.7 nmol, 4.5-5.4 MBq) was injected intravenously with 4 mg gelofusine for renal protection (*5*).

At 1 and 24 h after injection, mice were euthanized and relevant organs were dissected and weighed. Tumors were fixed in 4% paraformaldehyde. For biodistribution studies at 1 h after injection, radioactivity in each organ was determined in a γ-counter by measuring the γ-emission of ^{213}Bi (440 kEv), and the percentage of the injected dose per gram (%ID/g) was calculated. After radioactive decay, fixed tissues were embedded in paraffin.

Immunofluorescence Staining

To analyze the DNA damage response induced by the DSBs, fixed cells or 4-µm tissue sections were stained with primary antibodies [anti-53BP1 (NB100-304, Novus Biologicals, dilution 1/1000) or anti-γH2AX (05-636, Merck-Millipore, dilution 1/500)] and secondary antibodies (Alexa Fluor 594 or 488, Life Technologies). γH2AX and 53BP1 imaging was performed using a TCS SP5 confocal microscope (Leica).

RESULTS

^{213}Bi-Radiolabeling of PSMA I&T and JVZ-008

The labeling procedure is depicted in **Figure 1**. Radiolabeling with ^{213}Bi was achieved within 15 min with a specific activity (non-decay-corrected) of 58 MBq/nmol and 29 MBq/nmol for ^{213}Bi-PSMA I&T and ^{213}Bi-JVZ-008, respectively. Incorporation yield was > 95%.

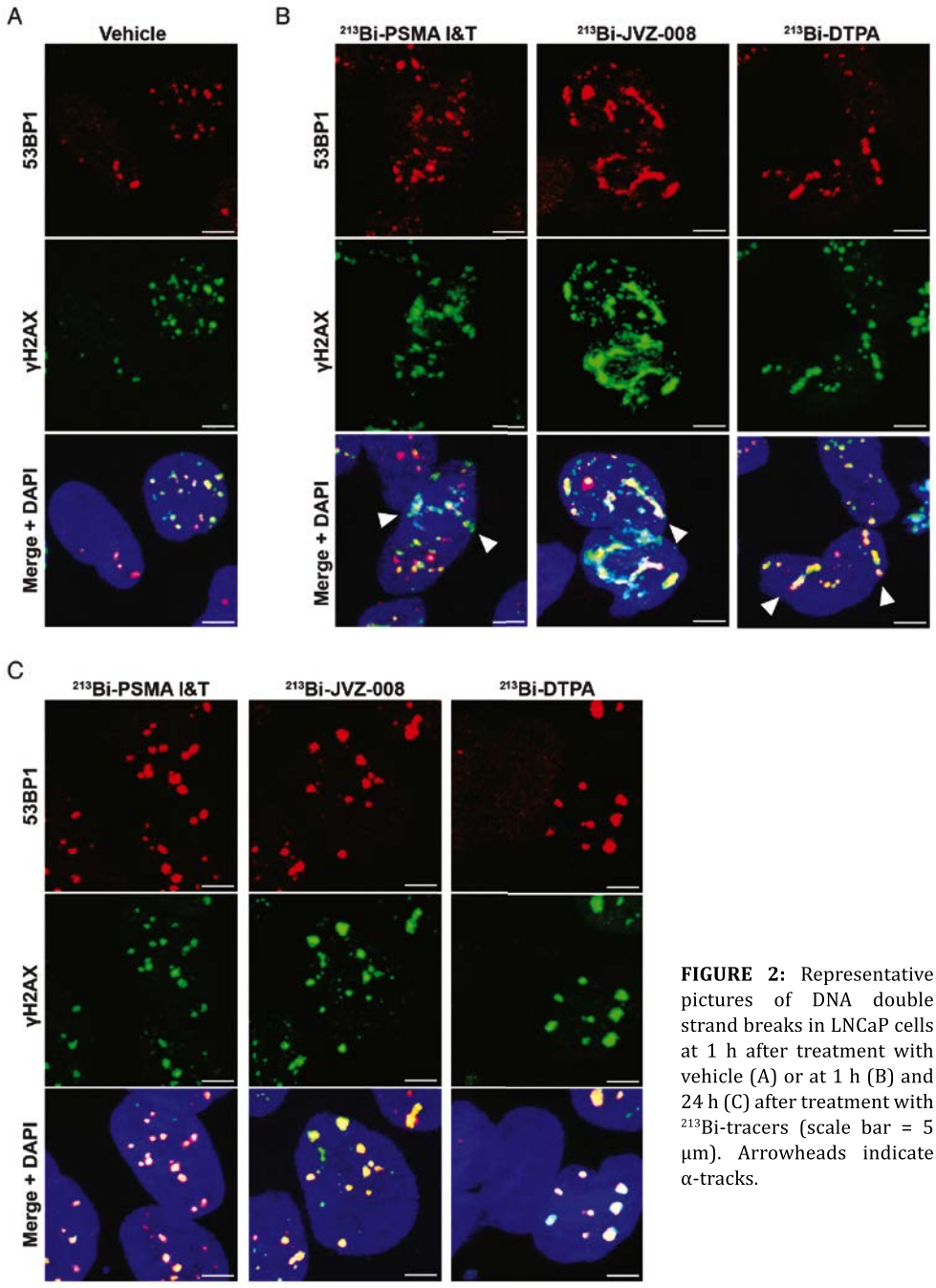

FIGURE 2: Representative pictures of DNA double strand breaks in LNCaP cells at 1 h after treatment with vehicle (A) or at 1 h (B) and 24 h (C) after treatment with ^{213}Bi-tracers (scale bar = 5 µm). Arrowheads indicate α-tracks.

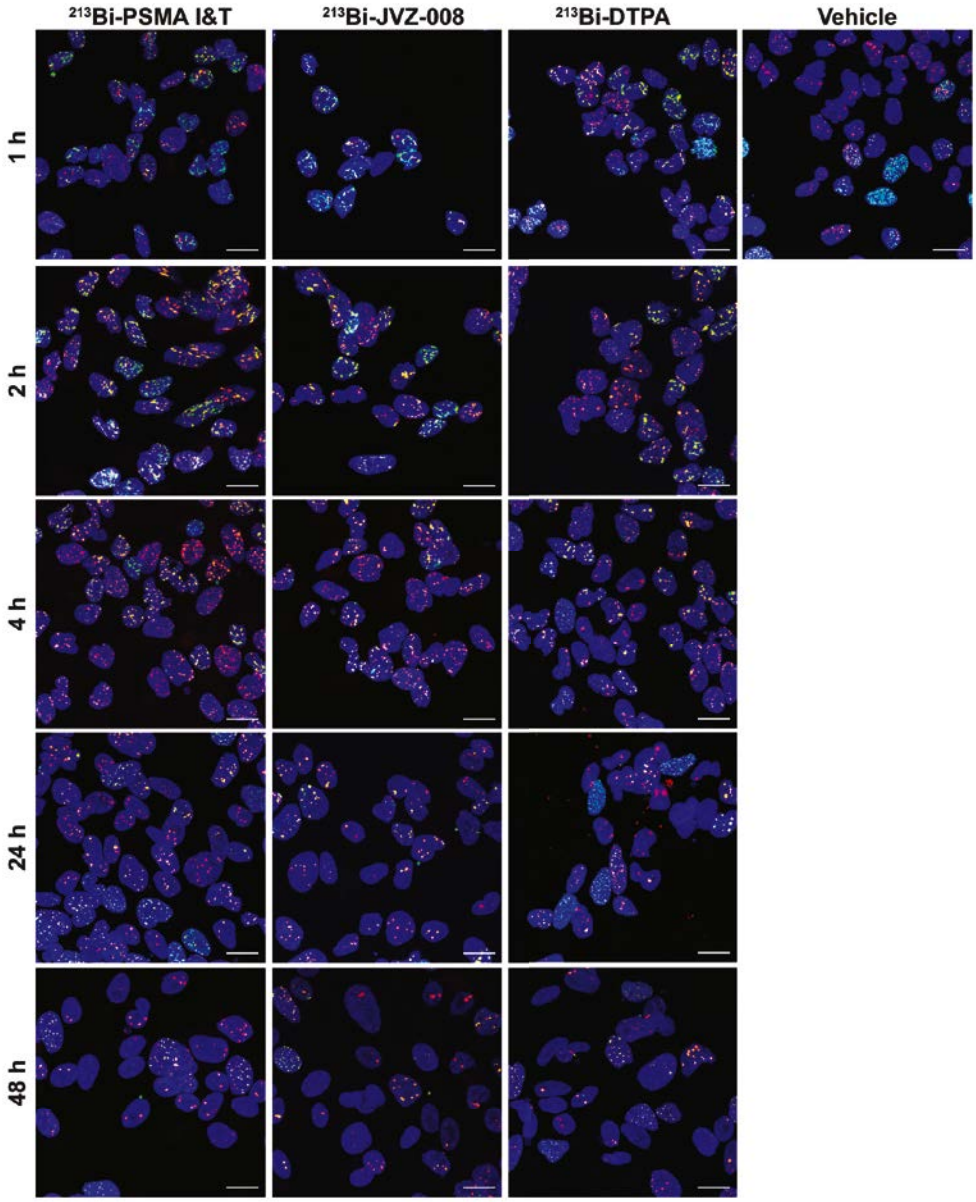

FIGURE 3. Representative overlay field pictures of DNA double strand breaks in LNCaP cells at 1 h after treatment with vehicle or at different time points after ^{213}Bi-tracer treatment (scale bar = 20 µm). Blue = DAPI, green = γH2AX, red = 53BP1.

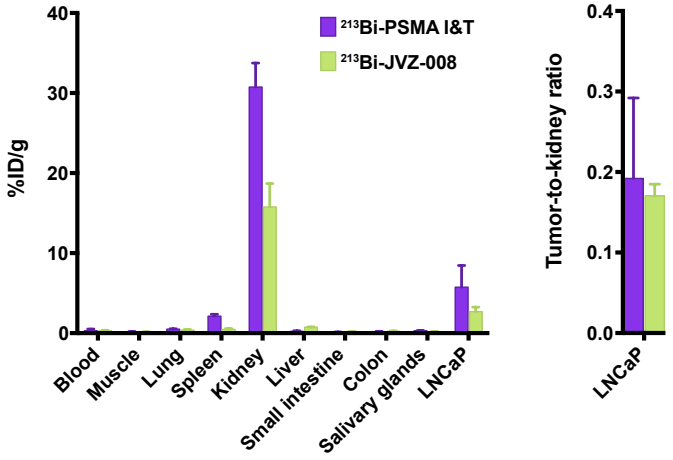

FIGURE 4: Biodistribution of ^{213}Bi-PSMA I&T and ^{213}Bi-JVZ-008 in LNCaP xenografts.

^{213}Bi-PSMA I&T and ^{213}Bi-JVZ-008 Induce DSBs in LNCaP Cells In Vitro

Phosphorylation of histone H2AX (γH2AX) and accumulation of p53-binding protein 1 (53BP1) at the site of DSBs are biomarkers of radiation-induced DSBs (*7*). Background 53BP1 and γH2AX nuclear foci, most likely arising from replication stress, were observed in vehicle-treated LNCaP cells. Treatment of LNCaP cells with the targeted tracers ^{213}Bi-PSMA I&T and ^{213}Bi-JVZ-008 and the nontargeted tracer ^{213}Bi-DTPA all induced DSBs, as indicated by the presence of 53BP1 and γH2AX foci (**Figure 2 and 3**). At early time points, the DNA damage was visible as single foci and linear tracks, i.e. α-tracks. Tracks were visible at least until 4 h after treatment, but were lost at 24 and 48 h after treatment. Single DSB foci were still present at these later time points.

^{213}Bi-PSMA I&T and ^{213}Bi-JVZ-008 Accumulate in LNCaP Tumors in Mice

Accumulation of ^{213}Bi-PSMA I&T and ^{213}Bi-JVZ-008 was observed in LNCaP tumors and in kidneys (**Figure 4**). Tumor uptake at 1 h after injection was 5.75±2.70 %ID/g and 2.68±0.56 %ID/g for ^{213}Bi-PSMA I&T and ^{213}Bi-JVZ-008, respectively. Tumor-to-kidney uptake ratios of both compounds were similar.

^{213}Bi-PSMA I&T and ^{213}Bi-JVZ-008 Induce DSBs in LNCaP Tumors in Mice

^{213}Bi-PSMA I&T and ^{213}Bi-JVZ-008 induced DSBs in LNCaP tumors, as reflected by increased numbers of 53BP1 and γH2AX foci 1 h after injection, as compared to nontreated mice. DSBs were still observed 24 h after injection (**Figure 5 and 6**). α-tracks were observed shortly after treatment and were no longer detectable 24 h after injection, in line with the in vitro observations.

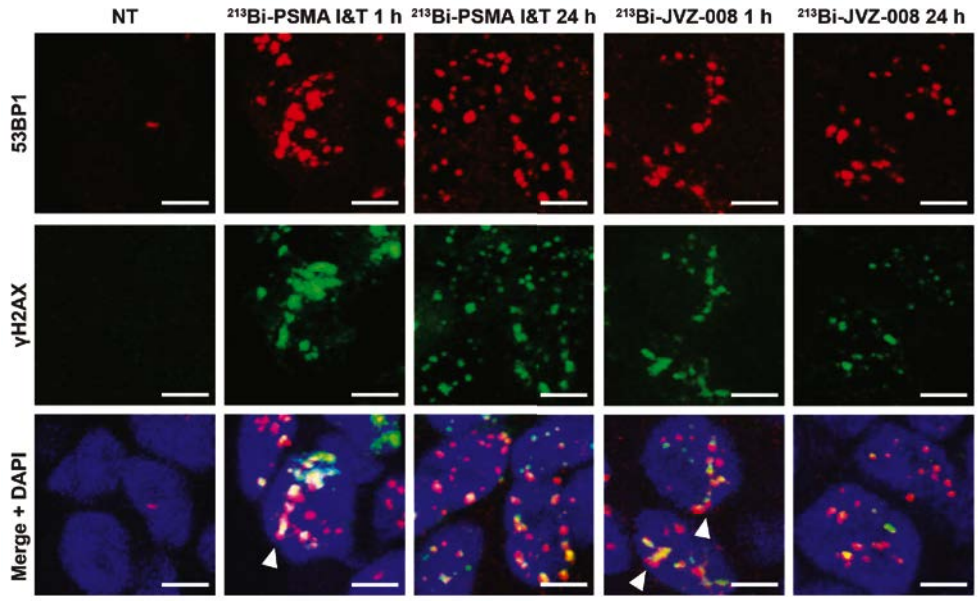

FIGURE 5: Representative pictures of DNA double strand breaks in LNCaP xenografts of nontreated (NT) mice or at 1 and 24 h after injection of ^{213}Bi-PSMA I&T or ^{213}Bi-JVZ-008 (scale bar = 5 μm). Arrowheads indicate α-tracks.

DISCUSSION

Here, we report on the preclinical results of PSMA-targeted α radionuclide therapy with 2 novel PSMA-targeting agents–the small-molecule PSMA inhibitor ^{213}Bi-PSMA I&T and the anti-PSMA nanobody ^{213}Bi-JVZ-008.

PSMA has emerged as a valuable target for specific delivery of diagnostic and therapeutic radionuclides to prostate tumors, owing to its high expression in the majority of PCa tumors. Up to now, PSMA-targeted radionuclide therapy strategies have mainly focused on β-emitting radionuclides. Studies with small molecule inhibitors and antibodies, such as ^{131}I-MIP-1095, ^{177}Lu-PSMA-617, ^{177}Lu-PSMA I&T, and ^{177}Lu-J591 have shown the safety and therapeutic efficacy of this approach (*3, 4, 8-11*).

α-particles have higher energies (4–9 MeV) and shorter path lengths (40–100 μm) than β-particles (energy: 0.1–2.2 MeV, path length: 1–10 mm). The high LET of α-particles causes complex DSBs (*12*), resulting in deletions, chromosome aberrations and cell death (*13*). High LET radionuclides therefore have a higher relative biological effectiveness for cell killing (*14, 15*) and may significantly enhance the efficacy of radionuclide therapy.

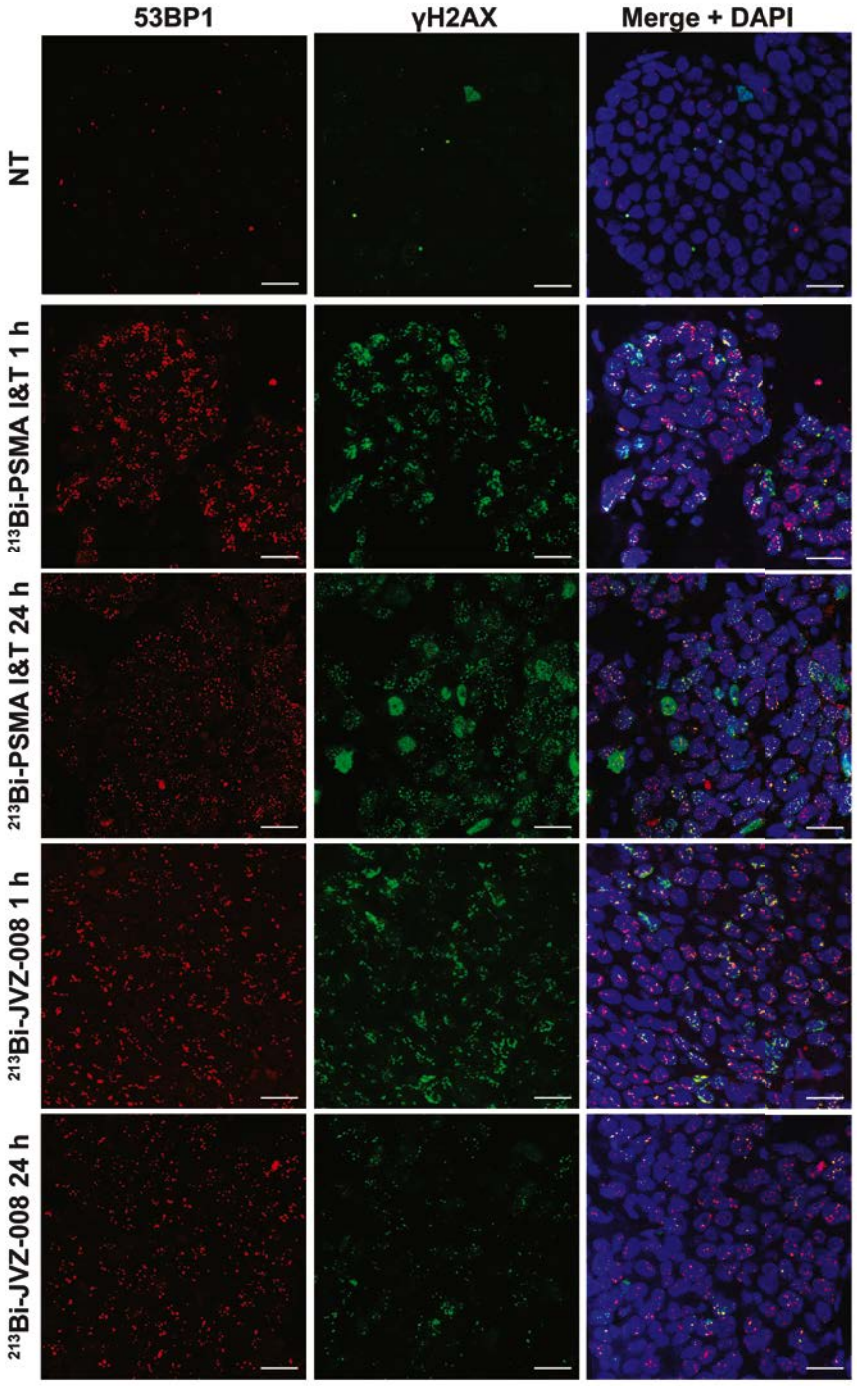

FIGURE 6: Representative pictures of DNA double strand breaks in LNCaP xenografts of nontreated (NT) mice or at 1 and 24 h after injection of ^{213}Bi-PSMA I&T or ^{213}Bi-JVZ-008 (scale bar = 20 µm).

Four studies have reported on PSMA-targeted radionuclide therapy using α-emitting radionuclides. In vitro and in vivo treatment with the monoclonal antibody J591 labeled with ^{213}Bi showed promising results (*16, 17*). However, in vivo application of this tracer appeared challenging because the short ^{213}Bi half-life (45.6 min) does not match with slow antibody pharmacokinetics. Two studies showed the ability of anti-PSMA-targeted liposomes/lipid vesicles loaded with the α-emitter ^{225}Ac to kill PSMA-expressing cells in vitro (*18, 19*). However, because of the high recoil energy when daughter products are released, in vivo stability of these nanocarriers should be addressed (*20*).

In the present study, we show for the first time the application of ^{213}Bi with low-molecular weight PSMA-targeting agents. Treatment of LNCaP cells with ^{213}Bi-PSMA I&T and ^{213}Bi-JVZ-008 resulted in production of DSBs, both in vitro and in vivo. However, induction of DSBs was also observed in vitro after treatment with the nontargeted agent ^{213}Bi-DTPA, with similar DSB foci kinetics as ^{213}Bi-PSMA I&T and ^{213}Bi-JVZ-008. This suggests that DNA damage was already induced by ^{213}Bi-DTPA from the medium during the 20 min incubation period. Because of the high cytotoxicity of ^{213}Bi and its short half-life, this in vitro model appeared suboptimal and the tracers were further evaluated in vivo. In our xenograft model, a 2-fold higher tumor uptake was observed for ^{213}Bi-PSMA I&T than for ^{213}Bi-JVZ-008. DSBs (including α-tracks) were induced by both tracers in LNCaP tumors. α-tracks were no longer detectable at 24 h after treatment, indicating that a fraction of the DSBs in the tracks was repaired.

For clinical translation, it is important to note that PSMA is also expressed in normal tissues and dosimetric calculations predict the highest absorbed doses in salivary glands and kidneys (*4, 9*). However, so far studies with β-emitting radionuclides reported only mild early side effects, such as xerostomia, mild hematotoxicity and mild nephrotoxicity in a minority of the treated-patients (*10*).

CONCLUSION

Preclinical evaluation of ^{213}Bi-PSMA I&T and ^{213}Bi-JVZ-008 revealed good tumor targeting and production of DSBs in PSMA-expressing LNCaP tumors in vivo. These results warrant further evaluation of therapeutic efficacy and toxicity. Providing a favorable safety profile, these novel tracers could offer a promising new treatment option for PCa patients with metastatic lesions.

REFERENCES

1. Heidenreich A, Bastian PJ, Bellmunt J, et al. EAU guidelines on prostate cancer. Part II: Treatment of advanced, relapsing, and castration-resistant prostate cancer. Eur Urol. 2014;65:467-479.
2. Parker C, Nilsson S, Heinrich D, et al. Alpha emitter radium-223 and survival in metastatic prostate cancer. N Engl J Med. 2013;369:213-223.
3. Weineisen M, Schottelius M, Simecek J, et al. 68Ga- and 177Lu-labeled PSMA I&T: optimization of a PSMA-targeted theranostic concept and first proof-of-concept human studies. J Nucl Med. 2015;56:1169-1176.
4. Herrmann K, Bluemel C, Weineisen M, et al. Biodistribution and radiation dosimetry for a probe targeting prostate-specific membrane antigen for imaging and therapy. J Nucl Med. 2015;56:855-861.
5. Chatalic KL, Veldhoven-Zweistra J, Bolkestein M, et al. A novel (111)In-labeled anti-prostate-specific membrane antigen nanobody for targeted SPECT/CT imaging of prostate cancer. J Nucl Med. 2015;56:1094-1099.
6. Kratochwil C, Giesel FL, Leotta K, et al. PMPA for nephroprotection in PSMA-targeted radionuclide therapy of prostate cancer. J Nucl Med. 2015;56:293-298.
7. Sak A, Stuschke M. Use of gammaH2AX and other biomarkers of double-strand breaks during radiotherapy. Semin Radiat Oncol. 2010;20:223-231.
8. Zechmann CM, Afshar-Oromieh A, Armor T, et al. Radiation dosimetry and first therapy results with a (124)I/ (131)I-labeled small molecule (MIP-1095) targeting PSMA for prostate cancer therapy. Eur J Nucl Med Mol Imaging. 2014;41:1280-1292.
9. Delker A, Fendler WP, Kratochwil C, et al. Dosimetry for Lu-DKFZ-PSMA-617: a new radiopharmaceutical for the treatment of metastatic prostate cancer. Eur J Nucl Med Mol Imaging. August 29, 2015 [Epub ahead of print].
10. Ahmadzadehfar H, Rahbar K, Kurpig S, et al. Early side effects and first results of radioligand therapy with (177)Lu-DKFZ-617 PSMA of castrate-resistant metastatic prostate cancer: a two-centre study. EJNMMI Res. 2015;5:114.
11. Tagawa ST, Milowsky MI, Morris M, et al. Phase II study of Lutetium-177-labeled anti-prostate-specific membrane antigen monoclonal antibody J591 for metastatic castration-resistant prostate cancer. Clin Cancer Res. 2013;19:5182-5191.
12. Milenic DE, Brady ED, Brechbiel MW. Antibody-targeted radiation cancer therapy. Nat Rev Drug Discov. 2004;3:488-499.
13. Ritter MA, Cleaver JE, Tobias CA. High-LET radiations induce a large proportion of non-rejoining DNA breaks. Nature. 1977;266:653-655.
14. Rydberg B, Cooper B, Cooper PK, Holley WR, Chatterjee A. Dose-dependent misrejoining of radiation-induced DNA double-strand breaks in human fibroblasts: experimental and theoretical study for high- and low-LET radiation. Radiat Res. 2005;163:526-534.
15. Mulford DA, Scheinberg DA, Jurcic JG. The promise of targeted {alpha}-particle therapy. J Nucl Med. 2005;46(Suppl 1):199s-204s.
16. Li Y, Tian Z, Rizvi SM, Bander NH, Allen BJ. In vitro and preclinical targeted alpha therapy of human prostate cancer with Bi-213 labeled J591 antibody against the prostate specific membrane antigen. Prostate Cancer Prostatic Dis. 2002;5:36-46.
17. Ballangrud AM, Yang WH, Charlton DE, et al. Response of LNCaP spheroids after treatment with an alpha-particle emitter (213Bi)-labeled anti-prostate-specific membrane antigen antibody (J591). Cancer Res. 2001;61:2008-2014.

18. Bandekar A, Zhu C, Jindal R, Bruchertseifer F, Morgenstern A, Sofou S. Anti-prostate-specific membrane antigen liposomes loaded with 225Ac for potential targeted antivascular alpha-particle therapy of cancer. J Nucl Med. 2014;55:107-114.
19. Zhu C, Bandekar A, Sempkowski M, et al. Nanoconjugation of PSMA-targeting ligands enhances perinuclear localization and improves efficacy of delivered alpha-particle emitters against tumor endothelial analogues. Mol Cancer Ther. November 19, 2015 [Epub ahead of print].
20. de Kruijff RM, Wolterbeek HT, Denkova AG. A Critical Review of Alpha Radionuclide Therapy-How to Deal with Recoiling Daughters? Pharmaceuticals (Basel). 2015;8:321-336.

Epilogue

4

General Discussion and Concluding Remarks

Summary

Samenvatting

Curriculum Vitae

PhD Portfolio

Acknowledgments

4

General Discussion and Concluding Remarks

Prostate cancer (PCa) is the second most frequently diagnosed cancer in men and the fifth leading cause of cancer death worldwide (*1*). Early detection of PCa is essential, as treatment options for advanced disseminated PCa are limited. A single tool that can be applied for diagnosis and therapy in a "theranostic" approach for PCa would be a major breakthrough. This powerful combination would not only allow non-invasive detection of PCa lesions, but also to monitor disease progression and treatment efficacy. However, a few pitfalls have to be considered if this goal is to be realized.

Theranostic agents are designed to accumulate in tumors, either by nontargeted mechanisms, e.g. the enhanced permeability and retention (EPR) effect, or by targeted mechanisms. Nontargeted mechanisms have a broader applicability, but do not provide the same uptake ratio between tumor target tissues and healthy nontarget tissues. Theranostic agents can be designed to specifically target tumor-associated

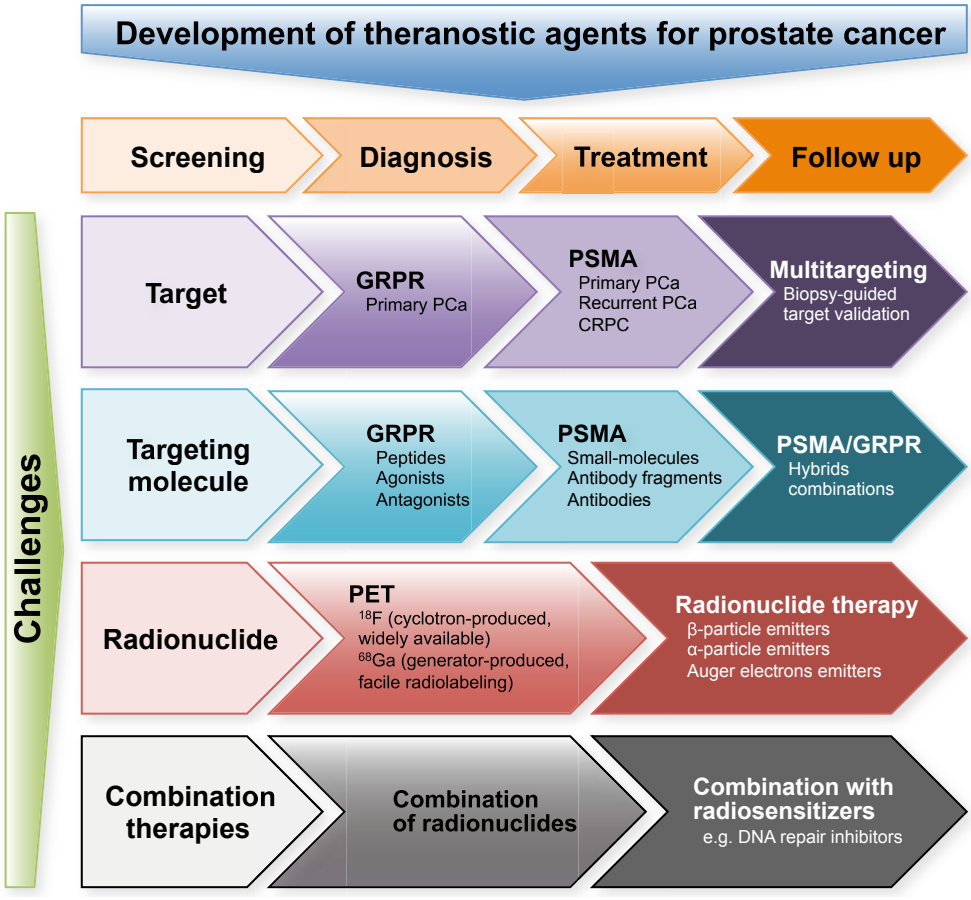

Figure 1. Factors to be considered for the design of theranostic agents for prostate cancer in nuclear medicine.

biomarkers, which are overexpressed on PCa cells. Several biomarkers have been identified as interesting targets for radionuclide imaging and therapy of PCa, including prostate-specific membrane antigen (PSMA), prostate stem cell antigen (PSCA), and gastrin-releasing peptide receptor (GRPR). The important factors to be considered for the development of theranostic agents for PCa in nuclear medicine are depicted in **Figure 1**.

Which Target?

PSMA is overexpressed on 90-100% of PCa, including lymph node and bone metastases (*2-4*). However, it is also expressed in various normal organs, such as prostate, kidneys, and salivary glands (*5*). Although PSMA is an excellent target for imaging of metastatic spread of PCa, its expression in normal prostate may limit the performance of PSMA-targeted tracers for initial staging. Furthermore, expression of PSMA on kidneys and salivary gland might be a limiting factor for the successful application of PSMA-targeted radionuclide therapy.

PSCA is overexpressed in about 90-100% of PCa and increased expression is found in advanced PCa and bone metastases (*6-9*). A study from Ananias et al. has shown overexpression of PSCA in 95% of lymph node metastases and 94% of bone metastases, although staining intensity was lower than for PSMA (*9*). Exploration of this target as imaging agent has been more limited than GRPR and PSMA. One of the main factors driving radiotracer development towards GRPR and PSMA might have been the availability of peptide ligands binding GRPR, and small-molecule inhibitors of PSMA, which are easy to produce and show favorable pharmacokinetics.

GRPR appears as a promising target for detection of primary PCa, as its expression on normal prostate is relatively low. GRPR is overexpressed in a majority of primary PCa, and in about 50% of lymph node metastases and bone metastases (*10*). It has been shown that GRPR-expression is down-regulated by androgen deprivation, limiting the use of GRPR-targeted tracer for anti-androgen treated recurrent PCa (*11*). GRPR could be a promising target for radionuclide therapy as well, owing to its low expression on normal tissues, except for the pancreas. However, radionuclide therapy is usually only applied in late-stage disease. Therefore more studies are needed to define the expression of GRPR in late-stage hormonally treated, castration-resistant prostate cancer (CRPC). The expression of GRPR on CRPC has not been studied extensively. This lack of information is mainly due to the absence of a validated and specific GRPR-antibody. Alternatively, GRPR mRNA expression levels have been quantified using polymerase chain reaction.

A multitargeting approach has been proposed, using bispecific tracers targeting PSMA and GRPR, which would enable tumor-targeting in different stages of PCa progression (*12, 13*). However, it should be noted that the combination of PSMA and GRPR targeting might lead to a combination of disadvantages of both approaches, e.g.

tracer uptake in organs expressing PSMA, e.g. kidneys and salivary gland, as well as in those expressing GRPR, e.g. pancreas. Alternatively, a more personalized multitracer approach could effectively contribute to individual management of PCa patients. In such an approach, the most suitable tracer (combination) would be selected based on target expression as determined on biopsy material. This strategy is not without pitfalls, as biopsy material might not represent the heterogeneity and complexity of the patient's tumor, and hence may only serve as an indication.

Which Targeting Molecule?

Next to selecting the most suitable target, the most appropriate targeting molecule should be identified. Targeting molecules should meet important criteria, such as easy manufacturing, low immunogenicity, in vivo stability, efficient tumor targeting, tumor specificity, fast clearance, and low uptake in healthy organs.

Peptides usually meet most of these criteria, and therefore represent a promising class of targeting molecules. However, natural peptides are prone to in vivo degradation by proteolytic enzymes. Strategies have been implemented to increase radiopeptide in vivo stability by introducing structural modifications (e.g. key amino acid substitution by D-amino acids or unnatural amino acids, cyclization, etc.), although such modifications can cause undesired changes in pharmacokinetics or impair receptor affinity. Alternatively, radiopeptides can be administered together with an enzyme inhibitor to protect them from enzymatic degradation. It has recently been shown that coinjection of a neutral endopeptidase (NEP) inhibitor, such as phosphoramidon (PA), can stabilize radiolabeled bombesin, minigastrin, and somatostatin analogs in vivo, leading to enhanced tumor uptake and improved tumor visualization (**4**). In **Chapter 2.2** of this thesis, we have shown that in vivo stabilization of the GRPR-antagonist peptide JMV4168 enhanced PET imaging and radionuclide therapy in a preclinical model of PCa.

For PSMA, there is no naturally occurring peptide ligand. Different classes of molecules have been considered, ranging from small-molecule inhibitors, antibody fragments, to antibodies. Antibodies have very good targeting properties, but show slow accumulation in tumors and slow clearance from the blood pool and background organs. Alternatively, antibody fragments (Fab, $F(ab')_2$, scFv, diabodies, minibodies, a.o.) can be used, but these usually show less affinity for their targets, and lower absolute uptake in tumor. In addition, high renal retention is often observed with antibody fragments. In some cases, renal reabsorption in proximal tubular cells can be diminished with compounds such as lysine, arginine, gelofusine, and albumin fragments. In **Chapter 3.1** of this thesis, we have designed a PSMA-targeting nanobody for imaging and radionuclide therapy of PCa. This tracer displays specific tumor targeting and, more importantly, low renal retention. Unfortunately, tumor targeting remained lower than the clinically used small-molecule inhibitor PSMA I&T. Small-molecule inhibitors, which specifically bind to the catalytic site of PSMA,

have shown efficient and fast accumulation at tumor sites, accompanied by mostly low background radioactivity. However, high uptake in kidneys and salivary glands is observed as well. In **Chapter 3.2** of this thesis, we have shown that renal and spleen uptake of an ^{111}In-labeled small-molecule PSMA inhibitor, ^{111}In-PSMA I&T, could be significantly reduced by coinjection of a small hydrophilic PSMA inhibitor. This led to improvement of metastatic lesion visualization near the spleen and kidneys, and protection of the kidneys from radiation-induced damage during radionuclide therapy in mice. However, the translation of this concept into a clinical setting might be challenging, mainly because the patterns of expression of human PSMA/FOLH1 and its mouse ortholog Folh1 differ in mice and humans (*15*). In patients, dosimetry calculations have shown that salivary glands might be the most at risk during radionuclide therapy. First radionuclide therapy results using ^{177}Lu-PSMA-617 and ^{177}Lu-PSMA I&T have shown no major renal toxicity (*16-19*), however it should be kept in mind that chronic renal toxicity is a late-occurring side effect. Reports have shown that expression of PSMA in normal organs is 100-1,000 fold lower than in tumors. It is not clear why the small-molecule inhibitors have such a high uptake in salivary glands. Better accessibility of the binding sites in the salivary glands to small molecules, or cross-reactivity with other receptors, splice variants or paralogs of PSMA might be an explanation. Anti-PSMA antibodies (e.g J591) do not accumulate in kidneys and salivary glands, and are therefore interesting for PSMA-targeted radionuclide therapy. To circumvent the long circulation time of antibodies, a pretargeting approach could be used, in which a radiolabeled hydrophilic molecule is "clicked" to a functionalized PSMA-targeted antibody after leaving sufficient time for antibody accumulation at the tumor site and clearance of unbound antibody from the circulation. The use of an antibody with a low internalization rate is required for this approach.

Which Radionuclide?

The choice of the radionuclide is essential in the design of tracers for imaging and therapy.

For PET imaging, ^{68}Ga emerges as a useful radionuclide, which can be eluted from a commercially available ^{68}Ge/^{68}Ga generator and offers straightforward radiolabeling procedures. Because of its short half-life (68 min), the use of ^{68}Ga-radiopharmaceuticals is limited to centers equipped with a ^{68}Ge/^{68}Ga generator. ^{18}F is more widely applied. ^{18}F can be produced in large quantities in a cyclotron, and because of the longer half-life (110 min), ^{18}F-radiopharmaceuticals can be shipped to hospitals within a range of ca. 200 km. However, most methods for labeling peptides with ^{18}F are laborious and require multistep procedures with moderate labeling yields. A good alternative is the Al^{18}F labeling method (*20*), allowing fast and facile labeling of peptides in a 1-step procedure. In **Chapter 2.1** of this thesis, we designed a new GRPR-antagonist conjugate, JMV5132 (NODA-MPAA-βAla-βAla-(H-D-Phe-Gln-Trp-Ala-Val-Gly-His-Sta-Leu-NH_2), with a NODA-MPAA chelator for high-yield complexation of Al^{18}F. Labeling of JMV5132 with Al^{18}F was completed within 20 minutes without a need for purification. PET images obtained with Al^{18}F-JMV5132 showed a higher resolution

than with ^{68}Ga-JMV4168 (DOTA-βAla-βAla-[H-D-Phe-Gln-Trp-Ala-Val-Gly-His-Sta-Leu-NH_2]), but Al^{18}F-JMV5132 showed higher hepatobiliary excretion. JMV5132 could be further improved by adding a hydrophilic glycosylated spacer, which would reduce lipophilicity and hepatobiliary excretion of the Al^{18}F-labeled tracer.

For PSMA targeting, several ^{18}F-labeled PSMA ligands have been developed for PET imaging of PCa. Recently, a promising ^{18}F-labeled PSMA ligand was introduced, [^{18}F]-DCFPyL [2-(3-(1-carboxy-5-[(6-[^{18}F]fluoro-pyridine-3-carbonyl)-amino]-pentyl)-ureido)-pentanedioic acid] (*21*). A direct comparison of [^{18}F]-DCFPyL with ^{68}Ga-HBED-CC-PSMA has indicated that [^{18}F]-DCFPyL could detect all lesions detected by ^{68}Ga-HBED-CC-PSMA, with significantly higher SUVmax values and higher tumor-to-background ratios. Moreover, in 3/14 patients, [^{18}F]-DCFPyL detected additional suspicious PCa lesions.

For therapy, β-particle emitting radionuclides are the most widely applied. ^{177}Lu-PSMA-617 and ^{177}Lu-PSMA I&T have been recently introduced for the treatment of metastatic castration-resistant PCa (*16-19*). Additionally, there is an increasing interest for α-particle emitting radionuclides. α-particles have higher energies and shorter path lengths than β-particles. The high linear energy transfer of alpha particles causes more complex DNA double-strand breaks (DSBs), resulting in a higher relative biological effectiveness for cell killing (*22, 23*). Therefore the use of alpha-emitters may significantly enhance the efficacy of radionuclide therapy. Two studies have reported on PSMA-targeted radionuclide therapy using the ^{213}Bi-labeled monoclonal antibody J591 (*24, 25*). However, the slow pharmacokinetics of antibodies do not match with the short half-life of ^{213}Bi. In **Chapter 3.3** of this thesis, we have shown the application of two ^{213}Bi-labeled low-molecular weight PSMA-targeting agents, the DOTAGA-conjugated small-molecule inhibitor PSMA I&T and the DOTA-conjugated anti-PSMA Nanobody JVZ-008, for alpha radionuclide therapy of PCa. These novel tracers could offer a promising new treatment option for PCa patients with metastatic lesions. However, because of the PSMA-mediated uptake in kidneys and salivary gland, toxicity should be investigated carefully. Alternatively, a pretargeting approach using e.g. J591 could be considered to overcome slow antibody pharmacokinetics and toxicity to kidneys and salivary glands.

How to Prevent Tumor Regrowth?

Even though radionuclide therapy can elicit tumor shrinkage, tumor regrowth is often observed after a few weeks or months. It is essential to determine the causes of tumor regrowth in order to maximize the radiotherapeutic effect. Regrowth of tumor cells may be caused by several factors, such as heterogeneous target expression, heterogeneity of tracer uptake, or radioresistance of tumor cells. Depending on the underlying cause, combination of treatments can be tailored to improve treatment efficacy. To achieve targeting of a wider range of tumor lesions, the combination of radionuclides with different penetration ranges in tissues has been considered (*26*). Combination with agents that inhibit DNA damage repair has been considered to circumvent resistance to radiation-induced DNA damage. A recent paper described

a sensitization strategy to enhance EGFR-targeted alpha-particle radiotherapy with a small-molecule inhibitor of DNA-dependent protein kinase, catalytic subunit (PKcs) (*27*). More recently, inhibition of heat shock protein 90 (HSP90), a protein associated with radioresistance, was used to potentiate radiation effects in tumorigenic cell lines (*28*). The genetic changes and the underlying pathways that are induced by radionuclide therapy are not well understood. More knowledge on these mechanisms and identifying the crucial checkpoints will allow development of novel combination strategies to improve efficacy of radionuclide therapy and prevent development of radioresistance.

CONCLUDING REMARKS

In conclusion, there is no perfect theranostic agent for imaging and therapy of PCa at all disease stages yet, but the studies described in this thesis have shown strategies that could be implemented to improve the detection and treatment of PCa at a specific stage of the disease. Early diagnosis of PCa may be achieved using GRPR antagonists (in combination with a NEP inhibitor), or small-molecules PSMA inhibitors. Detection of PCa recurrence and metastatic spread may be best achieved using small-molecule PSMA inhibitors, which offer very high imaging contrast. Expression of GRPR in late stage PCa should be investigated further to assess the applicability of GRPR antagonists for radionuclide therapy of metastatic CRPC. Small-molecule PSMA inhibitors are promising for treatment of late-stage PCa, but the use of a pretargeting approach using antibodies could potentially spare healthy tissues such as kidneys and salivary glands. Finally, a multitracer-based selection platform could be helpful for theranostic strategies to be implemented in a personalized approach in the management of PCa.

REFERENCES

1. Torre LA, Bray F, Siegel RL, Ferlay J, Lortet-Tieulent J, Jemal A. Global cancer statistics, 2012. CA Cancer J Clin. 2015;65:87-108.
2. Bostwick DG, Pacelli A, Blute M, Roche P, Murphy GP. Prostate specific membrane antigen expression in prostatic intraepithelial neoplasia and adenocarcinoma: a study of 184 cases. Cancer. 1998;82:2256-2261.
3. Silver DA, Pellicer I, Fair WR, Heston WD, Cordon-Cardo C. Prostate-specific membrane antigen expression in normal and malignant human tissues. Clin Cancer Res. 1997;3:81-85.
4. Wright GL, Jr., Haley C, Beckett ML, Schellhammer PF. Expression of prostate-specific membrane antigen in normal, benign, and malignant prostate tissues. Urol Oncol. 1995;1:18-28.
5. Sokoloff RL, Norton KC, Gasior CL, Marker KM, Grauer LS. A dual-monoclonal sandwich assay for prostate-specific membrane antigen: levels in tissues, seminal fluid and urine. Prostate. 2000;43:150-157.
6. Reiter RE, Gu Z, Watabe T, et al. Prostate stem cell antigen: a cell surface marker overexpressed in prostate cancer. Proc Natl Acad Sci U S A. 1998;95:1735-1740.
7. Gu Z, Thomas G, Yamashiro J, et al. Prostate stem cell antigen (PSCA) expression increases with high gleason score, advanced stage and bone metastasis in prostate cancer. Oncogene. 2000;19:1288-1296.
8. Han KR, Seligson DB, Liu X, et al. Prostate stem cell antigen expression is associated with gleason score, seminal vesicle invasion and capsular invasion in prostate cancer. J Urol. 2004;171:1117-1121.
9. Ananias HJ, van den Heuvel MC, Helfrich W, de Jong IJ. Expression of the gastrin-releasing peptide receptor, the prostate stem cell antigen and the prostate-specific membrane antigen in lymph node and bone metastases of prostate cancer. Prostate. 2009;69:1101-1108.
10. Ischia J, Patel O, Bolton D, Shulkes A, Baldwin GS. Expression and function of gastrin-releasing peptide (GRP) in normal and cancerous urological tissues. BJU Int. 2014;113 Suppl 2:40-47.
11. Schroeder RP, de Visser M, van Weerden WM, et al. Androgen-regulated gastrin-releasing peptide receptor expression in androgen-dependent human prostate tumor xenografts. Int J Cancer. 2010;126:2826-2834.
12. Bandari RP, Jiang Z, Reynolds TS, et al. Synthesis and biological evaluation of copper-64 radiolabeled [DUPA-6-Ahx-(NODAGA)-5-Ava-BBN(7-14)NH2], a novel bivalent targeting vector having affinity for two distinct biomarkers (GRPr/PSMA) of prostate cancer. Nucl Med Biol. 2014;41:355-363.
13. Eder M, Schafer M, Bauder-Wust U, Haberkorn U, Eisenhut M, Kopka K. Preclinical evaluation of a bispecific low-molecular heterodimer targeting both PSMA and GRPR for improved PET imaging and therapy of prostate cancer. Prostate. 2014;74:659-668.
14. Nock BA, Maina T, Krenning EP, de Jong M. "To serve and protect": enzyme inhibitors as radiopeptide escorts promote tumor targeting. J Nucl Med. 2014;55:121-127.
15. Bacich DJ, Pinto JT, Tong WP, Heston WD. Cloning, expression, genomic localization, and enzymatic activities of the mouse homolog of prostate-specific membrane antigen/NAALADase/folate hydrolase. Mamm Genome. 2001;12:117-123.
16. Schuchardt C, Wiessalla S, Ozkan A, et al. Therapy of Metastasized Prostate Cancer Using a Lu-177 Labeled PSMA Inhibitor (I&T): First Dosimetric Results in Patients. European Journal of Nuclear Medicine and Molecular Imaging. 2015;42:S99-S99.

17. Kulkarni HR, Singh A, Schuchardt C, Klette I, Wester HJ, Baum RP. Peptide Radioligand Therapy (PRLT) Using Lu-177 Labeled DOTAGA-PSMA Inhibitor Yields Objective Responses in Metastatic Castrate-resistant Prostate Cancer. European Journal of Nuclear Medicine and Molecular Imaging. 2015;42:S59-S60.
18. Ahmadzadehfar H, Rahbar K, Kurpig S, et al. Early side effects and first results of radioligand therapy with (177)Lu-DKFZ-617 PSMA of castrate-resistant metastatic prostate cancer: a two-centre study. EJNMMI Res. 2015;5:114.
19. Afshar-Oromieh A, Hetzheim H, Kratochwil C, et al. The novel theranostic PSMA-ligand PSMA-617 in the diagnosis of prostate cancer by PET/CT: biodistribution in humans, radiation dosimetry and first evaluation of tumor lesions. J Nucl Med. 2015.
20. McBride WJ, Sharkey RM, Karacay H, et al. A novel method of 18F radiolabeling for PET. J Nucl Med. 2009;50:991-998.
21. Chen Y, Pullambhatla M, Foss CA, et al. 2-(3-{1-Carboxy-5-[(6-[18F]fluoro-pyridine-3-carbonyl)-amino]-pentyl}-ureido)-pen tanedioic acid, [18F]DCFPyL, a PSMA-based PET imaging agent for prostate cancer. Clin Cancer Res. 2011;17:7645-7653.
22. Rydberg B, Cooper B, Cooper PK, Holley WR, Chatterjee A. Dose-dependent misrejoining of radiation-induced DNA double-strand breaks in human fibroblasts: experimental and theoretical study for high- and low-LET radiation. Radiat Res. 2005;163:526-534.
23. Mulford DA, Scheinberg DA, Jurcic JG. The promise of targeted {alpha}-particle therapy. J Nucl Med. 2005;46(Suppl 1):199s-204s.
24. Li Y, Tian Z, Rizvi SM, Bander NH, Allen BJ. In vitro and preclinical targeted alpha therapy of human prostate cancer with Bi-213 labeled J591 antibody against the prostate specific membrane antigen. Prostate Cancer Prostatic Dis. 2002;5:36-46.
25. Ballangrud AM, Yang WH, Charlton DE, et al. Response of LNCaP spheroids after treatment with an alpha-particle emitter (213Bi)-labeled anti-prostate-specific membrane antigen antibody (J591). Cancer Res. 2001;61:2008-2014.
26. Radojewski P, Dumont R, Marincek N, et al. Towards tailored radiopeptide therapy. Eur J Nucl Med Mol Imaging. 2015;42:1231-1237.
27. Song H, Hedayati M, Hobbs RF, et al. Targeting aberrant DNA double-strand break repair in triple-negative breast cancer with alpha-particle emitter radiolabeled anti-EGFR antibody. Mol Cancer Ther. 2013;12:2043-2054.
28. Spiegelberg D, Dascalu A, Mortensen AC, et al. The novel HSP90 inhibitor AT13387 potentiates radiation effects in squamous cell carcinoma and adenocarcinoma cells. Oncotarget. 2015;6:35652-35666.

4

Summary

The aim of the studies described in this thesis was to develop and optimize theranostic strategies for imaging and radionuclide therapy of prostate cancer (PCa). These theranostic approaches might ultimately contribute to a more personalized management of PCa patients.

Section 1 of this thesis introduces the concept of theranostics in nuclear medicine. In **Chapter 1.1** an introduction to PCa is provided, describing current diagnosis and staging procedures, treatment planning, and follow-up methods. Next, the clinical relevance of theranostic approaches is described, and the principles of molecular imaging and radionuclide therapy are laid out, together with the radionuclides used for imaging and therapy. Finally, molecular targets for PCa are introduced, with a focus on the gastrin-releasing peptide receptor (GRPR) and prostate-specific membrane antigen (PSMA). Moreover, PCa-targeted molecular imaging and radionuclide therapy approaches are discussed. **Chapter 1.2** describes novel strategies to improve the application of radiopeptides for imaging and therapy. After the successful application of ^{111}In-octreotide for imaging of neuroendocrine tumors in the clinic, radiopeptides targeting different receptor families have been developed for imaging of several types of diseases as well as for radionuclide therapy. Several approaches have been considered to improve the imaging performance of radiopeptides, including the use of receptor antagonists, in vivo stabilization of radiopeptides by in vivo enzyme inhibition, the use of positron-emitting radionuclides for positron emission tomography (PET) imaging, and the combination of nuclear and optical imaging. Strategies used to improve therapeutic efficacy of radiopeptides include the use of receptor antagonists, the combination of radionuclides with different penetration ranges, the combination of radionuclide therapy with chemotherapeutics, the introduction of α-particle-emitting radionuclides, and the introduction of methods to predict therapy response. Some of these strategies have been implemented in this thesis, as described below.

Section 2 of this thesis focuses on the development of GRPR-targeted theranostic strategies for PCa. GRPR antagonists have attracted considerable attention after reports have shown that GRPR antagonists show higher tumor uptake and lower accumulation in GRPR-positive nontarget tissues than GRPR agonists. More importantly, GRPR antagonists do not elicit side effects. The statin-based GRPR antagonist JMV594 (H-D-Phe-Gln-Trp-Ala-Val-Gly-His-Sta-Leu-NH_2) has been widely used in the design of GRPR-targeted imaging agents. In **Chapter 2.1** of this thesis, we describe the development of an ^{18}F-labeled GRPR antagonist for high resolution and sensitive PET imaging of PCa and compared the imaging properties of this tracer with those of ^{68}Ga-labeled analogs. For this purpose, J594 was conjugated to a NODA-MPAA chelator for high-yield complexation of Al^{18}F. The resulting compound, JMV5132 (NODA-MPAA-βAla-βAla-JMV594), was labeled with Al^{18}F in a 1-step procedure within 20 min. JMV5132 and the DOTA-analog JMV4168 (DOTA-βAla-βAla-JMV594) were radiolabeled with ^{68}Ga for comparison. Al^{18}F-JMV5132, ^{68}Ga-JMV5132, and ^{68}Ga-JMV4168 were evaluated in vivo in mice with subcutaneous PC-3 xenografts. Two hours after injection, uptake values of ^{68}Ga-JMV4168, ^{68}Ga-JMV5132 and Al^{18}F-JMV5132 in PC-3 tumors were similar. PET images obtained with Al^{18}F-JMV5132

showed a higher resolution than with ^{68}Ga-JMV4168, but Al^{18}F-JMV5132 showed higher hepatobiliary excretion than ^{68}Ga-JMV4168. In **Chapter 2.2** of this thesis, the application of DOTA analog JMV4168 in a theranostic approach for PC is described. In this study we demonstrated that in vivo stabilization of the GRPR antagonist JMV4168 could enhance PET imaging and radionuclide therapy in a preclinical model of PCa. Neutral endopeptidase (NEP) is a key proteolytic enzyme responsible for in vivo degradation of several peptide families, amongst which bombesin analogs. We have shown that coinjection of a NEP inhibitor (e.g. phosphoramidon (PA)) can protect ^{68}Ga- and ^{177}Lu-JMV4168 from enzymatic degradation, leading to a remarkable enhancement of diagnostic sensitivity and therapeutic efficacy. In PC-3 tumor-bearing mice, tumor uptake of ^{68}Ga-/^{177}Lu-JMV4168 at 1 h after injection was increased by a factor of 2 when PA was coadministered. PA coinjection also enhanced PC-3 tumor signal intensity in PET imaging with ^{68}Ga-JMV4168. Treatment of PC-3 tumor-bearing mice with ^{177}Lu-JMV4168 plus PA showed increased DNA damage, slower tumor regrowth and higher survival rates as compared to mice treated with ^{177}Lu-JMV4168 without PA. We concluded that this strategy might be beneficial to improve diagnosis and treatment of PCa and other GRPR-expressing malignancies and warrants clinical translation.

Despite the promise of GRPR antagonists in (pre)clinical studies, recent efforts for imaging and therapy of PCa in nuclear medicine have focused mainly on the development of PSMA-targeted tracers. In **Section 3** of this thesis, the development and optimization of imaging and therapeutic tracers targeting PSMA are described. Small-molecule PSMA inhibitors have attracted considerable attention for imaging of PCa, due to their efficient accumulation in tumor lesions and fast clearance from nontarget tissues. However, their application in radionuclide therapy could be hampered by their high uptake in some PSMA-positive nontarget organs, such as kidneys and salivary glands. In **Chapter 3.1** of this thesis, we describe the development of a Nanobody targeting PSMA for targeted imaging and therapy of PCa. Nanobodies are the smallest antibody-based fragments and possess valuable molecular imaging properties, such as high target specificity and rapid background clearance. In this study we described the application of the ^{111}In-labeled anti-PSMA Nanobody JVZ-007 for SPECT/CT imaging of PCa. JVZ-007 was initially produced with a c-*myc*-hexahistidine (his) tag allowing purification and detection. ^{111}In-JVZ007-c-*myc*-his showed good tumor targeting properties in vivo and in vitro, but had unfavorable renal retention. Renal uptake of ^{111}In-JVZ-007-c-*myc*-his was effectively reduced by coinjection of gelofusine and lysine. Subsequently, the c-*myc*-his tag was replaced by a single cysteine at the C terminus, allowing site-specific conjugation of chelates for radiolabeling. The replacement of the c-*myc*-his tag by the cysteine contributed to further reduction of renal uptake without loss of targeting. Because of its low renal uptake, this novel anti-PSMA Nanobody JVZ-007-cys could offer an advantage compared to small-molecule PSMA inhibitor for radionuclide therapy.

Alternatively, strategies to reduce uptake of small-molecule PSMA inhibitors in PSMA-positive nontarget tissues can be considered. In **Chapter 3.2** of this thesis, we

describe the application of the small-molecule PSMA inhibitor PSMA I&T for single photon emission computed tomography/computed tomography (SPECT/CT) imaging and radionuclide therapy of PCa. In this study we showed that PSMA-specific uptake in normal organs can be reduced using blocking agents such as 2-(phosphonomethyl) pentane-1,5-dioic acid (2-PMPA). In mice with subcutaneous PSMA-expressing xenografts, ^{111}In-PSMA I&T showed dose-dependent uptake in PSMA-expressing tumors, kidneys, spleen, adrenals, lung and salivary glands. PSMA-mediated renal uptake was efficiently reduced by co-administration of 2-PMPA, with the highest tumor/kidney ratios being obtained at 50 nmol 2-PMPA. In SPECT/CT imaging experiments, co-administration of 2-PMPA with ^{111}In-PSMA I&T improved visualization of sub-millimeter intraperitoneal metastases near the kidneys and spleen. Moreover, co-administration of 2-PMPA increased the tumor-to-kidney absorbed dose ratio during ^{177}Lu-PSMA I&T radionuclide therapy. As a result, mice injected with ^{177}Lu-PSMA I&T showed signs of nephrotoxicity at 3 months after therapy, whereas mice injected with vehicle or ^{177}Lu-PSMA I&T + 2-PMPA showed no signs of nephrotoxicity.

Despite the encouraging results of radionuclide therapy using ^{177}Lu-PSMA I&T, tumor regrowth was observed a few weeks after therapy. To improve the efficacy of PSMA-targeted radionuclide therapy, we investigated the feasibility of alpha radionuclide therapy using ^{213}Bi-labeled PSMA I&T and anti-PSMA nanobody JVZ-007 (**Chapter 3.3**). Labeling of PSMA I&T and JVZ-007-cys-DOTA (JVZ-008) with ^{213}Bi was optimized, and preliminary in vitro and in vivo evaluation were performed using LNCaP cells and LNCaP xenografts. ^{213}Bi-PSMA I&T and ^{213}Bi-JVZ-008 induced DNA double-strand breaks (DSBs) in LNCaP cells in vitro and in LNCaP-xenografts in vivo, as indicated by the presence of increased numbers of 53BP1 and γH2AX nuclear foci. Linear tracks of foci (alpha tracks) were observed in the nucleus at early time points, but were no longer visible after 24 h. However, single foci were still observed 24 h after treatment. ^{213}Bi-PSMA I&T showed a 2-fold higher tumor uptake than ^{213}Bi-JVZ-008 in LNCaP-xenografts. Further studies are required to determine the benefits of PSMA-targeted alpha radionuclide therapy over beta radionuclide therapy.

These preclinical studies have highlighted the challenges in the development of theranostic agents for PCa. Strategies have been implemented in this thesis to improve PET/SPECT imaging quality and therapeutic efficacy of GRPR- and PSMA-targeting theranostic agents. These encouraging preclinical findings warrant further clinical studies to elucidate the value of GRPR- and PSMA-targeted imaging and radionuclide therapy in PCa patients.

4

Samenvatting

SAMENVATTING

Het doel van het onderzoek beschreven in dit proefschrift is de ontwikkeling en het verbeteren van het gebruik van radioactieve tracers voor het afbeelden (imaging) en behandelen (radionucliden-therapie) van prostaatkanker. De zogenaamde theranostische benaderingswijze (gebruik van tracers die voor zowel diagnostiek als voor therapie gebruikt kunnen worden) kan uiteindelijk bijdragen aan een meer op de patiënt toegesneden therapie voor prostaatkankerpatiënten.

Sectie 1 van dit proefschrift introduceert het concept van theranostics in de nucleaire geneeskunde. In **Hoofdstuk 1.1** worden prostaatkanker, de huidige diagnostiek- en stageringsmogelijkheden en opties voor behandelingen kort beschreven. Vervolgens worden de klinische relevantie van theranostische toepassingen en de principes achter moleculaire beeldvorming en radionuclidentherapie, alsmede diverse radionucliden die toegepast worden voor beeldvorming, diagnose en therapie beschreven. Tenslotte worden moleculaire doeleiwitten (targets) aanwezig op prostaatkankercellen en waaraan de tracers kunnen binden, geïntroduceerd en bediscussieerd. In dit proefschrift is de nadruk gelegd op de "gastrin-releasing peptide receptor" (GRPR) en het "prostate-specific membrane antigen" (PSMA), twee belangrijke targets op prostaatkanker. **Hoofdstuk 1.2** beschrijft nieuwe strategieën voor de toepassing van kleine tracer moleculen (in dit geval "radiopeptiden") om tumoren zichtbaar te maken en te behandelen. Een mede door ons ontwikkelde tracer, indium-111 (^{111}In)-gelabeld octreotide, bleek neuroendocriene tumoren in patiënten heel goed te kunnen afbeelden, en volgens hetzelfde principe worden nu radiopeptiden ontwikkeld voor zowel het afbeelden als voor radionuclidentherapie van andere typen tumoren, zoals prostaatkanker.

Om beeldvorming met behulp van radiopeptiden te verbeteren, zijn verschillende strategieën toegepast en beschreven: het gebruik van receptor-antagonisten, het verhogen van de stabiliteit van radiopeptiden door het remmen van peptidase activiteit in het lichaam, het gebruik van positron-emitterende radionucliden voor zeer gevoelige positron emission tomography (PET) imaging en de combinatie van nucleaire en optische imaging technieken.

Om daarnaast de therapeutische effectiviteit van radiopeptiden te verbeteren, zijn de volgende benaderingen toegepast en beschreven: het gebruik van receptor-antagonisten, de combinatie van radionuclidentherapie met andere stoffen die gezonde organen beschermen of die de gevoeligheid van het tumorweefsel voor radioactieve straling verhogen en het gebruik van alfa-emitters, radionucliden die radioactieve deeltjes uitzenden met hoge energie maar over een kortere afstand (penetratie range) en dus veiliger voor omliggend weefsel.

Sectie 2 van dit proefschrift beschrijft de ontwikkeling van theranostische strategieën voor prostaatkanker via de GRPR. Verschillende studies hebben aangetoond dat, in vergelijking met GRPR agonisten, GRPR antagonisten een hogere opname in de tumor

en een lagere opname in gezonde weefsels laten zien. Daarnaast induceren GRPR antagonisten geen biologische effect na binding aan de receptor en daarom hebben zij minder bijwerkingen. In onze studies is de GRPR antagonist JMV594 (H-D-Phe-Gln-Trp-Ala-Val-Gly-His-Sta-Leu-NH_2) gebruikt als basis voor de ontwikkeling van nieuwe GRPR-tracers. In **Hoofdstuk 2.1** wordt de ontwikkeling van een fluor-18 (^{18}F)-gelabelde GRPR antagonist beschreven, waarmee met hoge resolutie en een hoge sensitiviteit prostaatkanker met de PET imaging techniek afgebeeld kan worden. Daarnaast worden de imaging-eigenschappen van deze tracer vergeleken met gallium-68 (^{68}Ga)-gelabelde analoga. Deze ^{68}Ga-gelabelde tracers hebben een kortere halfwaardetijd, wat een nadeel kan zijn tijdens imaging studies in patiënten. Voor de nieuwe ^{18}F-labeling is J594 geconjugeerd aan een andere chelator, NODA-MPAA, voor stabiele labeling met $Al^{18}F^{2+}$. Het product, JMV5132 (NODA-MPAA-βAla-βAla-JMV594), hebben we vervolgens gelabeld met $Al^{18}F^{2+}$ via een geoptimaliseerde 1-staps procedure, die in minder dan 20 minuten uitgevoerd kan worden. JMV5132 en het DOTA-analogon ervan, JMV4168 (DOTA-βAla-βAla-JMV594), zijn in deze studies beide radioactief gelabeld met ^{68}Ga en ter vergelijking meegenomen. $Al^{18}F$-JMV5132, ^{68}Ga-JMV5132 en ^{68}Ga-JMV4168 zijn vervolgens onderzocht in muizen met subcutane humane prostaattumoren. Twee uur na injectie van de tracer was de opname van ^{68}Ga-JMV4168, ^{68}Ga-JMV5132 en $Al^{18}F$-JMV5132 in de tumoren vergelijkbaar. PET afbeeldingen verkregen met $Al^{18}F$-JMV5132 waren van een hogere kwaliteit, maar lieten helaas ook een hogere ongewenste uitscheiding via de lever zien. In **Hoofdstuk 2.2** wordt een nieuwe en verbeterde toepassing van JMV4168, een DOTA-analogon, voor diagnose en therapie van prostaatkanker beschreven. Deze studie laat in een preklinisch model (een muis met een humane prostaattumor) zien dat de stabilisatie van de GRPR-antagonist JMV4168 leidt tot betere PET beelden en radionuclidentherapie. Het enzym neutral endopeptidase (NEP) is één van de belangrijkste enzymen in ons lichaam verantwoordelijk voor de afbraak van diverse peptiden, waaronder die van de door ons toegepaste GRPR-tracers. In dit hoofdstuk wordt beschreven dat co-injectie van een NEP-remmer, zoals phosphoramidon (PA), het ^{68}Ga- en lutetium-177 (^{177}Lu)-gelabelde JMV4168-peptide kan beschermen tegen enzymatische afbraak. Dit leidt tot een aanzienlijke verbetering van de diagnostische sensitiviteit en de therapeutische effectiviteit in dit muizenmodel. Het gelijktijdig toedienen van de enzymremmer PA resulteerde in een verdubbeling van de opname van ^{68}Ga-/^{177}Lu-JMV4168 in prostaattumoren. Het gelijktijdig toedienen van PA verhoogde tevens de intensiteit van het PET imaging signaal van ^{68}Ga-JMV4168 in de tumor. De behandeling van prostaattumoren in muizen met het therapeutische ^{177}Lu-JMV4168 peptide met gelijktijdige toediening van PA resulteerde ook in een toename van DNA schade in de tumorcellen, resulterend in een vertraagde tumorgroei en een verhoogde overleving van de muizen ten opzichte van muizen behandeld met alleen ^{177}Lu-JMV4168. Deze strategie zou mogelijk toegepast kunnen worden in de kliniek en de diagnose en behandeling van prostaatkanker en andere GRPR-positieve tumoren kunnen verbeteren.

Naast aandacht voor GRPR antagonisten, is er momenteel veel belangstelling voor de ontwikkeling en toepassing van tracers die binden aan PSMA. In **Sectie 3** van dit

proefschrift wordt de ontwikkeling en optimalisatie van verschillende van dergelijke tracers beschreven. Zogeheten “small-molecule PSMA-remmers” (PSMA-remmers met een laag molecuulgewicht) lokaliseren heel efficiënt in PSMA-positieve tumoren en worden snel uitgescheiden uit bijna alle gezonde weefsels. Echter, er werd een hoge opname van deze tracers gevonden in nieren en speekselklieren, wat een struikelblok zou kunnen vormen voor veilige toepassing van radionuclidentherapie met deze PSMA-bindende tracers.

In **Hoofdstuk 3.1** wordt de ontwikkeling van een nieuwe, PSMA-bindend Nanobody voor imaging en therapie van prostaatkanker beschreven. Nanobodies zijn kleine antilichaam eiwitten, die met hoge affiniteit binden aan hun doelwit, in dit geval PSMA. Nanobodies zijn kleiner en stabieler dan gewone antilichamen en ze worden sneller uitgescheiden. In deze studie worden de ontwikkeling en toepassing van ^{111}In-gelabeld anti-PSMA Nanobody JVZ-007 voor zogenaamde SPECT/CT imaging van prostaatkanker beschreven. JVZ-007 hebben we aanvankelijk geproduceerd met een aminozuurstaart van *c-myc*-hexahistidine (*c-myc*-his-tag) om de Nanobody te kunnen zuiveren en meten. In muizen met prostaattumoren toonde ^{11}In-JVZ007-*c-myc*-his inderdaad de gewenste hoge opname in de tumoren, maar ook een ongewenste hoge opname in de nieren. Deze opname in de nieren konden we verminderen door co-injectie van gelofusine en lysine. In vervolgexperimenten hebben we de *c-myc*-his-tag vervangen door een enkel cysteine-aminozuur aan de zogenaamde C-terminus van het eiwit, waardoor site-specifieke koppeling van chelatoren voor het radioactief labelen mogelijk werd. Het vervangen van de *c-myc*-his tag droeg sterk bij aan het reduceren van Nanobody opname in de nier zonder daarbij de binding aan de tumoren te verminderen. De lagere nieropname van het anti-PSMA Nanobody JVZ-007-cys in vergelijking met toepassing van de populaire “small-molecule PSMA-remmers”, die een hoge nieropname laten zien, zou een belangrijk voordeel op kunnen leveren tijdens radionuclidentherapie.

Vervolgens hebben we mogelijkheden onderzocht om de ongunstige hoge opname van de al genoemde “small-molecule PSMA-remmers” in nieren en speekselklieren te reduceren. In **Hoofdstuk 3.2** van dit proefschrift hebben we de toepassing beschreven van de small-molecule PSMA-remmer PSMA I&T voor toepassing in SPECT/CT imaging en radionuclidentherapie van prostaatkanker. In deze studie laten we zien dat PSMA-specifieke opname in gezonde organen verminderd kan worden door gebruik te maken van PSMA-bindende stoffen zoals bijvoorbeeld 2-(phosphonomethyl)pentane-1,5-dioic acid (2-PMPA). In muizen met een prostaattumor laat ^{111}In-PSMA I&T een dosisafhankelijke opname in PSMA-positieve tumoren en in organen zoals nieren, bijnieren, milt, long en speekselklieren zien. De nieropname konden we heel efficiënt reduceren door het gelijktijdig toedienen van 2-PMPA. De beste effecten werden verkregen bij 50 nmol 2-PMPA. In SPECT/CT experimenten verbeterde het gelijktijdig toedienen van 2-PMPA en ^{111}In-PSMA I&T de beeldvorming van uitzaaiingen bij de nieren en de milt. Daarnaast verbeterde 2-PMPA de mogelijkheden om ^{177}Lu-PSMA I&T te gebruiken voor radionuclidentherapie. Muizen behandeld met alleen ^{177}Lu-PSMA I&T ontwikkelden 3 maanden na therapie nierschade door de hoge dosis ^{177}Lu in de

nieren, maar muizen geïnjecteerd met een combinatie van ^{177}Lu-PSMA I&T en 2-PMPA vertoonden geen tekenen van nierschade.

Na de aanvankelijk bemoedigende effecten van ^{177}Lu-PSMA I&T-therapie, toonden de muizen enkele weken na therapie opnieuw tumorgroei. Om de werking van PSMA-radionuclidentherapie verder te verbeteren werden daarom de mogelijkheden van zogenaamde alfa-radionuclidentherapie, een therapie met uiterst effectieve alfastraling, onderzocht. Hiervoor werden PSMA I&T en anti-PSMA Nanobody JVZ-007 gelabeld met de alfastraler bismuth-213 (^{213}Bi), (**Hoofdstuk 3.3**). Nadat eerst de labeling van PSMA I&T en JVZ-007-cys-DOTA (JVZ-008) werd geoptimaliseerd, hebben we proeven uitgevoerd met prostaattumorcellen in vitro en muizen met humane prostaattumoren. ^{213}Bi-PSMA I&T en ^{213}Bi-JVZ-008 bleken meer schade in tumorcellen te veroorzaken dan de eerder toegepaste ^{177}Lu-gelabelde tracers. Lineaire sporen van schade (de kenmerkende alfasporen) waren zichtbaar in de celkern in de eerste 24 uur na bestraling. De opname van ^{213}Bi-PSMA I&T in de tumoren was twee keer zo hoog als die van ^{213}Bi-JVZ-008. Om alle voor- en nadelen van PSMA-gerichte alfa radionuclidentherapie goed in kaart te brengen is echter verder onderzoek nodig.

In onze preklinische studies hebben wij diverse mogelijkheden voor de ontwikkeling van imaging- en therapiestrategieën voor prostaatkanker onderzocht. In dit proefschrift staan diverse benaderingen beschreven die de kwaliteit van PET en SPECT imaging en de therapeutische werking van GRPR- en PSMA-bindende tracers kunnen verbeteren. Na de positieve preklinische bevindingen beschreven in dit proefschrift zijn er nu klinische studies nodig om GRPR- en PSMA-gerichte imaging en radionuclidentherapie van prostaatkanker verder te ontwikkelen.

4

Curriculum Vitae

Kristell Chatalic was born on June 3rd 1986 in Vitry-sur-Seine, France. After obtaining her Baccalaureate with distinction, she engaged in a prestigious competitive program at Lycée Saint-Louis (Paris) for entry into Engineering Schools. In 2006, she started her chemical engineering studies at the Engineering School of Chemistry, Polymers and Material Science (Ecole Européenne de Chimie, Polymères et Matériaux, ECPM) in Strasbourg (France), where she specialized in organic chemistry. She discovered her passion for molecular imaging and nuclear medicine during her first internship at Philips Healthcare in Eindhoven, The Netherlands. She worked on the synthesis of precursors for a pretargeting approach using "Click Chemistry" under the supervision of Dr. Marc Robillard. Her interest for biology and cancer research grew during this period, and drove her to carry out her Master's research thesis at the medicinal chemistry group directed by Prof. Martine Smit at the Vrije Universiteit (VU) in Amsterdam, the Netherlands. During this internship, she studied the interaction between the chemokine receptor CXCR7 and small organic molecules, under the supervision of Dr. David Maussang. In 2010, she obtained her "Diplôme d'Ingénieur" in organic chemistry and her Master's Degree in "Molecular and Supramolecular Chemistry" at Strasbourg University. She pursued her goal to become a researcher in the field of nuclear medicine, and started a PhD study in 2012 under the supervision of Prof. Marion de Jong and Dr. Wytske M. van Weerden at the Erasmus MC in Rotterdam. Part of her research was performed under supervision of Prof. Otto C. Boerman at the Radboud University Medical Center in Nijmegen. She has been working on a project at the interface of radiochemistry, molecular imaging and radionuclide therapy. Her research focuses on the development of theranostic approaches using tumor-targeted radiolabeled agents to achieve personalized treatment of prostate cancer. In 2014 she obtained a poster presentation award at the European Molecular Imaging Meeting in Antwerp. In 2015 she obtained the Alavi-Mandell Publication Award from the Society of Nuclear Medicine and Molecular Imaging for her publication in the *Journal of Nuclear Medicine*.

4

List of Publications

Chatalic KL, Konijnenberg M, Nonnekens J, de Blois E, Hoeben S, de Ridder C, Fehrentz JA, van Gent DC, Nock BA, Maina T, van Weerden WM, de Jong M. **In Vivo Stabilization of a Gastrin-Releasing Peptide Receptor Antagonist enhances PET Imaging and Radionuclide Therapy of Prostate Cancer in Preclinical Studies.** Theranostics. 6(1):104-117 (2016)

Chatalic KL, Kwekkeboom D, de Jong M. **Radiolabeled Peptides for Imaging and Therapy: A Radiant Future**. J Nucl Med. 56(12):1809-12 (2015)

Chatalic KL, Veldhoven-Zweistra J, Bolkestein M, Hoeben S, Koning GA, Boerman OC, de Jong M, van Weerden WM. **A Novel ^{111}In-labeled Anti-PSMA Nanobody for Targeted SPECT/CT Imaging of Prostate Cancer**. J Nucl Med. 56(7):1094-9 (2015)

Chatalic KL, Franssen GM, van Weerden WM, McBride WJ, Laverman P, de Blois E, Hajjaj B, Brunel L, Goldenberg DM, Fehrentz JA, Martinez J, Boerman OC, de Jong M. **Preclinical Comparison of Al^{18}F- and ^{68}Ga-Labeled Gastrin-Releasing Peptide Receptor Antagonists for PET Imaging of Prostate Cancer**. J Nucl Med. 55(12):2050-6 (2014)

Wijtmans M, Maussang D, Sirci F, Scholten DJ, Canals M, Mujić-Delić A, Chong M, **Chatalic KL**, Custers H, Janssen E, de Graaf C, Smit MJ, de Esch IJ, Leurs R. **Synthesis, modeling and functional activity of substituted styrene-amides as small-molecule CXCR7 agonists**. Eur J Med Chem. 51:184-92 (2012)

CONFERENCE PRESENTATIONS

Kristell L.S. Chatalic, Sandra Heskamp, et al. (2015) **Targeted Alpha Radionuclide Therapy of Prostate Cancer Using a Small Molecule Inhibitor of Prostate-Specific Membrane Antigen (PSMA).** Oral presentation delivered at the EANM conference, October 2015, Hamburg, Germany.

Kristell L.S. Chatalic, J. Veldhoven-Zweistra, et al. (2015) **Novel nanobody targeting prostate-specific membrane antigen: A promising tracer for imaging of prostate cancer**. Oral presentation at the European Association of Urology (EAU) annual Conference, March 2015, Madrid, Spain.

Kristell L.S. Chatalic, Joke Veldhoven-Zweistra et al. (2014). **SPECT/CT and PET Imaging of Prostate Cancer Xenografts using a novel anti-PSMA Nanobody.** Poster presentation delivered at the EANM conference, October 2014, Gothenburg, Sweden.

Kristell L.S. Chatalic, Mark Konijnenberg et al. (2014) **Enhancing the Theranostic Potential of the GRPR-antagonist JMV4168 for PET Imaging and Radionuclide Therapy of Prostate Cancer.** Oral presentation delivered at the EANM conference, October 2014, Gothenburg, Sweden.

Kristell L.S. Chatalic, Joke Veldhoven-Zweistra et al. (2014). **SPECT/CT Imaging of Prostate Cancer Using a Novel ^{111}In-labeled anti-PSMA Nanobody.** Poster presentation delivered at EMIM conference, June 2014, Antwerpen, Belgium. Poster presentation award in the category cell and receptor imaging.

Kristell L.S. Chatalic, Gerben. M. Franssen et al. (2013). **Preclinical Evaluation of Al^{18}F- and ^{68}Ga-labeled GRPR-antagonists for PET Imaging of Gastrin-Releasing Peptide Receptor Expression in Prostate Cancer.** Oral presentation delivered at the EANM conference, 2013, Lyon, France.

4

PhD Portfolio

SUMMARY OF PHD TRAINING AND TEACHING

Name PhD student: Kristell L.S. Chatalic
Erasmus MC Departments: Nuclear Medicine, Radiology, and Urology
Research School: Molecular Medicine

PhD period: 01-03-2012 – 16-03-2016
Promotors: Prof.dr.ir. M. de Jong, Prof.dr. O.C. Boerman
Co-promotor: Dr.ir. W.M. van Weerden

PhD training	Year	ECTS
General courses		
Endnote course	2013	0.3
Indesign CS5 Workshop (MolMed)	2014	0.15
Laboratory skills		
Safely working in the laboratory (LUMC Boerhaave)	2011	0.15
"Radiation safety, level 5B" course	2012	1
"Article 9" course (animal experimentation)	2012	4
Specialized courses and workshops		
Using R for data analysis (LUMC Boerhaave)	2011	1
Analysis of microarray gene expression data using R/BioC and web tools (LUMC Boerhaave)	2011	2
Signal transduction pathways regulating aging and disease (LUMC Boerhaave)	2011	1.4
Cursus ^{18}F Radiochemie (VU, Amsterdam)	2012	0.6
^{89}Zr-labeling training course (VU, Amsterdam)	2014	1
The translational imaging workshop by AMIE 'From mouse to man' (MolMed)	2012	1.4
Symposium: Visualising the Invisible: from single molecule Super-Resolution to Patient (MolMed)	2013	0.3
Workshop Nanobody Theranostics (Brussels)	2014	1.4
Workshops NKRV (Nijmegen, Delft, Amsterdam, Rotterdam)	2012-2015	1.4

Nuclear Medicine Research Meetings (Erasmus MC)	2012-2015	1
Urology Research Meetings (Erasmus MC)	2012-2015	1
JNI Meetings (Erasmus MC)	2012-2015	0.3
International conferences		
EANM Annual Congress 2013, Lyon, France	2013	1.25
EMIM Annual Congress 2014, Antwerpen, Belgium	2014	1
EANM Annual Congress 2014, Gothenburg, Sweden	2014	1.25
9th Symposium on Targeted Alpha Therapy 2015, Warsaw, Poland	2015	1
EANM Annual Congress, October 2015, Hamburg, Germany	2015	1

Teaching activities	**Year**	**ECTS**
Supervising trainees	2013-2014	10
Journal clubs Nuclear Medicine	2012-2015	1

Peer-review activities	**Year**	**ECTS**
Nuclear Medicine and Biology	2014	0.3
Journal of Nuclear Medicine	2015	0.3
Cancer Letters	2015	0.3

Total		**34.1**

4

Acknowledgments

ACKNOWLEDGMENTS

This PhD thesis is the result of 4 years of hard work and dedication, and the work described in this thesis would not have been possible without the help of many people. I would like to take the opportunity to thank those who stood by me and contributed to this achievement.

My interest for nuclear medicine was triggered during my first research internship at the High Tech Campus of Philips Healthcare in the Netherlands in 2008. **Dr. Robillard**, dear Marc, you inspired me to pursue my scientific career in nuclear medicine, for which I would like to express my biggest thanks.

During this internship, I also met my partner, a smart Dutch biologist. **Caesar Roseboom**, dear Caes, you made me see the Netherlands from a complete different perspective. All of a sudden this country was not that boring anymore, and the rain did not bother me, because I had you at my side. And you stood by me ever since. You followed me in my adventures to Brazil, Switzerland, Strasbourg, until we finally returned back to the Netherlands. You supported me all these years and I cannot thank you enough for that.

In 2010 I started an internship at the Vrije Universiteit Amsterdam in the department of medicinal chemistry, to study the interactions of molecules with cancer cells. **Dr. Maussang**, dear David, you also started as a chemist and ended up in cancer biology, and you believed in me. Thank you for all the support and valuable lessons. They have proven very helpful in my scientific career!

After doing some research in Leiden, I realized I wanted to pursue a PhD study in nuclear medicine.

Prof. de Jong, dear Marion, you offered me a position in nuclear medicine. You supported me, provided all the trainings I needed, and most importantly: you BELIEVED IN ME! I felt encouraged and motivated enough to push forward multiple projects from which the results can be read in this thesis. I am very proud to have been part of your research group and to have you as my first promoter. I cannot express in words how much I am grateful for your support and the multiple opportunities you have created for me, in order to develop myself as a scientist. Amongst those opportunities, you supported me in carrying out a research stay in Nijmegen. There I have been able to collaborate with other talented researchers, which resulted in several successful projects that can be read in this thesis.

Prof. Boerman, dear Otto, you welcomed me to your lab in Nijmegen and provided everything I needed to learn and progress rapidly in the research topic. I felt like I had so much to learn in Nijmegen, that I could not just leave after 2 weeks. You were closely involved in the research projects and thanks to your expert advice I progressed very

quickly. I always kept an impression of the lab in Nijmegen as an ideal place to work in, and we collaborated on many projects ever since. I am very proud to have you as my second promoter. Thank you for all the support you gave me during my PhD study!

Dr. van Weerden, dear Wytske, thanks to your expertise in prostate cancer, you provided another dimension to my project. We worked together on the anti-PSMA nanobody project and PSMA rapidly became an integral part of my PhD project. It was quite the challenge to work on the GRPR and PSMA projects simultaneously, but I am so grateful for all the support you provided. The end result has proven to be worth the effort! Thanks to your critical point of view, we achieved studies of high quality and I am very grateful for that.

Prof. Verzijlbergen, **Prof. Bangma**, **Prof. Krestin**, thank you for giving me the opportunity to start this collaborative PhD project in the departments of Nuclear Medicine, Urology and Radiology. I am very proud to have been part of these 3 outstanding departments.

I would like to thank all my colleagues from the Nuclear Medicine, Radiology and Urology labs in Rotterdam for the great atmosphere and work discussions. In particular the following people with whom I actively collaborated:

Dear **Joke**, it was a great pleasure to work with you. Your enthusiasm and kindness is refreshing, and you were so dedicated to the nanobody production, next to your busy life of being a mom of 3. **Sander** and **Corrina**, you were of such a big help in the lab! You were flexible, hard working, and you both did such an extraordinary job! You deserve a BIG THANKS!

Dr. Melis, dear Marleen, thank you for your help and involvement at the early stage of my PhD study. I appreciate your enthusiasm and energy and I value your honesty and integrity. **Dr. Konijnenberg**, dear Mark, you made a significant contribution to the quality of the papers with your valuable expertise in dosimetry. Thank you for all of your efforts! **Dr. Nonnekens**, dear Julie, you are a very nice person to collaborate with, and your expertise in radiation induced-DNA damage has added great value to my projects. **Erik** and **Wout**, you taught me a lot about radiolabeling of peptides and stability of radiopeptides. Thank you for sharing your expertise with me!

Simone, **Ingrid**, **Costanza**, and **Hendrik**, you were great fun to have as PhD roommates for almost 3 years. **Simone**, you were my confidant. We supported each other, advised each other, thank you for always being there! **Ingrid** and **Costanza**, thank you for your enthusiasm and for bringing joy and a great atmosphere into our group. I would also like to thank the rest of the **SPECTRIM team**, in particular **Dr. Monique Bernsen**, **Jan**, **Gaby**, **Sandra**, **Joost**, **Marcel**, **Ho Sze**, **Harald**, **Stuart**, **Linda** and **Saskia** for the interesting work discussions, the good work atmosphere and the nice lab outings. Thanks to all the students, in particular **Thomas**, **Sally** and **Evelyn** for your great

contribution. **Jacqueline**, thank you for the energy you put into arranging so many things for the department, thank you for supporting us during the EANM conferences throughout the years.

Since I have also spent a significant amount of time in Nijmegen, I would also like to thank everyone from the lab in Nijmegen for the great experience.

Gerben Franssen and **Dr. Peter Laverman**, thank you for teaching me the $Al^{18}F$ labeling technique, and sharing all your tips and tricks related to radiolabeling. Working together was an exciting opportunity, and a great experience!

Dr. Heskamp, dear Sandra, you are a kind, smart, ambitious and modest researcher. We have worked on 2 projects together, and I must say that this has been the most efficient period of my PhD study. In 5 months we produced enough data for 2 very good papers. We had similar research interests and a similar pace of working. A perfect combination! I had great fun working together with you. Even though you had a busy post-doc life, trying to get funds to secure your position at the university, you always had time for our projects. And at the most hectic of times at the end of my PhD study, you supported me and took over our last experiment. I am really happy I met you! You are a role model of successful post-doc for me.

Janneke and **Gerben**, thank you for your exceptional involvement into the research projects, and thank you for being so flexible. I cannot give you enough chocolate to thank you for the extraordinary job you did! **Danny**, **Cathelijn**, **Bianca**, **Kitty**, **Iris** and **Henk**, you have been very helpful during my experiments in Nijmegen. You were always there when I needed help. Thank you so much for all the good work you did! Thank you to the other team members, in particular **Tessa**, **Marteen**, **Stefanie**, **Willem**, **Inge**, **Stijn**, **Marlène**, **Charlotte**, **Lieke**, **Desirée**, **Wael**, **Wietske**, **Samantha**, **Floor**, **Mark** and **Annemarie** for being such nice colleagues and for the fun time in Nijmegen.

Prof. Martinez, **Dr. Fehrentz**, **Dr. Hajjaj**, **Luc Brunel**, thank you for your collaborative effort in the synthesis of chelated GRPR antagonists. Without your great expertise in peptide synthesis and pharmacology, this project would not have been possible. **Dr. Maina-Nock**, Dr. Nock, dear Thea, dear Berthold, I extremely value our collaboration, your kindness, and the interesting scientific discussions we had. **Prof. Wester**, **Dr. Schottelius**, I am very grateful for your collaboration on the PSMA projects, and for your critical review of my manuscripts and thesis. **Dr. Morgenstern**, **Dr. Bruchertseifer**, thank you for your valuable collaboration on the alpha emitter project.

Ton Everaers, you did such a great job with the layout of my thesis and the cover design! Thank you for investing so much time and energy in this!

Graag wil ik ook mijn schoonfamilie bedanken voor de ontzettende steun in de laatste jaren. Beste **Arda** en **Harry**, jullie zijn zo lief! Jullie hebben mij als een dochter in de familie opgenomen. Daarnaast hebben jullie mij in de laatste maanden enorm veel geholpen met het oppassen op de konijnen en vissen en bij het verhuizen naar Engeland. Heel erg bedankt! **Thierry**, ook bedankt voor jouw hulp (ja, je bent de sterkste) en voor de gezelligheid!

Finally, I would like to thank my family. **Céline**, ma grande sœur, tu es un modèle pour moi. Ambitieuse, intelligente, tu es devenue docteur en médecine, et mère de 3 enfants adorables dont je suis très fière d'être tata. Merci pour tes conseils de grande sœur, je suis très fière de devenir docteur ès sciences, et j'espère bientôt devenir une super maman comme toi. **Geoffrey**, tu es presque comme mon frère. Merci pour ton amitié qui a persisté depuis notre enfance jusqu'à ce jour. **Papa**, **Maman**, je ne pourrai jamais vous remercier autant de m'avoir soutenue toutes ces années. Merci de m'avoir guidée dans mes choix d'études et de carrières et de m'avoir laissé la liberté de faire mes propres choix. J'espère que vous êtes fiers de vos filles, et de ce livre qui vous est dédié.